

PLAXIS

Internal Report

**Groundwater flow, fully coupled flow deformation
and undrained analyses in PLAXIS 2D and 3D**

Vahid Galavi

Research department

Preface

The main goal of this research was to implement groundwater flow and fully coupled flow-deformation analysis in PLAXIS 2D and 3D to enhance the code to simulate flow and deformation in saturated and partially saturated soils. The existing undrained analysis of PLAXIS has also been modified for partially saturated soils. The mechanical behaviour of unsaturated soil is described by the well-known Barcelona Basic Model (developed for PLAXIS 3D via user defined soil model option by Nubia Gonzalez), Gonzalez & Gens (2008).

It is acknowledged that the scientific part of the fully coupled flow-deformation analysis is mainly based on the report written by Radu Schwab (2008).

The outline of the work presented in this study is the following:

Chapter 1 presents basic equations and definitions.

Chapter 2 presents the governing equations of flow and deformation. First of all Darcy's law is described and then the continuity equation and deformation equations are derived.

The finite element formulation of the flow and the deformation equations derived in Chapter 2 is presented in Chapter 3.

Chapter 4 presents available boundary conditions for groundwater flow calculation.

Hydraulic models, implemented in PLAXIS 2D and 3D, are discussed in Chapter 5.

Barcelona Basic Model is briefly described in chapter 6. This chapter gives the basic features of the model which is written by Gonzalez & Gens (2008).

Chapters 7 to 10 present numerical verification of the code. Verification of one-dimensional groundwater flow problems is given chapter 7, while the two problems are discussed in Chapter 8. Fully coupled-flow deformation analysis and unsaturated soil model are verified in Chapter 9 and 10 respectively.

In chapter undrained analysis of PLAXIS is reviewed and the bulk modulus of water used in different types of calculation is summarised. At the end of this chapter some examples are given.

Table of contents

List of symbols

1	Introduction	1
2	Governing equations	7
3	Finite element formulations	15
4	Boundary conditions	21
5	Hydraulic models	27
6	Barcelona Basic model	33
7	Groundwater flow verification: 1D	47
8	Groundwater flow verification: 2D & 3D	117
9	Coupled analysis verification	175
10	Unsaturated soil model verifications	235
11	Undrained analysis in PLAXIS	247
12	Bibliography	273
	Appendices	277

1 Introduction

To analyse mechanical behaviour of saturated or partially saturated soils by means of numerical methods (e.g. finite element method) in proper manner, it is necessary to take into account both deformation and groundwater flow. For time dependent behaviour, this leads to mixed equations of displacement and pore pressure, called coupled hydro-mechanical approach, which have to be solved simultaneously. For applications which involve a horizontal phreatic surface, the equations can be simplified by decomposing the total pore pressure into a constant component (steady state pore pressure) and a time dependent component (excess pore pressure). But in many practical cases the distribution of stationary pore pressure is unknown in the beginning of the calculation stage (undrained excavations with dewatering or simulation of wave loading in off-shore conditions). Therefore a more general formulation according to Biot's theory of consolidation is needed which enables the user to simultaneously calculate deformation and groundwater flow with time-dependent boundary conditions in saturated and partially saturated soils, as presented here. The main challenge in this case is the need to use the consolidation theory for unsaturated soil conditions at least due to the need to simulate the phreatic line. Due to elastoplastic behaviour of soil skeleton and suction dependency of degree of saturation and relative permeability, all coefficients of the global stiffness matrix in the finite element formulations of Biot theory are non-linear. This case is completely different from the equations of saturated soils where only the elastoplastic stiffness matrix is non-linear. Therefore efficient numerical procedures are required, as implemented in PLAXIS. Accuracy, robustness and efficiency of the calculation depend on the method that selects the time increments. PLAXIS 2D and 3D utilise a fully implicit scheme which is unconditionally stable (Booker & Small, 1975).

Another essential issue for modelling the mechanical behaviour of unsaturated soils is the constitutive model implemented in a coupled flow-deformation analysis. A conceptually similar model to the well-known Barcelona Basic Model (BBM) (Alonso et al., 1990), developed by Gonzalez & Gens (2008), has been implemented in PLAXIS via user defined soil model option. The main features of the implemented model is that it utilises Bishop stress and suction as state variables (Sheng et al., 2003; Gallipoli et al., 2003) instead of net stress and suction as utilised in the original BBM. In addition to an implicit stress integration scheme based on backward Euler algorithm, a sub-stepping scheme proposed by Pérez et al. (2001) is used to integrate the strain-stress relations. The input variables of the constitutive model are the increment of total strain and increment of suction.

Two types of calculations, namely steady state and transient groundwater flow calculations for saturated and unsaturated soils have been fully implemented in PLAXIS kernels. According to the type of element used for deformation analysis, the new kernel uses the same type of element for groundwater flow calculation. Usually higher order elements do not behave as well as lower order elements for groundwater flow calculation. But additional procedures are utilised in the kernel to overcome the problems related to higher order elements. It is shown that the model is capable of calculating groundwater flow with a good accuracy.

Five types of hydraulic models have been implemented in PLAXIS kernels, namely Van Genuchten, Mualem (simplified Van Genuchten which has been called Van Genuchten in PlaxFlow kernel developed by GeoDelft), linearized Van Genuchten, spline and fully saturated.

In the following all features of the new implementations are presented.

1.1 Basic equations

Representation of formulations is based on the mechanical sign conventions, in which compressive stresses and strains are *negative*. In the same manner, pore water pressure p_w and pore air pressure p_a are considered to be *negative* in compression. Water discharge is assumed to be *positive* for inflow.

The porosity n is the ratio of the volume of voids to the total volume, and the saturation S is the ratio of free water volume to void volume:

$$n = \frac{dV_v}{dV} \quad S = \frac{dV_w}{dV_v} \quad (1.1)$$

The volumetric moisture content is:

$$\theta = \frac{dV_w}{dV} = S n \quad (1.2)$$

The water content is the ratio of the weight (or mass) of the water and the solids:

$$w = \frac{dW_w}{dW_s} = S \frac{n}{1-n} \frac{\rho_w}{\rho_s} \quad (1.3)$$

The density of the multiphase medium ρ is:

$$\rho = (1-n) \rho_s + n S \rho_w \quad (1.4)$$

where ρ_s stands for the density of the solid particles and ρ_w is the water density.

The stress state of the groundwater can be expressed in terms of groundwater heads as well. The hydraulic head ϕ can be decomposed in the elevation head z and the pressure head ϕ_p :

$$\phi = z - \frac{P_w}{\gamma_w} = z + \phi_p \quad (1.5)$$

The equations are presented in a three-dimensional space with a vertical and upwards oriented z-axis. For two dimensional problems the y-axis is vertical and the range of the vectors and matrices is correspondingly reduced.

The vector format of the gradient operator ∇ is:

$$\nabla^T \equiv \left| \frac{\partial}{\partial x} \quad \frac{\partial}{\partial y} \quad \frac{\partial}{\partial z} \right| \quad (1.6)$$

The differential operator corresponding to the definitions of engineering strains $\underline{\underline{L}}$ is defined as:

$$\underline{\underline{L}}^T = \begin{vmatrix} \frac{\partial}{\partial x} & 0 & 0 & \frac{\partial}{\partial y} & 0 & \frac{\partial}{\partial z} \\ 0 & \frac{\partial}{\partial y} & 0 & \frac{\partial}{\partial x} & \frac{\partial}{\partial z} & 0 \\ 0 & 0 & \frac{\partial}{\partial z} & 0 & \frac{\partial}{\partial y} & \frac{\partial}{\partial x} \end{vmatrix} \quad (1.7)$$

1.2 Unsaturated soil behaviour

Granular matrix, such as soil, is a mixture of solid particles in which pore spaces can be filled with liquids and gas. In geotechnical engineering the common fluids are air and water. The mechanical behaviour of soil is simplified in classical soil mechanics, by considering only two states where soil is fully dry, i.e. all pores are filled with air, or soil is fully saturated, i.e. all pores are filled with water. In the dry case, it is often assumed that the pores are empty and the compressibility of fluid and the degree of saturation are neglected. In contrast, in unsaturated soil mechanics the pores are considered to be filled with both liquid (water) and gas (air) and the relative proportion of liquid and gas plays a significant role in the mechanical behaviour of unsaturated soils. If degree of saturation of liquid is less than 1, the soil is called unsaturated or partially saturated which generally appears above the phreatic level and the pore water pressure is positive with respect to the atmospheric pressure. Below the phreatic level, the pore water pressures are negative and the soil is usually saturated. The position of phreatic level and the distribution of pore water pressure governed by climate conditions

(groundwater flow boundary conditions). In the areas where the upward flux (i.e. evaporation and evapotranspiration) exists, suction above phreatic level increases (and degree of saturation decreases) and the water level is lowered with time while in the case of downward flux (i.e. precipitation) suction decreases (and degree of saturation increases) and the water level rises with time. In the case of zero net surface flux, the pore water pressure profile become in equilibrium at a hydrostatic condition (Figure 1.1).

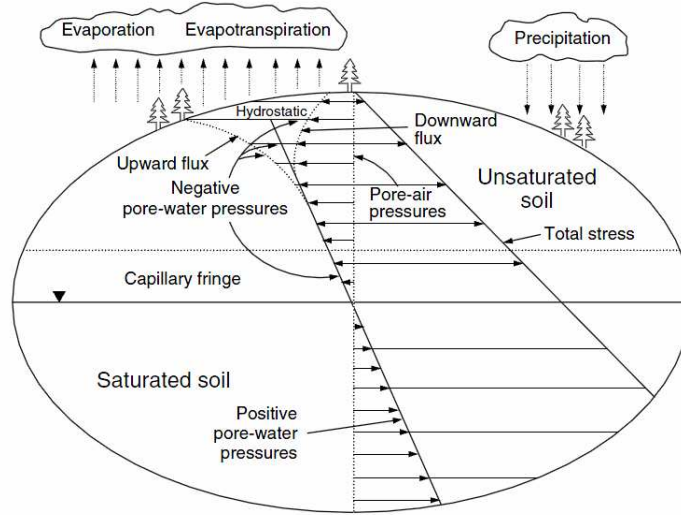


Fig. 1.1: A visualisation of soil mechanics showing the role of the surface flux boundary conditions (Fredlund, 1996)

1.3 Suction

Water potential is the potential work of pure water relative to a reference. This causes to flow water in porous media from an area with higher water potential to an area with lower water potential. The total water potential can be considered as the summation of water potential due to matric, osmotic, gas pressures and gravity. Flow in unsaturated zones relates to total suction which summation of matric S and osmotic suction π :

$$S_t = S + \pi \quad (1.8)$$

In most practical applications, osmotic suction does not exist, therefore:

$$S_t = S \quad (1.9)$$

Matric suction is related to soil matrix (adsorption and capillarity due to soil matrix) and it is the difference between soil water pressure and gas pressure:

$$S = p_a - p_w \quad (1.10)$$

where, p_w and p_a are the pore water pressure and the pore air pressure, respectively. In most cases, the pore air pressure is constant and small enough to be neglected. Therefore the matric suction is negative of the pore water pressure:

$$S = -p_w \quad (1.11)$$

1.4 Bishop effective stress

The governing equations of consolidation based on total pore pressure approach as used in PLAXIS follow Biot's theory (Biot, 1941). The formulation is based on small strain theory and Darcy's law for fluid flow is assumed. Bishop's effective stress (Bishop & Blight, 1963) is utilised in this formulation defined by Eq. (1.8). Note that the mechanical sign convention is used, i.e. compressive stresses are considered to be negative.

$$\boldsymbol{\sigma} = \boldsymbol{\sigma}' + \mathbf{m}(\chi p_w + (1 - \chi)p_a) \quad (1.12)$$

where:

$$\boldsymbol{\sigma} = (\sigma_{xx} \quad \sigma_{yy} \quad \sigma_{zz} \quad \sigma_{xy} \quad \sigma_{yz} \quad \sigma_{zx})^T \quad (1.13a)$$

$$\mathbf{m} = (1 \quad 1 \quad 1 \quad 0 \quad 0 \quad 0)^T \quad (1.13b)$$

$\boldsymbol{\sigma}$ is the vector with total stresses, $\boldsymbol{\sigma}'$ contains the effective stresses, p_w and p_a are the pore water pressure and the pore air pressure, respectively, and \mathbf{m} is a vector containing unity terms for normal stress components and zero terms for the shear stress components. χ is an effective stress parameter called matric suction coefficient and varies from 0 to 1 covering the range from dry to fully saturated conditions. Considering these two special cases shows that for a fully saturated soil ($\chi = 1$), the classical effective stress equation for compressive pore pressure is obtained as:

$$\boldsymbol{\sigma} = \boldsymbol{\sigma}' + \mathbf{m}p_w \quad (1.14)$$

and for a fully dry soil ($\chi = 0$) the effective stress is

$$\boldsymbol{\sigma} = \boldsymbol{\sigma}' + \mathbf{m}p_a \quad (1.15)$$

This concept can be simplified for practical application assuming that the pore air pressure is constant and is small enough to be neglected (i.e. $p_a \approx 0$). Therefore for a completely dry soil, effective and total stresses are essentially equal. The matric suction coefficient χ is generally determined experimentally. This parameter depends on the degree of saturation, porosity and on the matric suction

$(p_a - p_w)$ (e.g. Bolzon et al., 1996; Bishop & Blight, 1963). The experimental evidences on the matric suction coefficient χ are quite sparse and therefore this parameter is often assumed to be equal to the effective saturation in PLAXIS. Now the effective stress formulation can be simplified to

$$\boldsymbol{\sigma} = \boldsymbol{\sigma}' + \mathbf{m}(S_e p_w) \quad (1.16)$$

in which S_e is the effective saturation which is a function of the suction pore pressure.

2 Governing equations

2.1 Darcy's law

The flow of water in a *saturated* soil is commonly described using Darcy's law (1856). He postulated that the rate of water flow through a soil mass is proportional to the hydraulic head gradient. The equations of equilibrium for groundwater flow are:

$$\nabla p_w + \rho_w \underline{g} + \underline{\varphi} = 0 \quad (2.1)$$

where $\underline{g} = (0, -g, 0)^T$ is the vector of gravitational acceleration and $\underline{\varphi}$ the vector of the friction force, per unit volume, between the flowing fluid and the soil skeleton. This force is linearly dependent on the fluid velocity and acts in opposite direction. The relations are:

$$\underline{\varphi} = -\underline{m}^{\text{int}} \underline{q} \quad (2.2)$$

where \underline{q} is the *specific discharge* (fluid velocity), and $\underline{m}^{\text{int}}$ is:

$$\underline{m}^{\text{int}} = \begin{vmatrix} \mu/\kappa_x & 0 & 0 \\ 0 & \mu/\kappa_y & 0 \\ 0 & 0 & \mu/\kappa_z \end{vmatrix} \quad (2.3)$$

with μ the *dynamic viscosity* of the fluid and κ_i the *intrinsic permeability* of the porous medium. From (2.1) and (2.2) results:

$$-\nabla p_w - \rho_w \underline{g} + \underline{m}^{\text{int}} \underline{q} = 0 \quad (2.4)$$

which can be also written as:

$$\underline{q} = \underline{k}^{\text{int}} (\nabla p_w + \rho_w \underline{g}) \quad (2.5)$$

where $\underline{k}^{\text{int}}$ is:

$$\underline{k}^{\text{int}} = \begin{vmatrix} \kappa_x/\mu & 0 & 0 \\ 0 & \kappa_y/\mu & 0 \\ 0 & 0 & \kappa_z/\mu \end{vmatrix} \quad (2.6)$$

In soil mechanics the *coefficient of permeability* k_i^{sat} (or *hydraulic conductivity*) is used instead of both intrinsic permeability and viscosity:

$$k_i^{sat} = \rho_w g \frac{K_i}{\mu} \quad i = x, y, z \quad (2.7)$$

In an unsaturated state the coefficient of permeability depends on the soil saturation. The relative permeability $k_{rel}(S)$ is defined as the ratio of the permeability at a given saturation to the permeability in saturated state. The coefficients of permeability defined in (2.7) represent the full saturation, for an unsaturated state the permeability is:

$$k_i = k_{rel} k_i^{sat} \quad i = x, y, z \quad (2.8)$$

The basic form of Darcy's law is:

$$\underline{q} = \frac{k_{rel}}{\rho_w g} \underline{k}^{sat} (\nabla p_w + \rho_w \underline{g}) \quad (2.9)$$

where \underline{k}^{sat} is the saturated permeability matrix.

$$\underline{k}^{sat} = \begin{vmatrix} k_x^{sat} & 0 & 0 \\ 0 & k_y^{sat} & 0 \\ 0 & 0 & k_z^{sat} \end{vmatrix} \quad (2.10)$$

2.2 Compressibility of water

The compression modulus of the air-water mixture is the inverse of the *compressibility*:

$$(K_w = 1/\beta) \quad (2.11)$$

where

$$\beta = \frac{dV_w/V_w}{dp} \quad (2.12)$$

where dV_w and V_w are volume of the water and volume variation due to the variation of the pressure.

For unsaturated groundwater flow the compressibility of water can be expressed as follows (Bishop & Eldin, 1950; Fredlund & Rahardjo, 1993).

$$\beta = S \beta_w + \frac{1 - S + h S}{K_{air}} \quad (2.13)$$

where S = degree of saturation; β_w = compressibility of pure water (4.58×10^{-7} kPa⁻¹); h = volumetric coefficient of air solubility (0.02); K_{air} = Bulk modulus of air (100 kPa at atmospheric pressure). The equation can be simplified by neglecting the air solubility (Verruijt 2001):

$$\beta = S \beta_w + \frac{1 - S}{K_{air}} \quad (2.14)$$

2.3 Continuity equation

The mass concentration of water (residual water) in each elemental volume of the medium is equal to $\rho_w n S$. The mass continuity equation of the water states that the water outflow from the volume is equal to the changes in the mass concentration. While the water outflow is the divergence of the mass flux density of the residual water ($\nabla^T \rho_w \underline{q}$). Therefore the continuity equation has the form (Song 1990):

$$\nabla^T \left[\rho_w \frac{k_{rel}}{\rho_w g} k^{sat} (\nabla p_w + \rho_w \underline{g}) \right] = - \frac{\partial}{\partial t} (\rho_w n S) \quad (2.15)$$

The right hand side of equation (2.15) can be written as:

$$- \frac{\partial}{\partial t} (\rho_w n S) = -n S \frac{\partial \rho_w}{\partial t} - \rho_w n \frac{\partial S}{\partial t} - \rho_w S \frac{\partial n}{\partial t} \quad (2.16)$$

These three terms represent the changes in water density, saturation and soil porosity, respectively.

According to the principle of mass conservation, for different corresponding values of pressure and volume, the mass is constant, i.e.:

$$m_w = \rho_w V_w = c \quad (2.17)$$

Thus:

$$dm_w = \rho_w dV_w + d\rho_w V_w = 0 \quad (2.18)$$

or

$$-\frac{dV_w}{V_w} = \frac{d\rho_w}{\rho_w} \quad (2.19)$$

Introducing the definition of water compressibility, we have

$$\frac{d\rho_w}{\rho_w} = -\beta dp \quad (2.20)$$

The time derivative of the equation is

$$\frac{1}{\rho_w} \frac{\partial \rho_w}{\partial t} = -\beta \frac{\partial p}{\partial t} = -\frac{1}{K_w} \frac{\partial p}{\partial t} \quad (2.21)$$

Now, the term containing the derivative of ρ_w with respect to time can be expressed as:

$$-n S \frac{\partial \rho_w}{\partial t} = -n S \frac{\partial \rho_w}{\partial p_w} \frac{\partial p_w}{\partial t} = \frac{n \rho_w}{K_w} S \frac{\partial p_w}{\partial t} \quad (2.22)$$

The second term of the right hand side of Eq. (2.16) has the form:

$$\rho_w n \frac{\partial S}{\partial t} = n \rho_w \frac{\partial S}{\partial p_w} \frac{\partial p_w}{\partial t} \quad (2.23)$$

The term representing the changes in porosity is composed of:

- The overall compression of the soil structure due to effective stresses and pore pressure:

$$-\frac{\partial \varepsilon_v}{\partial t} = -\underline{m}^T \frac{\partial \underline{\varepsilon}}{\partial t} \quad (2.24)$$

- The compression of the solid particles due to the changes of the pore pressure:

$$-\frac{(1-n)}{K_s} S \frac{\partial p_w}{\partial t} \quad (2.25)$$

where K_s is the bulk modulus of the solid particles forming the soil skeleton and

- The compression of the solid particles due to the changes in effective stresses:

$$\frac{1}{3K_s} \underline{m}^T \underline{M} \left(\frac{\partial \underline{\varepsilon}}{\partial t} - \frac{1}{3K_s} S \frac{\partial p_w}{\partial t} \underline{m} \right) \quad (2.26)$$

Substituting all the factors in Eq. (2.15) and neglecting the second order infinitesimal terms the continuity equation is obtained as:

$$\rho_w S \frac{\partial \varepsilon}{\partial t} - \rho_w S \left(\frac{n}{K_w} + \frac{(1-n)}{K_s} \right) \frac{\partial p_w}{\partial t} + n \rho_w \frac{\partial S}{\partial p_w} \frac{\partial p_w}{\partial t} + \nabla^T \left[\rho_w \frac{k_{rel}}{\rho_w g} k^{sat} (\nabla p_w + \rho_w \underline{g}) \right] = 0 \quad (2.27)$$

Equation (2.27) can be reformulated for the flow problem by neglecting the deformations of the solid particles and the density gradients of water (Boussinesq's approximation):

$$S \frac{\partial \varepsilon}{\partial t} - n \left(\frac{S}{K_w} - \frac{\partial S}{\partial p_w} \right) \frac{\partial p_w}{\partial t} + \nabla^T \left[\frac{k_{rel}}{\rho_w g} k^{sat} (\nabla p_w + \rho_w \underline{g}) \right] = 0 \quad (2.28)$$

2.4 Steady state and transient groundwater flow

Steady state is defined as an analysis, in which the hydraulic head and the coefficient of permeability at any point in the soil mass remain constant with respect to time which can be consider as a situation of groundwater flow when time tends to infinity. In contrast, in transient analyses, the hydraulic head (and possibly the coefficient of permeability) change with respect to time. Changes are usually in respect to a change in the boundary conditions with respect to time.

Equation (2.28) can be simplified for transient analysis by neglecting the displacements of solid particles, i.e.:

$$-n \left(\frac{S}{K_w} - \frac{\partial S}{\partial p_w} \right) \frac{\partial p_w}{\partial t} + \nabla^T \left[\frac{k_{rel}}{\rho_w g} k^{sat} (\nabla p_w + \rho_w \underline{g}) \right] = 0 \quad (2.29)$$

The above equation is a form of the well-known Richards equation which describes saturated-unsaturated groundwater flow. The Richards equation has the following form (e.g. Dogan & Motz (2005)):

$$\left\{ \frac{\partial}{\partial x} \left[K_x(h) \frac{\partial h}{\partial x} \right] + \frac{\partial}{\partial y} \left[K_y(h) \frac{\partial h}{\partial y} \right] + \frac{\partial}{\partial z} \left[K_z(h) \left(\frac{\partial h}{\partial z} + 1 \right) \right] \right\} = [C(h) + S \cdot S_s] \frac{\partial h}{\partial t} \quad (2.30)$$

where K_x , K_y and K_z are permeability coefficients in x , y and z directions, respectively. $C(h) = (\partial \theta / \partial h)$ is the specific moisture capacity (L^{-1}) and S_s is the

specific storage (L^{-1}). The specific storage S_s is a material property which can be expressed as:

$$S_s = \rho_w g \left(\frac{1-n}{K_s} + \frac{n}{K_w} \right) \quad (2.31)$$

The compressibility of soil particles can be neglected, therefore:

$$S_s = \frac{n \rho_w g}{K_w} \quad (2.32)$$

The term $C(h)$ in the Richards equation can be expanded as:

$$C(h) = \frac{\partial \theta}{\partial h} = \frac{\partial}{\partial h} (nS) = n \frac{\partial S}{\partial h} \quad (2.33)$$

By substituting equations (2.32) and (2.33) in the Richards equation (Eq. 2.30) and changing from head based equation to pore water pressure based equation, equation (2.29) is obtained.

For steady state groundwater flow, in which variation of pore water pressure with respect to time is zero, the continuity condition applies:

$$\nabla^T \left[\frac{k_{rel}}{\rho_w g} k^{sat} (\nabla p_w + \rho_w \underline{g}) \right] = 0 \quad (2.34)$$

This equation expresses that there is no net inflow or outflow in an elementary area, as illustrated in Figure (2.1).

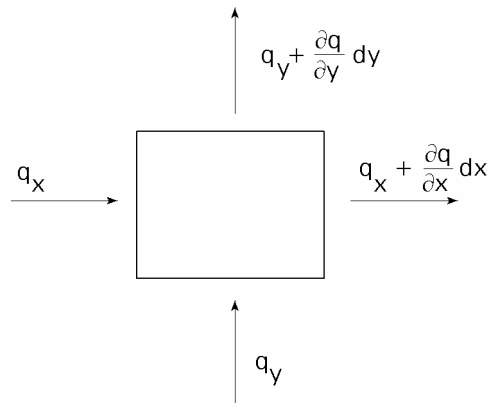


Fig. 2.1: Illustration of the continuity condition

2.5 Deformation equations

For a representative elemental volume of the soil the linear momentum balance is given by:

$$\underline{\underline{L}}^T (\underline{\underline{\sigma}}' + S_e p_w \underline{\underline{m}}) + \rho \underline{\underline{g}} = \underline{\underline{0}} \quad (2.35)$$

where

$$\rho = (1-n) \rho_s + n S \rho_w \quad (2.36)$$

is the density of the multiphase medium, $\underline{\underline{g}}$ is a vector containing the gravity acceleration $\underline{\underline{g}}^T = (0, -g, 0)^T$ in the 3D space and $\underline{\underline{L}}^T$ is the transpose of the differential operator $\underline{\underline{L}}$ (Eq. 1.7).

Assuming infinitesimal strain theory, the relationship between strain and displacements can be formulated as:

$$d\underline{\underline{\varepsilon}} = \underline{\underline{L}} d\underline{\underline{u}} \quad (2.37)$$

Rewriting the effective stress equation (1.12) in incremental form as:

$$d\underline{\underline{\sigma}} = d\underline{\underline{\sigma}}' + S_e dp_w \underline{\underline{m}} \quad (2.38)$$

The constitutive relation using effective stresses is written as:

$$d\underline{\underline{\sigma}}' = \underline{\underline{M}} d\underline{\underline{\varepsilon}} \quad (2.39)$$

$\underline{\underline{M}}$ represents the material stress-strain matrix. The governing equation for the deformation model is obtained:

$$\underline{\underline{L}}^T [\underline{\underline{M}} (\underline{\underline{L}} d\underline{\underline{u}}) + S_e dp_w \underline{\underline{m}}] + d(\rho \underline{\underline{g}}) = \underline{\underline{0}} \quad (2.40)$$

3 Finite element formulation

3.1 Deformation problem

In finite element method the displacement field in an element \underline{u} results from the nodal values of the displacements \underline{v} using interpolation (shape) functions assembled in a matrix \underline{N} :

$$\underline{u} = \underline{N} \underline{v} \quad (3.1)$$

Substitution of (3.1) in (2.33) gives:

$$\underline{\varepsilon} = \underline{L} \underline{N} \underline{v} = \underline{B} \underline{v} \quad (3.2)$$

where \underline{B} is a matrix containing the spatial derivatives of the shape functions. The virtual work equation is:

$$\int_V \delta \underline{\varepsilon}^T \underline{\sigma} dV = \int_V \delta \underline{u}^T \underline{b} dV + \int_\Gamma \delta \underline{u}^T \underline{t} d\Gamma \quad (3.3)$$

where \underline{b} is the body force vector in the volume V and \underline{t} is the traction on the boundary Γ . The stresses can be computed incrementally:

$$\underline{\sigma}^i = \underline{\sigma}^{i-1} + \Delta \underline{\sigma} = \underline{\sigma}^{i-1} + \int_{t^{i-1}}^{t^i} \dot{\underline{\sigma}} dt \quad (3.4)$$

If Eq. (3.3) is considered for the actual state i , the unknown $\underline{\sigma}^i$ can be eliminated using Eq. (3.4), therefore:

$$\int_V \delta \underline{\varepsilon}^T \Delta \underline{\sigma} dV = \int_V \delta \underline{u}^T \underline{b}^i dV + \int_\Gamma \delta \underline{u}^T \underline{t}^i d\Gamma - \int_V \delta \underline{\varepsilon}^T \underline{\sigma}^{i-1} dV \quad (3.5)$$

Equation (3.5) can be reformulated in discretised form as:

$$\int_V \underline{B}^T \Delta \underline{\sigma} dV = \int_V \underline{N}^T \underline{b}^i dV + \int_\Gamma \underline{N}^T \underline{t}^i d\Gamma - \int_V \underline{B}^T \underline{\sigma}^{i-1} dV \quad (3.6)$$

By writing the body forces and the boundary tractions in incremental form the following equation is obtained:

$$\int_V \underline{B}^T \Delta \underline{\sigma} dV = \int_V \underline{N}^T \Delta \underline{b} dV + \int_\Gamma \underline{N}^T \Delta \underline{t} d\Gamma + \underline{r}_v^{i-1} \quad (3.7)$$

with the residual force vector \underline{r}^{i-1} :

$$\underline{r}^{i-1} = \int_V \underline{N}^T \underline{b}^{i-1} dV + \int_\Gamma \underline{N}^T \underline{t}^{i-1} d\Gamma - \int_V \underline{B}^T \underline{\sigma}^{i-1} dV \quad (3.8)$$

The residual force vector should be equal zero if the solution of step i is accurate. Plaxis uses in the consolidation analyses the same shape functions for displacements¹ and for pore pressures, i.e.:

$$\underline{p}_w = \underline{N} \underline{p}_n \quad (3.9)$$

The principle of effective stresses Eq. (1.12) can be written in the following form:

$$\underline{\sigma}^{i-1} = \underline{\sigma}'^{i-1} + S_e^{i-1} p_w^{i-1} \underline{m} \quad (3.10)$$

$$\Delta \underline{\sigma} = \Delta \underline{\sigma}' + S_e^{i-1} \Delta p_w \underline{m} \quad (3.11)$$

By substituting Eq. (3.11) in Eq. (3.7) one obtains:

$$\int_V \underline{B}^T (\Delta \underline{\sigma}' + S_e^i \Delta p_w \underline{m}) dV = \int_V \underline{N}^T \Delta \underline{b} dV + \int_\Gamma \underline{N}^T \Delta \underline{t} d\Gamma + \underline{r}_v^{i-1} \quad (3.12)$$

Substitution of the stress-strain relationship (Eq. 2.35) in Eq. (3.12), we have:

$$\int_V \underline{B}^T \underline{M} \underline{B} \Delta \underline{v} dV + \int_V S_e^i \underline{B}^T \underline{m} \Delta p_w dV = \int_V \underline{N}^T \Delta \underline{b} dV + \int_\Gamma \underline{N}^T \Delta \underline{t} d\Gamma + \underline{r}_v^i \quad (3.13)$$

or in matrix form:

$$\underline{K} \Delta \underline{v} + \underline{Q} \Delta p_w = \Delta \underline{f}_u + \underline{r}_v^i \quad (3.14)$$

where \underline{K} , \underline{Q} and $\Delta \underline{f}_u$ are the stiffness matrix, the coupling matrix and the increment of the load vector, respectively.

$$\underline{K} = \int_V \underline{B}^T \underline{M} \underline{B} dV \quad (3.15)$$

¹ For generality, different sets of shape functions may be used to describe the variation of the displacements and the pore pressure rates. This implies that the nodes in the finite element mesh may have varying degrees of freedom, with some being associated with displacements, some being associated with pore pressure, and some being associated with both. In order for the pore pressure rates to be consistent with the stress rates, one can choose the polynomial describing the pore pressure rates to be one order lower than the polynomial describing the displacements. This approach leads to less accurate estimates of the displacements but smaller oscillations in the pore pressures (see Abbo, 1997)

$$\underline{\underline{Q}} = \int_V S_e \underline{\underline{B}}^T \underline{\underline{m}} \underline{\underline{N}} dV \quad (3.16)$$

$$\Delta \underline{\underline{f}}_u = \int_V \underline{\underline{N}}^T \Delta \underline{\underline{b}} dV + \int_{\Gamma} \underline{\underline{N}}^T \Delta \underline{\underline{t}} dS \quad (3.17)$$

The actual changes of the degree of saturation are included in the increments of the body forces (Eq. 3.17).

3.2 Flow problem

Galerkin approach with the same shape functions for pore pressure and for displacements is applied to Eq. (2.27). By using the Green's theorem the differential order of the equation is reduced and the discretised mass conservation equation results in the form of:

$$\begin{aligned} & \int_V \underline{\underline{N}}^T S \underline{\underline{m}}^T \underline{\underline{L}} \underline{\underline{N}} \frac{dv}{dt} dV - \int_V \underline{\underline{N}}^T n \left(\frac{S}{K_w} - \frac{\partial S}{\partial p_w} \right) \underline{\underline{N}} \frac{dp_w}{dt} dV - \int_V (\nabla \underline{\underline{N}})^T \frac{k_{rel}}{\gamma_w} k^{sat} \nabla \underline{\underline{N}} p_w dV \\ & - \int_V (\nabla \underline{\underline{N}})^T \frac{k_{rel}}{\gamma_w} k^{sat} \rho_w \underline{\underline{g}} dV - \int_{\Gamma} \underline{\underline{N}} \hat{q} dS = 0 \end{aligned} \quad (3.18)$$

and in matrix form:

$$-\underline{\underline{H}} \underline{\underline{p}}_w - \underline{\underline{S}} \frac{d \underline{\underline{p}}_w}{dt} + \underline{\underline{C}} \frac{dv}{dt} = \underline{\underline{G}} + \underline{\underline{q}}_p \quad (3.19)$$

where $\underline{\underline{H}}$, $\underline{\underline{Q}}$, $\underline{\underline{C}}$ and $\underline{\underline{S}}$ are the permeability matrix, the coupling matrix and the compressibility matrix. $\underline{\underline{q}}_p$ is the flux on boundaries. $\underline{\underline{G}}$ is a vector in which effect of gravity on flow in vertical direction is considered. This vector is a part of external flux.

$$\underline{\underline{H}} = \int_V (\nabla \underline{\underline{N}})^T \frac{k_{rel}}{\gamma_w} k^{sat} (\nabla \underline{\underline{N}}) dV \quad (3.20)$$

$$\underline{\underline{S}} = \int_V \underline{\underline{N}}^T \left(\frac{n S}{K_w} - n \frac{dS}{dp_w} \right) \underline{\underline{N}} dV \quad (3.21)$$

$$\underline{\underline{C}} = \int_V \underline{\underline{N}} S \underline{\underline{L}} \underline{\underline{N}} dV \quad (3.22)$$

$$\underline{\underline{G}} = \int_V (\nabla \underline{\underline{N}})^T \frac{k_{rel}}{\gamma_w} k^{sat} \rho_w \underline{\underline{g}} dV \quad (3.23)$$

$$\underline{q}_p = \int_{\Gamma} \underline{N}^T \hat{q}_w dS \quad (3.24)$$

For transient calculation displacements of particles can be neglected. Therefore the coupling matrix is zero. Now Eq. (3.19) can be simplified to the following form:

$$-\underline{H} \underline{p}_w - \underline{S} \frac{d \underline{p}_w}{dt} = \underline{G} + \underline{q}_p \quad (3.25)$$

For steady state calculation, time derivative of pore pressure is zero, therefore:

$$-\underline{H} \underline{p}_w = \underline{G} + \underline{q}_p \quad (3.26)$$

3.3 Coupled problem

The formulation of Biot's equation presented above contains a coupled behaviour which is represented by both the equilibrium equation and the continuity equation of the water-soil mixture. The displacements of the solid skeleton and the pore water pressure are chosen as basic variables of the problem. The spatial discretisation yields the following system of equations, which is non symmetric:

$$\begin{bmatrix} \underline{K} & \underline{Q} \\ 0 & -\underline{H} \end{bmatrix} \begin{bmatrix} \underline{v} \\ \underline{p}_w \end{bmatrix} + \begin{bmatrix} 0 & 0 \\ \underline{C} & -\underline{S} \end{bmatrix} \begin{bmatrix} \frac{d \underline{v}}{dt} \\ \frac{d \underline{p}_w}{dt} \end{bmatrix} = \begin{bmatrix} \underline{f}_u \\ \underline{G} + \underline{q}_p \end{bmatrix} \quad (3.27)$$

The symmetry of the system (Eq. 3.27) can be restored by the time differentiation of the first equation:

$$\begin{bmatrix} \underline{K} & \underline{Q} \\ \underline{C} & -\underline{S} \end{bmatrix} \begin{bmatrix} \frac{d \underline{v}}{dt} \\ \frac{d \underline{p}_w}{dt} \end{bmatrix} = \begin{bmatrix} 0 & 0 \\ 0 & \underline{H} \end{bmatrix} \begin{bmatrix} \underline{v} \\ \underline{p}_w \end{bmatrix} + \begin{bmatrix} \frac{d \underline{f}_u}{dt} \\ \underline{G} + \underline{q}_p \end{bmatrix} \quad (3.28)$$

3.4 Solving procedure

Equation (3.28) can be integrated in time, using a first order finite difference method. The equations are written in a more concise form:

$$\underline{\underline{B}} \frac{d\underline{X}}{dt} + \underline{\underline{C}} \underline{X} = \underline{F} \quad (3.29)$$

where $\underline{X}^T = [\underline{v} \quad \underline{p}_w]$. The matrices $\underline{\underline{B}}$, $\underline{\underline{C}}$ and \underline{F} are dependent on \underline{X} . The discretisation is carried out by the generalised midpoint rule which approximates

$$\left(\frac{d\underline{X}}{dt} \right)^{i+\alpha} = \frac{\Delta \underline{X}}{\Delta t} = \frac{\underline{X}^{i+1} - \underline{X}^i}{\Delta t} \quad \underline{X}^{i+\alpha} = (1-\alpha) \underline{X}^i + \alpha \underline{X}^{i+1} \quad (3.30)$$

Eq. (3.29) at time $t^{i+\alpha}$ becomes:

$$[\underline{\underline{B}} + \alpha \Delta t \underline{\underline{C}}]^{i+\alpha} \underline{X}^{i+1} = [\underline{\underline{B}} - (1-\alpha) \Delta t \underline{\underline{C}}]^{i+\alpha} \underline{X}^i + \Delta t \underline{F}^{i+\alpha} \quad (3.31)$$

where Δt is the time step and α is a parameter $0 \leq \alpha \leq 1$. In Plaxis a full implicit procedure is utilised with $\alpha = 1$. Application of this procedure to Eq. (3.28) yields:

$$\begin{bmatrix} \underline{\underline{K}} & \underline{\underline{Q}} \\ \underline{\underline{C}} & -\underline{\underline{S}}^* \end{bmatrix}^{i+\alpha} \begin{bmatrix} \Delta \underline{v} \\ \Delta \underline{p}_w \end{bmatrix} = \begin{bmatrix} 0 & 0 \\ 0 & \Delta t \underline{\underline{H}} \end{bmatrix}^{i+\alpha} \begin{bmatrix} \underline{v}^i \\ \underline{p}_w^i \end{bmatrix} + \begin{bmatrix} \Delta f_u \\ \Delta t \underline{G} + \Delta t (\underline{q}_p^i + \alpha \Delta \underline{q}_p) \end{bmatrix} \quad (3.32)$$

with

$$\underline{\underline{S}}^* = (\underline{\underline{S}} + \alpha \Delta t \underline{\underline{H}}) \quad (3.33)$$

$$\underline{\underline{H}} = \int_V (\nabla \underline{N})^T \frac{k_{rel}}{\gamma_w} k^{sat} (\nabla \underline{N}) dV \quad (3.34)$$

$$\underline{\underline{S}} = \int_V \underline{N}^T \left(\frac{nS}{K_w} - n \frac{dS}{dp_w} \right) \underline{N} dV \quad (3.35)$$

$$\underline{\underline{G}} = \int_V (\nabla \underline{N})^T \frac{k_{rel}}{\gamma_w} k^{sat} \rho_w \underline{g} dV \quad (3.36)$$

$$\underline{\underline{q}}_p = \int_{\Gamma} \underline{N}^T \hat{q}_w dS \quad (3.37)$$

$$\underline{\underline{K}} = \int_V \underline{\underline{B}}^T \underline{\underline{M}} \underline{\underline{B}} dV \quad (3.38)$$

$$\underline{\underline{Q}} = \int_V \underline{S} \underline{\underline{B}}^T \underline{m} \underline{N} dV \quad (3.39)$$

$$\underline{\underline{C}} = \int_V \underline{\underline{N}} \underline{\underline{S}} \underline{\underline{L}} \underline{\underline{N}} dV \quad (3.40)$$

$$\Delta \underline{\underline{f}}_u = \int_V \underline{\underline{N}}^T \Delta \underline{\underline{b}} dV + \int_\Gamma \underline{\underline{N}}^T \Delta \underline{\underline{t}} dS \quad (3.41)$$

In the case of consolidation of unsaturated soils all matrices and the external flux (right hand vector) are nonlinear. In this respect the following issues should be taken into account:

- The stiffness matrix $\underline{\underline{K}}$ is usually stress-dependent.
- The permeability in the permeability matrix $\underline{\underline{H}}$ and in the vector $\underline{\underline{G}}$ is pressure dependent, due to suction dependency of relative permeability k_{rel} .
- The coupling matrices $\underline{\underline{Q}}$ and $\underline{\underline{C}}$ as well as the compressibility matrix $\underline{\underline{S}}$ are suction dependent. The latter is also depends on the derivative of saturation
- In addition, the boundary conditions for the seepage line and drains are also nonlinear.
- The right hand side of both equilibrium and mass conservation equations are nonlinear terms for unsaturated soils. The nonlinearity of the first equation is due to the weight of the soil which is a function of the degree of saturation and the nonlinearity of the right side of the second equation is due to the suction dependency of the relative permeability and the variable Neumann boundary conditions.

For both equations the Cauchy BC are imposed directly in the equation system.

4 Boundary conditions

The following boundary conditions are available in PLAXIS:

4.1 Closed

This type of boundary conditions specifies a zero Darcy flux over the boundary as

$$\underline{q} \cdot \underline{n} = q_x n_x + q_y n_y + q_z n_z = 0 \quad (4.1)$$

where n_x , n_y and n_z are the outward pointing normal vector components on the boundary.

4.2 Inflow

A non-zero Darcy flux over a boundary is set by a prescribed recharge value $|\bar{q}|$ and reads

$$\underline{q} \cdot \underline{n} = q_x n_x + q_y n_y + q_z n_z = -|\bar{q}| \quad (4.2)$$

This indicates that the Darcy flux vector and the normal vector on the boundary are pointing in opposite directions.

4.3 Outflow

For outflow boundary conditions the direction of the prescribed Darcy flux, $|\bar{q}|$, should equal the direction of the normal on the boundary, i.e.:

$$\underline{q} \cdot \underline{n} = q_x n_x + q_y n_y + q_z n_z = |\bar{q}| \quad (4.3)$$

4.4 Head

For prescribed head boundaries the value of the head $\bar{\phi}$ is imposed as

$$\phi = \bar{\phi} \quad (4.4)$$

Alternatively prescribed pressure conditions can be given. Overtopping conditions for example can be formulated as prescribed pressure boundaries.

$$p = 0 \quad (4.5)$$

These conditions directly relate to a prescribed head boundary condition and are implemented as such.

4.5 Infiltration/evaporation

This type of boundary conditions poses a more complex mixed boundary condition. An inflow value \bar{q} may depend on time and as in nature the amount of inflow is limited by the capacity of the soil. If the precipitation rate exceeds this capacity, ponding takes place at a depth $\bar{\phi}_{\max}$ and the boundary condition switches from inflow to prescribed head. As soon as the soil capacity meets the infiltration rate the condition switches back.

This boundary condition simulates evaporation for negative values of \bar{q} . The outflow boundary condition takes place, when the groundwater head is higher than the minimum head specified by the user $\bar{\phi}_{\min}$.

These boundary conditions are expressed as

$$\left\{ \begin{array}{ll} \phi = y + \bar{\phi}_{\max} & \text{if } \text{ponding} \\ \underline{q} \cdot \underline{n} = q_x n_x + q_y n_y + q_z n_z = -\bar{q} & \text{if } y + \bar{\phi}_{\min} < y + \phi < y + \bar{\phi}_{\max} \\ \phi = y + \bar{\phi}_{\min} & \text{if } \text{drying} \end{array} \right. \quad (4.6)$$

4.6 Seepage

Flow problems with a free water level may involve a seepage surface on the downstream boundary, as shown in Figure 4.1. A seepage surface will always occur when the water level touches an open downstream boundary. The seepage surface is not a streamline (in contrast to the water level) or an equi-potential line. It is a line on which the groundwater head, h , equals the elevation head y (= vertical position). This condition arises from the fact that the water pressure is zero on the seepage surface, which is the same condition as that exists at the water level.

It is not necessary to know the exact length of the seepage surface before the calculation begins, since the same boundary conditions ($h = y$) may be used along the whole boundary line where seepage is expected to occur. Free boundaries with $h = y$ may therefore be specified for all boundaries where the hydraulic head is unknown. Alternatively, for boundaries well above the water level where it is obvious that a seepage surface does not occur, it may also be appropriate to prescribe those boundaries as closed flow boundaries.

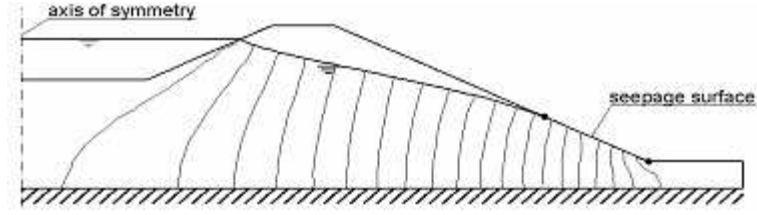


Fig. 4.1: Seepage surface

The water line option generates phreatic/seepage conditions by default. An external head $\bar{\phi}$ is prescribed on the part of the boundary beneath the water line, seepage or free conditions are applied to the rest of the line. The phreatic/seepage condition reads

$$\left\{ \begin{array}{ll} \phi = \bar{\phi} & \text{if below phreatic level} \\ \phi = z & \text{if above phreatic level and outflow} \\ q \cdot n = q_x n_x + q_y n_y + q_z n_z = 0 & \text{if above phreatic level and suction} \end{array} \right. \quad (4.7)$$

The seepage condition only allows for outflow of groundwater at atmospheric pressure. For unsaturated conditions at the boundary the boundary is closed. The external head $\bar{\phi}$ may vary in a time dependent way.

4.7 Infiltration well

Inside the domain wells are modelled as source terms, $|\bar{Q}|$ where specifies the inflowing flux per meter.

$$Q = |\bar{Q}| \quad (4.8)$$

As the source term in the governing equation simulates water flowing in the system, the source term is positive for a recharge well.

4.8 Extraction well

A discharge rate $|\bar{Q}|$ simulates an amount of water leaving the domain

$$Q = -|\bar{Q}| \quad (4.9)$$

The source term in the governing equation is negative for a discharge well.

4.9 Drain

Drains are handled as seepage boundaries. However, drains are located inside the domain. In reality drains cannot work perfectly and do not permit water leaving

the domain at atmospheric pressure, therefore a prescribed head $\bar{\phi}$ should be considered for the part of the drain below the water level. The condition is written as

$$\begin{cases} \phi = \bar{\phi} & \text{if } outflow \\ \underline{q} \cdot \underline{n} = q_x n_x + q_y n_y + q_z n_z = 0 & \text{if } suction \end{cases} \quad (4.10)$$

The drain itself does not generate a resistance against flow.

4.10 Interfaces

Interface elements are used to simulate impermeable structural elements. In such an element there is no connection between both sides of the element and therefore a zero Darcy flux over internal boundary is obtained.

Initial conditions are generated as a steady state solution for a problem with a given set of boundary conditions.

4.11 Time dependent conditions

PLAXIS provides several features for analysis of transient groundwater flow and fully coupled flow-deformation problems with varying conditions in time (time-dependent conditions). Time-dependent conditions can only be applied in a transient or in a fully coupled flow-deformation analysis.

Seasonal or irregular variations in water levels can be modelled using linear, harmonic or user-defined time distributions. Four different functions can be assigned for this purpose, namely constant, linear, harmonic and user-defined functions.

Linear (function 1): This option can be used to describe the increase or decrease of a condition linearly in time. For a linear variation of groundwater head, the inputs of the following parameters are required:

Δt : This parameter represents the time interval for the calculation phase, expressed in unit of time. Its value is equal to the Time interval parameter as specified in the Parameters tab sheet of the Phase list window. The value is fixed and cannot be changed in the Time-dependent head window.

H_0 : This parameter represents the actual height of the water level, expressed in unit of length. Its value is automatically calculated in the kernel based on the initial pore pressures.

H_{ult} : This parameter, specified in unit of length, represents the ultimate value

of head for the current calculation phase. Hence, together with the time interval this parameter determines the rate of the water level increase or decrease.

For a linear variation of infiltration, inflow or outflow the inputs of the following parameters are required:

Q_0 : This parameter is the initial specific discharge through the geometry line under consideration, expressed in unit of length per unit of time.

Q_{ult} : This parameter, specified in unit of length per unit of time, represents the ultimate specific discharge in the time interval of the current calculation phase.

Harmonic (function 2): This option can be used when a condition varies harmonically in time. The harmonic variation of the water level is described as:

$$y(t) = y_0 + 0.5H \sin(\omega_0 t + \varphi_0) \quad (4.11)$$

with

$$\omega_0 = 2\pi/T$$

in which H , T and φ_0 are the wave height in the unit of length, the wave period in the unit of time and the initial phase angle, respectively.

In case of infiltration, inflow or outflow, the parameter Q_A needs to be entered instead of H . Q_A represents the amplitude of the specific discharge and is specified in unit of length per unit of time.

Table (function 3): In addition to the pre-defined functions for variations with time, PLAXIS provides the possibility to enter user-defined time series. This option can be useful for a back-analysis when measurements are available. In the table, time always starts from zero which is related to the beginning of the calculation phase.

5 Hydraulic models

5.1 Van Genuchten model

There are many material models which describe the hydraulic behaviour of unsaturated soils. The most common in the groundwater literature is the model of Van Genuchten (1980) relationship, which is used in PlaxFlow. This relationship is a more general case of Mualem (1976) function. Van Genuchten function is a three-parameter equation and relates the *saturation* to the suction pore pressure head ϕ_p :

$$S(\phi_p) = S_{residu} + (S_{sat} - S_{residu}) \left[1 + (g_a |\phi_p|)^{g_n} \right]^{g_c} \quad (5.1)$$

where

$$\phi_p = -P_w / \rho_w g$$

S_{residu} is the residual saturation which describes the part of water that remains in soil even at high suction heads. S_{sat} is the saturation when the pores are filled with water. In general, the pores at saturated conditions the pores cannot be completely filled with water and some air bubbles can be present in water therefore in this case S_{sat} will be less than 1. g_a , g_n and g_c are empirical parameters. If the following assumption is made, as used in Plaxis, Eq. (5.1) converts to Mualem (1976) function which is a two-parameter equation.

$$g_c = \frac{1 - g_n}{g_n} \quad (5.2)$$

Figure 5.1 shows the effect of the parameter g_a on the shape of retention curve. This parameter is related to the air entry value (AEV) of the soil.

The effect of the parameter g_n , which is a function of the rate of water extraction from the soil once the AEV has been exceeded, is plotted in Figure 5.2.

The parameter g_c is a function of the residual water content (related to the curvature in the high suction range), Figure 5.3.

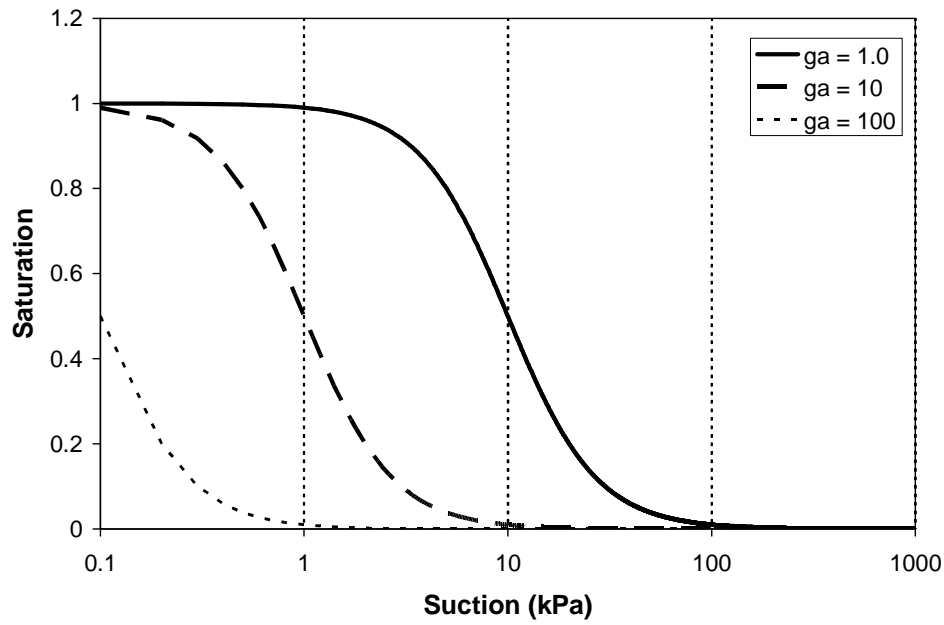


Fig. 5.1: Effect of the parameter g_a on the retention curve, ($g_n = 2.0$ and $g_c = -1.0$)

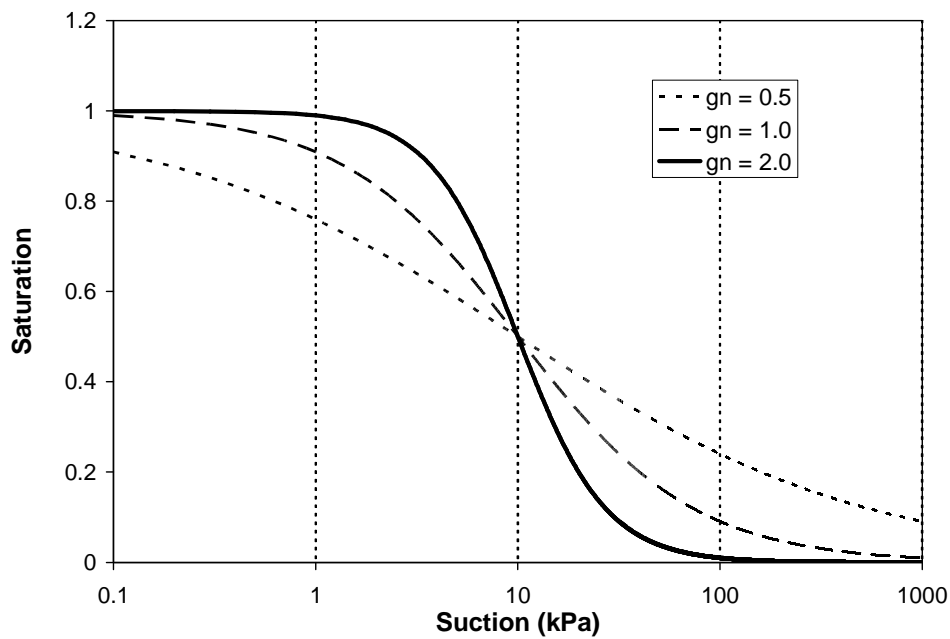


Fig. 5.2: Effect of the parameter g_n on the retention curve, ($g_a = 1.0$ and $g_c = -1.0$)

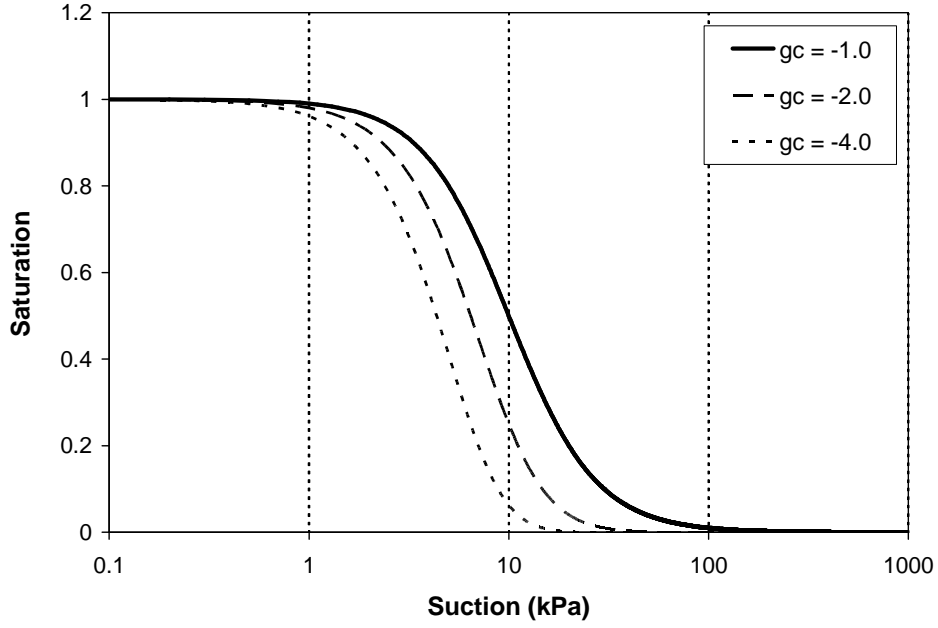


Fig. 5.3: Effect of the parameter g_c on the retention curve, ($g_a = 1.0$ and $g_n = 2.0$)

The effective saturation is defined as:

$$S_e = \frac{S - S_{residu}}{S_{sat} - S_{residu}} \quad (5.3)$$

The *relative permeability* according to Mualem - Van Genuchten is:

$$k_{rel}(S) = (S_e)^{g_l} \left[1 - \left(1 - S_e^{\frac{g_n}{g_n-1}} \right)^{\frac{g_n-1}{g_n}} \right]^2 \quad (5.4)$$

g_l is an empirical parameter. g_a , g_l and g_n have to be measured. In Plaxis 2D the parameters can be directly specified or can be chosen using a database of soil properties.

The derivative of saturation in respect to pore pressure reads:

$$\frac{\partial S(p_w)}{\partial p_w} = \begin{cases} 0 & \text{if } (p_w \leq 0) \\ (S_{sat} - S_{residu}) \left(\frac{1-g_n}{g_n} \right) \left[g_n \left(\frac{g_a}{\gamma_w} \right)^{g_n} \cdot p_w^{g_n-1} \right] \left[1 + \left(g_a \cdot \frac{p_w}{\gamma_w} \right)^{g_n} \right]^{\left(\frac{1-2g_n}{g_n} \right)} & \text{if } (p_w > 0) \end{cases} \quad (5.5)$$

Figure 5.1 and Figure 5.2 present the Mualem - Van Genuchten relations for a sandy material with parameters $S_{sat} = 1.0$, $S_{res} = 0.027$, $g_a = 2.24 \text{ m}^{-1}$, $g_l = 0.0$ and $g_n = 2.286$ graphically.

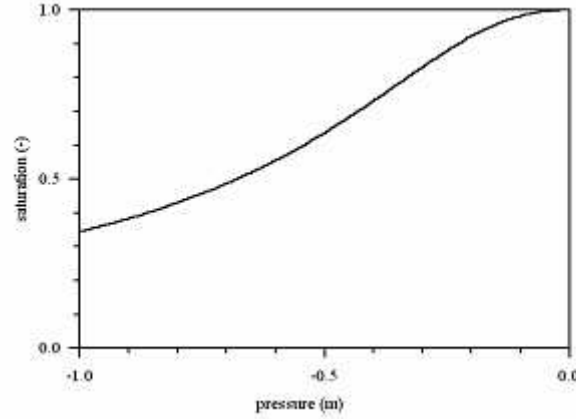


Fig. 5.4: Mualem – Van Genuchten: head – degree of saturation

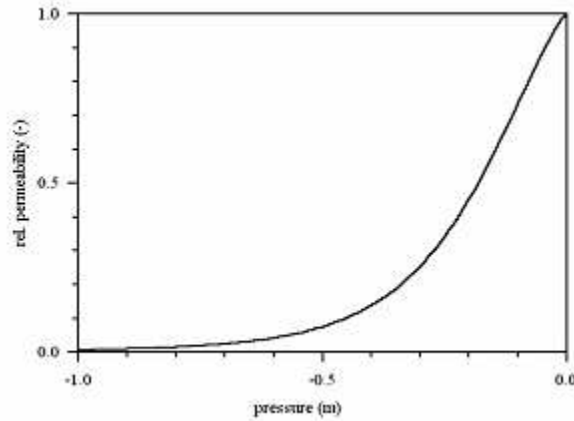


Fig. 5.5: Mualem – Van Genuchten: head – relative permeability

5.2 Linearized Van Genuchten model

A linearised form of the Van Genuchten's model is also used as alternative in Plaxis 2D. The *saturation* is defined as:

$$S(\phi_p) = \begin{cases} 1 & \text{if } \phi_p \geq 0 \quad (p_w \leq 0) \\ 1 + \frac{\phi_p}{|\phi_{ps}|} \left(1 - \frac{p_w}{|p_{ws}|} \right) & \text{if } \phi_{ps} < \phi_p < 0 \quad (p_{ws} > p_w > 0) \\ 0 & \text{if } \phi_p < \phi_{ps} \quad (p_w > p_{ws}) \end{cases} \quad (5.6)$$

and its derivative in respect to pore pressure is:

$$\frac{\partial S(p_w)}{\partial p_w} = \begin{cases} 0 & \text{if } \phi_p \geq 0 & (p_w \leq 0) \\ -\frac{1}{|p_{ws}|} & \text{if } \phi_{ps} < \phi_p < 0 & (p_{ws} > p_w > 0) \\ 0 & \text{if } \phi_p < \phi_{ps} & (p_w > p_{ws}) \end{cases} \quad (5.7)$$

The variable ϕ_{ps} represents the threshold of the unsaturated condition and can be derived from Van Genuchten model:

$$\phi_{ps} = \frac{1}{S_{\phi_p = -1,0m} - S_{sat}} \quad (5.8)$$

The *relative permeability* is approximate as:

$$k_{rel}(\phi_p) = \begin{cases} 1 & \text{if } \phi_p \geq 0 & (p_w \leq 0) \\ 10^{\frac{4\phi_p}{\phi_{pk}}} & \text{if } \phi_{pk} < \phi_p < 0 & (p_{wk} > p_w > 0) \\ 10^{-4} & \text{if } \phi_p < \phi_{pk} & (p_w > p_{wk}) \end{cases} \quad (5.9)$$

where ϕ_{pk} is the pressure head at which the relative permeability is reduced to 10^{-4} , but is limited to a value between 0.5 and 0.7 m.

Figure 5.3 and Figure 5.4 present the linearized Van Genuchten relations for a sandy material with parameters $\phi_{ps} = 1.48$ m, $\phi_{pk} = 1.15$ m graphically.

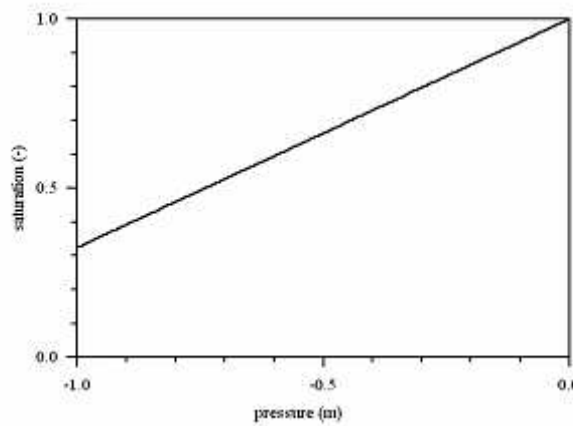


Fig. 5.6: Linearized Van Genuchten: head – degree of saturation

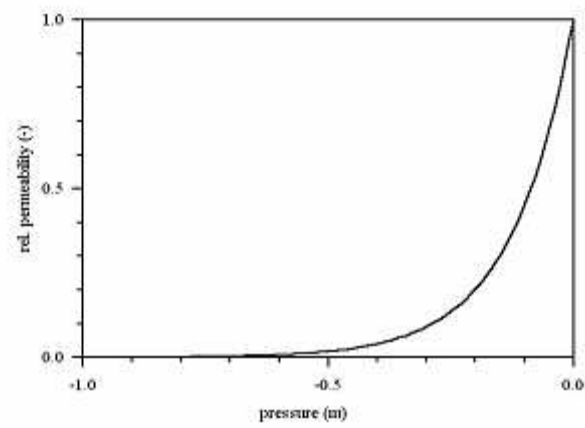


Fig. 5.7: Linearized Van Genuchten: head – relative permeability

6 Barcelona Basic Model

6.1 Introduction

The unsaturated soil model implemented to account for effects of suction follows the well-known Barcelona Basic Model (Alonso et al., 1990) which is an extension of the Modified Cam Clay model (Roscoe & Burland, 1968) by introducing suction to its formulation. Bishop stress and suction are used as state variables in this model. The model switches from fully saturated constitutive model to partially saturated soil model, as suction increases.

The main features of the model are:

- To follow the Barcelona Basic Model (BBM) characteristics to account the behaviour of unsaturated soils (Alonso et al., 1990)
- To work with Bishop stress (Sheng, et al., 2003, Gallipoli et al., 2003) and suction as the state variables a difference of the BBM which use the net stress and suction
- To consider an independent elastic strain component associated to suction (the elastic strain increment is then split into the elastic strain increment due to Bishop stress changes and the elastic strain increment due to suction changes.

In the following the model is described briefly. Stress invariants and derivatives are given in Appendix A.

6.2 Yield function

To define the yield function it assumes that:

- The behaviour of saturated soil is represented by the Modified Cam Clay model (MCC).
- The yield surface of the MCC model is valid for suction $s > 0$.
- The preconsolidation pressure P_c is a function of suction like to BBM model

The yield function is defined as:

$$F = 3J^2 - \left(\frac{g(\theta)}{g(-30^\circ)} \right)^2 M^2 (p + p_s)(P_c - p) \quad (6.1)$$

Where, p' is the mean effective stress, J is the square root of the second stress invariant of deviatoric stress tensor, $J = \left(\frac{1}{2} \text{trace}(\sigma_{ij} - p' \delta_{ij}) \right)^{1/2}$. The function $g(\theta)$ is defined as:

$$g(\theta) = \frac{\sin \phi'}{\cos \theta + \frac{\sin \theta \sin \phi'}{\sqrt{3}}} \quad (6.2)$$

where θ is Lode angle. P'_c is assumed to vary with suction according to

$$P'_c = P'_r \left(\frac{P'_o}{P'_r} \right)^{\frac{\lambda_o^* - \kappa^*}{\lambda_s^* - \kappa^*}} \quad (6.3)$$

where P'_0 is the yield surface location at zero suction and is also the hardening parameter, P'_r is a reference mean stress, λ_o^* is the modified compression index for saturated soil, λ_s^* is the slope modified of the NCL for unsaturated soil and κ^* is the modified swelling index which is assumed to be independent of suction. The increase in cohesion follows a linear relationship with suction, i.e.:

$$p_s = k_s s \quad (6.4)$$

where, κ_s describe the increase in cohesion with suction. The slope λ_s^* is assumed to vary with the suction according to:

$$\lambda_s^* = \lambda_o \left[(1-r) \exp(-\beta s) + r \right] \quad (6.5)$$

Where r and β are two additional material constants that can be determined experimentally. The first is a constant related to the maximum stiffness of the soil (for an infinite suction), $r = \lambda_s(s \rightarrow \infty) / \lambda_o$, and the second controls the rate of increase of soil stiffness with suction.

6.3 Elastic response

The mechanical elastic behaviour is the same as in the Cam –clay models with the tangent modulus (K) and shear modulus (G) being defined by the following expressions (a constant Poisson's ratio (μ) is assumed):

$$K = \frac{p'}{\kappa^*} \quad (6.6)$$

$$G = \frac{3(1-2\mu)K}{2(1+\mu)} \quad (6.7)$$

In the model a change in suction produces a volumetric elastic strain given by:

$$d\epsilon_{ij}^{e,s} = \frac{\kappa_s}{3(s + p_{atm})} ds \delta_{ij} = \frac{1}{3K_s} ds \delta_{ij} \quad (6.8)$$

κ_s , is the elastic stiffness for changes in suction.

6.4 Flow rule and hardening parameters

The yield surface location at zero suction P'_0 , defines the hardening parameter (as in the BBM model) and the hardening law is described as:

$$dP'_0 = \frac{P'_0}{\lambda_o^* - \kappa^*} d\epsilon_v^p \quad (6.9)$$

The plastic flow rule is defined as,

$$G = \alpha 3J^2 - \left(\frac{g(\theta)}{g(-30^\circ)} \right)^2 M^2 (p + p_s)(P_c - p) \quad (6.10)$$

where α can be chosen to obtain Jaky's formula for one dimensional consolidation for normally consolidated materials. Following the procedure used by Alonso et al., 1990, the expression for α is:

$$\alpha = \frac{M(M-9)(M-3)}{9(6-M)} \left[1 / (1 - \kappa^* / \lambda_o^*) \right] \quad (6.11)$$

6.5 Implicit integration of unsaturated soil model

The implementation is based on Backward Euler algorithm following the application to three invariants isotropic hardening models developed by Jeremic

and Sture (1997) and Pérez et al., (2001). The solution is sought by using the flow direction $m_{ij} = \partial G / \partial \sigma_{ij}$ at the final stress state.

The variables given as input of the mechanical constitutive subroutine are the increment of total strain and increment of suction.

6.6 Constitutive relations for infinitesimal plasticity

The constitutive equations which characterize the elastoplastic material can be briefly stated as follow,

$$d\boldsymbol{\varepsilon}_{ij} = d\boldsymbol{\varepsilon}_{ij}^e + d\boldsymbol{\varepsilon}_{ij}^p + d\boldsymbol{\varepsilon}_{ij}^{e,s} \quad (6.12)$$

$$d\boldsymbol{\sigma}_{ij} = D_{ijkl} d\boldsymbol{\varepsilon}_{kl}^e = D_{ijkl} (d\boldsymbol{\varepsilon}_{kl} - d\boldsymbol{\varepsilon}_{kl}^p - d\boldsymbol{\varepsilon}_{kl}^{e,s}) \quad (6.13)$$

$$d\boldsymbol{\varepsilon}_{ij}^p = d\lambda \frac{\partial G(\boldsymbol{\sigma}_{ij}, \boldsymbol{\chi}, s)}{\partial \boldsymbol{\sigma}_{ij}} \quad (6.14)$$

$$d\boldsymbol{\chi} = \frac{\partial \boldsymbol{\chi}}{\partial \boldsymbol{\varepsilon}_{ij}^p} d\boldsymbol{\varepsilon}_{ij}^p \quad (6.15)$$

where, $d\boldsymbol{\varepsilon}_{ij}$, $d\boldsymbol{\varepsilon}_{ij}^e$ and $d\boldsymbol{\varepsilon}_{ij}^p$ are increments of the total elastic and plastic strain tensors respectively and $d\boldsymbol{\varepsilon}_{ij}^{e,s}$ is the contribution of suction to increment of elastic strain tensor. $d\boldsymbol{\chi}$ represents the increment of hardening parameters (in this case of P_0) and $d\lambda$ is the plastic multiplier to be determined with the aid of the loading-unloading criterion, which can be expressed in terms of the Kuhn Tucker conditions as,

$$\begin{aligned} F(\boldsymbol{\sigma}_{ij}, \boldsymbol{\chi}, s) &\leq 0 \\ d\lambda &\geq 0 \\ F d\lambda &= 0 \end{aligned} \quad (6.16)$$

During any process of loading, conditions (Eq. 6.16) must hold simultaneously.

6.7 Backward Euler algorithm

Fully implicit, Backward Euler schemes are given in the following form:

$$\begin{aligned}
\sigma_{ij}^{(n+1)} &= \sigma_{ij}^{(n)} + \Delta \sigma_{ij}^{(n+1)} \\
\epsilon_{kl}^p{}^{(n+1)} &= \epsilon_{kl}^p{}^{(n)} + \Delta \epsilon_{kl}^p{}^{(n+1)} \\
\chi^{(n+1)} &= \chi^{(n)} + \Delta \chi^{(n+1)} \\
F^{(n+1)} &= 0
\end{aligned} \tag{6.17}$$

where,

$$\Delta \sigma_{ij}^{(n+1)} = D_{ijkl} \left(\Delta \epsilon_{kl} - \Delta \epsilon_{kl}^p - \Delta \epsilon_{kl}^{e,s} \right) \tag{6.18}$$

$$\Delta \epsilon_{ij}^p{}^{(n+1)} = \Delta \lambda^{(n+1)} \left(\frac{\partial G}{\partial \sigma_{ij}} \right)^{(n+1)} \tag{6.19}$$

$$\Delta \chi^{(n+1)} = \left(\frac{\partial \chi}{\partial \epsilon_{ij}^p} \right)^{(n+1)} \Delta \epsilon_{ij}^p{}^{(n+1)} \tag{6.20}$$

Where (n+1) is the actual load step and (n) is the converged step.

Time-integration of equation (6.17) with backward Euler scheme yields the following nonlinear local problem (in compact notation),

$$\begin{aligned}
\sigma^{(n+1)} &= \sigma^{(n)} + \mathbf{D} : \Delta \epsilon - \Delta \lambda^{(n+1)} \mathbf{D} : \mathbf{m}^{(n+1)} - \mathbf{D} : \Delta \epsilon_s^e \\
\chi^{(n+1)} &= \chi^{(n)} + \left(\frac{\partial \chi}{\partial \epsilon^p} \right)^{(n+1)} \mathbf{m}^{(n+1)} \Delta \lambda^{(n+1)} \\
F(\sigma^{(n+1)}, \chi^{(n+1)}, s) &= 0
\end{aligned} \tag{6.21}$$

In equation (6.21), the state at time $t^{(n)}$ (i.e., quantities $\sigma^{(n)}$ and $\chi^{(n)}$), the increment of total strains from time $t^{(n)}$ to time $t^{(n+1)}$, $\Delta \epsilon$, and the suction, s , are known. The unknowns of this local problem are the stresses $\sigma^{(n+1)}$ and the hardening parameters $\chi^{(n+1)}$ at time $t^{(n+1)}$, and the plastic multiplier $\Delta \lambda$.

Formulating the residual of the three non-linear equations (6.21), the local Newton-Raphson solver may be stated as follows:

$$\mathbf{R}\{\sigma^{(n+1)}, \chi^{(n+1)}, \Delta \lambda\} = \begin{cases} \sigma^{(n+1)} + \Delta \lambda \mathbf{D} : \mathbf{m}^{(n+1)} + \mathbf{D} : \Delta \epsilon_s^e - \sigma^{(n)} - \mathbf{D} : \Delta \epsilon = 0 \\ \chi^{(n+1)} - \left(\frac{\partial \chi}{\partial \epsilon^p} \right)^{(n+1)} \mathbf{m}^{(n+1)} \Delta \lambda - \chi^{(n)} = 0 \\ F(\sigma_{n+1}^{(k)}, \chi_{n+1}^{(k)}, s) = 0 \end{cases} \tag{6.22}$$

The non-linear system of eight equations is solved by linearizing the residual and expanding it into a Taylor series:

$$\mathbf{R}\{\boldsymbol{\sigma} + \delta\boldsymbol{\sigma}, \chi + \delta\chi, \Delta\lambda + \delta\lambda\} = \mathbf{R}\{\boldsymbol{\sigma}, \chi, \Delta\lambda\} + \frac{\partial \mathbf{R}\{\boldsymbol{\sigma}, \chi, \Delta\lambda\}}{\partial(\boldsymbol{\sigma}, \chi, \Delta\lambda)} \begin{bmatrix} \delta\boldsymbol{\sigma} \\ \delta\chi \\ \delta\lambda \end{bmatrix} + O[\delta^2] \quad (6.23)$$

The gradient expression $\frac{\partial \mathbf{R}\{\boldsymbol{\sigma}, \chi, \Delta\lambda\}}{\partial(\boldsymbol{\sigma}, \chi, \Delta\lambda)}$ renders the Jacobian of the residual \mathbf{R} :

$$\mathbf{J}\{\boldsymbol{\sigma}, \chi, \Delta\lambda\} = \begin{bmatrix} I + \Delta\lambda \mathbf{D} : \frac{\partial \mathbf{m}}{\partial \boldsymbol{\sigma}} & \Delta\lambda \mathbf{D} : \frac{\partial \mathbf{m}}{\partial \chi} & \mathbf{D} : \mathbf{m} \\ -\Delta\lambda \frac{\partial \chi}{\partial \boldsymbol{\varepsilon}^p} \frac{\partial \mathbf{m}}{\partial \boldsymbol{\sigma}} & 1 - \Delta\lambda \frac{\partial \chi}{\partial \boldsymbol{\varepsilon}^p} \frac{\partial \mathbf{m}}{\partial \chi} & -\frac{\partial \chi}{\partial \boldsymbol{\varepsilon}^p} \mathbf{m} \\ \frac{\partial F}{\partial \boldsymbol{\sigma}} & \frac{\partial F}{\partial \chi} & 0 \end{bmatrix} \quad (6.24)$$

Truncation after the first order terms, $O[\delta^2] \cong 0$, and letting the residual equation (6.23) go to zero, it obtains a set of linear equations for the corresponding increments of $[\boldsymbol{\sigma}, \chi, \Delta\lambda]$, that simultaneously reduces all three residuals to zero:

$$0 = \mathbf{R}\{\boldsymbol{\sigma}_k, \chi_k, \Delta\lambda_k\} + \mathbf{J}\{\boldsymbol{\sigma}_k, \chi_k, \Delta\lambda_k\} \begin{bmatrix} \delta\boldsymbol{\sigma}_{k+1} \\ \delta\chi_{k+1} \\ \delta\lambda_{k+1} \end{bmatrix} \quad (6.25)$$

Indices k and $k+1$ denote the iteration cycle. Solving the linearized system of equations the new iterative update of the eight variables is obtained:

$$\begin{bmatrix} \delta\boldsymbol{\sigma}_{k+1} \\ \delta\chi_{k+1} \\ \delta\lambda_{k+1} \end{bmatrix} = -[\mathbf{J}\{\boldsymbol{\sigma}_k, \chi_k, \Delta\lambda_k\}]^{-1} \mathbf{R}\{\boldsymbol{\sigma}_k, \chi_k, \Delta\lambda_k\} \quad (6.26)$$

Addition of the iterative corrector to the old values of the independent variables yields the eight updates:

$$\begin{bmatrix} \boldsymbol{\sigma}_{k+1} \\ \chi_{k+1} \\ \Delta\lambda_{k+1} \end{bmatrix} = \begin{bmatrix} \boldsymbol{\sigma}_k \\ \chi_k \\ \Delta\lambda_k \end{bmatrix} + \begin{bmatrix} \delta\boldsymbol{\sigma}_{k+1} \\ \delta\chi_{k+1} \\ \delta\lambda_{k+1} \end{bmatrix} \quad (6.27)$$

For starting the iteration, an initial solution is required. This solution is chosen to be the elastic solution at the contact point with the yield surface given by:

$$\begin{aligned}\boldsymbol{\sigma}_0 &= \boldsymbol{\sigma}^c = \boldsymbol{\sigma}^h + (1 - \alpha) \mathbf{D} : \Delta \boldsymbol{\epsilon} \\ \chi_0 &= \chi^h \\ s_0 &= s^c \\ \Delta \lambda_0 &= 0\end{aligned}\tag{6.28}$$

The trial stress state $\Delta \boldsymbol{\sigma}_{n+1}^{(\text{Trial})} = \mathbf{D} : \Delta \boldsymbol{\epsilon}$ and the elastic strain vector due to suction $\Delta \boldsymbol{\epsilon}_s^c$ are maintained fixed during the iteration process.

6.8 Consistent tangent stiffness matrix

To solve the global problem with quadratic convergence it is necessary to use a consistent tangent matrix. To compute this matrix, the consistent moduli $\mathbb{P}^{n+1} \mathbf{s} / \mathbb{P}^{n+1} \mathbf{D} \mathbf{e}$ at each Gauss point are needed. They are obtained by linearizing equation (6.21), the linearization is represented in a compact form as (Pérez et al., 2001):

$$\frac{\mathbb{P}^{n+1} \mathbf{s}}{\mathbb{P}^{n+1} \mathbf{D} \mathbf{e}} = \mathbf{P}^T (\mathbf{J}^{n+1})^{-1} \mathbf{P} \mathbf{D}\tag{6.29}$$

where $\mathbf{P}^T = (\mathbf{I}_{ns} \ 0_{ns \times nc+1})$ is the projection matrix on stress space (Pérez et al., 2001); note that $0_{ns \times nc+1}$ is a null rectangular matrix with ns rows and $nc + 1$ columns, ns is the number of stresses and nc is the number of hardening parameters.

Additionally, the above process will be combined with sub-incrementation of the prescribed strain (substepping) according to the recursive scheme proposed by Pérez-Foguet *et al.*, (2001), this implementation is in progress.

6.9 Description of the subroutine: unsat_model

The subroutine *Unsat_Model* has the same structure for input/output variables of the subroutine *User_Mod* of Plaxis to implement user-defined soil models. In the subroutine are expected as input variables (in addition to the standard input variables in User-defined soil models) the following:

Suction0: Previous or historical suction value of the current stress point

Suction: Suction value to be applied in the current stress point

Sig0: Bishop's effective stress at start of step

As output variables are expected (in addition to the standard input variables in User-defined soil models):

Sig: Bishop's effective stress computed in the subroutine

Error_code: Code assigned to the possible errors during the calculation process.

Input/output variables:

iMod = 1 : Number model

nProps = 18 : Model parameters

ParamName (1): Poisson ratio (μ)

ParamName (2): Slope of the unload/reload line (κ) of saturated soil

ParamName (3): Slope of the normal compression line (λ_0) of saturated soil

ParamName (4): Elastic stiffness due to suction (κ_s)

ParamName (5): Parameter to control the tensile strength due to suction (k)

ParamName (6): Slope of the Critical state line (M)

ParamName (7): Friction angle at CS (ϕ_{cs} [degrees])

ParamName (8): Initial void ratio (e_0)

ParamName (9): Preconsolidation pressure of saturated soil (P_o [kPa])

ParamName (10): Reference mean stress (P_r [kPa])

ParamName (11): Parameter to control infinite suction (r)

ParamName (12): Parameter to control soil stiffness with suction (β [kPa⁻¹])

ParamName (13): Van Genuchten Parameter (a [kPa])

ParamName (14): Van Genuchten Parameter (b)

ParamName (15): Van Genuchten Parameter (c)

ParamName (16): Parameter of non associated flow rule (α_g)

ParamName (17): Coefficient of earth pressure at rest (K_o)

ParamName (18): Overconsolidation ratio (OCR)

nStat = 6 : Number of state variables

stVar0 (1) = P_o (Preconsolidation pressure of the saturated soil)

stVar0 (2) = Suction (Actual suction value)

stVar0 (3) = S_r (Actual degree of saturation)

stVar0 (4) = Pc (Preconsolidation pressure of Unsaturated soil)
 stVar0 (5) = pt (Tensile strength due to suction)
 stVar0 (6) = F_result (Value of yield function)

Error_code (Scalar Integer): Code assigned to the possible errors

Contains the code assigned to the possible errors that can occur during the calculation process. If ierror_code is greater than zero, this parameter will force the calculation to stop. The possible errors and their codes are

Code	Description	Subroutine
101	Does not converge during elastic integration	Subroutine <i>Elastic integration</i>
102	Can not find crossing point with yield surface	Function <i>exit F_1</i>
103	Does not converge during plastic integration	Subroutine <i>Plastic integration</i>

Note: Internally the subroutine *Unsat_Model* groups some input data into a *derived data type* named Prop_model which has the follow fields:

Prop_model%Imod = Imod
 Prop_model%npar = Nprops
 Prop_model%n = Nstress
 Prop_model%nhv = Nstat
 Prop_model%par = Props()

Nstress is the number of stress components (6) plus the number of the hardening parameters in order to build a vector of generalized stress.

6.10 Proposition for determination of the unsaturated soil parameters

Table 6.1 describes the determination the unsaturated soil model and Table 6.2 gives parameters of Barcelona Basic Model for some soil types.

Tab. 6.1: User-defined soil model local property variables

No	Model parameters	Definition	Proposition for estimation	Typical values	Reference
10	P_r [F/L ²]	Reference mean stress at which one may reach the saturated virgin state, starting at a partially saturated condition, through a wetting path which involves only (elastic) swelling.	Upscaled from Isotropic compression tests or eodometric tests at different constant suctions. Fig 1. Relationships between preconsolidation stress (P_o , P_c) and the reference stress (P_r) - Fit of the Load-Collapse curve (LC): 	When $P_r = P_o$ (saturated condition) the LC yield curve becomes a straight line. In this case, changes in s do not result in plastic deformations.	Alonso et al (1990).
11	r	Parameter defining the maximum soil stiffness (for an infinite suction)	Upscaled from Isotropic compression tests or eodometric tests at different constant suctions. Fit of the Load-Collapse curve (LC).	See Table 1: Some values from literature.	Alonso, et al (1990). Barrera, et al (2002)

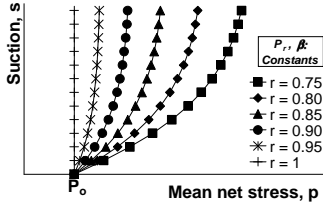
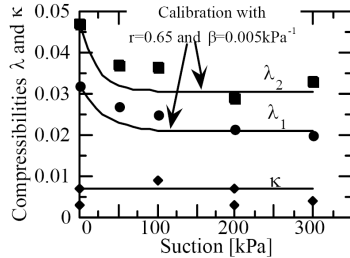
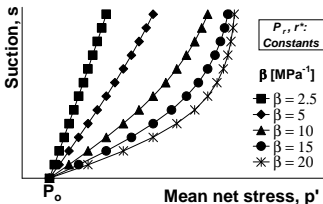
No	Model parameters	Definition	Proposition for estimation	Typical values	Reference
	r (cont.)		Influence of r on LC:		
					
			Fig 4. Influence of r^* in the shape of LC curve		
		Example of the influence of suction increase on the compressibility:			
		<i>Sion Silt</i> (Geiser et al., 2000):			Geiser et al (2000).
		$\lambda_s = \lambda_o \left[(1 - r^*) \exp(-\beta s) + r^* \right]$			
					
			Fig 5. Variation of the compressibility index with the suction		
12	β [F/L ²] ⁻¹	Parameter controlling the rate of increase of soil stiffness with suction	<p>Upscaled from Isotropic compression tests or eodometric tests at different constant suctions.</p> <p>Fit of the Load-Collapse curve (LC).</p> <p>Influence of β on LC:</p> 	See Table 1: Some values from literature.	Alonso, et al (1990) Barrera, et al (2002).

Fig 6. Influence of β in the shape of LC curve

Tab. 6.2: Parameters for the Barcelona Basic Model for different soil types

Soil type	μ	M	κ	$\lambda(0)$	r	β (MPa) ⁻¹	p _r (MPa)	Reference
BCN Silt	0.3 3	1.155	0.005	0.073	0.782	155	7.0 E-05	Barrera (2002)
Sion silt	0.4 0	1.33	0.007	0.032: p:100– 400 kPa 0.047: p>400 kPa	0.65	5	0.02	Geiser et al (2001)
Compacted kaolin, ML	G= 3.3 MPa	0.821	0.015	0.14	0.26	16.4	0.043	Josa (1988)
Compacted kaolin [w = 6% , S _r = 0.627]			0.011	0.065	0.75	20	0.01	Karube (1986)
Compacted kaolin			0.027	0.063	Variable 0.32 0.58 0.972	10		Thu, et al. (2007)
Sandy Clay (Lower Cromer till)	G= 7 MPa	1.2	0.0077	0.066	0.25	20	0.012	Maswoswe (1985)
Lower Cromer till	0.2	1.2	0.0077	0.066	0.35	16.4	0.012	Georgiadis (2003)
Lambeth Sand (London City)	0.2	0.9	0.005	0.06	0.25	20		Georgiadis (2003)
Metramo silty Sand	G = 45 MPa	1.54	0.0056	0.022	Variable 0.68 0.91 0.978	24	0.001	Rampino et al (2000)
Boom Clay Pellets			0.015	0.16	0.57	6	0.05	Sánchez (2004)
FEBEX Bentonite		1.24	0.005	0.080	0.90	1	0.50	Lloret et al (2003)
Silty sand from the Riverside		1.32	0.009	0.11	0.29	18.1	0.041	Mun B-J (2004)

Soil type	μ	M	κ	$\lambda(0)$	r	β (MPa) ⁻¹	p _r (MPa)	Reference
Campus								
Bentonite –Sand mixtures			0.008	0.25	0.85	0.05	8.0E-06	Alonso et al (2005)
Lixhe chalk	0.2		0.0085	0.18	0.95	8.0	0.003	Collin et al (2002)
Compacted silt. (clayey, slightly sandy Silt) [w = 23.1%, $\gamma_d = 15.6 \text{ kN/m}^3$]			0.004	0.052	0.17	1.8		Vasallo et al (2007)
Serrate bentonite	0.4	1.5	0.05	0.15	0.75	0.05	0.1	Zhang et al (2003)
Boom Clay	0.33	1.0	0.00265	0.26	0.564	0.544	0.06	Zhang et al (2003)
Reconstituid Kaolin			0.014	0.37	0.27	10		Slatter et al (2006)
Earth fill compacted with a soil with a lower than optimum water content			0.005	0.085	2	5		Cordao and Farias (2006)
Jossigny's Silt (silt of low plasticity)	0.3	1.0	0.015	0.108	0.911	5.75	6.55E-06	Vaunat et al (2000)
Residual granite soil (CH)	G=8.9 MPa	0.895	0.14	0.29	0.24	19.69	0.045	Mofiz et al (2005)

7 Verification of groundwater flow: One-Dimensional

In this section verification of the groundwater flow codes implemented in PLAXIS 2D and 3D kernels is given. As it is hard to derive an analytical solution for the examples given in this section, the results are compared with the existing Plaxflow code developed by GeoDelft. The examples are chosen from the first part of the report provided by GeoDelft, report co710201.101 v1, December 2002.

This chapter presents the results of 13 column tests, for which a flow problem has been solved. The column has a height of 2.0 m and a width of 0.05 m, vertical boundaries are closed and flow is strictly one-dimensional. The Van Genuchten and spline models are used. Most of available types of boundary conditions are imposed separately including constant head, constant pressure, inflow, outflow and seepage conditions. Precipitation conditions automatically apply the inflow and outflow conditions according to the function used for the prescribed flux. Right now, four functions can be used for varying prescribed flux in time, namely constant, linear, harmonic and the user defined function (table). The same functions can also be applied for water level varying. In the case of steady state calculation, only constant function is utilised, i.e. no variation. To have proper results, fine mesh used in both 2D and 3D, Figure 7.1.

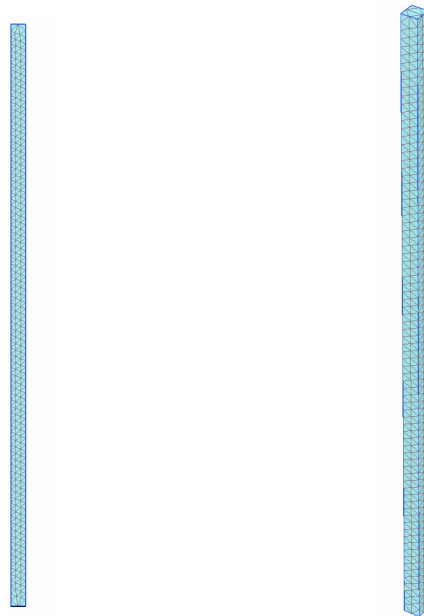


Fig. 7.1: finite element meshes used in 2D and 3D calculations; Left: 2D; Right 3D

7.1 Case A1: pressure head

Case A1 involves an infiltration situation and is shown in Figure A1.1. The left picture presents the initial boundary conditions from which a steady state flow situation is calculated. Imposing a head of -1.0 m at the bottom of the model and 1.0 m at the top generates unsaturated starting conditions. The right hand side picture shows the boundary conditions for the later time period. Boundary conditions change to 2.0 m at the top of the model, the bottom condition is not changed. Starting series O1 sand model describes hydraulic behaviour of material for which Van Genuchten relationship is applied. The properties of the soil are given in Table A1.1.

The following steps are performed in this case:

1. *Steady state*: Steady state groundwater flow calculation to generate initial pore pressure, (suction pore pressure of 10 kPa in the entire column).
2. *Transient*: The top boundary head is set. Infiltration takes place and the model gets more saturated in time. The infiltration front move downward in time until a new steady state situation is reached. Figure A1.2 and A1.3 show a vertical cross section of the calculated pore pressures and degree of saturation in time. The infiltration profiles are shown for steps given in Table A1.2.
3. *Steady state*: Steady state groundwater flow calculation to generate ultimate pore pressure.

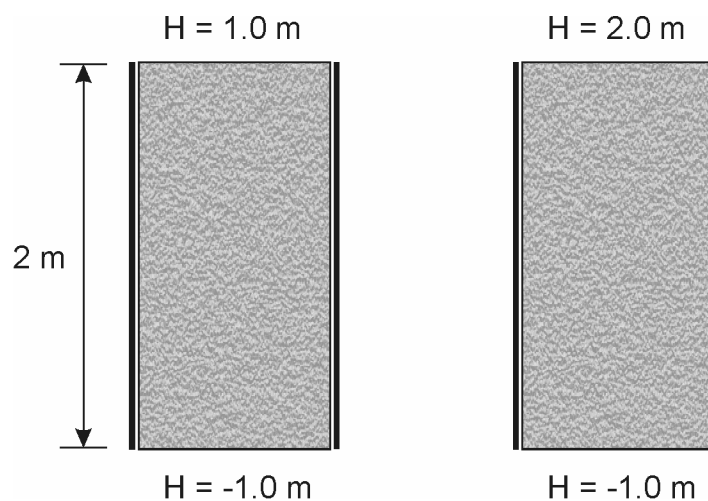


Fig. A1.1: Geometry of case A1

Tab. A1.1: Input data for case A1

Description	Symbol	Unit	Value
Permeability	k_x, k_y, k_z	[m/day]	0.1521
initial void ratio	e_{init}	[-]	0.5625
Elastic storage	$K_{w,ref}/n$	[kN/m ²]	4.875×10^5
Saturated saturation	S_{sat}	[-]	1.0
Residual saturation	S_{res}	[-]	0.06203
Van Genuchten	g_n	[-]	2.286
Van Genuchten	g_a	[m ⁻¹]	2.24
Van Genuchten	g_l	[-]	0

Tab. A1.2: Input data for case A1

Step	Time (day)
2	<i>Steady state</i>
20	0.232
32	0.463
44	0.694
56	0.926
68	1.16
80	1.39
126	2.31
156	3.47
194	<i>Steady state</i>

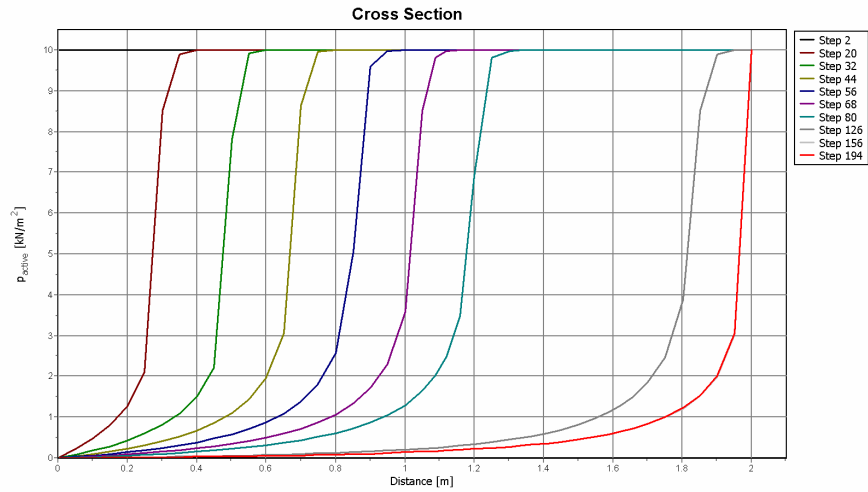


Fig. A1.2: Active pore pressure in time vs height in PLAXIS 2D

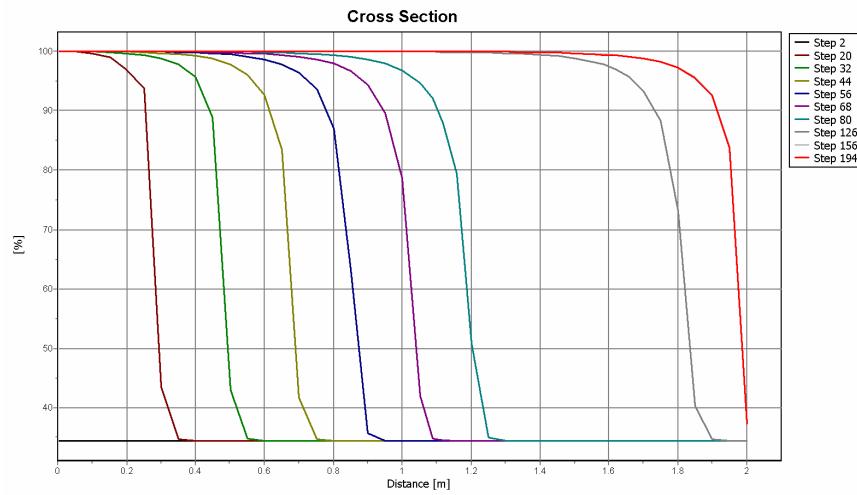


Fig. A1.3: Degree of saturation in time vs height in PLAXIS 2D

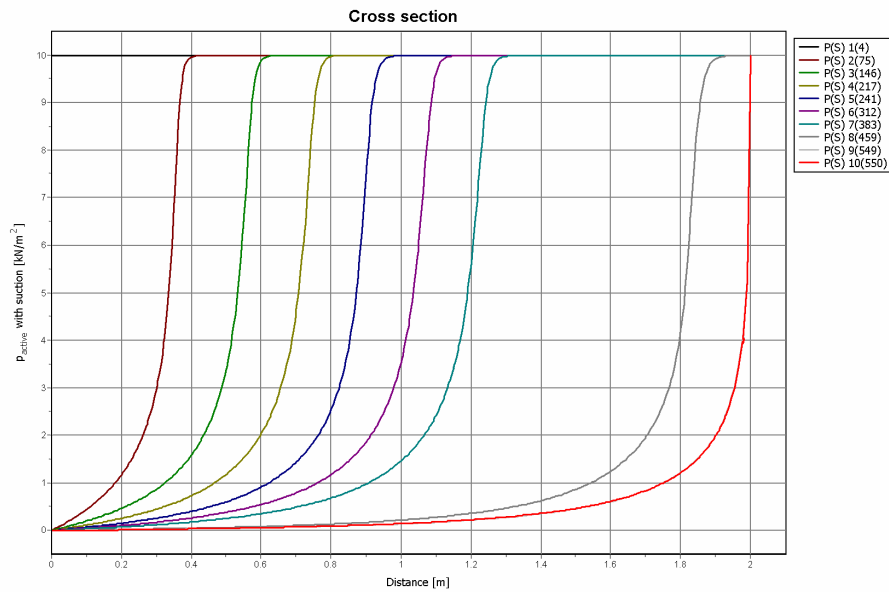


Fig. A1.4: Active pore pressure in time vs height in PLAXIS 3D

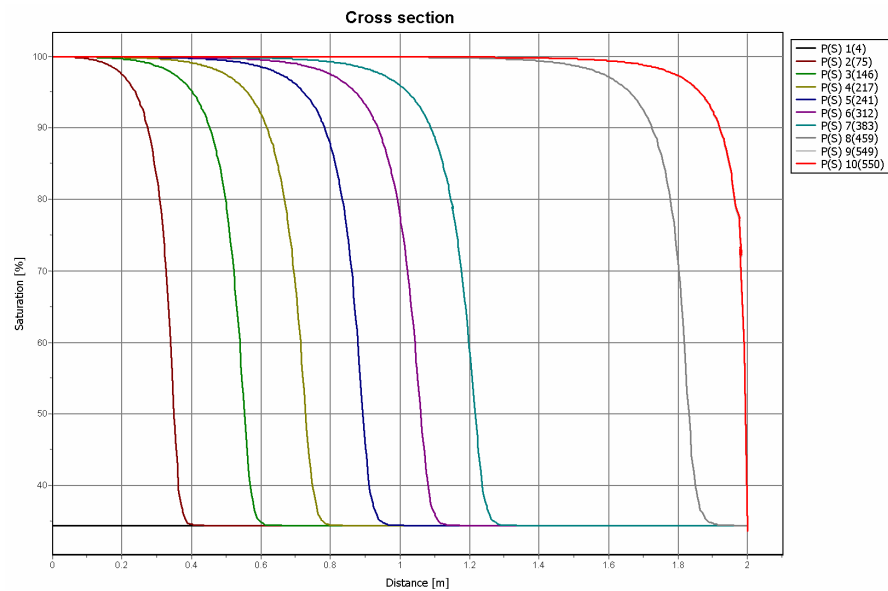


Fig. A1.5: Degree of saturation in time vs height in PLAXIS 3D

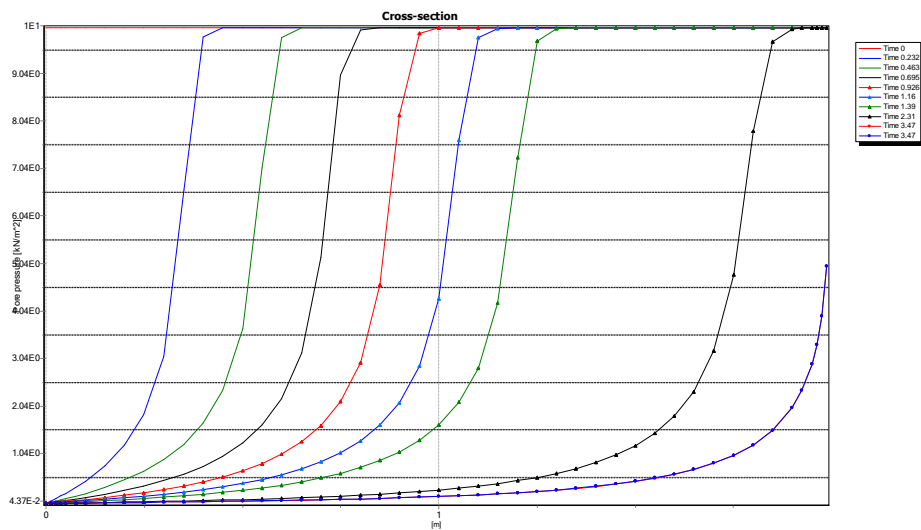


Fig. A1.6: Active pore pressure in time vs height (existing PlaxFlow)

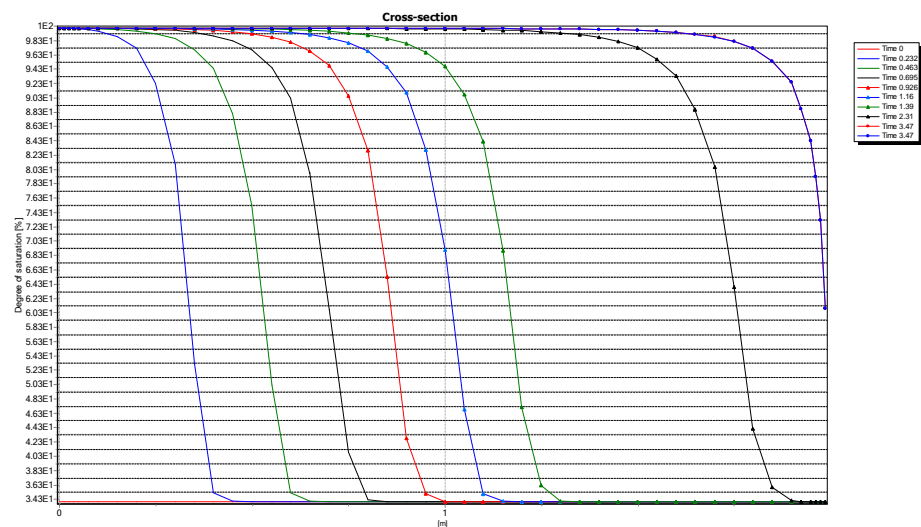


Fig. A1.7: Degree of saturation in time vs height (existing PlaxFlow)

Summary:

As seen the results from PLAXIS 2D, PLAXIS 3D and PlaxFlow are similar.

7.2 Case A3: Inflow boundary

Case A3 involves an infiltration situation and is shown in Figure A3.1. In this example the influx is constant in time and given as an prescribed boundary flux. The left picture presents the initial boundary conditions from which a steady state flow situation is calculated. Imposing a head of -1.0 m at the bottom of the model and 1.0 m at the top generates unsaturated starting conditions. The right hand side picture shows the boundary conditions for the later time period. Boundary conditions change to 0.152 m/day inflow at the top of the model, the bottom condition is not changed. Starting series O1 sand model describes hydraulic behaviour of material for which Van Genuchten relationship is applied. The properties of the soil are given in Table A3.1.

The following steps are performed in this case:

1. *Steady state*: Steady state groundwater flow calculation to generate initial pore pressure, (suction pore pressure of 10 kPa in the entire column).
2. *Transient*: The boundary prescribed flux is imposed. Infiltration takes place and the model gets more saturated in time. The infiltration front move downward in time until a new steady state situation is reached. Figure A3.2 and A3.3 show a vertical cross section of the calculated pore pressures and degree of saturation in time. The infiltration profiles are shown for steps given in Table A3.2.
3. *Steady state*: Steady state groundwater flow calculation to generate ultimate pore pressure.

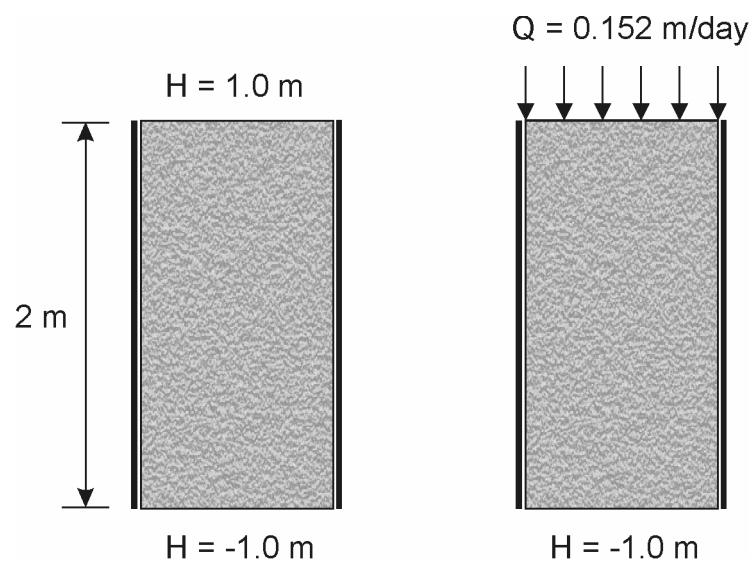


Fig. A3.1: Geometry of case A3

Tab. A3.1: Input data for case A3

Description	Symbol	Unit	Value
Permeability	k_x, k_y, k_z	[m/day]	0.1521
initial void ratio	e_{init}	[-]	0.5625
Elastic storage	$K_{w,ref}/n$	[kN/m ²]	4.875×10^5
Saturated saturation	S_{sat}	[-]	1.0
Residual saturation	S_{res}	[-]	0.06203
Van Genuchten	g_n	[-]	2.286
Van Genuchten	g_a	[m ⁻¹]	2.24
Van Genuchten	g_l	[-]	0

Tab. A3.2: Input data for case A3

Step	Time (day)
2	<i>Steady state</i>
39	0.232
76	0.463
113	0.694
150	0.926
187	1.16
224	1.39
372	2.31
557	3.47
643	<i>Steady state</i>

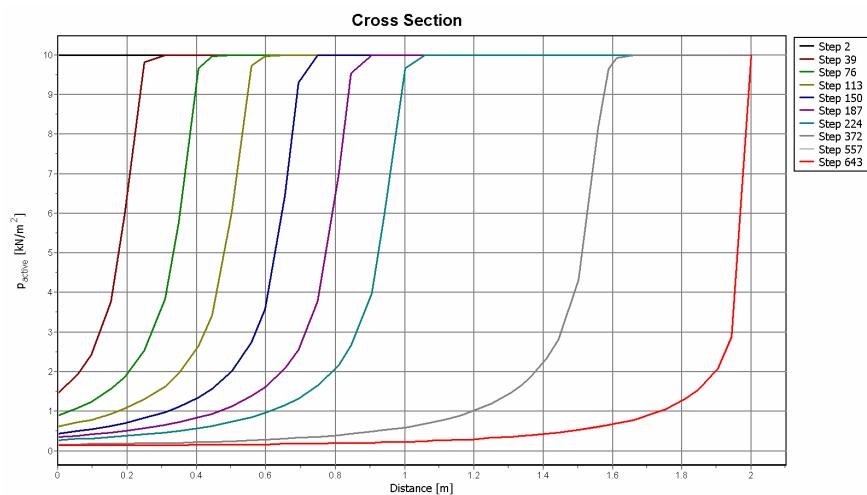


Fig. A3.2: Active pore pressure in time vs height in PLAXIS 2D

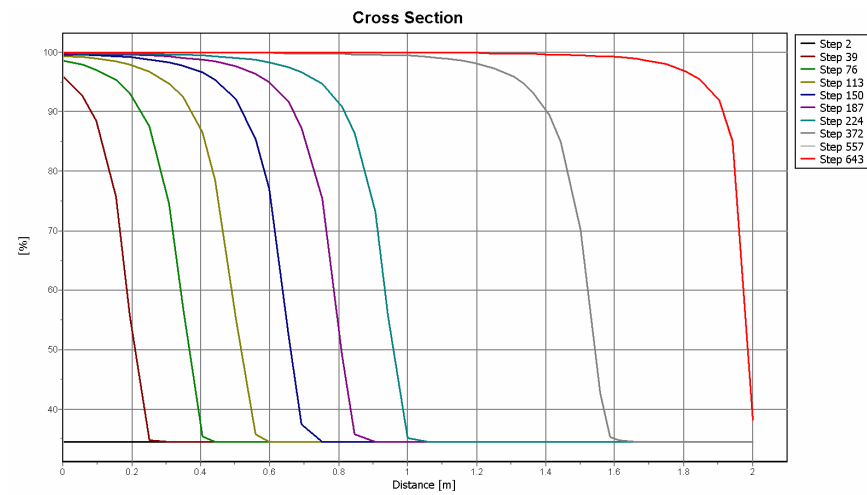


Fig. A3.3: Degree of saturation in time vs height in PLAXIS 2D

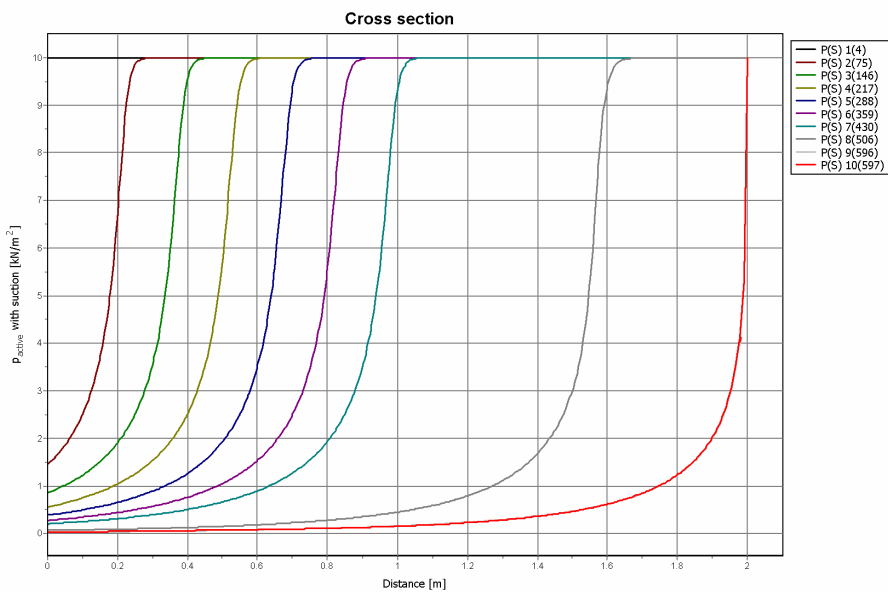


Fig. A3.4: Active pore pressure in time vs height in PLAXIS 3D

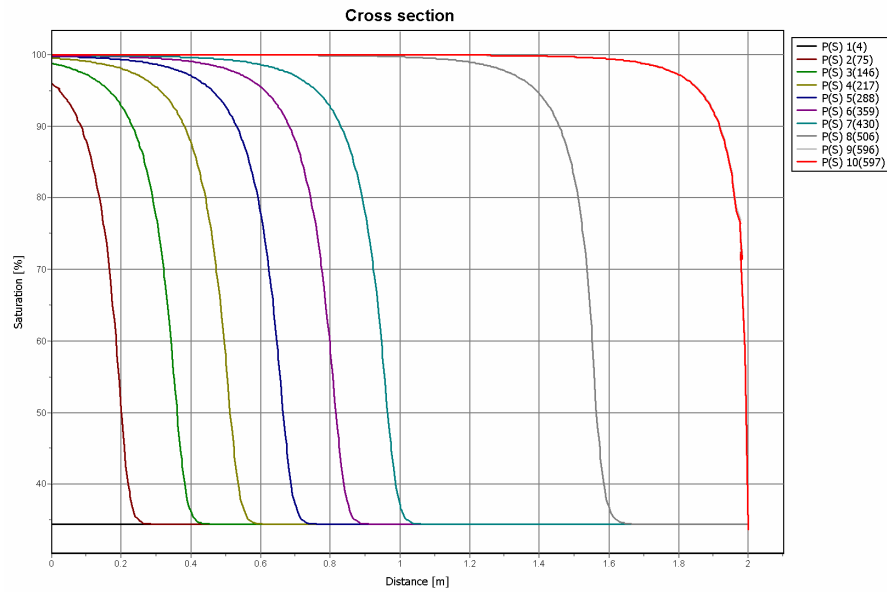


Fig. A3.5: Degree of saturation in time vs height in PLAXIS 3D

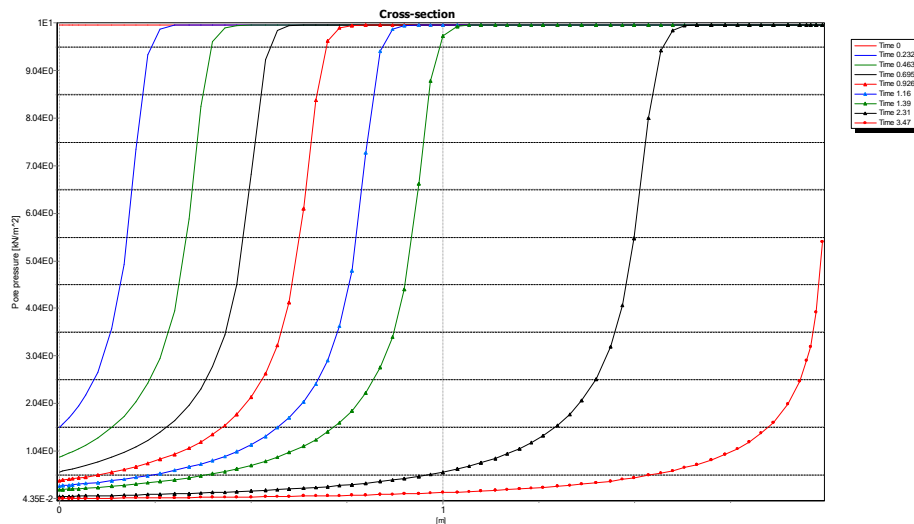


Fig. A3.6: Active pore pressure in time vs height (existing PlaxFlow)

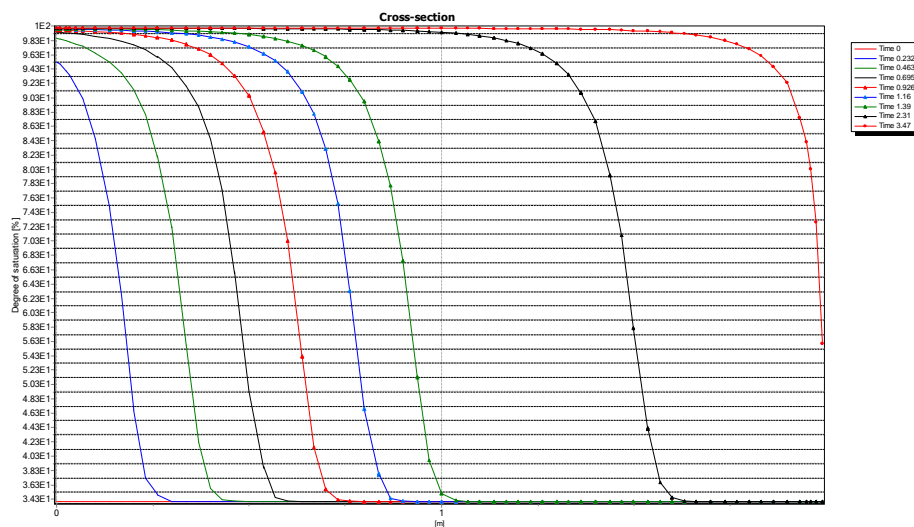


Fig. A3.7: Degree of saturation in time vs height (existing PlaxFlow)

Summary:

As seen the results from PLAXIS 2D, PLAXIS 3D and PlaxFlow are similar.

7.3 Case B1: Fixed head boundary

Case B1 involves a recharge situation and is shown in Figure B1.1. In this example the column is filled from the bottom in opposite direction of the gravitational force. The left picture presents the initial boundary conditions from which a steady state hydrostatic situation is calculated. Imposing a head of 0 m at the bottom of the model and seepage boundary condition (or closed) at the top generates unsaturated starting conditions. The right hand side picture shows the boundary conditions for the later time period. Boundary conditions change to 1.5 m at the bottom of the model, the top condition is not changed. Starting series O1 sand model describes hydraulic behaviour of material for which Van Genuchten relationship is applied. The properties of the soil are given in Table B1.1.

The following steps are performed in this case:

1. *Steady state*: Steady state groundwater flow calculation to generate initial pore pressure, (hydrostatic condition: suction pore pressure of 20 kPa at the top of the column).
2. *Transient*: The fixed boundary head of 1.5 m at the bottom is imposed. Recharge takes place and the model gets more saturated in time. The infiltration front move upward in time until a new steady state situation is reached. Figure B1.2 and B1.3 show a vertical cross section of the calculated pore pressures and degree of saturation in time. The infiltration profiles are shown for steps given in Table B1.2.
3. *Steady state*: Steady state groundwater flow calculation to generate ultimate pore pressure, (hydrostatic condition: suction pore pressure of 5 kPa at the top of the column).

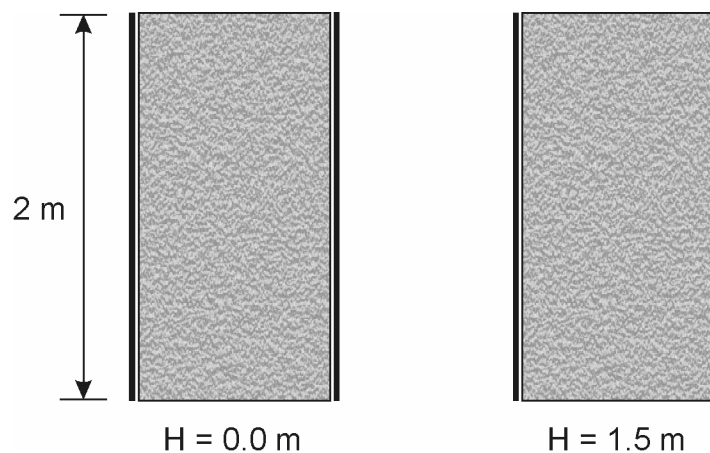


Fig. B1.1: Geometry of case B1

Tab. B1.1: Input data for case B1

Description	Symbol	Unit	Value
Permeability	k_x, k_y, k_z	[m/day]	0.1521
initial void ratio	e_{init}	[-]	0.5625
Elastic storage	$K_{w,ref}/n$	[kN/m ²]	4.875×10^5
Saturated saturation	S_{sat}	[-]	1.0
Residual saturation	S_{res}	[-]	0.06203
Van Genuchten	g_n	[-]	2.286
Van Genuchten	g_a	[m ⁻¹]	2.24
Van Genuchten	g_l	[-]	0

Tab. B1.2: Input data for case B1

Step	Time (day)
2	<i>Steady state</i>
3	<i>0.00579</i>
4	<i>0.0116</i>
7	<i>0.0694</i>
10	<i>0.127</i>
34	<i>0.706</i>
53	<i>1.28</i>
147	<i>7.07</i>
244	<i>12.9</i>
246	<i>Steady state</i>

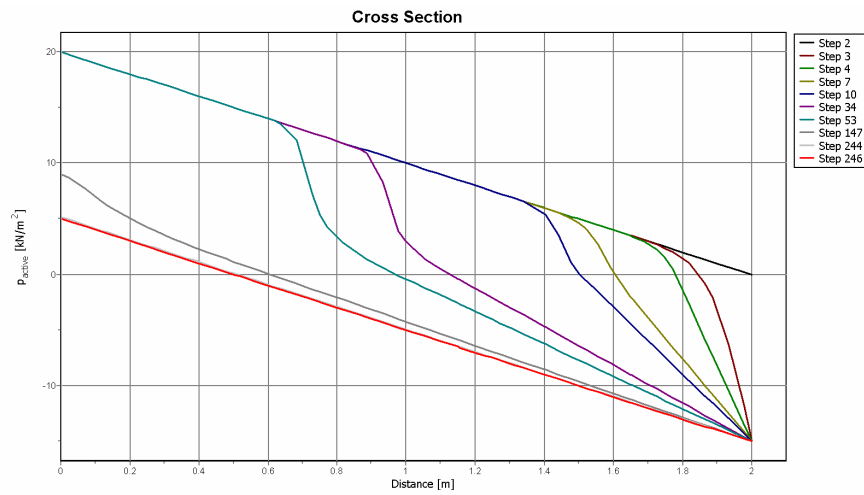


Fig. B1.2: Active pore pressure in time vs height in PLAXIS 2D

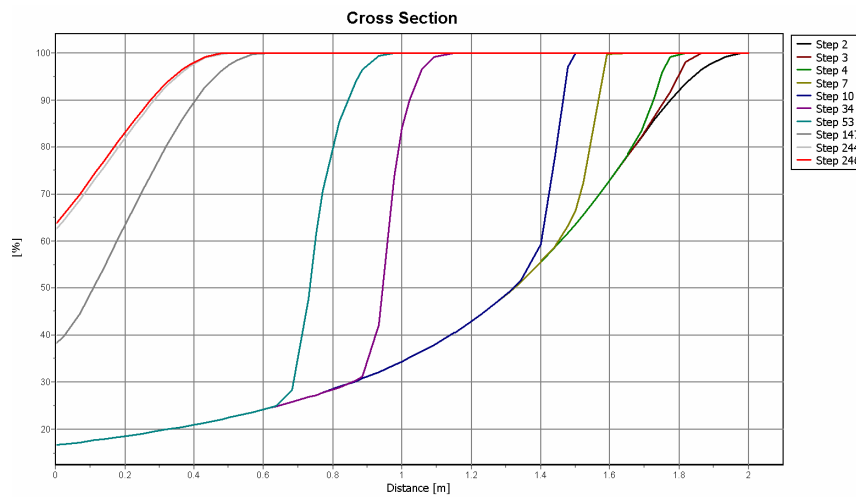


Fig. B1.3: Degree of saturation in time vs height in PLAXIS 2D

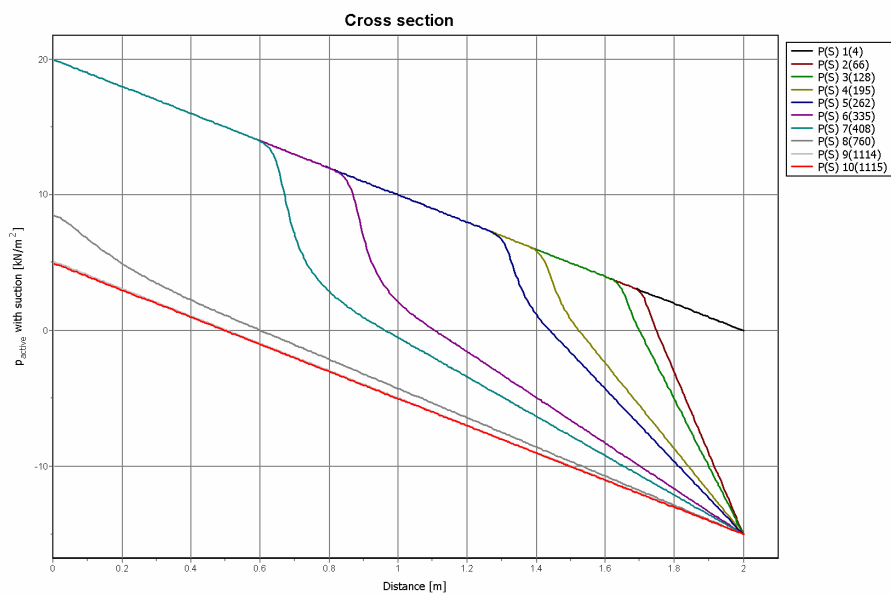


Fig. B1.4: Active pore pressure in time vs height in PLAXIS 3D

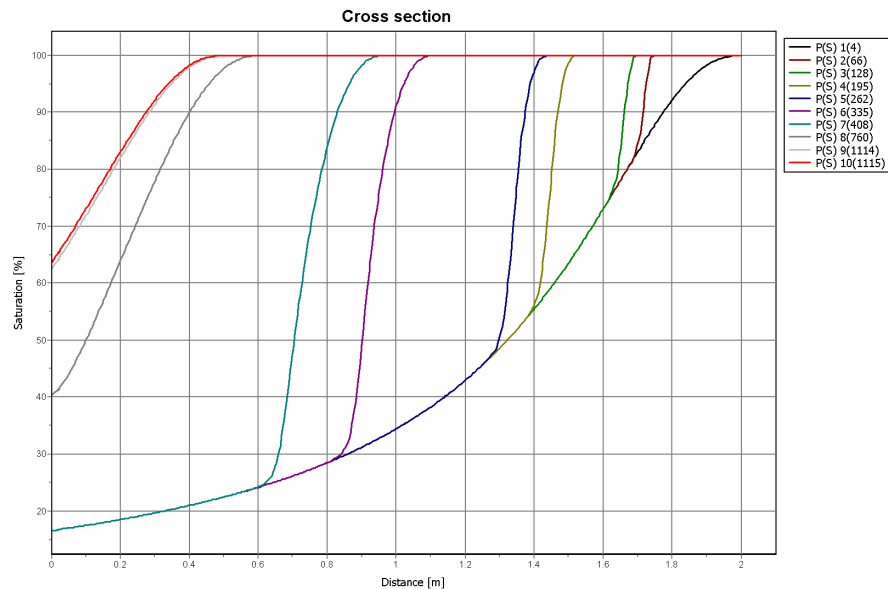


Fig. B1.5: Degree of saturation in time vs height in PLAXIS 3D

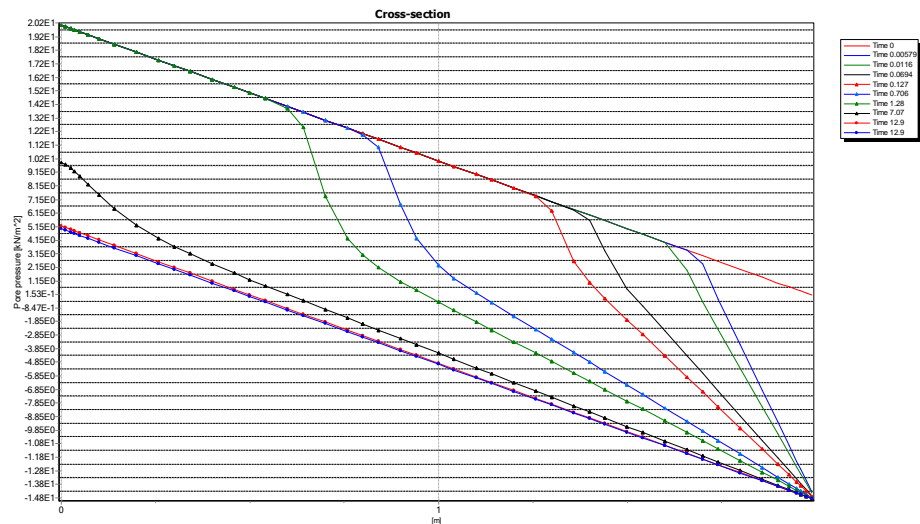


Fig. B1.6: Active pore pressure in time vs height (existing PlaxFlow)

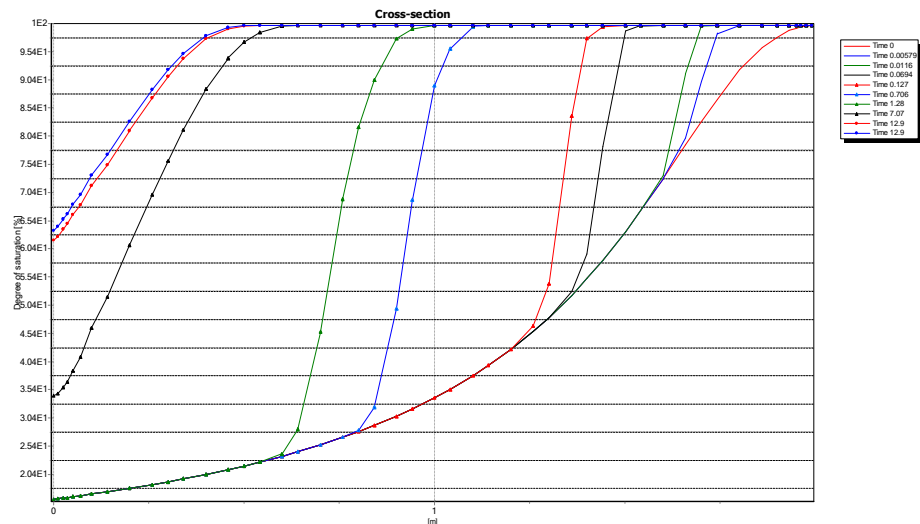


Fig. B1.7: Degree of saturation in time vs height (existing PlaxFlow)

Summary:

As seen the results from PLAXIS 2D, PLAXIS 3D and PlaxFlow are similar.

7.4 Case B3: Fixed head boundary

Case B3 involves a drainage situation and is shown in Figure B3.1. In this example the column is dried from the bottom in opposite direction of the gravitational force. The left picture presents the initial boundary conditions from which a constant suction of 0 kPa is generated in entire column. Imposing a head of 0 m at the bottom of the model and a head of 2.0 m at the top of the column generates the unsaturated starting conditions. The right hand side picture shows the boundary conditions for the later time period. Boundary conditions change to seepage (or closed) at the bottom of the model, the top condition is not changed. Starting series O1 sand model describes hydraulic behaviour of material for which Van Genuchten relationship is applied. The properties of the soil are given in Table B3.1.

The following steps are performed in this case:

1. *Steady state*: Steady state groundwater flow calculation to generate initial pore pressure, (constant suction pore pressure of 0 kPa in whole of the column).
2. *Transient*: The seepage boundary condition (or closed boundary condition) at the top is imposed. Drainage takes place and the model gets more unsaturated in time. Figure B3.2 and B3.3 show a vertical cross section of the calculated pore pressures and degree of saturation in time. The results are shown for steps given in Table B3.2.
3. *Steady state*: Steady state groundwater flow calculation to generate ultimate pore pressure, (hydrostatic condition: suction pore pressure of 20 kPa at the top of the column).

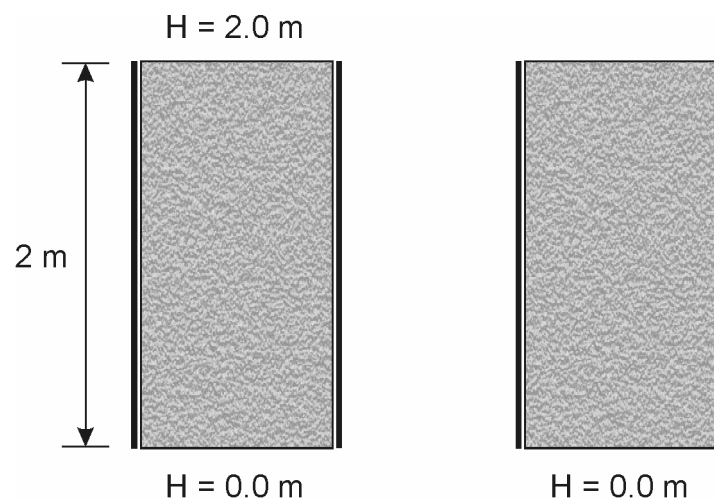


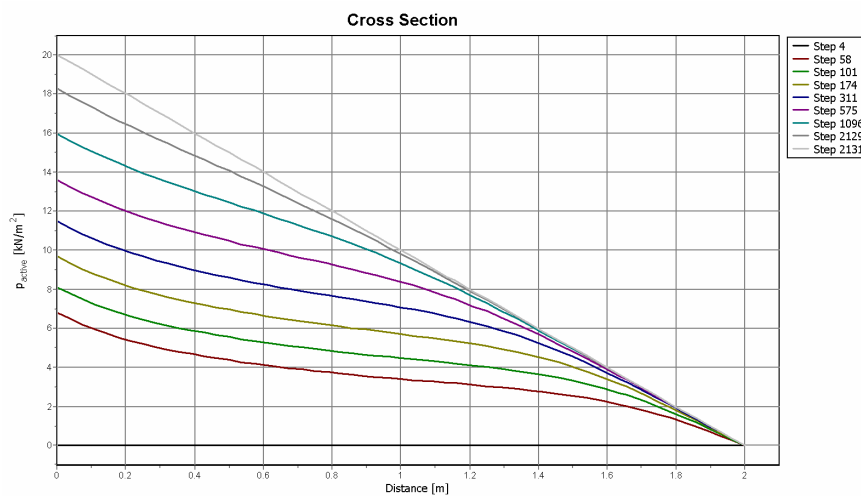
Fig. B3.1: Geometry of case B3

Tab. B3.1: Input data for case B3

Description	Symbol	Unit	Value
Permeability	k_x, k_y, k_z	[m/day]	0.1521
Initial void ratio	e_{init}	[-]	0.5625
Elastic storage	$K_{w,ref}/n$	[kN/m ²]	4.875×10^5
Saturated saturation	S_{sat}	[-]	1.0
Residual saturation	S_{res}	[-]	0.06203
Van Genuchten	g_n	[-]	2.286
Van Genuchten	g_a	[m ⁻¹]	2.24
Van Genuchten	g_l	[-]	0

Tab. B3.2: Input data for case B3

Step	Time (day)
4	<i>Steady state</i>
58	2
101	4
174	8
311	16
575	32
1096	64
2129	128
2131	<i>Steady state</i>

**Fig. B3.2:** Active pore pressure in time vs height in PLAXIS 2D

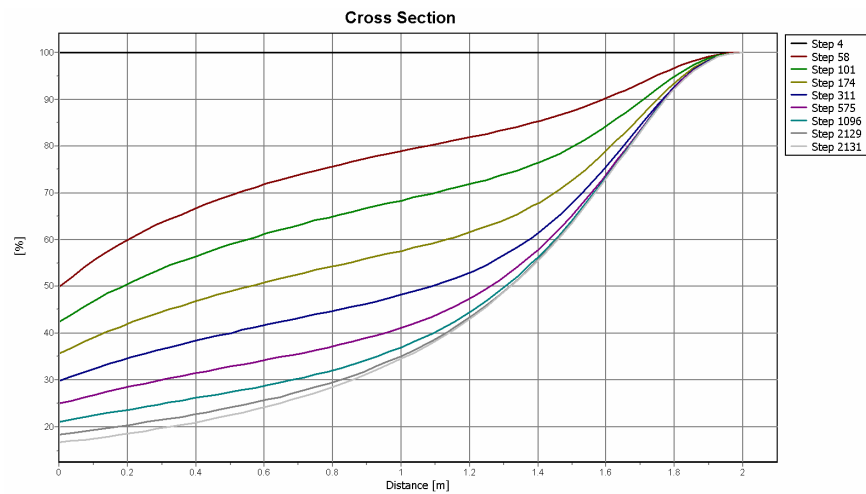


Fig. B3.3: Degree of saturation in time vs height in PLAXIS 2D

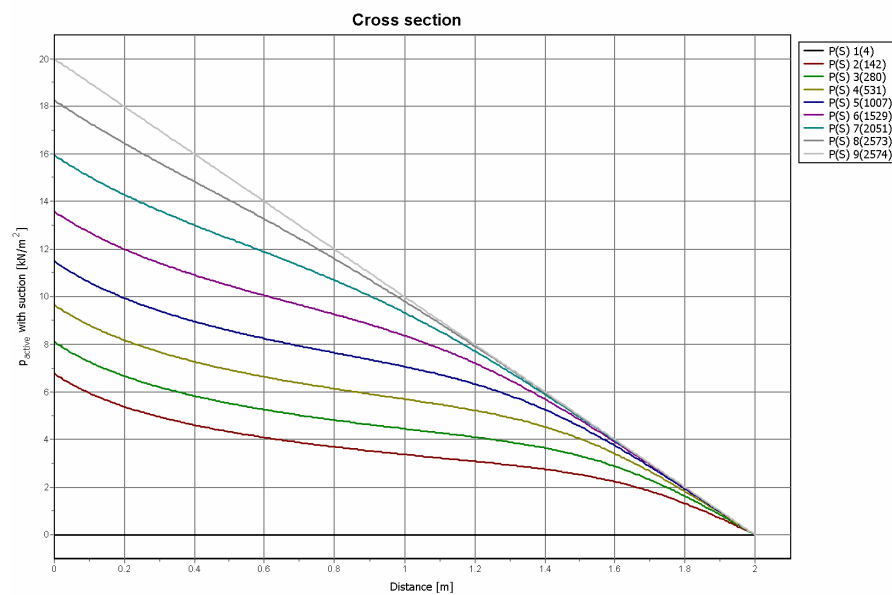


Fig. B3.4: Active pore pressure in time vs height in PLAXIS 3D

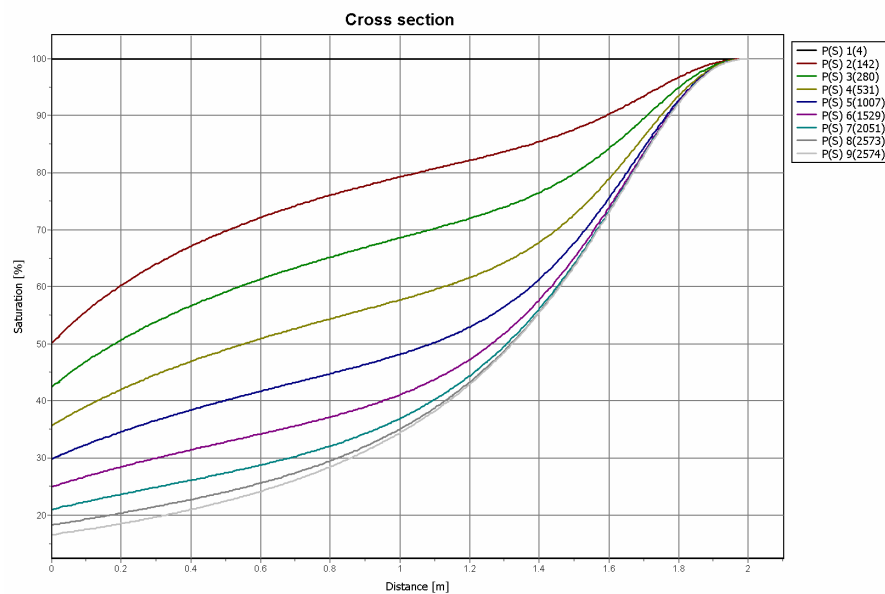


Fig. B3.5: Degree of saturation in time vs height in PLAXIS 3D

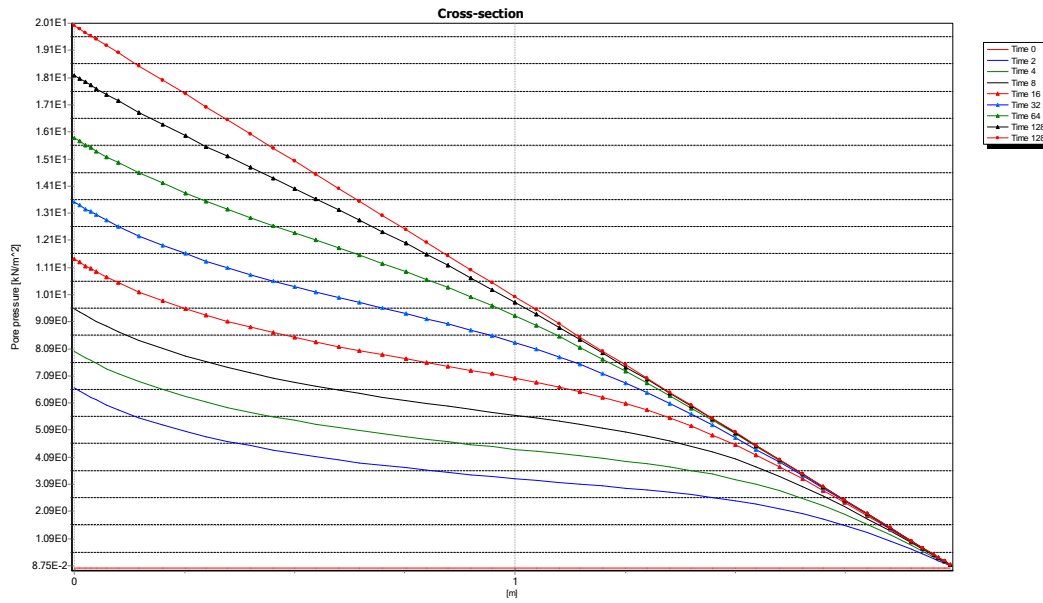


Fig. B3.4: Active pore pressure in time vs height (existing PlaxFlow)

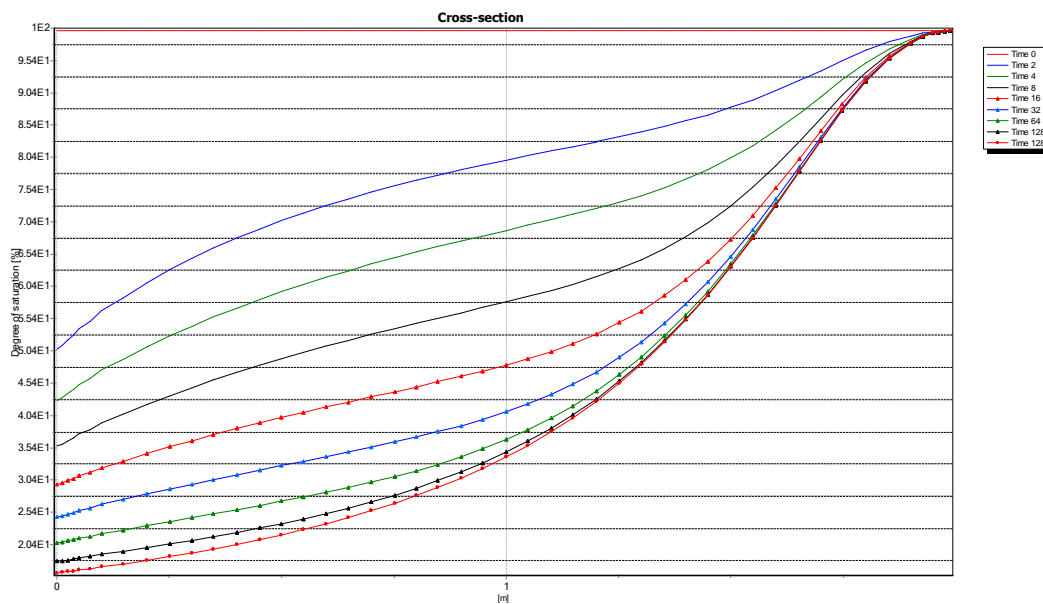


Fig. B3.5: Degree of saturation in time vs height (existing PlaxFlow)

Summary:

As seen the results from PLAXIS 2D, PLAXIS 3D and PlaxFlow are similar.

7.5 Case B4: Outflow boundary

Case B4 involves a drainage situation and is shown in Figure B4.1. In this example the column is dried from the bottom in opposite direction of the gravitational force by means of prescribed outflow boundary conditions. The left picture presents the initial boundary conditions from which a hydrostatic water pore pressure is generated in column. Imposing heads of 2 m at the bottom and at the top of the column generates the saturated starting conditions. The right hand side picture shows the boundary conditions for the later time period. Boundary conditions change to constant outflow of 0.152 m/day at the bottom of the model, the top condition is not changed. Staring series O1 sand model describes hydraulic behaviour of material for which Van Genuchten relationship is applied. The properties of the soil are given in Table B4.1.

The following steps are performed in this case:

4. *Steady state*: Steady state groundwater flow calculation to generate initial hydrostatic pore pressure.
5. *Transient*: The outflow boundary condition at the bottom is imposed. Drainage takes place in time. Figure B4.2 and B4.3 show a vertical cross section of the calculated pore pressures from the PLAXIS 2D and Plaxflow kernels, respectively. The results of PLAXIS 2D are shown for steps given in Table B4.2.
6. *Steady state*: Steady state groundwater flow calculation to generate ultimate pore pressure.

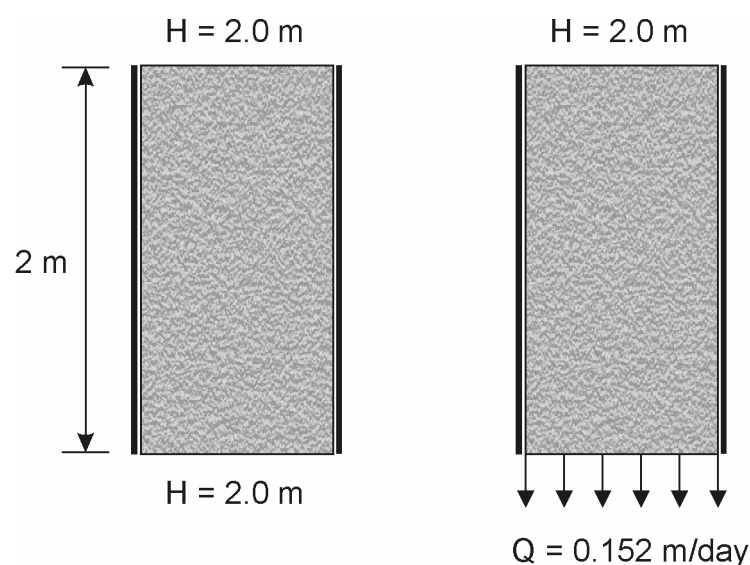


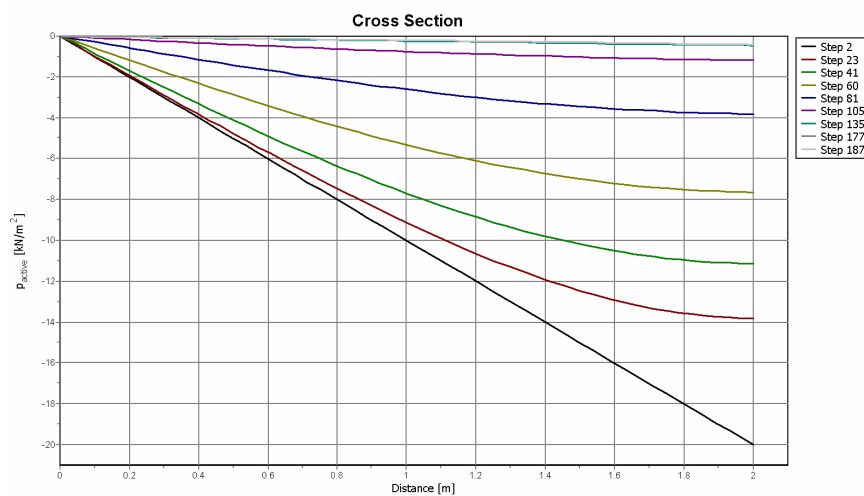
Fig. B4.1: Geometry of case B4

Tab. B4.1: Input data for case B4

Description	Symbol	Unit	Value
Permeability	k_x, k_y, k_z	[m/day]	0.1521
Initial void ratio	e_{init}	[-]	0.5625
Elastic storage	$K_{w,ref}/n$	[kN/m ²]	10.84
Saturated saturation	S_{sat}	[-]	1.0
Residual saturation	S_{res}	[-]	0.06203
Van Genuchten	g_n	[-]	2.286
Van Genuchten	g_a	[m ⁻¹]	2.24
Van Genuchten	g_l	[-]	0

Tab. B4.2: Input data for case B4

Step	Time (day)
2	<i>Steady state</i>
23	2
41	4
60	8
81	16
105	32
135	64
177	128
187	<i>Steady state</i>

**Fig. B4.2:** Active pore pressure in time vs height in PLAXIS 2D

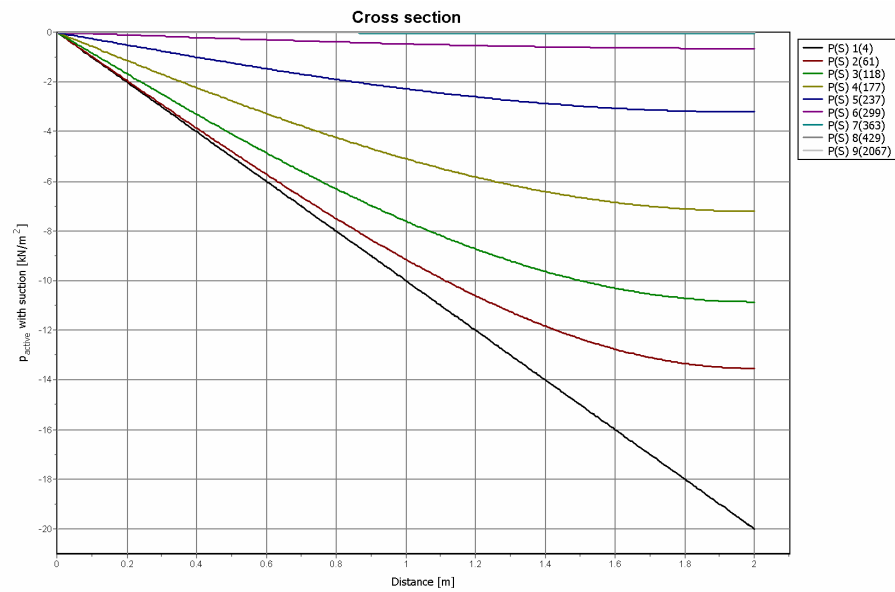


Fig. B4.3: Active pore pressure in time vs height in PLAXIS 3D

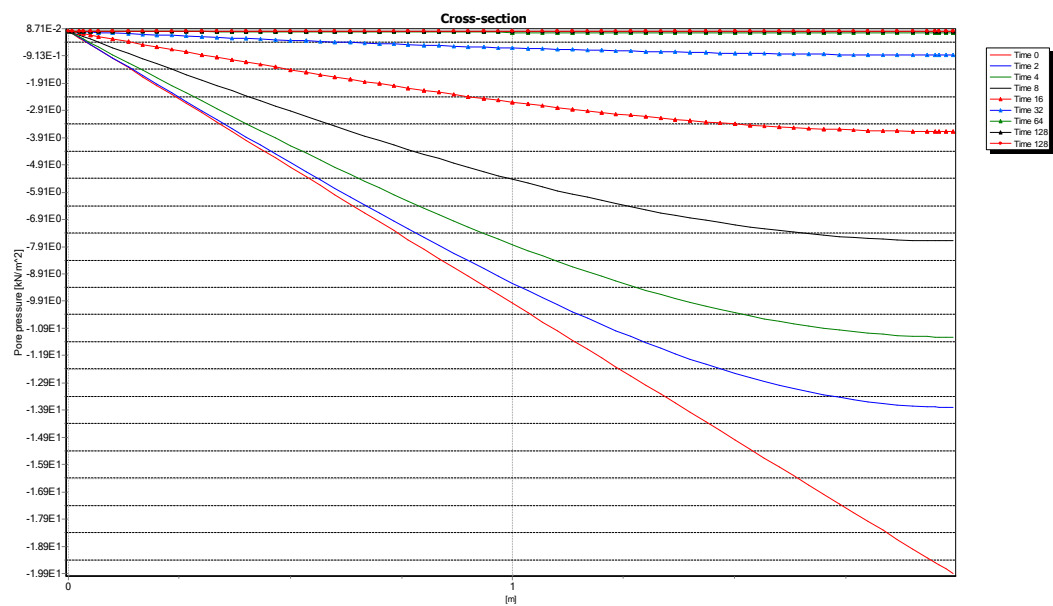


Fig. B4.4: Active pore pressure in time vs height (existing PlaxFlow)

Summary:

As seen the results from PLAXIS 2D, PLAXIS 3D and PlaxFlow are similar.

7.6 Case C1: pressure head (spline model: sand)

Case C1 involves an infiltration situation and is shown in Figure C1.1. The left picture presents the initial boundary conditions from which a steady state flow situation is calculated. Imposing a head of -1.0 m at the bottom of the model and 1.0 m at the top generates unsaturated starting conditions. The right hand side picture shows the boundary conditions for the later time period. Boundary conditions change to 2.0 m at the top of the model, the bottom condition is not changed. Haverkamp sand model describes hydraulic behaviour of material for which cubic Hermit spline interpolation is applied. The properties of the soil are given in Table C1.1 and Table C1.2.

The following steps are performed in this case:

4. *Steady state*: Steady state groundwater flow calculation to generate initial pore pressure, (suction pore pressure of 10 kPa in the entire column).
5. *Transient*: The top boundary head is set. Infiltration takes place and the model gets more saturated in time. The infiltration front move downward in time until a new steady state situation is reached. Figure C1.2 to C1.4 show a vertical cross section of the calculated pore pressures, degree of saturation and relative permeability in time. The infiltration profiles are shown for steps given in Table C1.3.
6. *Steady state*: Steady state groundwater flow calculation to generate ultimate pore pressure.

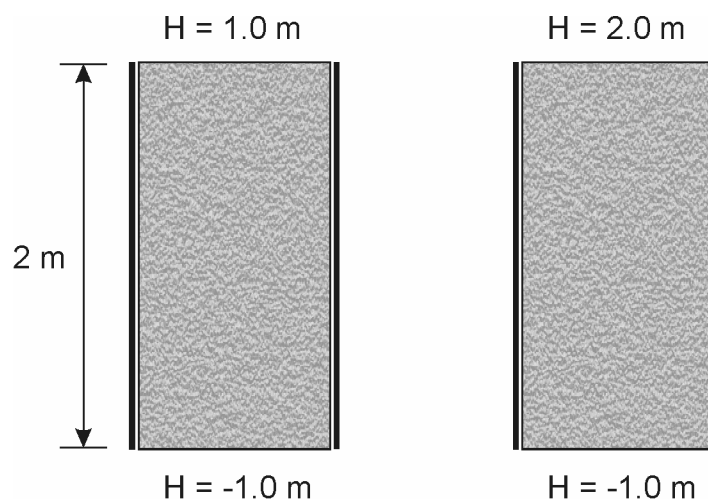


Fig. C1.1: Geometry of case C1

Tab. C1.1: Input data for case C1

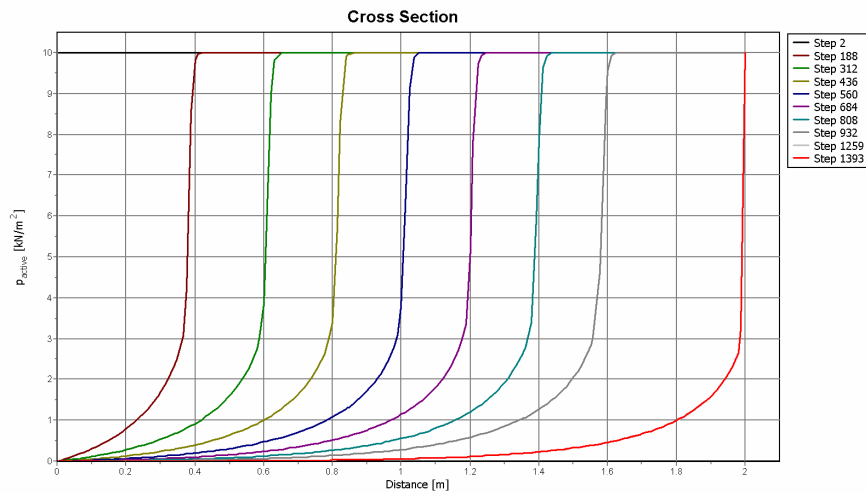
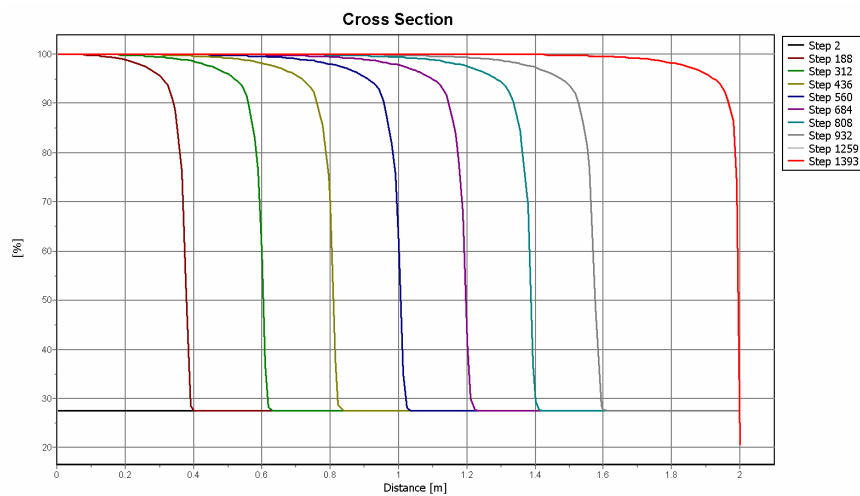
Description	Symbol	Unit	Value
Permeability	k_x, k_y, k_z	[m/day]	8.156
initial void ratio	e_{init}	[-]	0.403
Elastic storage	$K_{w,ref}/n$	[kN/m ²]	4.875×10^5

Tab. C1.2: Haverkamp sand data

- H (m)	k_r	S
0.00E+00	1.0	1.0
2.00E-01	0.44448	0.94019
4.00E-01	2.91E-02	0.57286
6.00E-01	4.36E-03	0.35567
8.00E-01	1.12E-03	0.29439
1.00E+00	3.89E-04	0.27536
1.20E+00	1.64E-04	0.26821
1.40E+00	7.90E-05	0.26508
1.60E+00	4.19E-05	0.26354
1.80E+00	2.40E-05	0.26272
2.00E+00	1.46E-05	0.26224
2.20E+00	9.27E-06	0.26195
2.40E+00	6.14E-06	0.26177
2.60E+00	4.20E-06	0.26165
2.80E+00	2.95E-06	0.26157
3.00E+00	2.13E-06	0.26151
3.20E+00	1.57E-06	0.26147
3.40E+00	1.18E-06	0.26144
3.60E+00	8.98E-07	0.26141
3.80E+00	6.95E-07	0.2614

Tab. C1.3: Input data for case C1

Step	Time (day)
2	<i>Steady state</i>
188	<i>0.00463</i>
312	<i>0.00926</i>
436	<i>0.0139</i>
560	<i>0.0185</i>
684	<i>0.0232</i>
808	<i>0.0278</i>
932	<i>0.0324</i>
1259	<i>0.0463</i>
1393	<i>Steady state</i>

**Fig. C1.2:** Active pore pressure in time vs height in PLAXIS 2D**Fig. C1.3:** Degree of saturation in time vs height in PLAXIS 2D

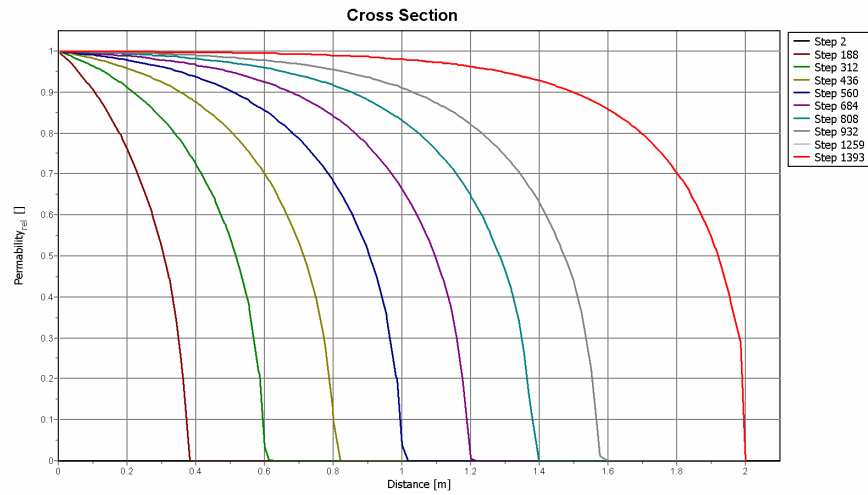


Fig. C1.4: Relative permeability in time vs height in PLAXIS 2D

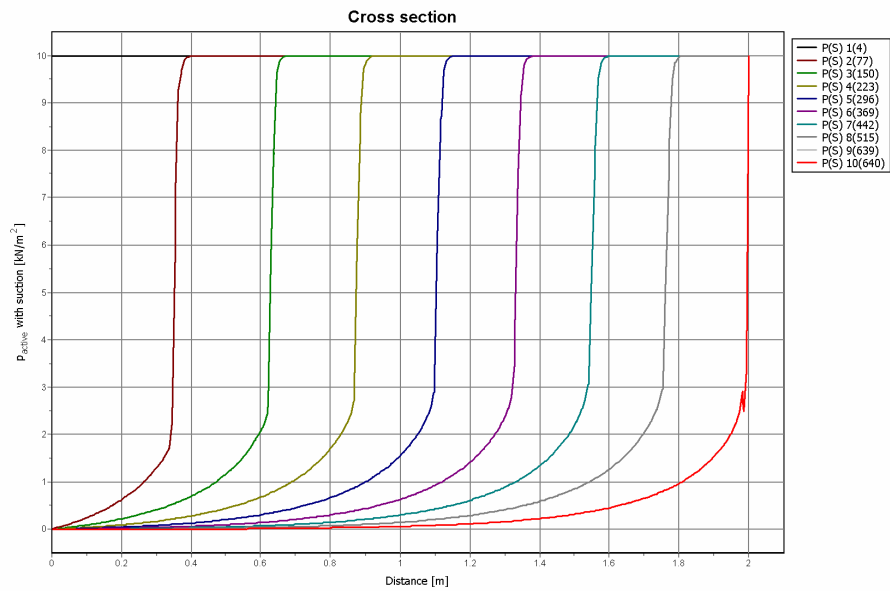


Fig. C1.5: Active pore pressure in time vs height in PLAXIS 3D

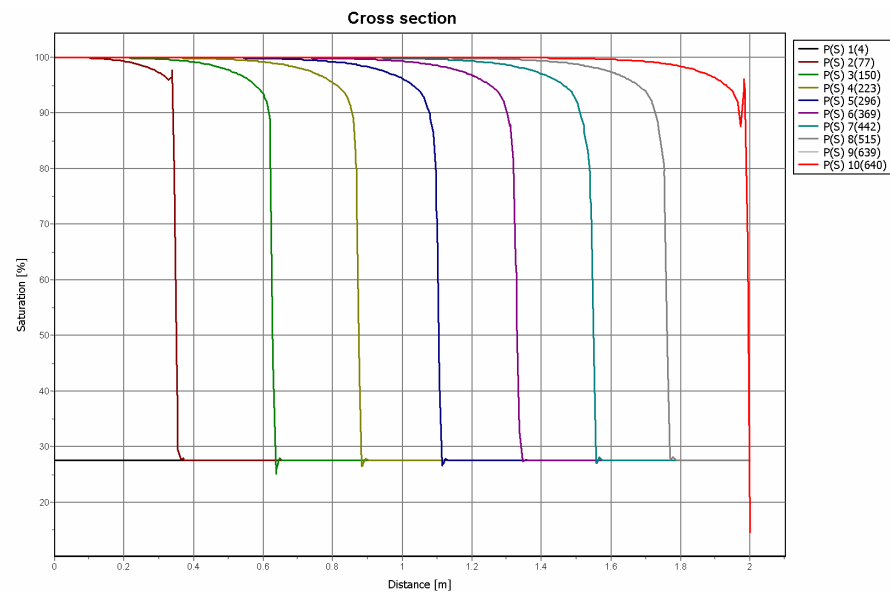


Fig. C1.6: Degree of saturation in time vs height in PLAXIS 3D

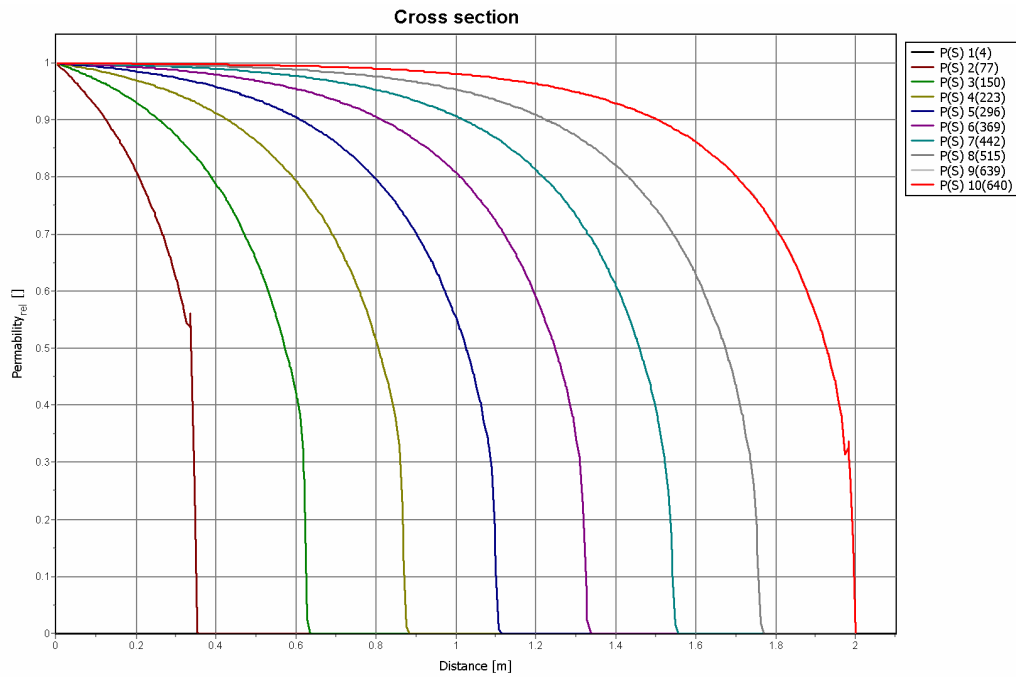


Fig. C1.7: Relative permeability in time vs height in PLAXIS 3D

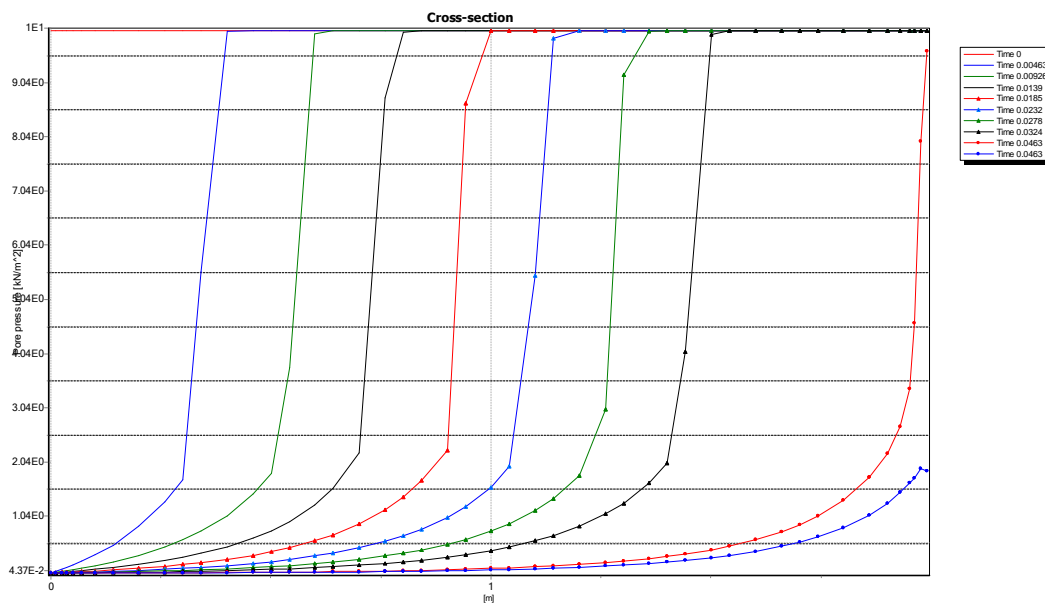


Fig. C1.8: Active pore pressure in time vs height (existing PlaxFlow)

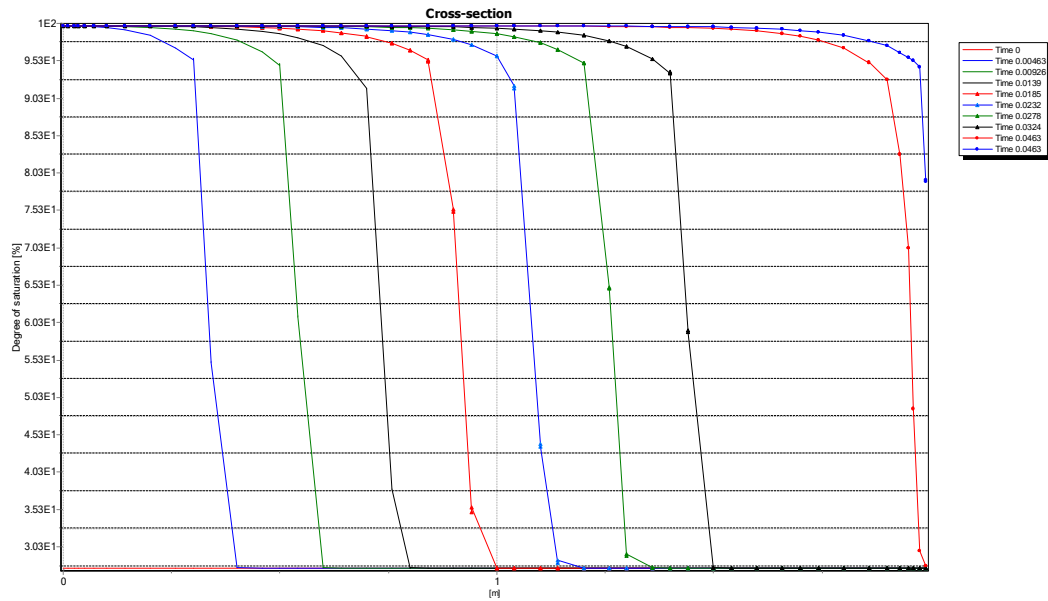


Fig. C1.9: Degree of saturation in time vs height (existing PlaxFlow)

Summary:

As seen the results from PLAXIS 2D, PLAXIS 3D and PlaxFlow are similar. The maximum suction pore pressure is 10 kPa ($H=-1.0$ m), therefore the minimum degree of saturation for all curves plotted in Figure C1.3 must be 27.5 % (Table C1.2). As seen the degrees of saturation for step 1259 and 1393 show lower values at distance 2 m which is a visualization problem due to extrapolation method used in the output program and this is not a serious problem.

7.7 Case C2: pressure head (spline model: clay)

Case C2 involves an infiltration situation and is shown in Figure C2.1. The left picture presents the initial boundary conditions from which a steady state flow situation is calculated. Imposing a head of -1.0 m at the bottom of the model and 1.0 m at the top generates unsaturated starting conditions. The right hand side picture shows the boundary conditions for the later time period. Boundary conditions change to 2.0 m at the top of the model, the bottom condition is not changed. Haverkamp clay model describes hydraulic behaviour of material for which cubic Hermit spline interpolation is applied. The properties of the soil are given in Table C2.1 and Table C2.2.

The following steps are performed in this case:

7. *Steady state*: Steady state groundwater flow calculation to generate initial pore pressure, (suction pore pressure of 10 kPa in the entire column).
8. *Transient*: The top boundary head is set. Infiltration takes place and the model gets more saturated in time. The infiltration front move downward in time until a new steady state situation is reached. Figure C2.2 to C2.4 show a vertical cross section of the calculated pore pressures, degree of saturation and relative permeability in time. The infiltration profiles are shown for steps given in Table C2.3.
9. *Steady state*: Steady state groundwater flow calculation to generate ultimate pore pressure.

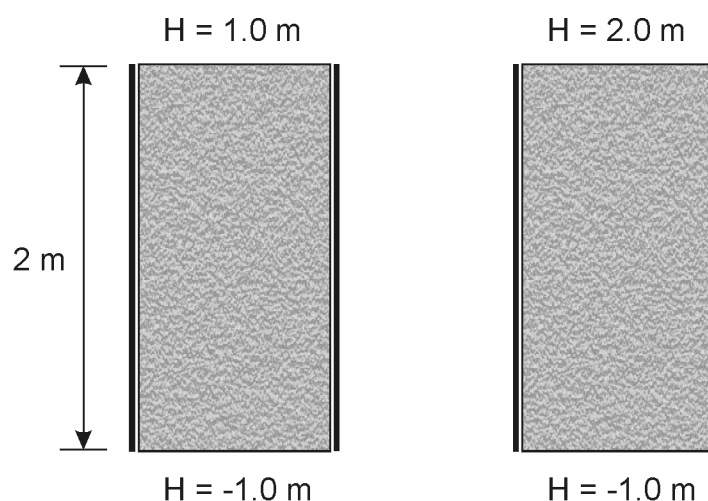


Fig. C2.1: Geometry of case C2

Tab. C2.1: Input data for case C2

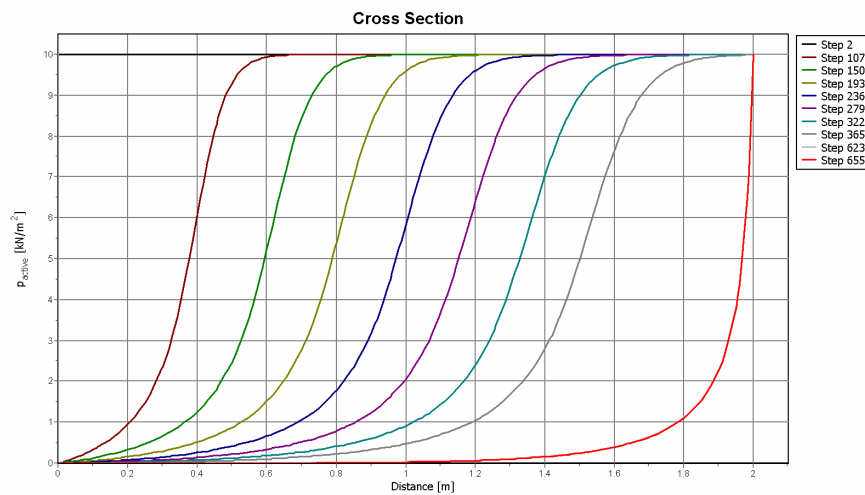
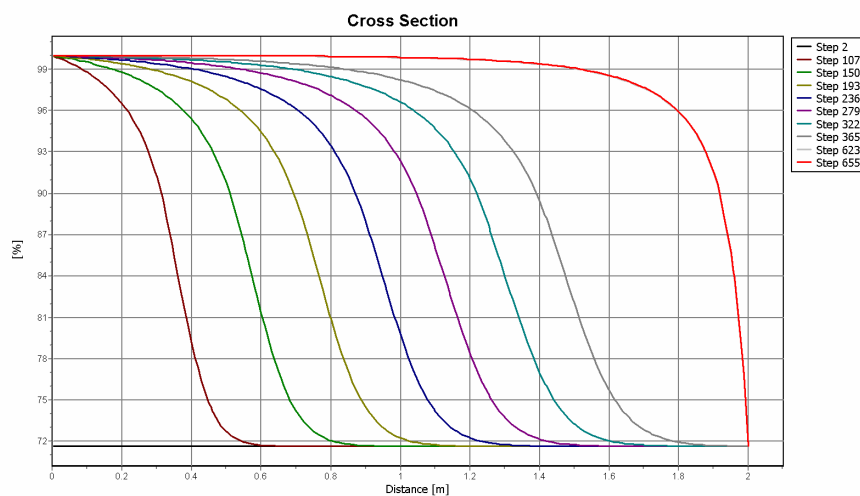
Description	Symbol	Unit	Value
Permeability	k_x, k_y, k_z	[m/day]	0.0106
Initial void ratio	e_{init}	[-]	0.98
Elastic storage	$K_{w,ref}/n$	[kN/m ²]	4.875×10^5

Tab. C2.2: Haverkamp clay data

- H (m)	k_r	S
0.00E+00	1.0	1.0
2.00E-01	0.3829	0.9263
4.00E-01	0.1539	0.8498
6.00E-01	8.15E-02	0.7935
8.00E-01	0.05064	0.7505
1.00E+00	0.03469	0.7164
1.20E+00	0.02536	0.6886
1.40E+00	0.01942	0.6653
1.60E+00	0.0154	0.6454
1.80E+00	0.01254	0.6283
2.00E+00	0.01043	0.6132
2.20E+00	0.008822	0.5999
2.40E+00	0.004573	0.588
2.60E+00	0.006579	0.5773
2.80E+00	0.005775	0.5675
3.00E+00	0.005114	0.5587
3.20E+00	0.004565	0.5505
3.40E+00	0.004102	0.543
3.60E+00	0.003709	0.5361
3.80E+00	0.003372	0.5297

Tab. C2.3: Input data for case C2

Step	Time (day)
2	<i>Steady state</i>
107	2.32
150	4.63
193	6.95
236	9.26
279	11.58
322	13.89
365	16.21
623	32.41
655	<i>Steady state</i>

**Fig. C2.2:** Active pore pressure in time vs height in PLAXIS 2D**Fig. C2.3:** Degree of saturation in time vs height in PLAXIS 2D

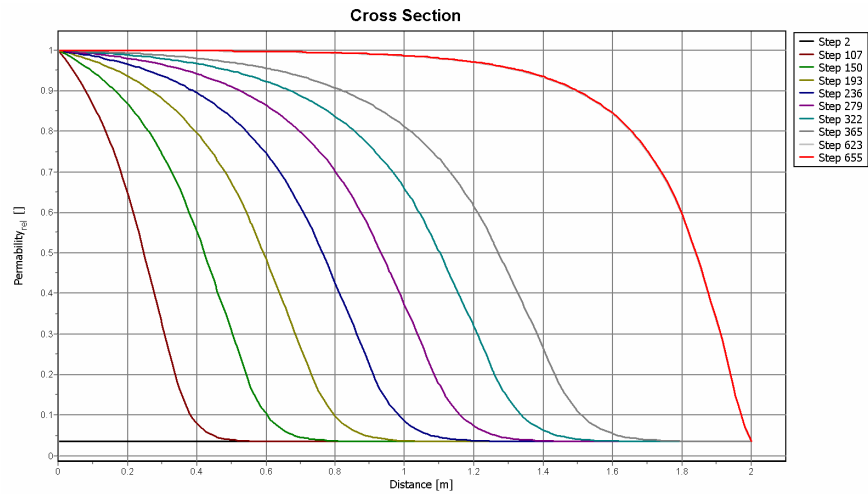


Fig. C2.4: Relative permeability in time vs height in PLAXIS 2D

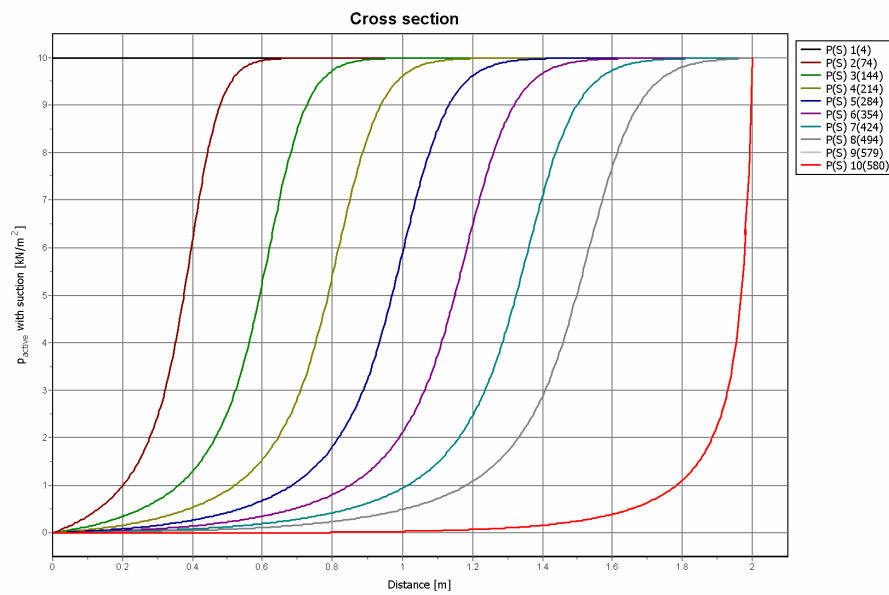


Fig. C2.5: Active pore pressure in time vs height in PLAXIS 3D

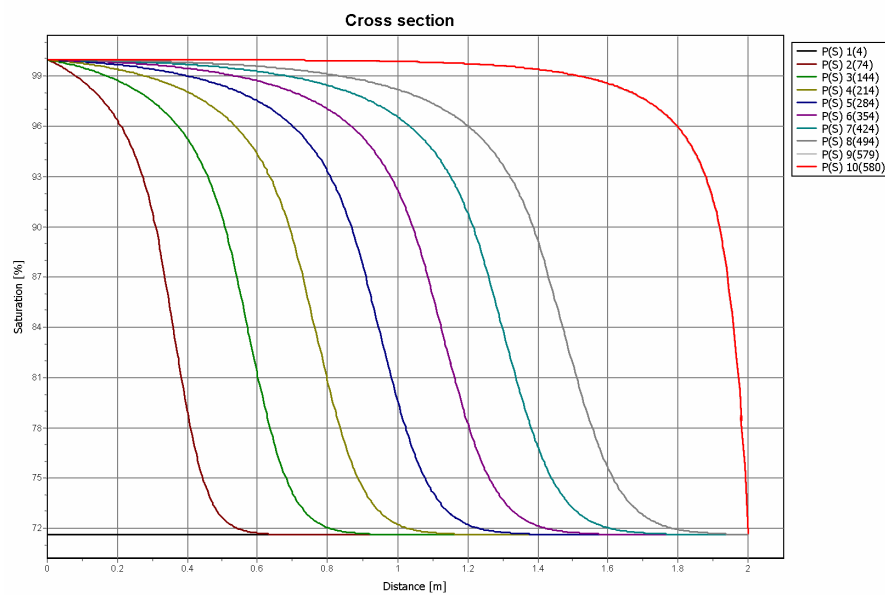


Fig. C2.6: Degree of saturation in time vs height in PLAXIS 3D

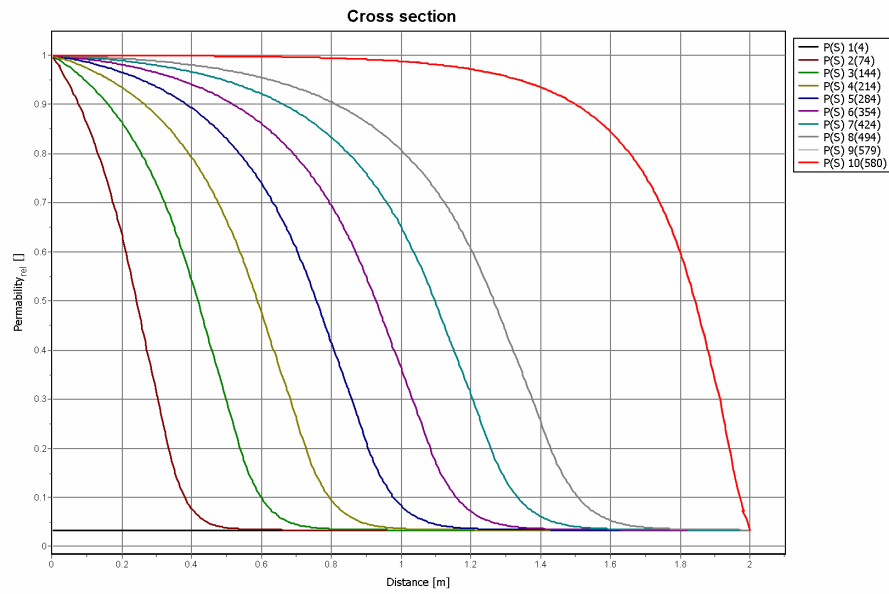


Fig. C2.7: Relative permeability in time vs height in PLAXIS 3D

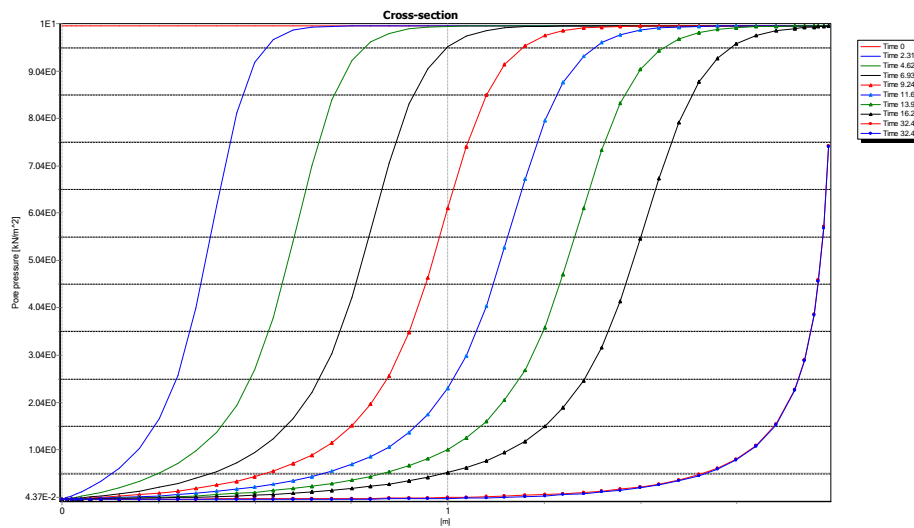


Fig. C2.8: Active pore pressure in time vs height (existing PlaxFlow)

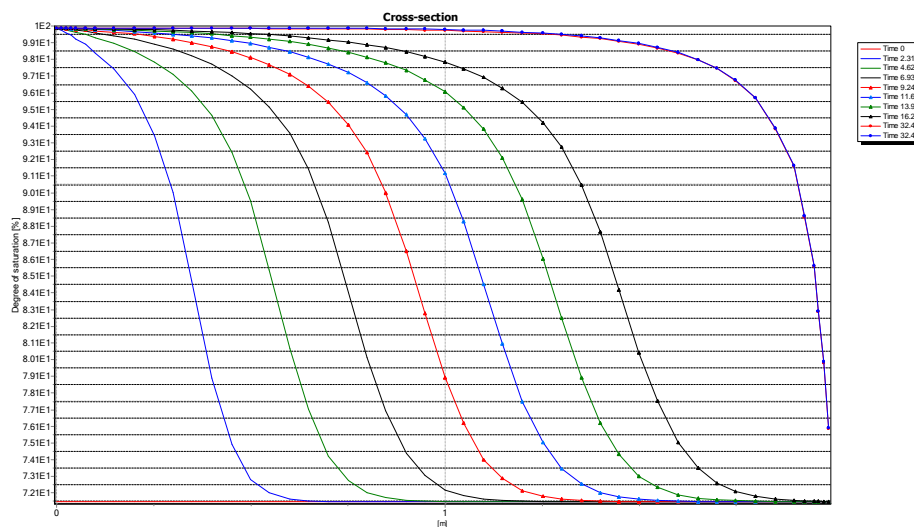


Fig. C2.9: Degree of saturation in time vs height (existing PlaxFlow)

Summary:

As seen the results from PLAXIS 2D, PLAXIS 3D and PlaxFlow are similar.

7.8 Case C3: material contrast high-low permeability

Case C3 involves an infiltration problem through a column composed of a sand layer on top of a clay layer as shown in Figure C3.1. The left picture presents the initial boundary conditions from which a steady state flow situation is calculated. Imposing a head of -1.0 m at the bottom of the model and 1.0 m at the top generates unsaturated starting conditions. The right hand side picture shows the boundary conditions for the later time period. Boundary conditions change to 2.0 m at the top of the model, the bottom condition is not changed. Haverkamp clay and Haverkamp sand models describe hydraulic behaviour of clay and sand materials for which cubic Hermit spline interpolation are applied. The properties of the layers are given in Table C1.1, Table C1.2, Table C2.1 and Table C2.2.

The following steps are performed in this case:

10. *Steady state*: Steady state groundwater flow calculation to generate initial pore pressure.
11. *Transient*: The top boundary head is set. Infiltration takes place and the model gets more saturated in time. The infiltration front move downward in time until a new steady state situation is reached. Figure C3.2 to C3.4 show a vertical cross section of the calculated pore pressures, degree of saturation and relative permeability in time. The infiltration profiles are shown for steps given in Table C3.1.
12. *Steady state*: Steady state groundwater flow calculation to generate ultimate pore pressure.

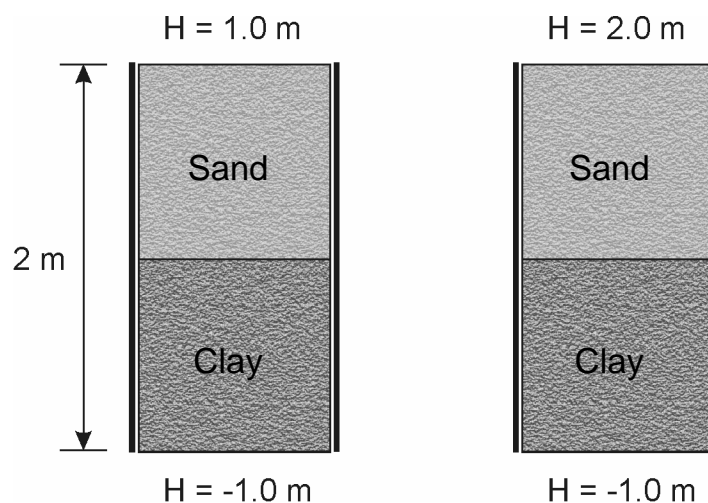
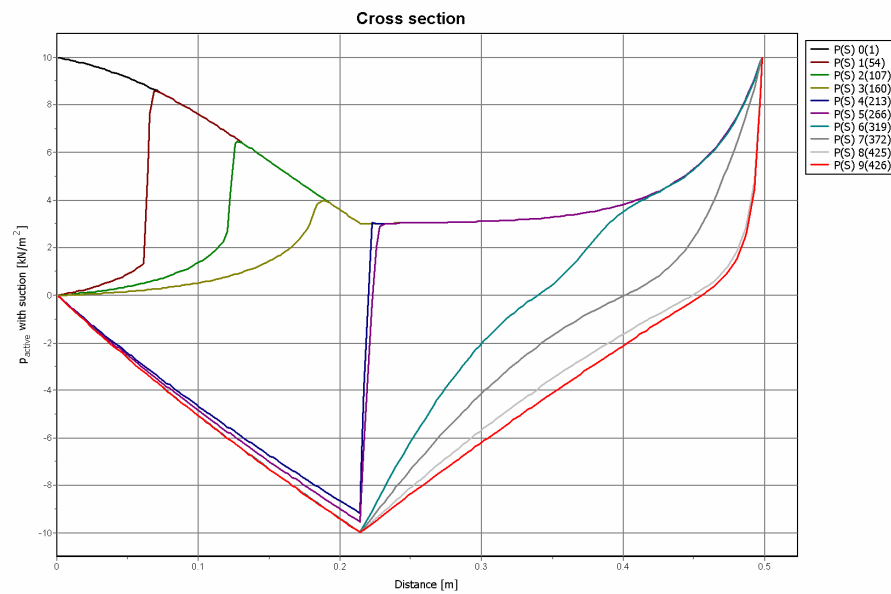


Fig. C4.1: Geometry of case C3

Tab. C3.1: Input data for case C3

Step	Time (day)
14	<i>Steady state</i>
40	<i>0.00463</i>
58	<i>0.00926</i>
76	<i>0.0139</i>
94	<i>0.0185</i>
107	<i>0.0232</i>
141	<i>1.07</i>
177	<i>2.22</i>
240	<i>4.54</i>
261	<i>Steady state</i>

**Fig. C3.2:** Active pore pressure in time vs height in PLAXIS 2D

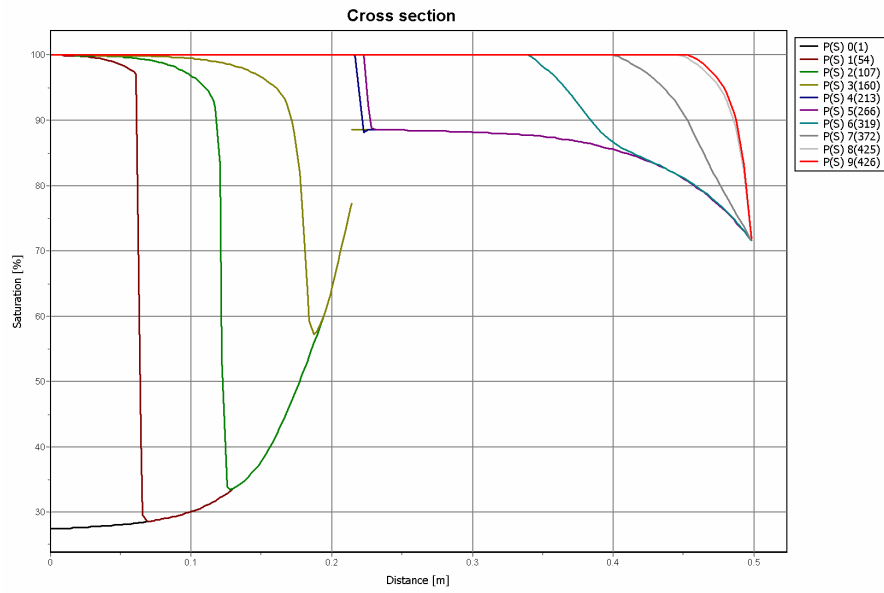


Fig. C3.3: Degree of saturation in time vs height in PLAXIS 2D

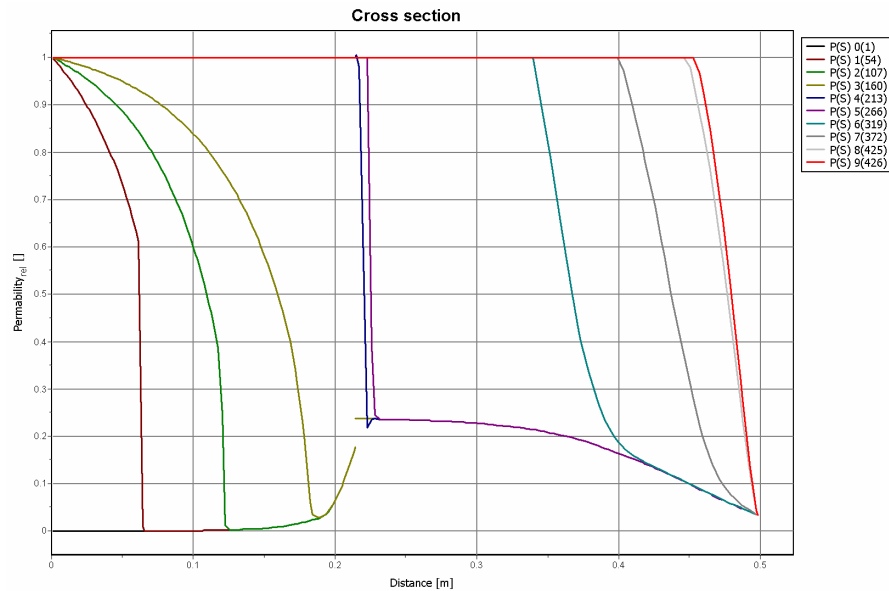


Fig. C3.4: Relative permeability in time vs height in PLAXIS 2D

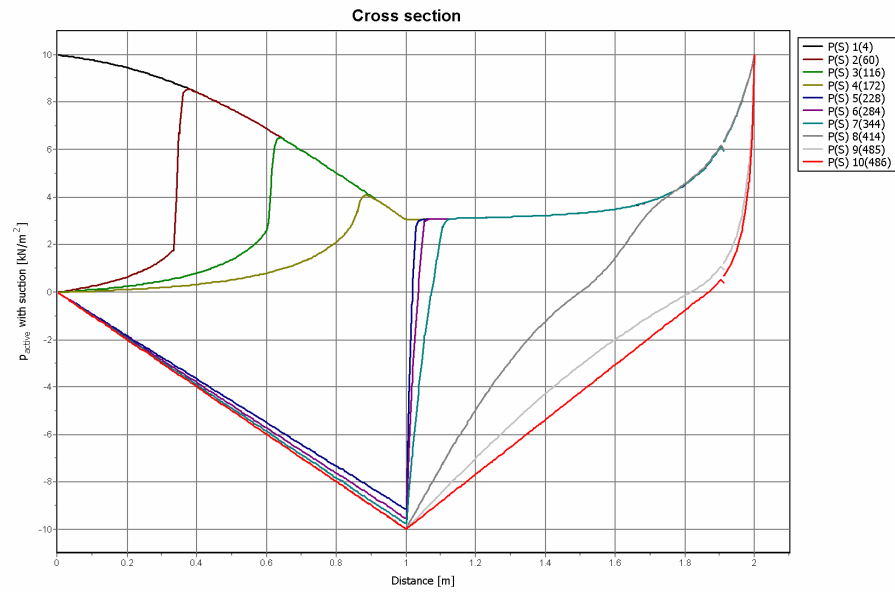


Fig. C3.5: Active pore pressure in time vs height in PLAXIS 3D

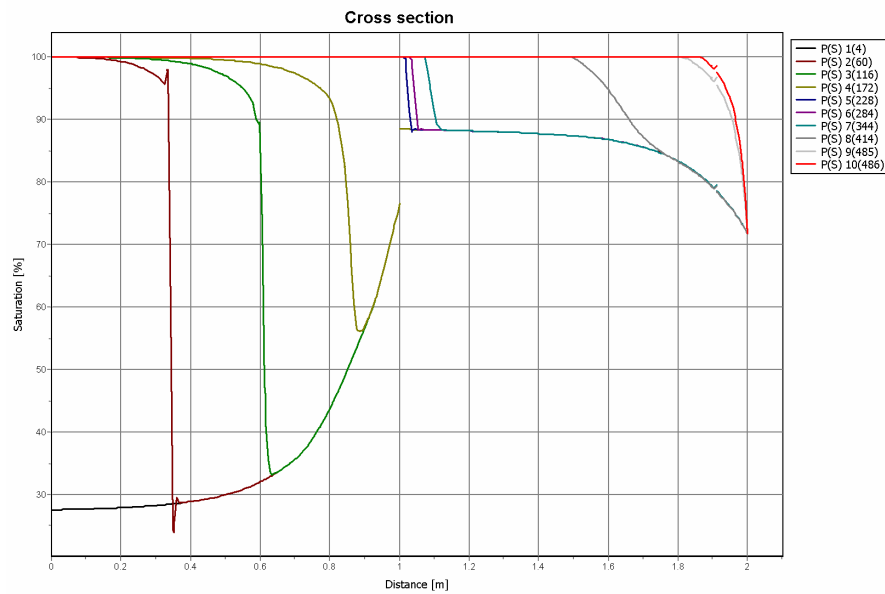


Fig. C3.6: Degree of saturation in time vs height in PLAXIS 3D

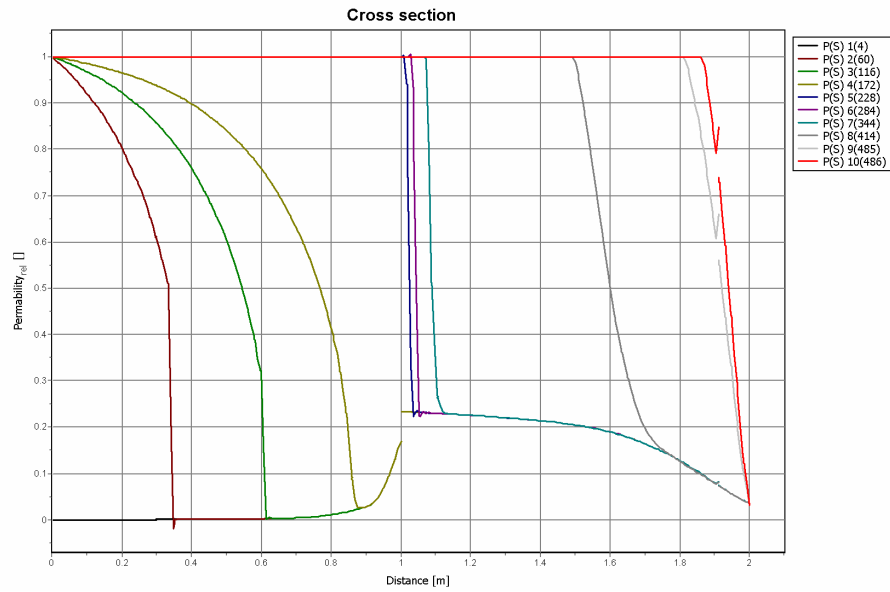


Fig. C3.7: Relative permeability in time vs height in PLAXIS 3D

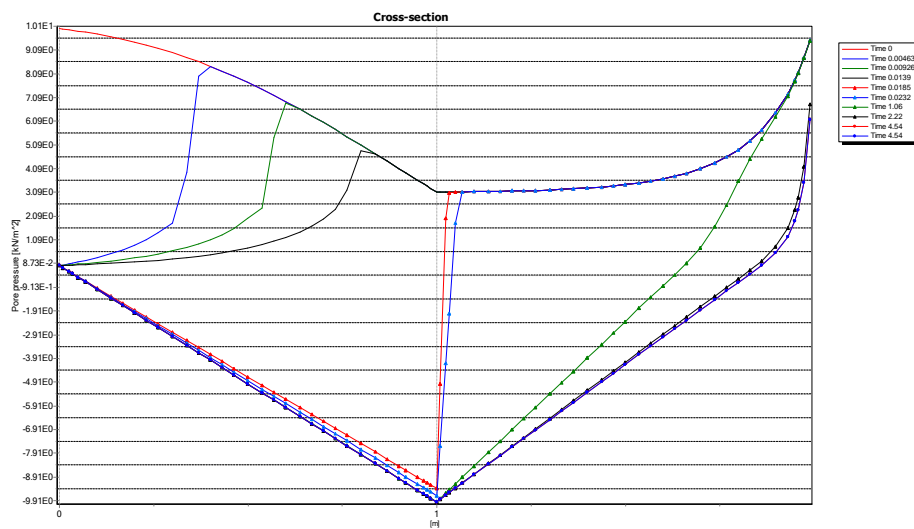


Fig. C3.8: Active pore pressure in time vs height (existing PlaxFlow)

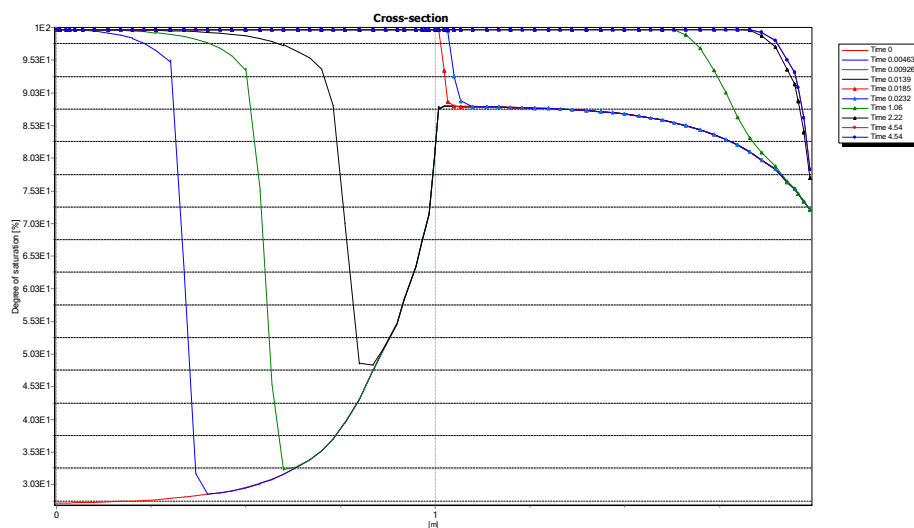


Fig. C3.9: Degree of saturation in time vs height (existing PlaxFlow)

Summary:

As seen the results from PLAXIS 2D, PLAXIS 3D and PlaxFlow are similar.

7.9 Case C4: material contrast low- high permeability

Case C4 involves an infiltration problem through a column composed of a clay layer on top of a sand layer as shown in Figure C4.1. The left picture presents the initial boundary conditions from which a steady state flow situation is calculated. Imposing a head of -1.0 m at the bottom of the model and 1.0 m at the top generates unsaturated starting conditions. The right hand side picture shows the boundary conditions for the later time period. Boundary conditions change to 2.0 m at the top of the model, the bottom condition is not changed. Haverkamp clay and Haverkamp sand models describe hydraulic behaviour of clay and sand materials for which cubic Hermit spline interpolation are applied. The properties of the layers are given in Table C1.1, Table C1.2, Table C2.1 and Table C2.2.

The following steps are performed in this case:

13. *Steady state*: Steady state groundwater flow calculation to generate initial pore pressure.
14. *Transient*: The top boundary head is set. Infiltration takes place and the model gets more saturated in time. The infiltration front move downward in time until a new steady state situation is reached. Figure C4.2 to C4.4 show a vertical cross section of the calculated pore pressures, degree of saturation and relative permeability in time. The infiltration profiles are shown for steps given in Table C4.1.
15. *Steady state*: Steady state groundwater flow calculation to generate ultimate pore pressure.

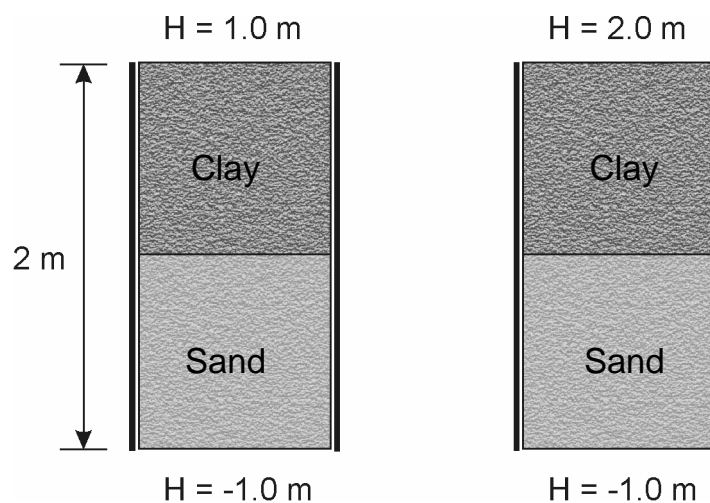
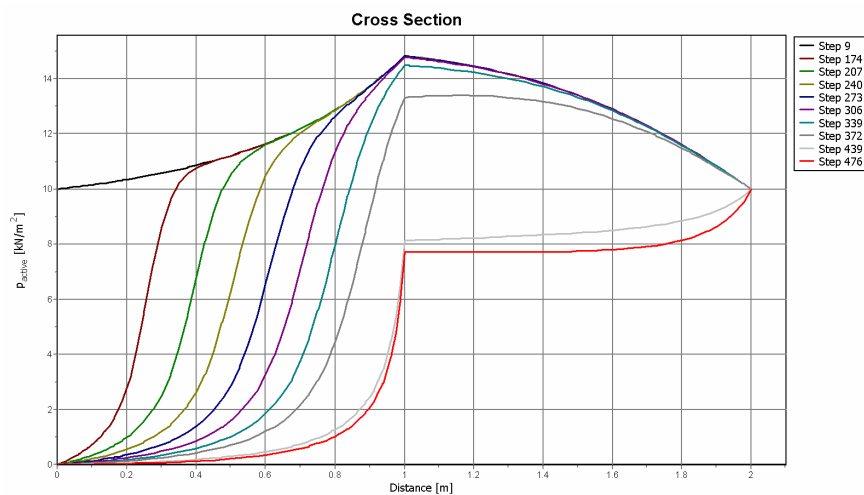
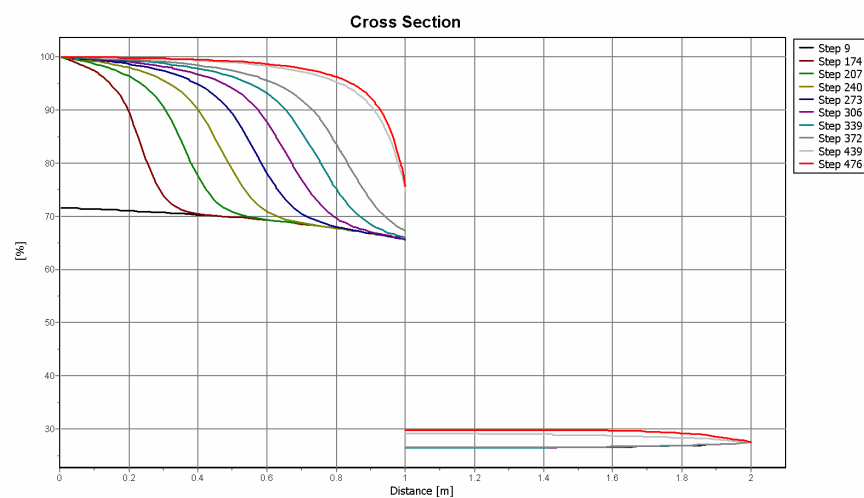


Fig. C4.1: Geometry of case C4

Tab. C4.1: Input data for case C4

Step	Time (day)
9	<i>Steady state</i>
174	<i>1.157</i>
207	<i>2.314</i>
240	<i>3.471</i>
273	<i>4.628</i>
306	<i>5.785</i>
339	<i>6.942</i>
372	<i>8.099</i>
439	<i>11.571</i>
476	<i>Steady state</i>

**Fig. C4.2:** Active pore pressure in time vs height in PLAXIS 2D**Fig. C4.3:** Degree of saturation in time vs height in PLAXIS 2D

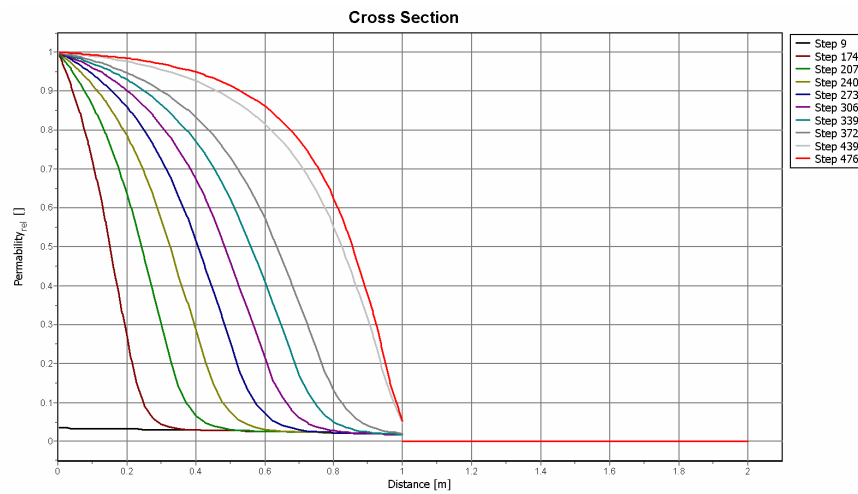


Fig. C4.4: Relative permeability in time vs height in PLAXIS 2D

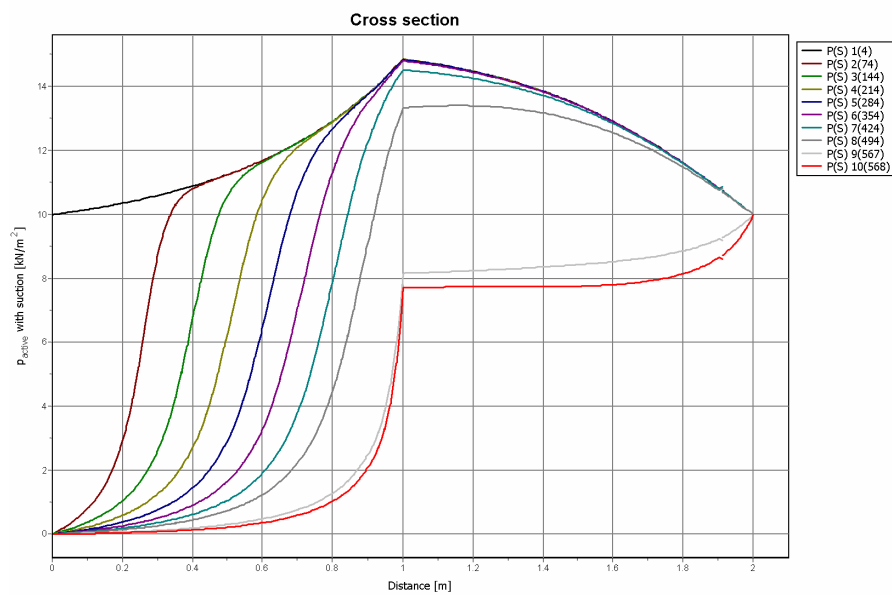


Fig. C4.5: Active pore pressure in time vs height in PLAXIS 3D

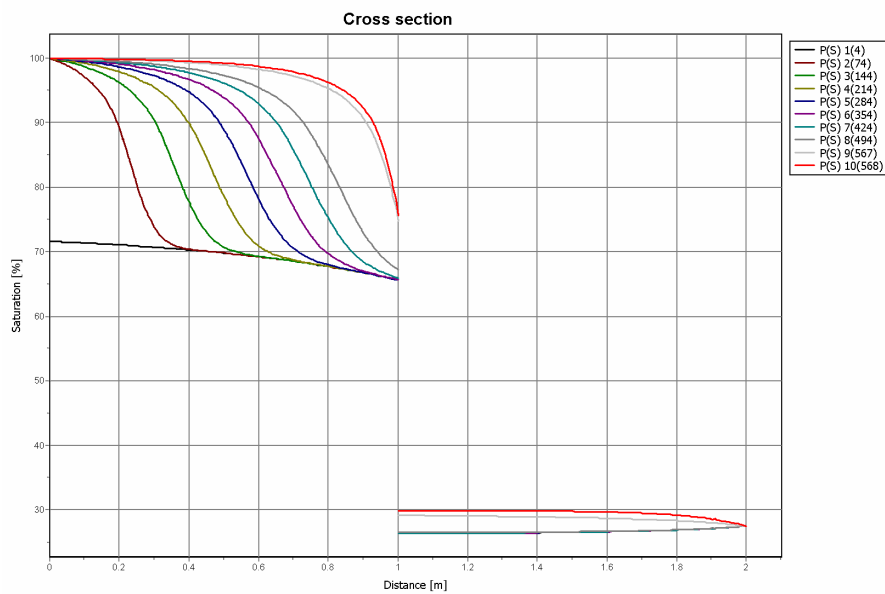


Fig. C4.6: Degree of saturation in time vs height in PLAXIS 3D

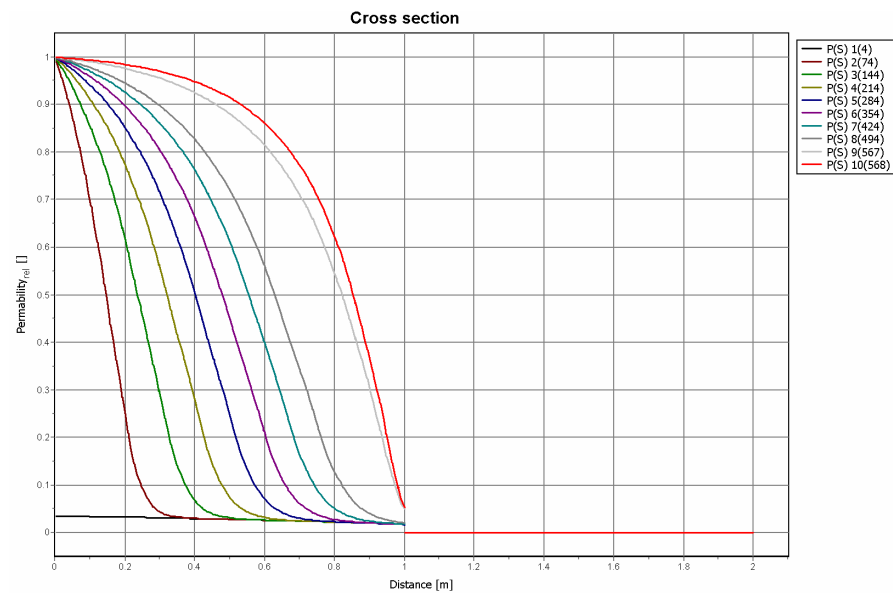


Fig. C4.7: Relative permeability in time vs height in PLAXIS 3D

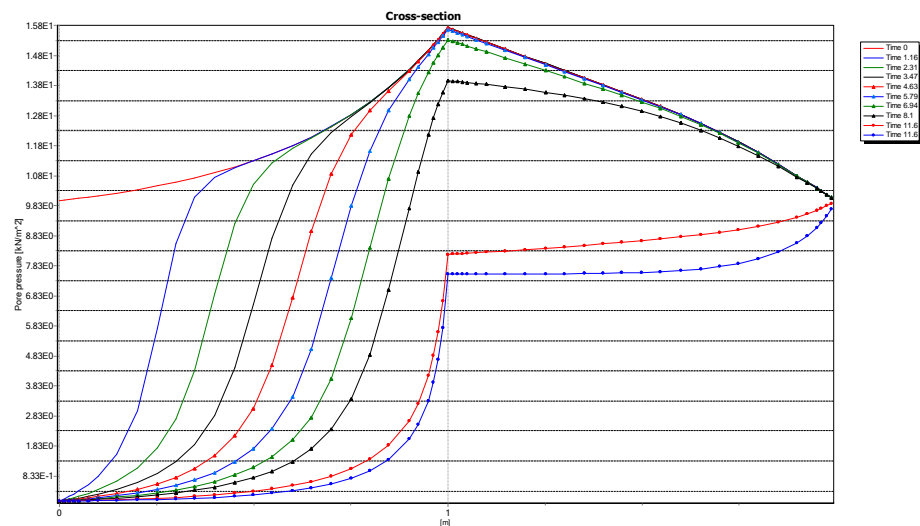


Fig. C4.8: Active pore pressure in time vs height (existing PlaxFlow)

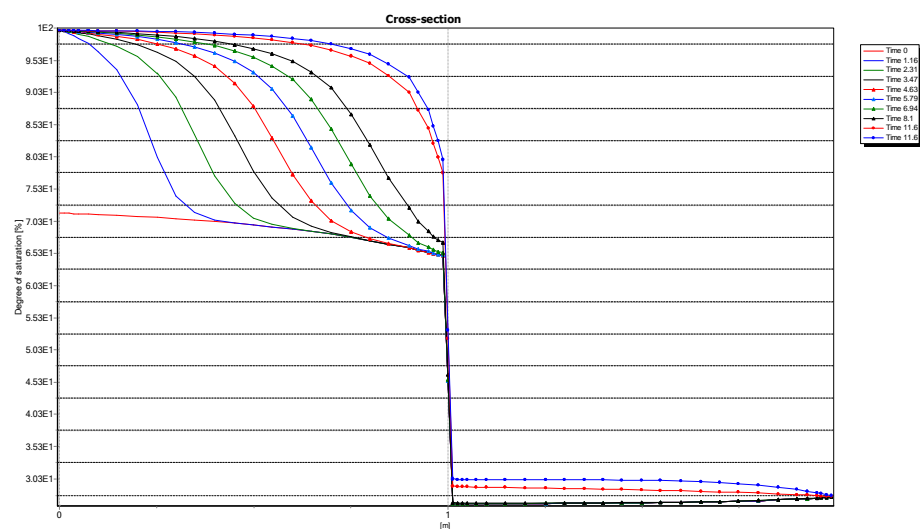


Fig. C4.9: Degree of saturation in time vs height (existing PlaxFlow)

Summary:

As seen the results from PLAXIS 2D, PLAXIS 3D and PlaxFlow are similar.

7.10 Case D1: Seepage face boundary

Case D1 involves a seepage problem and is shown in Figure D1.1. In this example the column is wetted from the bottom in opposite direction of the gravitational force. The left picture presents the initial boundary conditions from which suction pore pressure of 0 kPa at the bottom and 20 kPa at the top are generated. This is performed by imposing a head of 0 m at the bottom of the model and a seepage boundary condition at the top of the column. The middle and the right hand side pictures show the boundary condition used for later stages. For $t=0$ to 4.053 day the middle model is applied, in which a head of 3.0 m is imposed for the head of the bottom boundary, and then the head boundary at the bottom is changed to 0 m. The seepage boundary condition prescribes a closed boundary condition as long as the condition remains unsaturated, the condition changes to a pressure 0 Pa condition when the boundary starts to become saturated. For this condition, outflow may occur. Staring series O1 sand model describes hydraulic behaviour of material for which Van Genuchten relationship is applied. The properties of the soil are given in Table D1.1.

The following steps are performed in this case:

1. *Steady state*: Steady state groundwater flow calculation to generate initial pore pressure.
2. *Transient*: The bottom head boundary is changed to 3.0 for time until 4.053 day and then is changed to 0. Wetting and drying takes place. Figure D1.2 and D1.3 show a vertical cross section of the calculated pore pressures and degree of saturation in time. The results are shown for steps given in Table D1.2.

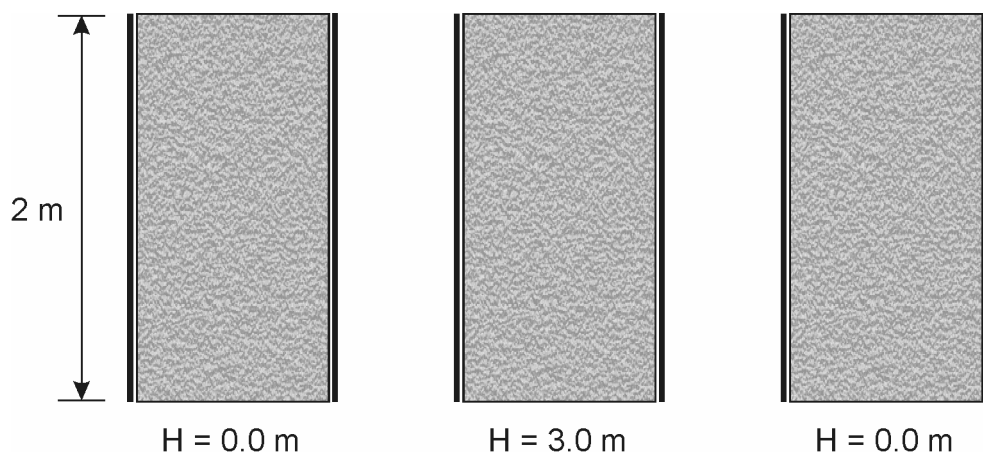


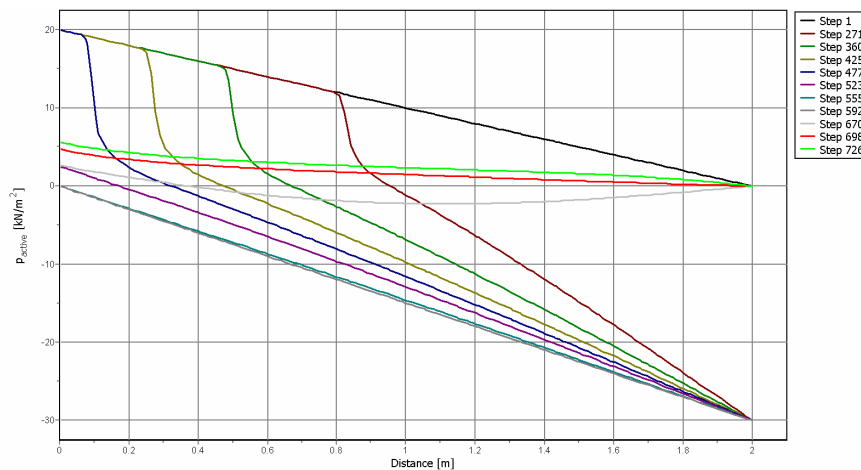
Fig. D1.1: Geometry of case D1

Tab. D1.1: Input data for case D1

Description	Symbol	Unit	Value
Permeability	k_x, k_y, k_z	[m/day]	0.1521
initial void ratio	e_{init}	[-]	0.5625
Elastic storage	$K_{w,ref}/n$	[kN/m ²]	98.39
Saturated saturation	S_{sat}	[-]	1.0
Residual saturation	S_{res}	[-]	0.06203
Van Genuchten	g_n	[-]	2.286
Van Genuchten	g_a	[m ⁻¹]	2.24
Van Genuchten	g_l	[-]	0

Tab. D1.2: Input data for case D1

Step	Time (day)
1	<i>Steady state</i>
271	<i>0.579</i>
360	<i>1.158</i>
425	<i>1.737</i>
477	<i>2.316</i>
523	<i>2.895</i>
555	<i>3.474</i>
592	<i>4.053</i>
670	<i>4.632</i>
698	<i>5.211</i>
726	<i>5.790</i>

**Fig. D1.2:** Active pore pressure in time vs height in PLAXIS 2D

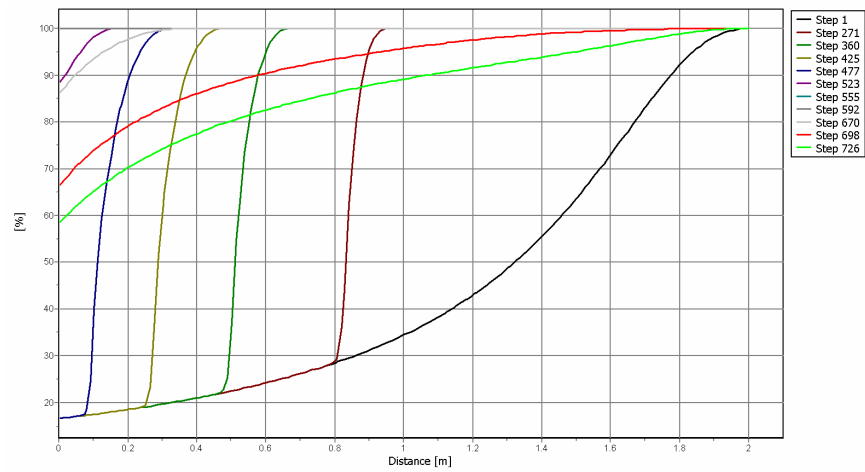


Fig. D1.3: Degree of saturation in time vs height in PLAXIS 2D

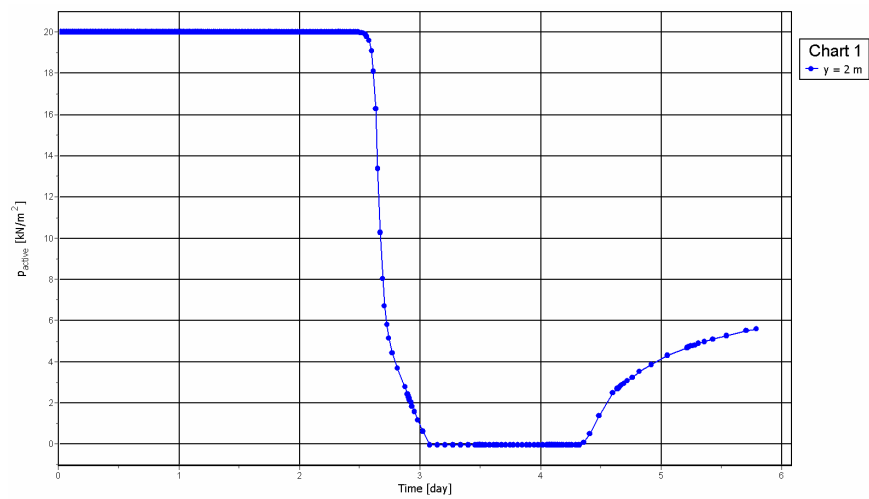


Fig. D1.4: Pore pressure at the Gauss point at the top of the column in time in PLAXIS 2D

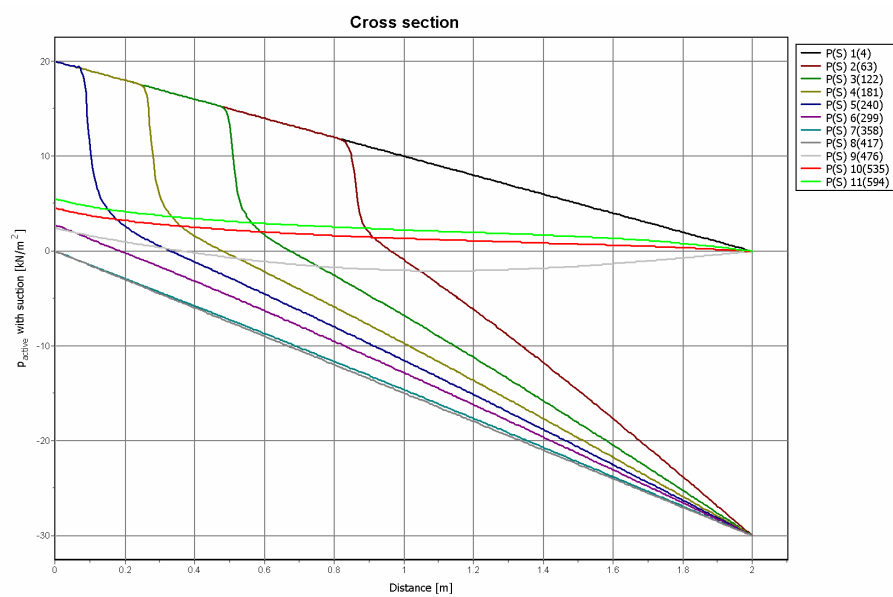


Fig. D1.5: Active pore pressure in time vs height in PLAXIS 3D

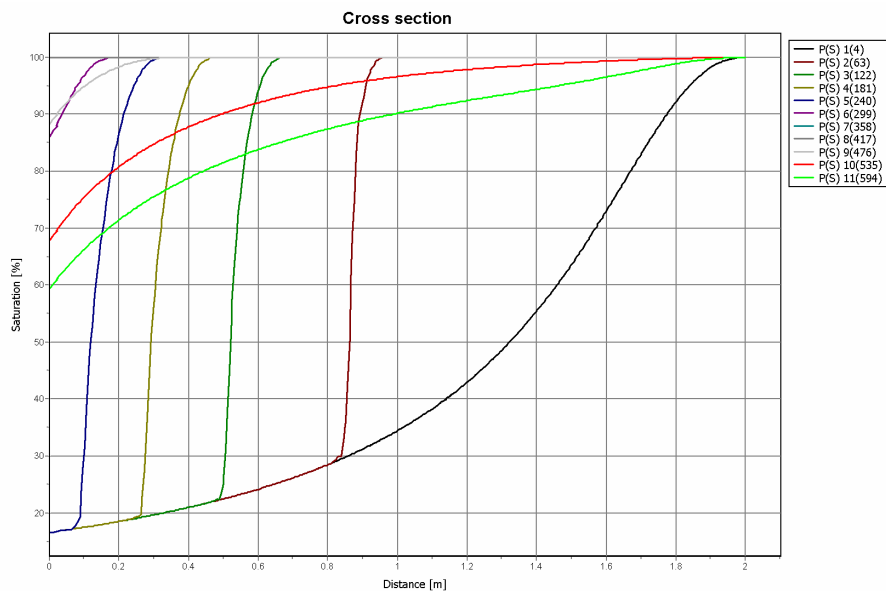


Fig. D1.6: Degree of saturation in time vs height in PLAXIS 3D

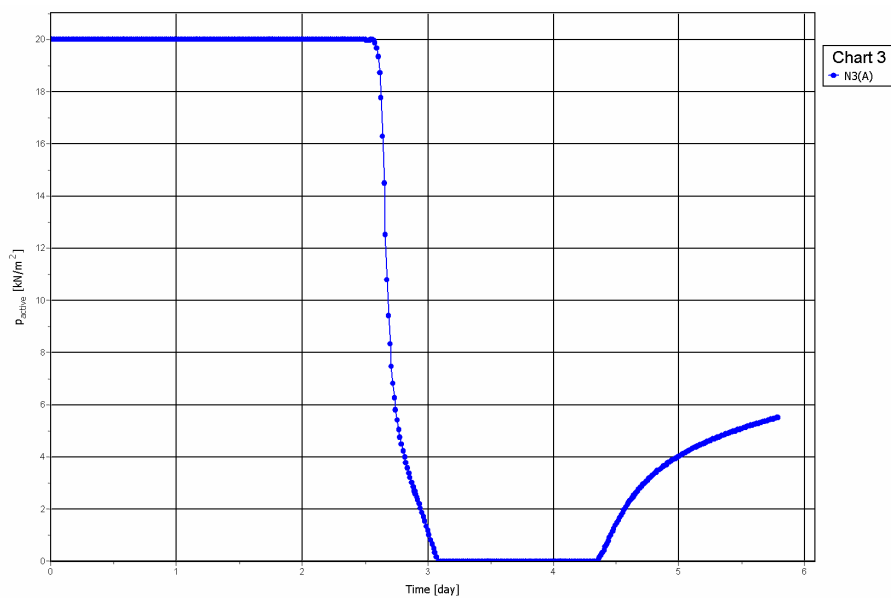


Fig. D1.7: Pore pressure at the Gauss point at the top of the column in time in PLAXIS 3D

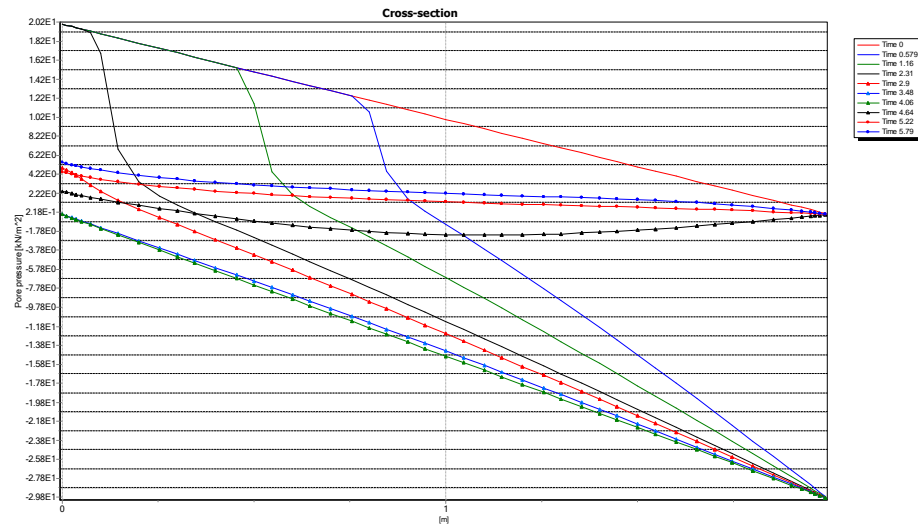


Fig. D1.8: Active pore pressure in time vs height (existing PlaxFlow)

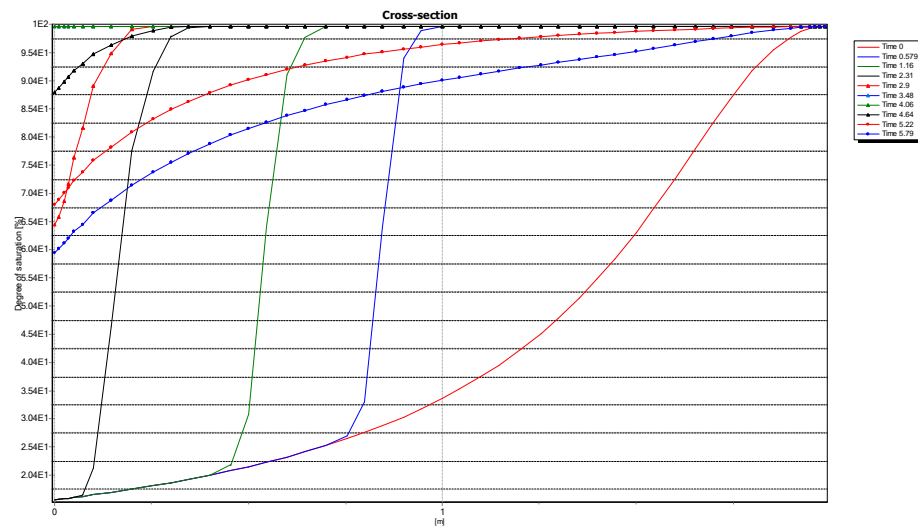


Fig. D1.9: Degree of saturation in time vs height (existing PlaxFlow)

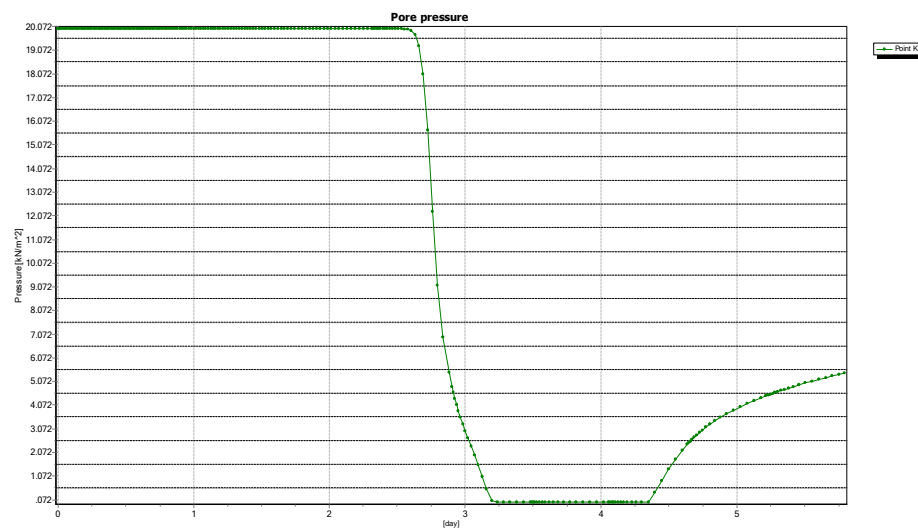


Fig. D1.10: Pore pressure at the Gauss point at the top of the column in time (existing PlaxFlow)

Summary:

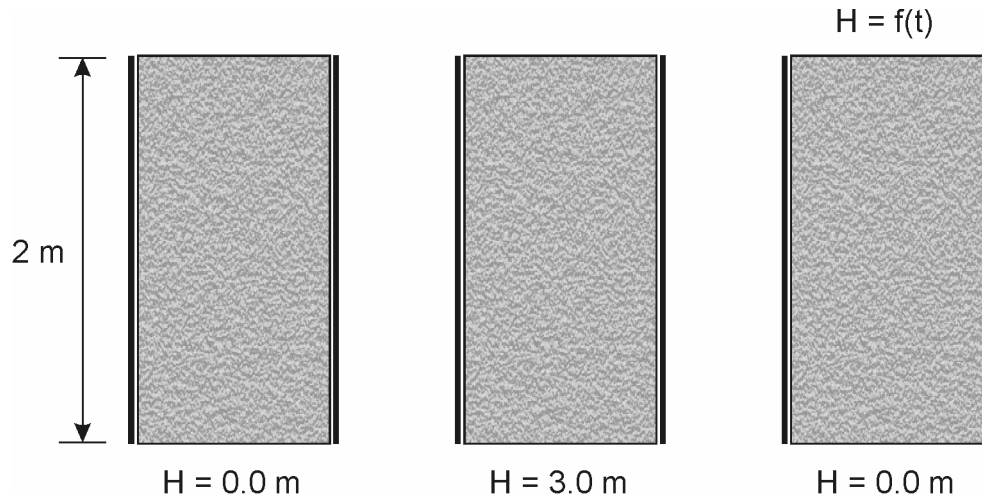
As seen the results from PLAXIS 2D, PLAXIS 3D and PlaxFlow are similar.

7.11 Case D2: Generalised seepage face boundary

Case D2 involves a generalised seepage problem and is shown in Figure D2.1. In this example the column is wetted from the bottom in opposite direction of the gravitational force. When the column is fully saturated, the top boundary is imposed to a harmonic head variation and simultaneously the column is imposed drainage from the bottom boundary. The left picture presents the initial boundary conditions from which suction pore pressure of 0 kPa at the bottom and 20 kPa at the top are generated. This is performed by imposing a head of 0 m at the bottom of the model and a seepage boundary condition at the top of the column. The middle and the right hand side pictures show the boundary condition used for later stages. For $t=0$ to 4.053 day the middle model is applied, in which a head of 3.0 m is imposed for the head of the bottom boundary and a seepage boundary condition with constant head is applied to the top boundary. The seepage boundary condition prescribes a closed boundary condition as long as the condition remains unsaturated, the condition changes to a pressure 0 Pa condition when the boundary starts to become saturated. For this condition, outflow may occur. After this stage ($t>4.053$ day) the right boundary conditions are plied, i.e. the bottom head is set to 0 and a seepage boundary condition with harmonic head is applied to the top boundary. As long as the top boundary is wet, the harmonic head is applied and when suction occurs the boundary becomes closed. For the harmonic function, $H=0.4$ m, $\omega_0 = 4.52$ rad/day ($T=1.39$ day) and $\phi_0=0$. Staring series O1 sand model describes hydraulic behaviour of material for which Van Genuchten relationship is applied. The properties of the soil are given in Table D2.1.

The following steps are performed in this case:

1. *Steady state*: Steady state groundwater flow calculation to generate initial pore pressure.
2. *Transient*: The bottom head boundary is changed to 3.0 for time until 4.053 day and a seepage boundary condition is applied to the top.
3. *Transient*: The bottom head boundary is changed to 0.0 for time greater than 4.053 day and a seepage boundary condition with harmonic head is applied to the top.

**Fig. D2.1:** Geometry of case D2**Tab. D2.1:** Input data for case D2

Description	Symbol	Unit	Value
Permeability	k_x, k_y, k_z	[m/day]	0.1521
initial void ratio	e_{init}	[-]	0.5625
Elastic storage	$K_{w,ref}/n$	[kN/m ²]	98.39
Saturated saturation	S_{sat}	[-]	1.0
Residual saturation	S_{res}	[-]	0.06203
Van Genuchten	g_n	[-]	2.286
Van Genuchten	g_a	[m ⁻¹]	2.24
Van Genuchten	g_l	[-]	0

Tab. D2.2: Input data for case D2

Step	Time (day)
1	<i>Steady state</i>
163	<i>0.579</i>
279	<i>1.158</i>
291	<i>1.737</i>
331	<i>2.316</i>
354	<i>2.895</i>
357	<i>3.474</i>
360	<i>4.053</i>
432	<i>4.632</i>
451	<i>5.211</i>
470	<i>5.790</i>

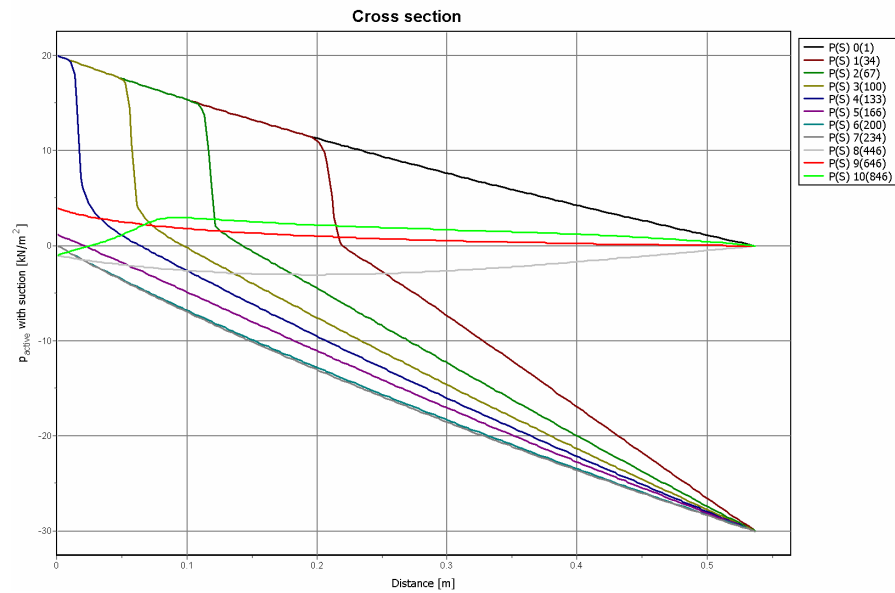


Fig. D2.2: Active pore pressure in time vs height in PLAXIS 2D

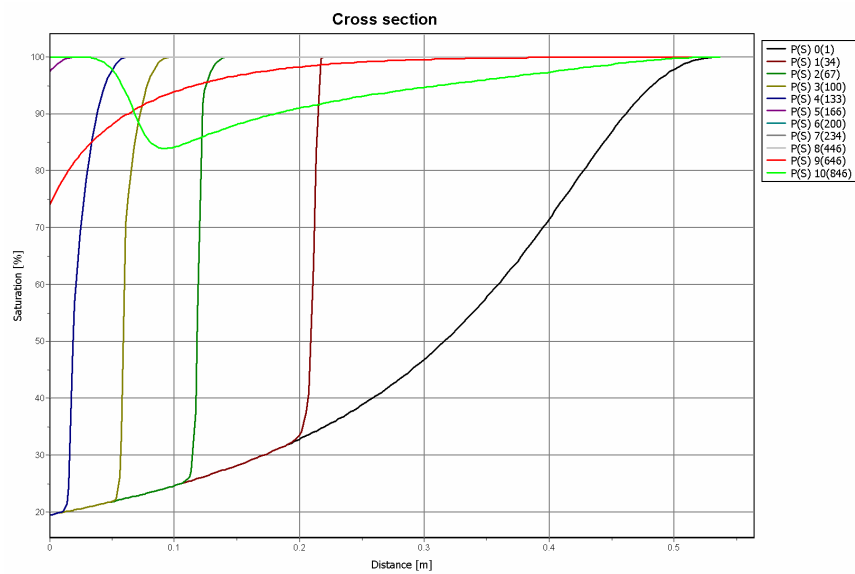


Fig. D2.3: Degree of saturation in time vs height in PLAXIS 2D

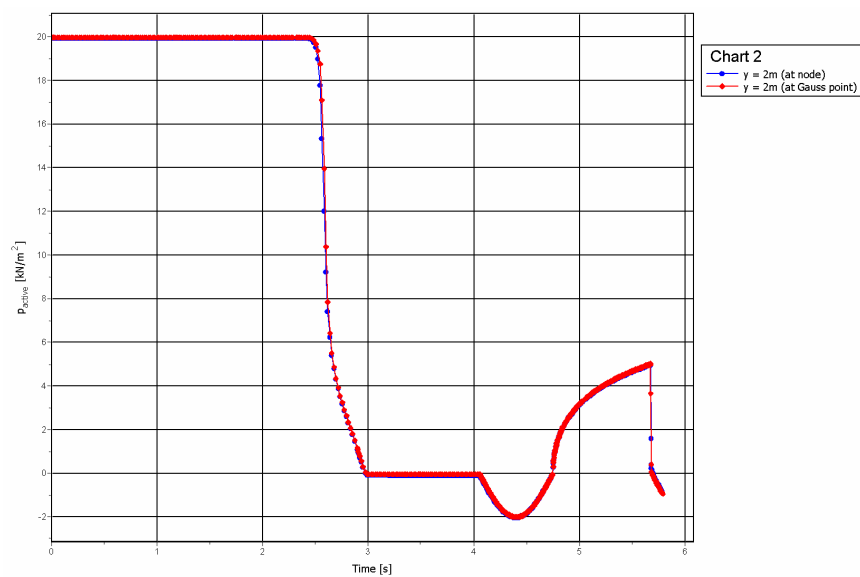


Fig. D2.4: Pore pressure the top of the column in time in PLAXIS 2D

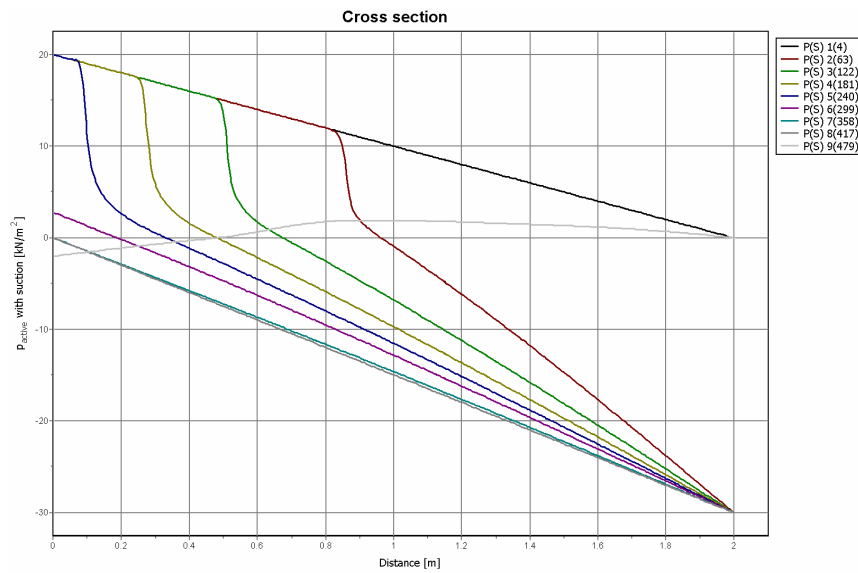


Fig. D2.5: Active pore pressure in time vs height in PLAXIS 3D

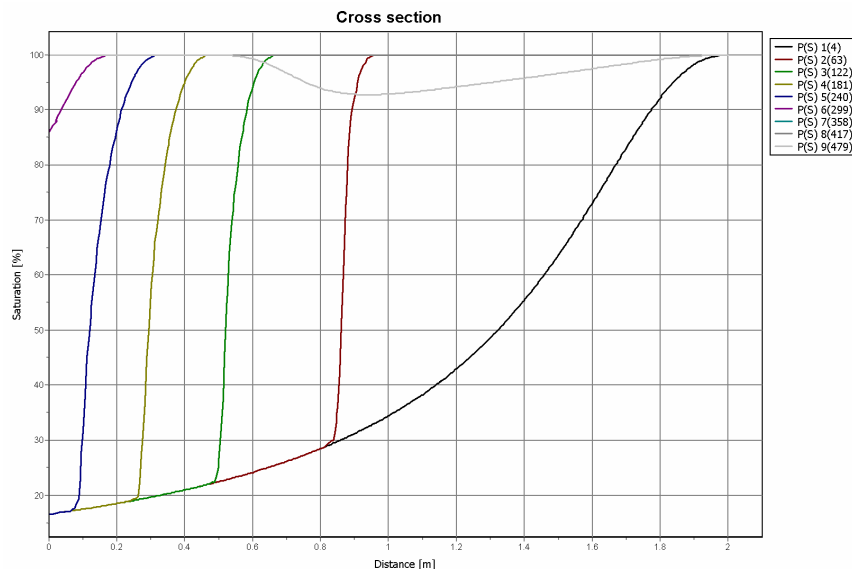


Fig. D2.6: Degree of saturation in time vs height in PLAXIS 3D

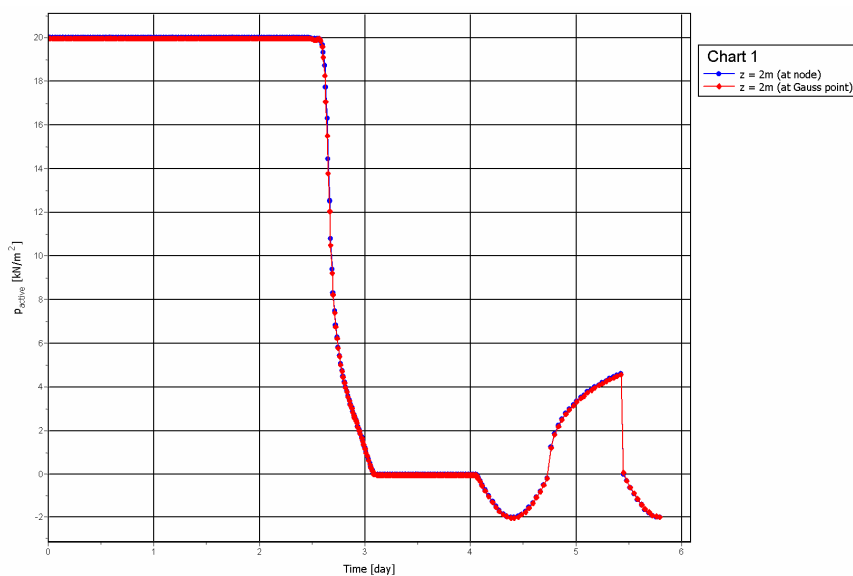


Fig. D2.7: Pore pressure the top of the column in time in PLAXIS 3D

Summary:

For this case, the existing PlaxFlow does not generate proper results and its results are different from the results of PlaxFlow verification report. However, it seems that PLAXIS 2D and PLAXIS 3D are capable of simulating this example and provide similar results to the above-mentioned report. In the case of PLAXIS 3D results at 4.632 day and 5.211 day are not shown because the harmonic phase is simulated in one phase.

7.12 Case D3: Infiltration boundary, ponding condition

Case D3 involves an infiltration problem driven by a constant influx restricted by a ponding condition as is shown in Figure D3.1. As long as the soil is able to handle the inflowing water the boundary flux will equal to the prescribed flux. As the column becomes more saturated the column capacity will decrease and depressions in the terrain get filled with water. Under these conditions the ponding depth gives the driving force. The left picture presents the initial boundary conditions from which a steady state flow situation is calculated. This condition generates suction pore pressure of 10 kPa in entire column. The right hand side picture shows the boundary condition used for later stages. Boundary conditions change to a time dependent influx given in Table D3.1 (and Figure D3.2) and restricted by a ponding depth of 0.1 m at the top of the model. The bottom condition is not altered during the simulation. Starting series O1 sand model describes hydraulic behaviour of material for which Van Genuchten relationship is applied. The properties of the soil are given in Table D3.2.

The following steps are performed in this case:

1. *Steady state*: Steady state groundwater flow calculation to generate initial pore pressure.
2. *Transient*: The top boundary is changed to prescribed flux. Figure D3.3 and D3.4 show a vertical cross section of the calculated pore pressures and degree of saturation in time. The results are shown for steps given in Table D3.3.

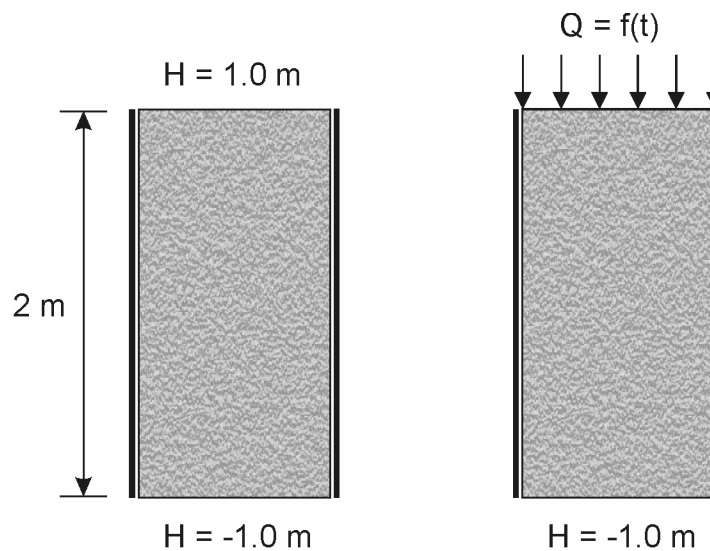
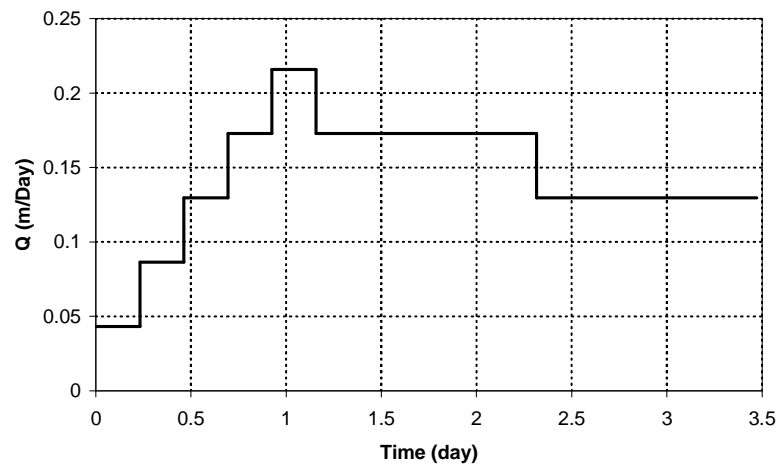


Fig. D3.1: Geometry of case D3

Tab. D3.1: Prescribed flux

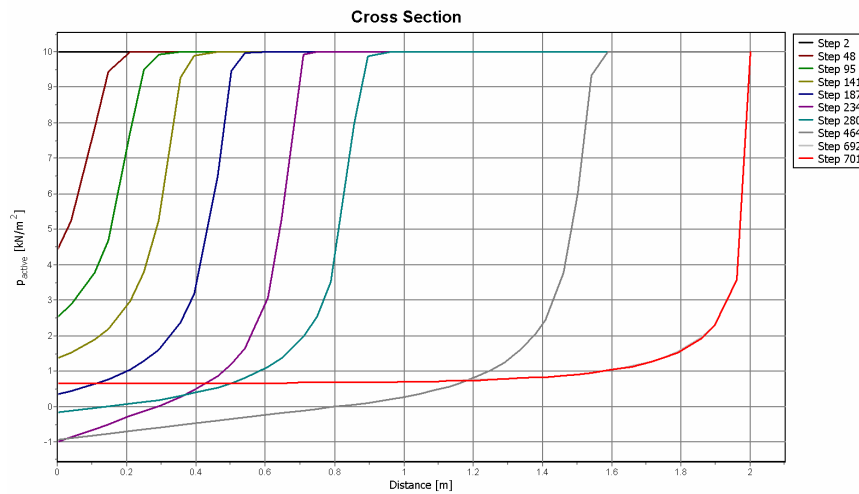
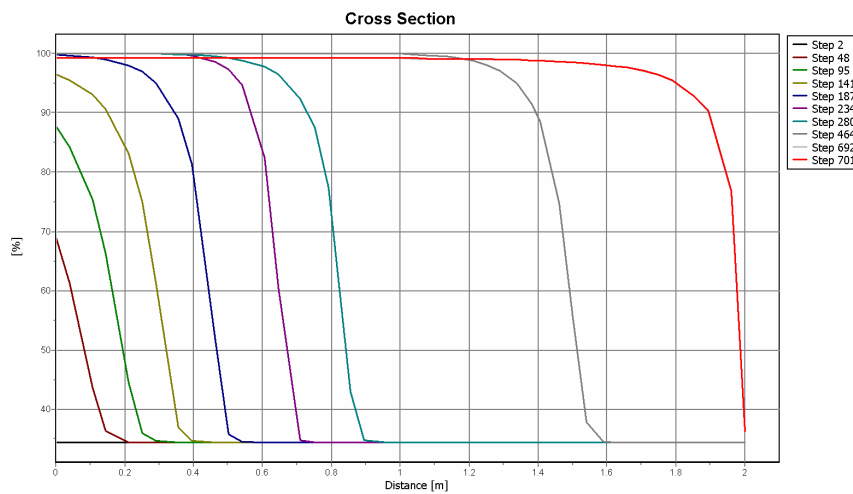
Time (day)	Q (m/day)
0	0.0432
0.2315	0.0432
0.2315	0.0864
0.463	0.0864
0.463	0.1296
0.6944	0.1296
0.6944	0.1728
0.9259	0.1728
0.9259	0.216
1.1574	0.216
1.1574	0.1728
2.3148	0.1728
2.3148	0.1296
3.4722	0.1296

**Fig. D3.2:** Prescribed flux**Tab. D3.2:** Input data for case D3

Description	Symbol	Unit	Value
Permeability	k_x, k_y, k_z	[m/day]	0.1521
initial void ratio	e_{init}	[-]	0.5625
Elastic storage	$K_{w,ref}/n$	[kN/m ²]	487.5e3
Saturated saturation	S_{sat}	[-]	1.0
Residual saturation	S_{res}	[-]	0.06203
Van Genuchten	g_n	[-]	2.286
Van Genuchten	g_a	[m ⁻¹]	2.24
Van Genuchten	g_l	[-]	0

Tab. D3.3: Input data for case D3

Step	Time (day)
2	<i>Steady state</i>
48	<i>0.23</i>
95	<i>0.465</i>
141	<i>0.695</i>
187	<i>0.925</i>
234	<i>1.16</i>
280	<i>1.39</i>
464	<i>2.31</i>
692	<i>3.45</i>
701	<i>3.494</i>

**Fig. D3.3:** Active pore pressure in time vs height in PLAXIS 2D**Fig. D3.4:** Degree of saturation in time vs height in PLAXIS 2D

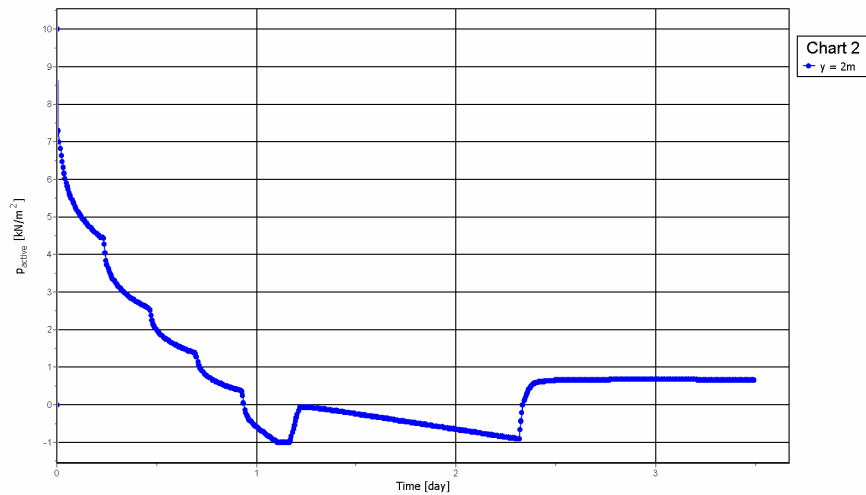


Fig. D3.5: Pore pressure at node and Gauss point at the top of the column in time in PLAXIS 2D

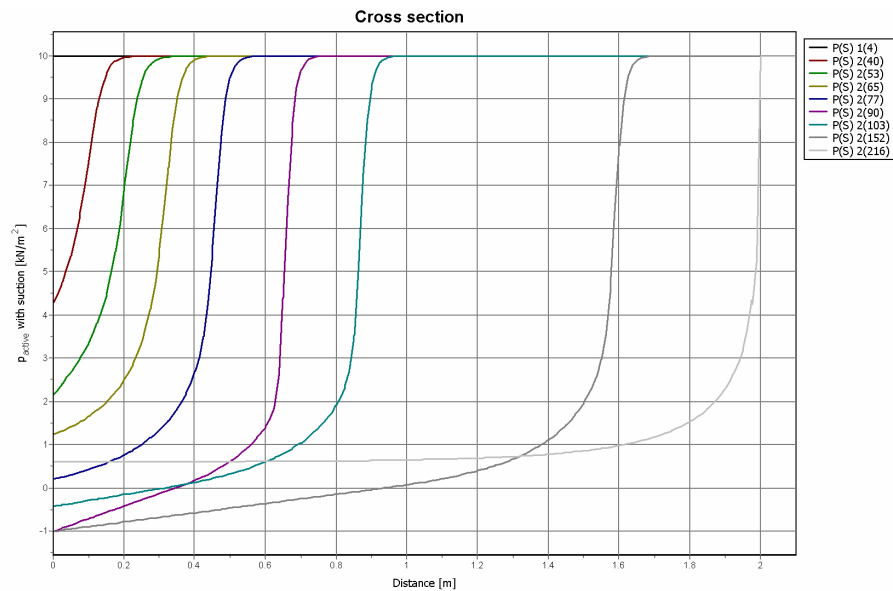


Fig. D3.6: Active pore pressure in time vs height in PLAXIS 3D

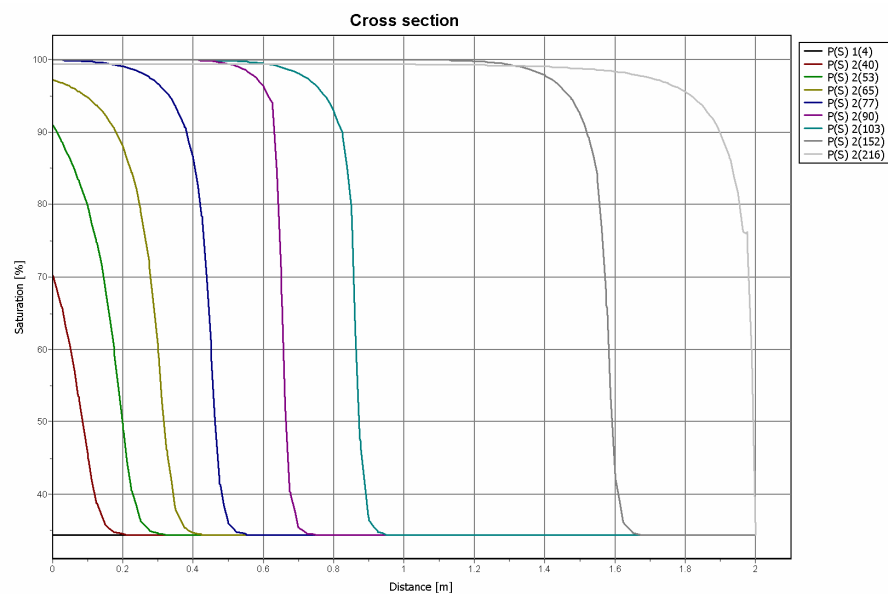


Fig. D3.7: Degree of saturation in time vs height in PLAXIS 3D

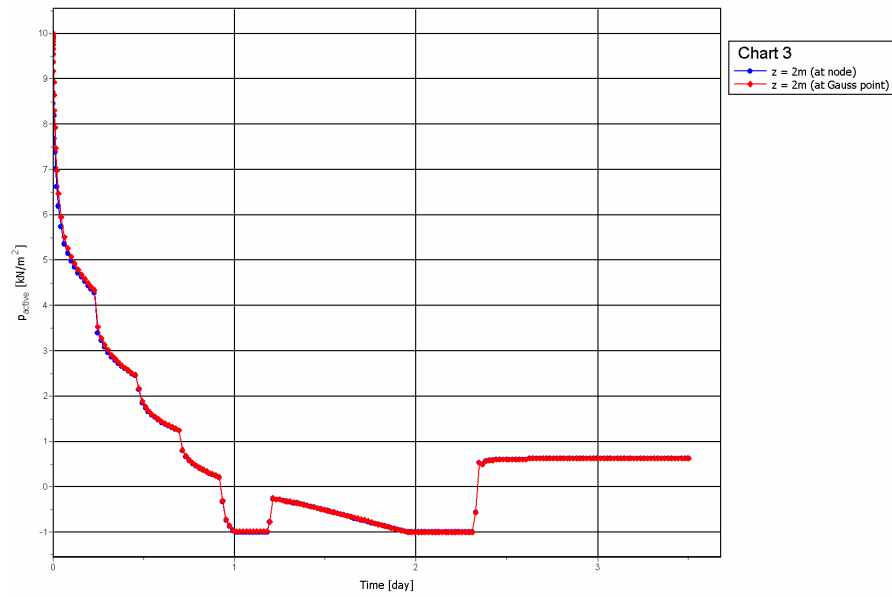


Fig. D3.8: Pore pressure at node and Gauss point at the top of the column in time in PLAXIS 3D

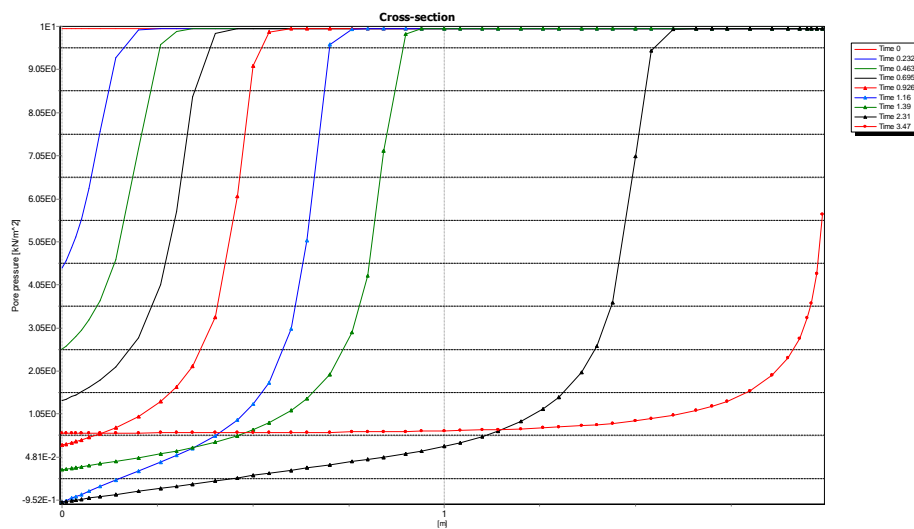


Fig. D3.9: Active pore pressure in time vs height (existing PlaxFlow)

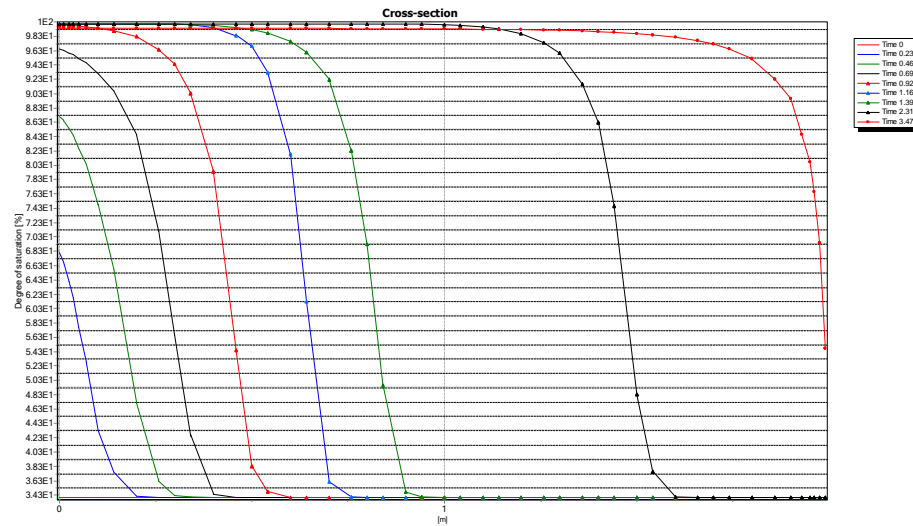


Fig. D3.10: Degree of saturation in time vs height (existing PlaxFlow)

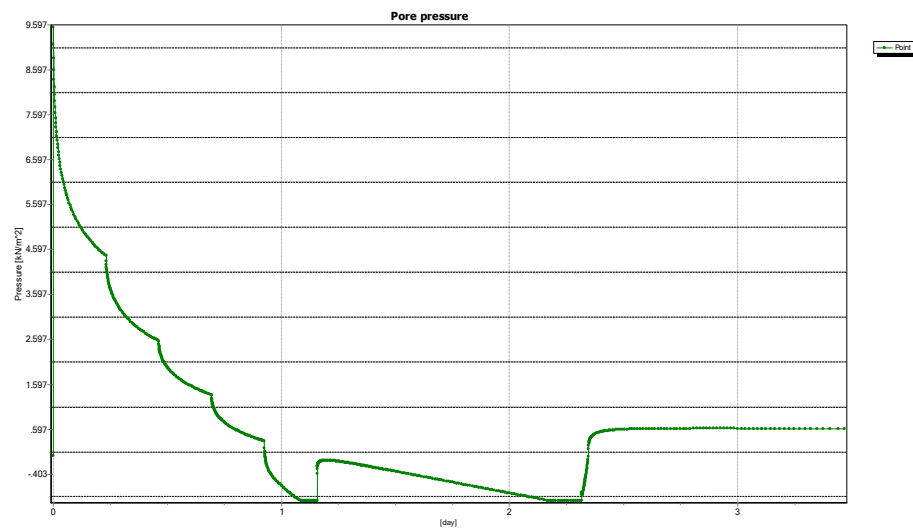


Fig. D3.11: Pore pressure at the Gauss point at the top of the column in time (existing PlaxFlow)

Summary:

As seen the results from PLAXIS 2D, PLAXIS 3D and PlaxFlow are similar.

7.13 Case D4: (evapo)transpiration boundary, ultimate condition

Case D4 involves a drying problem driven by a time dependent outflux restricted by a ponding condition as is shown in Figure D4.1. As long as the soil is able to handle the outflowing water the boundary flux will equal to the prescribed flux. As the column becomes more unsaturated the column capacity will decrease. Under these conditions the evapotranspiration depth gives the driving force. The left picture presents the initial boundary conditions from which a steady state flow situation is calculated. This condition generates suction pore pressure of 10 kPa in entire column. The right hand side picture shows the boundary condition used for later stages. Boundary conditions change to a time dependent outfluxes given in Table D4.1 (and Figure D4.2) and restricted by an evapotranspiration depth of -10. m at the top of the model. The bottom condition is not altered during the simulation. Starting series O1 sand model describes hydraulic behaviour of material for which Van Genuchten relationship is applied. The properties of the soil are given in Table D4.2.

The following steps are performed in this case:

1. *Steady state*: Steady state groundwater flow calculation to generate initial pore pressure.
2. *Transient*: The top boundary is changed to prescribed flux. Figure D4.3 and D4.4 show a vertical cross section of the calculated pore pressures and degree of saturation in time. The results are shown for steps given in Table D3.3.

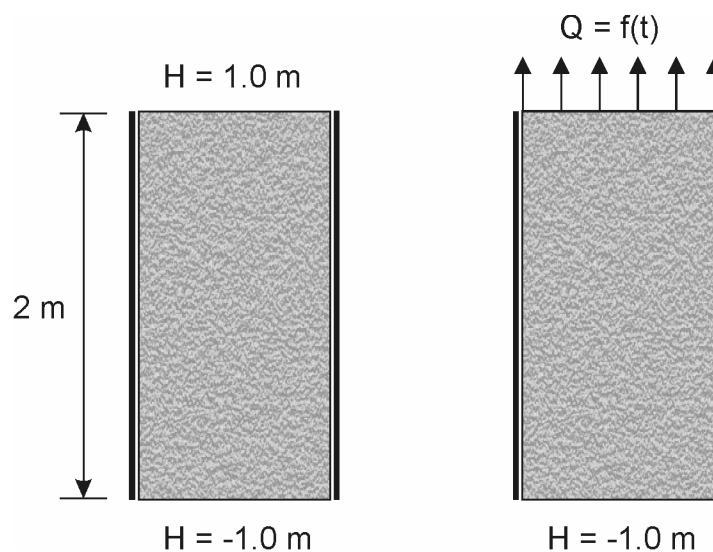
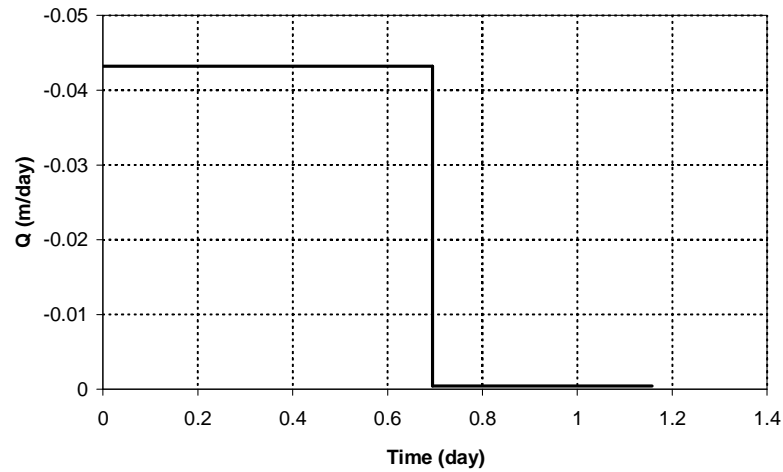


Fig. D4.1: Geometry of case D4

Tab. D4.1: Prescribed flux

Time (day)	Q (m/day)
0	-0.0432
0.6944	-0.0432
0.6944	-0.00043
1.1574	-0.00043

**Fig. D4.2:** Prescribed flux**Tab. D4.2:** Input data for case D4

Description	Symbol	Unit	Value
Permeability	k_x, k_y, k_z	[m/day]	0.1521
initial void ratio	e_{init}	[-]	0.5625
Elastic storage	$K_{w,ref}/n$	[kN/m ²]	487.5e3
Saturated saturation	S_{sat}	[-]	1.0
Residual saturation	S_{res}	[-]	0.06203
Van Genuchten	g_n	[-]	2.286
Van Genuchten	g_a	[m ⁻¹]	2.24
Van Genuchten	g_l	[-]	0

Tab. D4.3: Input data for case D4

Step	Time (day)
2	<i>Steady state</i>
48	<i>0.23</i>
95	<i>0.465</i>
141	<i>0.695</i>
187	<i>0.925</i>
234	<i>1.16</i>

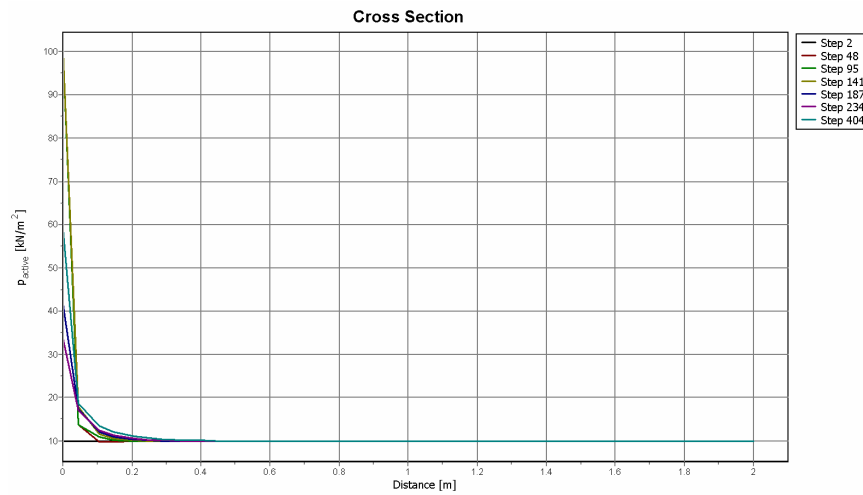


Fig. D4.3: Active pore pressure in time vs height in PLAXIS 2D

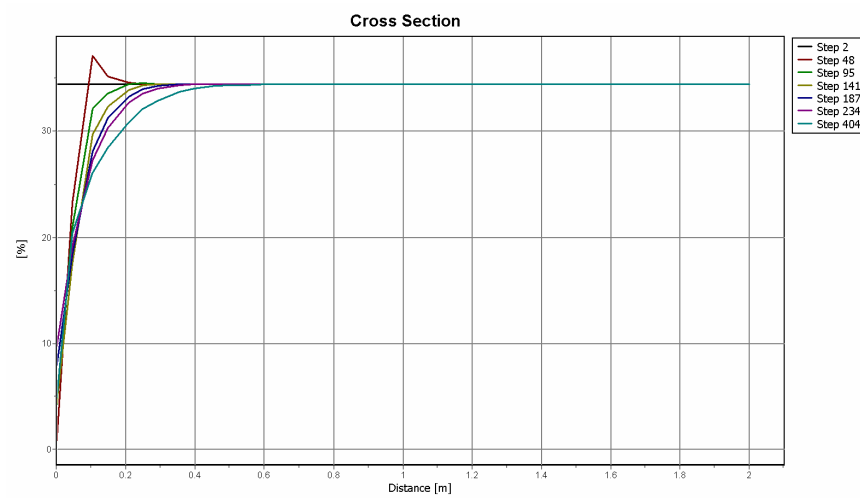


Fig. D4.4: Degree of saturation in time vs height in PLAXIS 2D

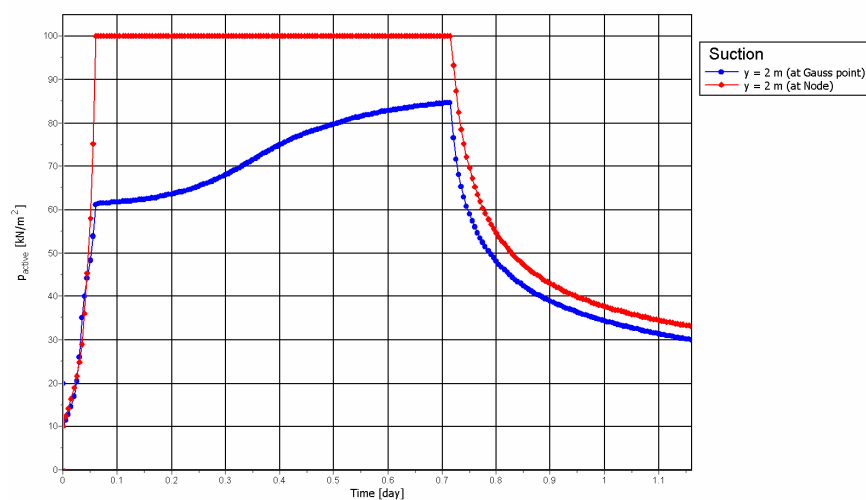


Fig. D4.5: Pore pressure at node and Gauss point at the top of the column in time in PLAXIS 2D

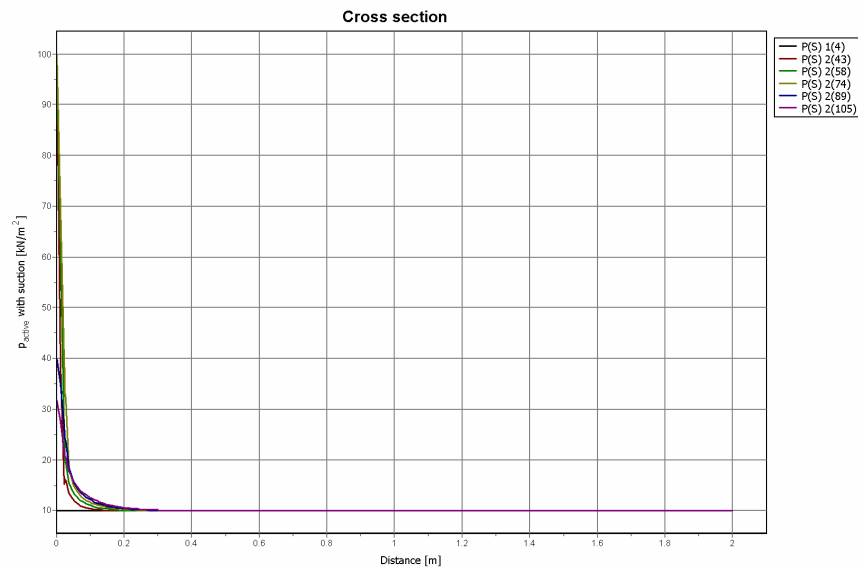


Fig. D4.6: Active pore pressure in time vs height in PLAXIS 3D

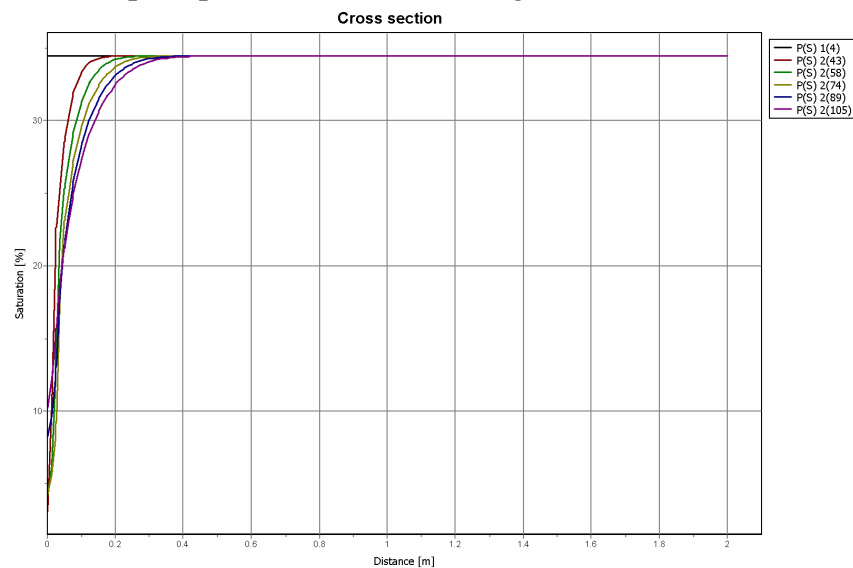


Fig. D4.7: Degree of saturation in time vs height in PLAXIS 3D

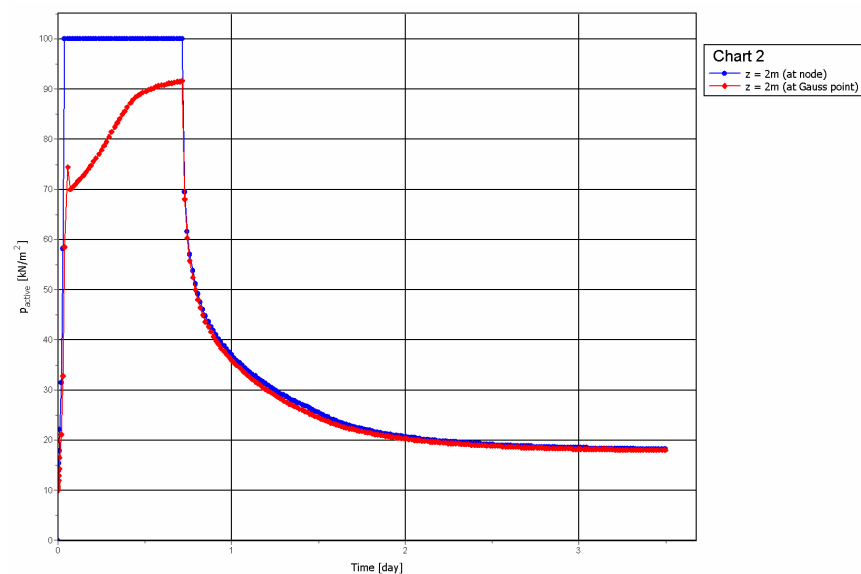


Fig. D4.8: Pore pressure at node and Gauss point at the top of the column in time in PLAXIS 3D

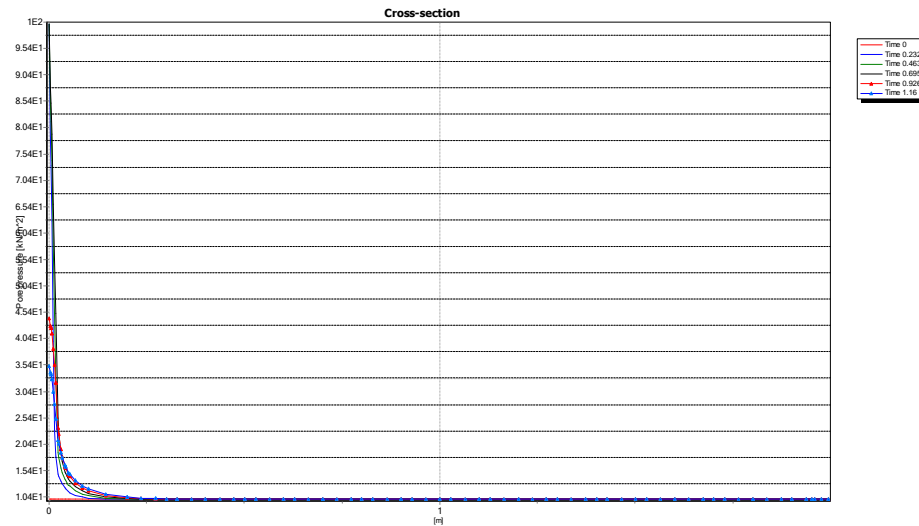


Fig. D4.9: Active pore pressure in time vs height (existing PlaxFlow)

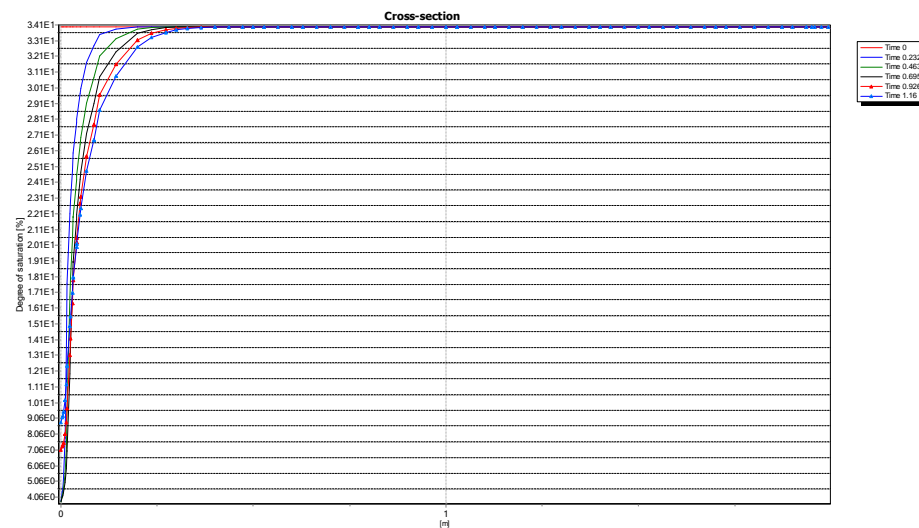


Fig. D4.10: Degree of saturation in time vs height (existing PlaxFlow)

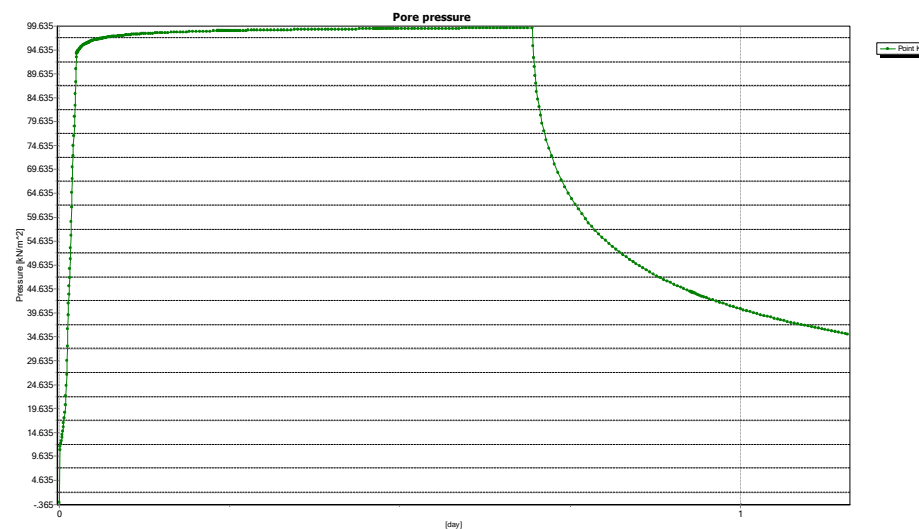


Fig. D4.8: Pore pressure at the Gauss point at the top of the column in time (existing PlaxFlow)

Summary:

The example given in this section is not a practical problem. In this example, it is intended to extract water from a very dry zone. By imposing a prescribed outflow boundary conditions, soil in the near of the boundary gets more unsaturated and the relative permeability becomes smaller and consequently extracting water becomes more difficult.

7.14 Conclusions

Results of 13 one dimensional flow problems, solved by the new PLAXIS 2D and 3D kernels, are shown in this chapter and most of them are compared with PlaxFlow results. As seen, results are in agreement in most cases with the results from PlaxFlow kernel.

For all examples very fine meshes with 15 noded elements in 2D and 10-noded tetrahedral elements in 3D are used.

The following features have been tested:

1. *Hydraulic models.* Van Genuchten and spline models have been tested. It has been found that the predefined parameters of linearised Van Genuchten relationship do not produce similar results to Van Genuchten relationship. Therefore, it is suggested to use Van Genuchten model and not the approximated one.
2. *Different material set.* The capability of the code to simulate hydraulic behaviour of soils has been shown for two types of material, namely sands and clay. It has been found that the models usually need finer mesh for sands compared to clays, as variation of relative permeability is higher for sands.
3. *Boundary conditions.* Almost all boundary conditions have been tested in this chapter, namely prescribed boundary head, seepage boundary condition, varying head (in PLAXIS 2D and 3D codes, this is a part of seepage boundary condition), inflow, outflow, precipitation and evaporation. The rest boundary conditions, namely wells and drains are tested in chapter 10 where groundwater flow analyses are verified against two and three dimensional problems.
4. *Automatic time stepping.* PLAXIS 2D and 3D kernels use an automatic time stepping. The kernel calculates the first (critical) time, maximum and minimum time steps in the beginning of calculation based on elements size and material parameters.
5. *Steady state and transient calculation.* Both steady state and transient types of calculations have been tested.
6. *Permeability contrasts.* Results of two cases, namely low-high and high-low permeability contrasts have been shown.

8 Verification of groundwater flow: Two and three dimensional problems

This chapter presents the results of 10 groundwater flow calculations for which a specific feature of flow problem has been solved. All examples have been analysed by both two and three dimensional codes (i.e. PLAXIS 2D and PLAXIS 3D). It is intended here to present the most important features of the code and to verify them against analytical solutions. In some case for which an analytical solution does not exist the results are compared with the results from the old 2D groundwater flow code developed by GeoDelft (PlaxFlow). In all cases the Van Genuchten model is used.

8.1 Case G1: Potato field moisture

This lesson demonstrates the applicability of PLAXIS to agricultural problems. The potato field lesson involves a loam layer on top of a sandy base. Regional conditions prescribe a water level at the position of the material interface. The water level in the ditches remains unchanged. The precipitation may vary on a daily basis due to weather conditions. The calculation aims to predict the variation of the water content in the loam layer in time as a result of time-dependent boundary conditions.

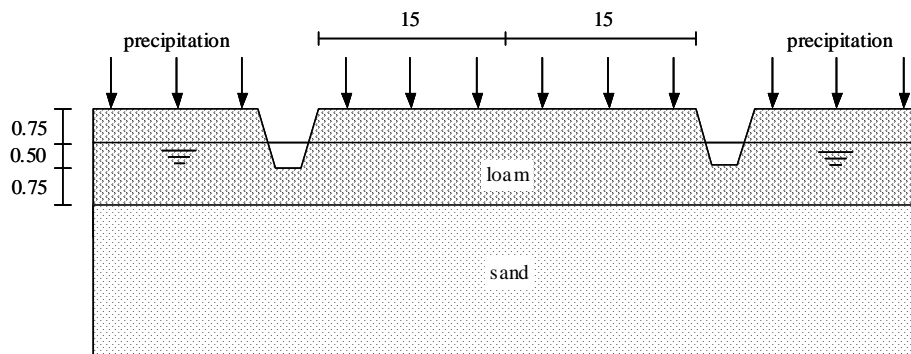


Fig. G1.1: Potato field geometry

Starting series B9 and O2 represent the top and the bottom layers. The parameters are given in Table G1.1 and G1.2, respectively.

Tab. G1.1: Input data for loam layer (B9)

Description	Symbol	Unit	Value
Permeability	k_x, k_y, k_z	[m/day]	0.0154
initial void ratio	e_{init}	[-]	0.754
Elastic storage	$K_{w,ref}/n$	[kN/m ²]	4.875×10^5
Van Genuchten	g_n	[-]	1.325
Van Genuchten	g_a	[m ⁻¹]	0.650
Van Genuchten	g_l	[-]	-2.161

Tab. G1.1: Input data for sand layer (O2)

Description	Symbol	Unit	Value
Permeability	k_x, k_y, k_z	[m/day]	0.1270
initial void ratio	e_{init}	[-]	0.62
Elastic storage	$K_{w,ref}/n$	[kN/m ²]	4.875×10^5
Van Genuchten	g_n	[-]	1.951
Van Genuchten	g_a	[m ⁻¹]	2.13
Van Genuchten	g_l	[-]	0.168

The precipitation fluxes are given in Table G1.3. The threshold values for ponding and precipitation (evapotranspiration) are chosen as 1 m and 0 at the top of the boundary, respectively.

Tab. G1.3: Prescribed flux ($\varphi_{min} = 0$ and $\varphi_{max} = 1$ m)

Time (day)	Q (m/day)
0	0
1	0
1	0.01
2	0.01
2	0.03
3	0.03
3	0
4	0
4	0.03
5	0.03
5	0
6	0
6	0.01
8	0.01
8	0
9	0
9	0.01

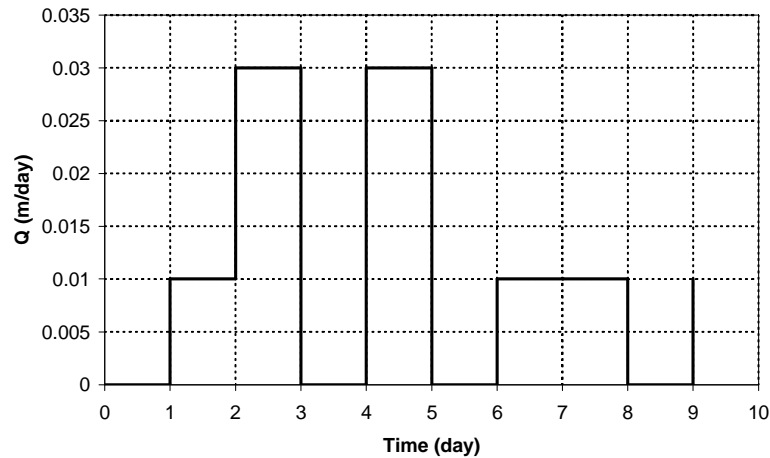


Fig. G1.2: Prescribed flux

Due to the symmetry of the problem, it is sufficient to simulate a strip with a width of 15.0 m, as indicated in Figure G1.3. The thickness of the loam layer is 2.0 m and the sand layer is 3.0 m deep.

The finite element mesh used for the calculation is depicted in Figure G1.3. The 2D and 3D meshes consists of 1032 15-noded elements and 20648 10 noded tetrahedral elements, respectively.

The following steps are performed in this case:

1. *Steady state*: Steady state groundwater flow calculation to generate initial pore pressure, (the bottom head is imposed to 3 m).
2. *Transient*: The top boundary head is set to influx.

Active pore pressure and degree of saturation are shown in Figures G1.4 to G1.9 for steady state, after 4.5 and after 9 days.

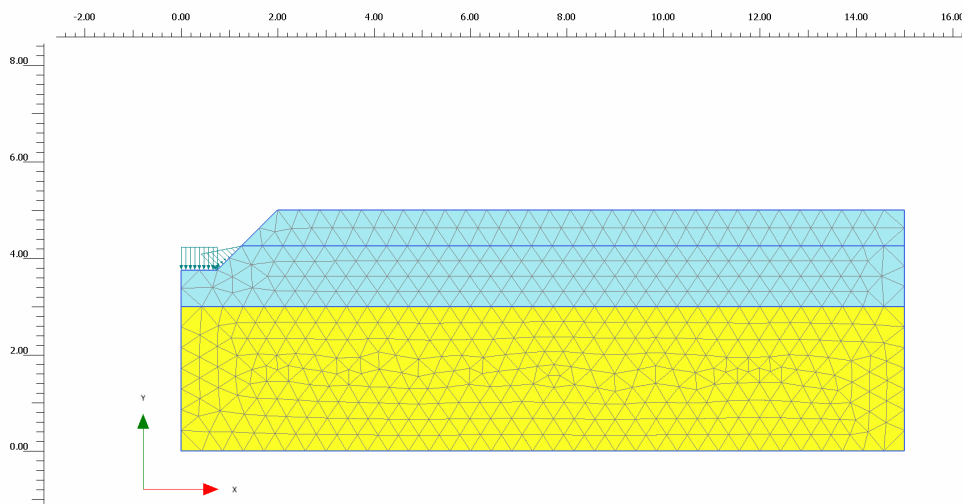


Fig. G1.3.2D: Finite element mesh (PLAXIS 2D - 15 noded elements)

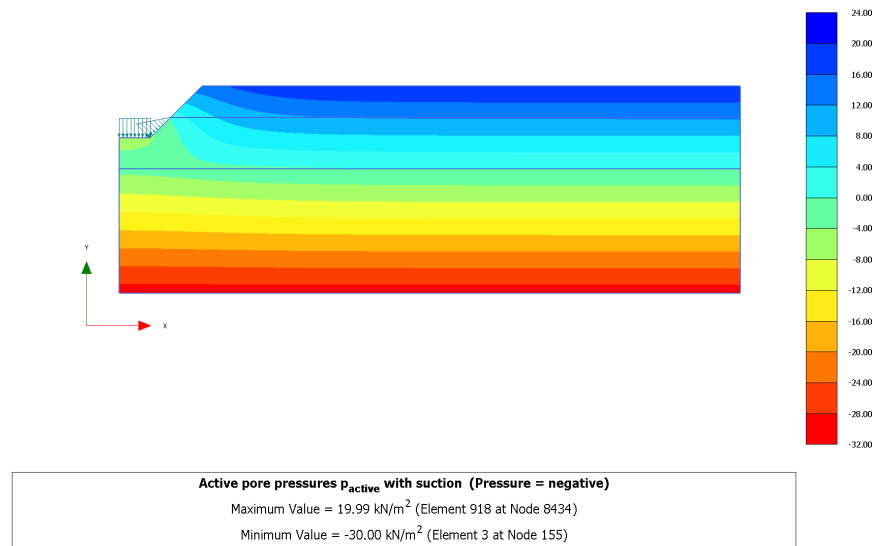


Fig. G1.4.2D: Active pore pressure after steady state calculation (PLAXIS 2D)

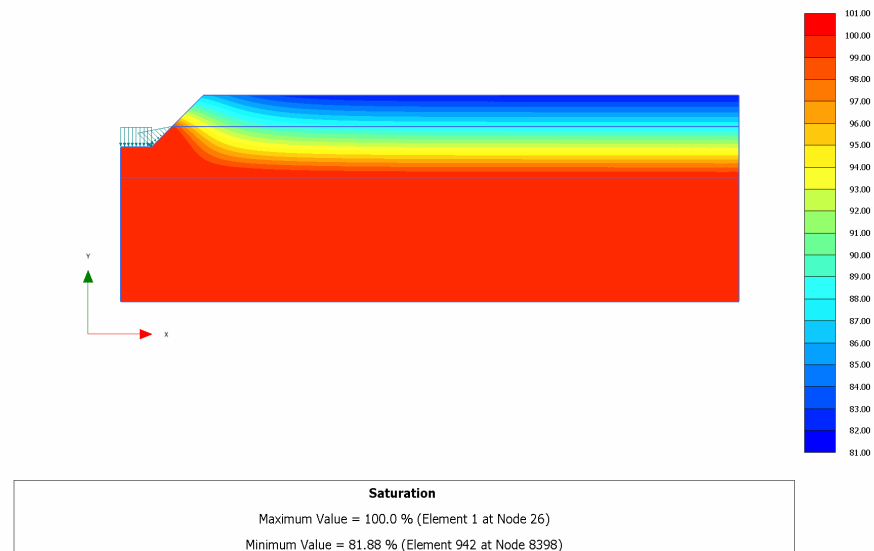


Fig. G1.5.2D: Degree of saturation after steady state calculation (PLAXIS 2D)

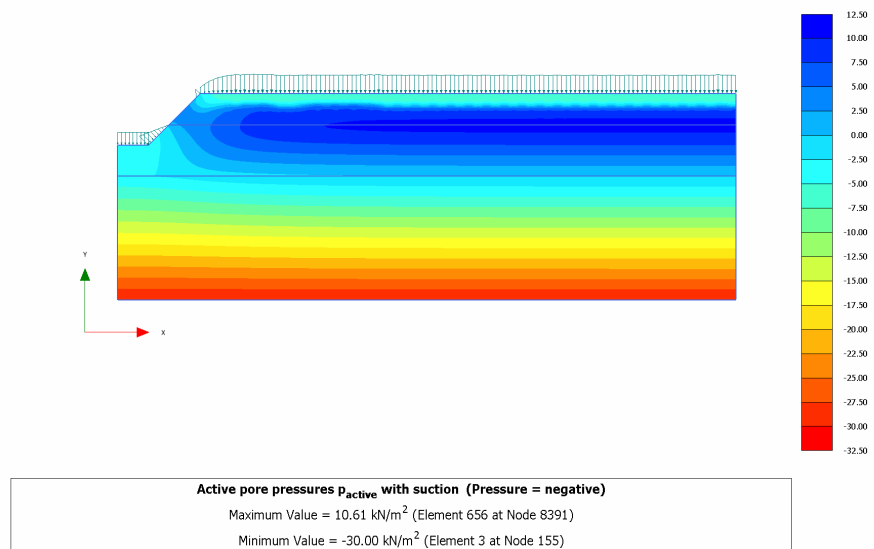


Fig. G1.6.2D: Active pore pressure after 4.5 days (PLAXIS 2D)

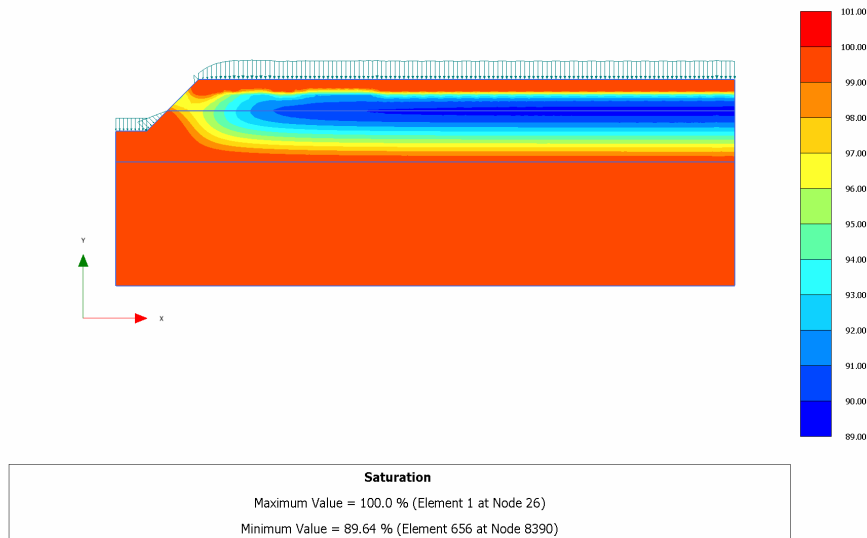


Fig. G1.7.2D: Degree of saturation after 4.5 days (PLAXIS 2D)

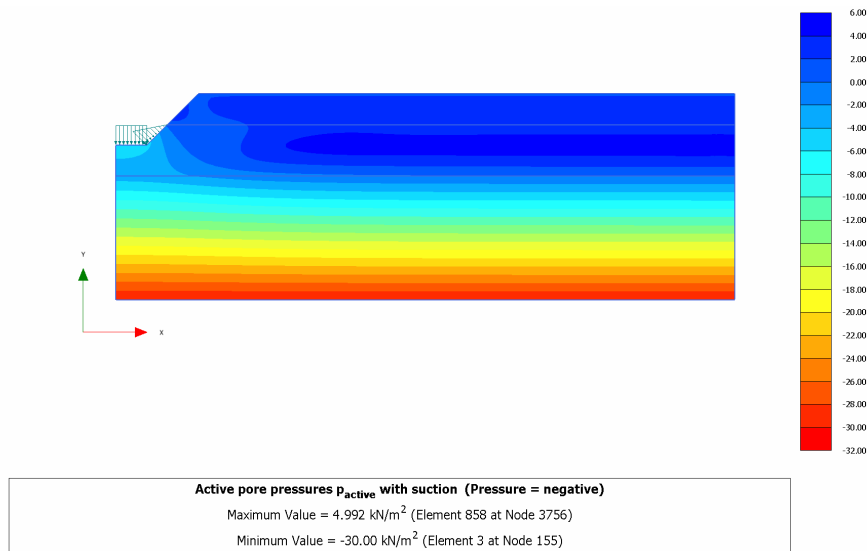


Fig. G1.8.2D: Active pore pressure after 9 days (PLAXIS 2D)

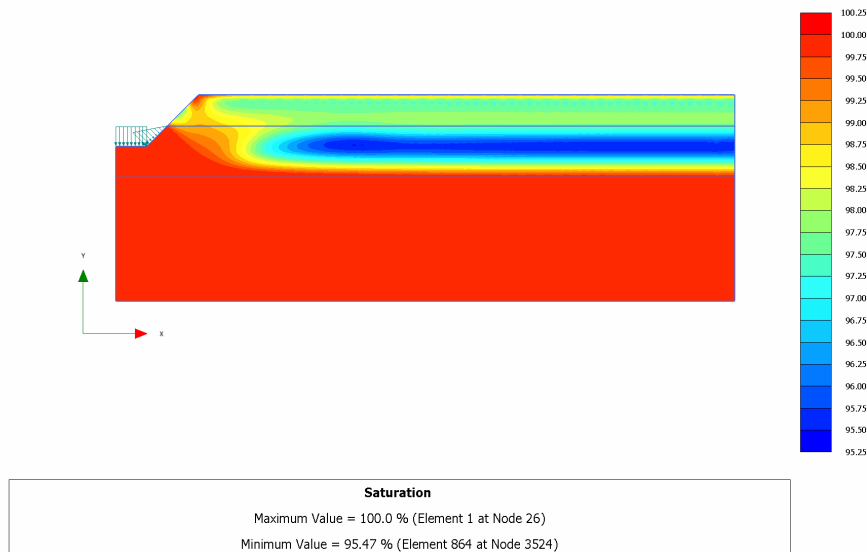


Fig. G1.9.2D: Degree of saturation after 9 days (PLAXIS 2D)

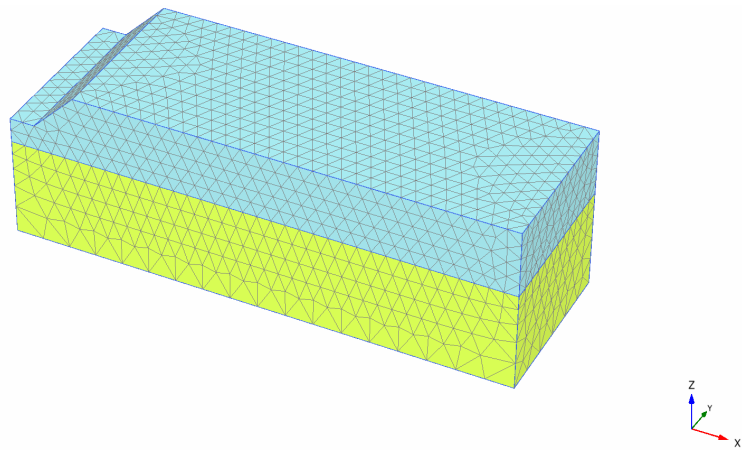


Fig. G1.3.3D: Finite element mesh (PLAXIS 3D - 10 noded elements)

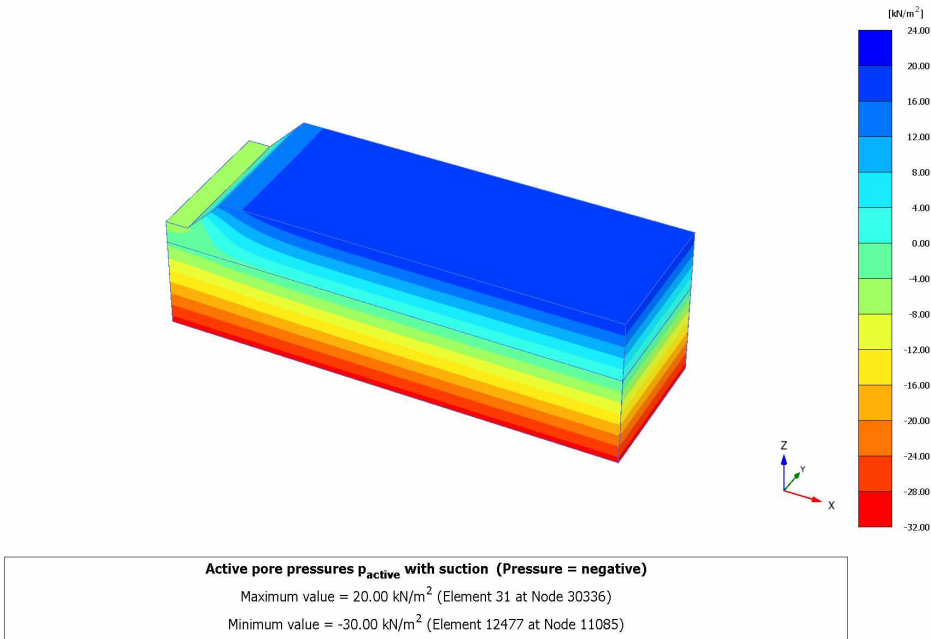


Fig. G1.4.3D: Active pore pressure after steady state calculation (PLAXIS 3D)

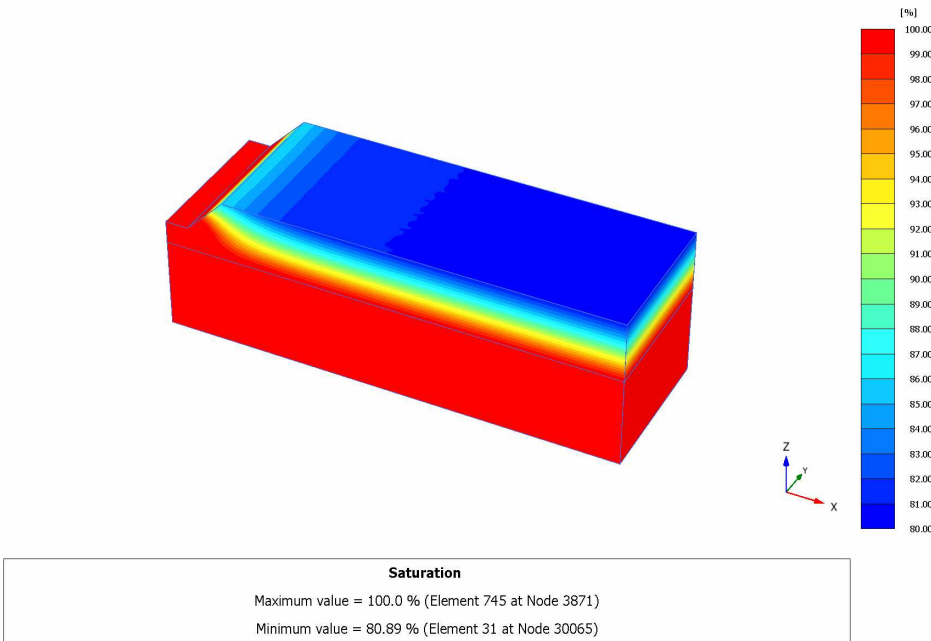


Fig. G1.5.3D: Degree of saturation after steady state calculation (PLAXIS 3D)

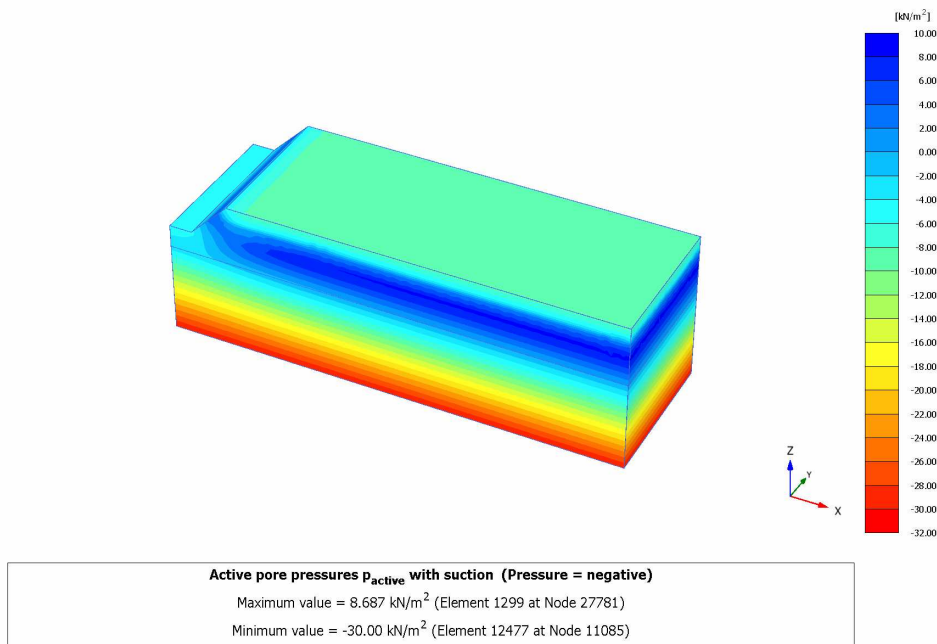


Fig. G1.6.3D: Active pore pressure after 4.5 days (PLAXIS 3D)

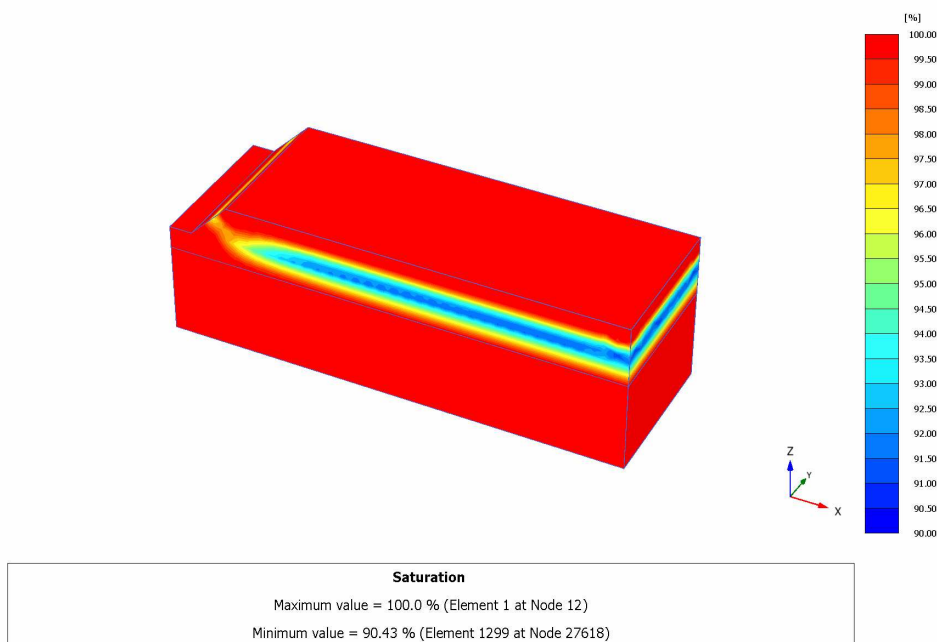


Fig. G1.7.3D: Degree of saturation after 4.5 days (PLAXIS 3D)

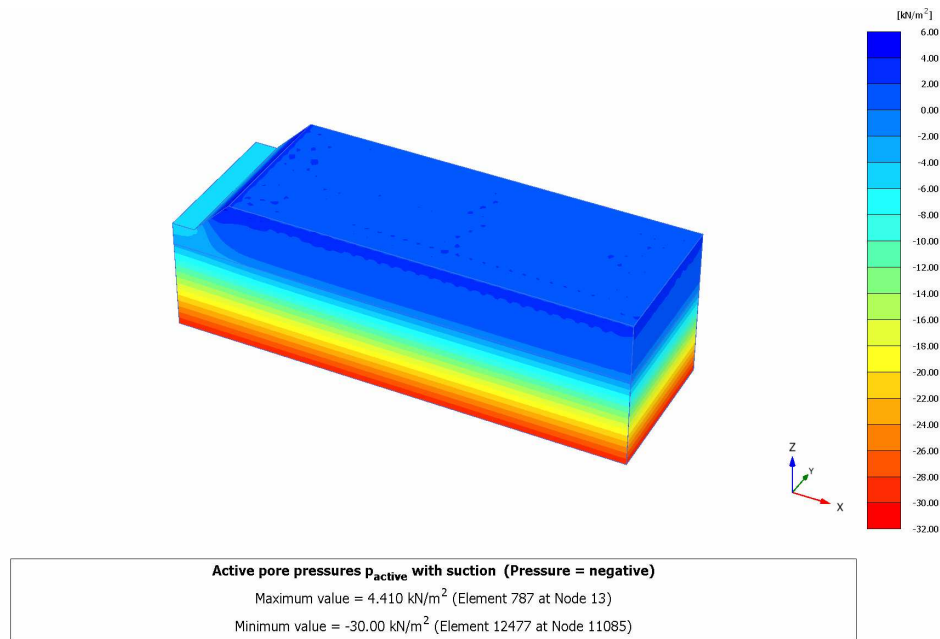


Fig. G1.8.3D: Active pore pressure after 9 days (PLAXIS 3D)

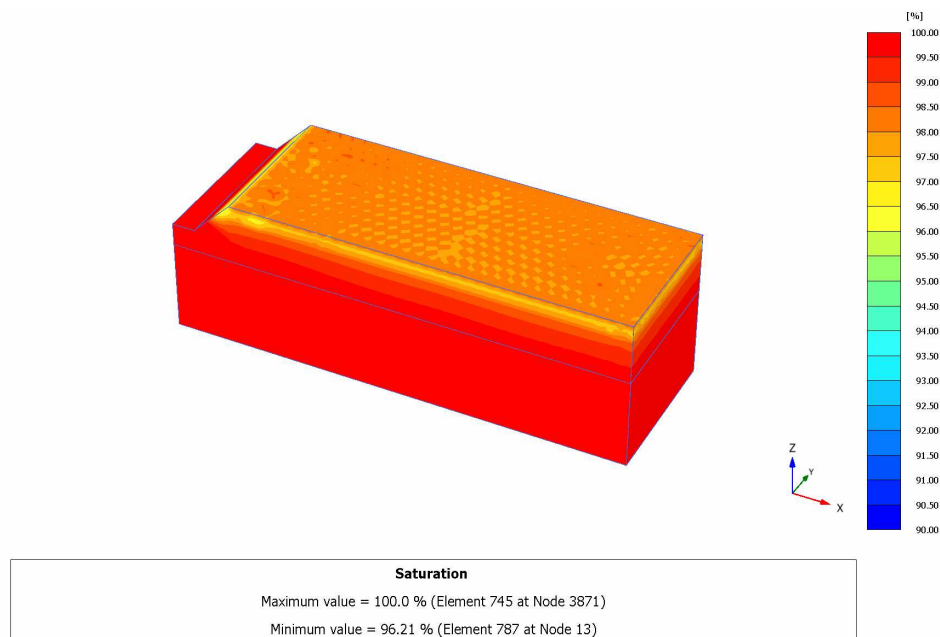
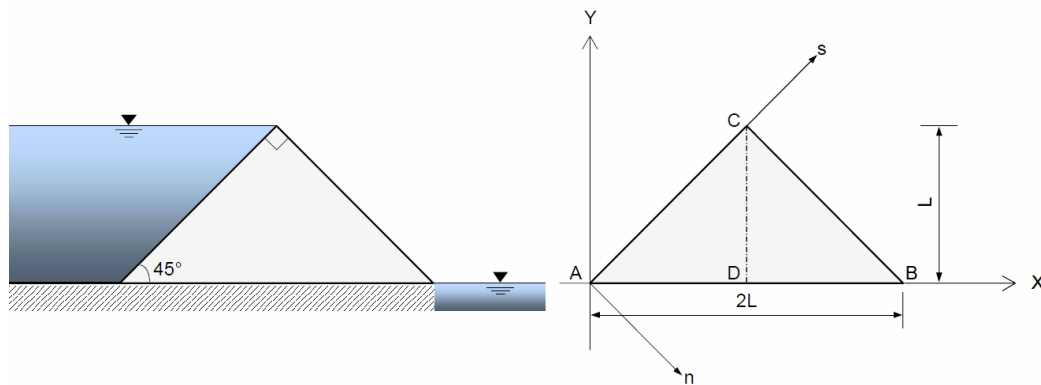


Fig. G1.9.3D: Degree of saturation after 9 days (PLAXIS 3D)

Summary:

This example has been chosen from the PlaxFlow manual. By comparing the results, it can be observed that the results from PLAXIS 2D, PLAXIS 3D and PlaxFlow (see the PlaxFlow manual) are similar.

This exercise illustrates groundwater flow in a triangular earth dam underlain by an impervious base. On the left side of the dam the water table is at the crest level and on the right side the water table is at the surface level. The base angles are 45° and the top angle is 90° , Figure G2.1.



In this case the entire slope CB is a seepage surface and no free surface exist, leading to a confined groundwater flow. Such a geometry and boundary conditions allow for solving the problem analytically. The solution of the problem was first introduced by Davison (see Harr, 1962). Here, the total discharge calculated by the analytical solution will be compared with that computed by PLAXIS. The total flow through the dam can be calculated as follows:

$$A(x,y) = (0,0), B(x,y) = (2L,0), C(x,y) = (L,L)$$
$$q_s = -k \frac{dh}{ds} = k \frac{n}{2L}$$

$$n = (x - y) / \sqrt{2}$$

$$s = (x + y) / \sqrt{2}$$

In xy -system:

$$h = L - \frac{x^2 - y^2}{4L}$$

$$q_x = -k \frac{dh}{dx} = k \frac{x}{2L}$$

$$q_y = -k \frac{dh}{dy} = k \frac{y}{2L}$$

$$\frac{dq_x}{dx} + \frac{dq_y}{dy} = \frac{dq_n}{dn} + \frac{dq_s}{ds} = 0$$

$$\text{Line AB: } n = s \text{ and } q_n = q_s, q_y = 0$$

$$\text{Line CD: } q_x = \frac{k}{2}$$

$$\text{total discharge } Q_x = \frac{k}{2} L$$

$$\text{Line AC: } q_n = k \frac{s}{2L}$$

$$\text{total discharge } Q_n = \frac{1}{2} \frac{kL\sqrt{2}}{2L} L\sqrt{2} = \frac{k}{2} L$$

$$\text{Line BC: } q_s = k \frac{n}{2L}$$

$$\text{total discharge } Q_s = \frac{1}{2} \frac{kL\sqrt{2}}{2L} L\sqrt{2} = \frac{k}{2} L$$

To compare results obtained from the analytical solution with that obtained from PLAXIS, a triangular dam, 2 m wide and 1 m high is considered. The head at the left side is assumed to be 1 m and the coefficient of permeability is 1 m/day. The geometry of the problem and the finite element mesh are presented in Figure G2.2. The width of the model is 1 m in the 3D calculations.

Following the analytical solution, the total discharge through the dam at sides CD and BC is:

$$Q = 0.50 \text{ m}^3/\text{day}/\text{m}$$

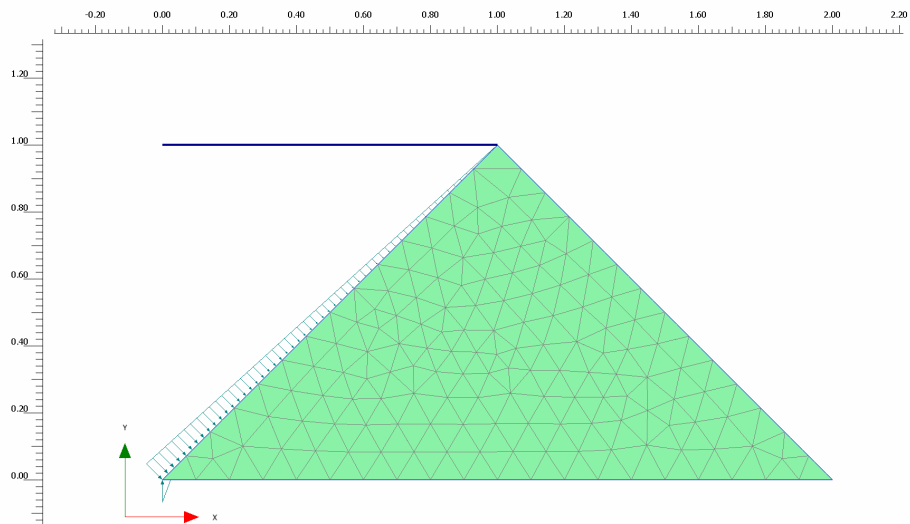


Fig. G2.2.2D: FE mesh, 15-noded elements (PLAXIS 2D)

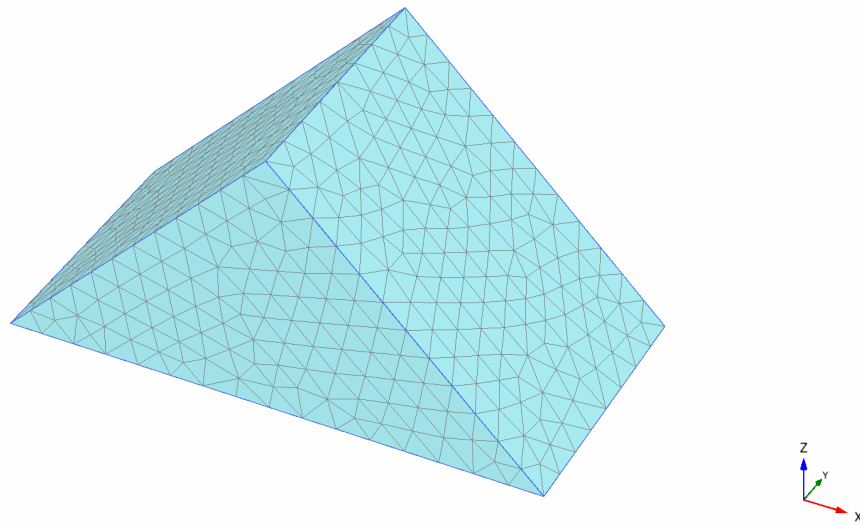


Fig. G2.2.3D: FE mesh, 10-noded tetrahedral elements (PLAXIS 3D)

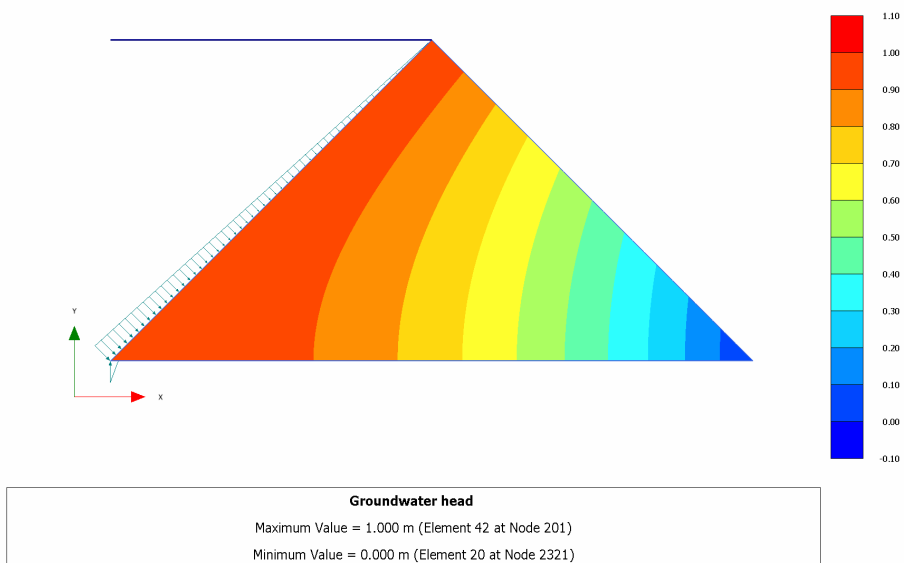
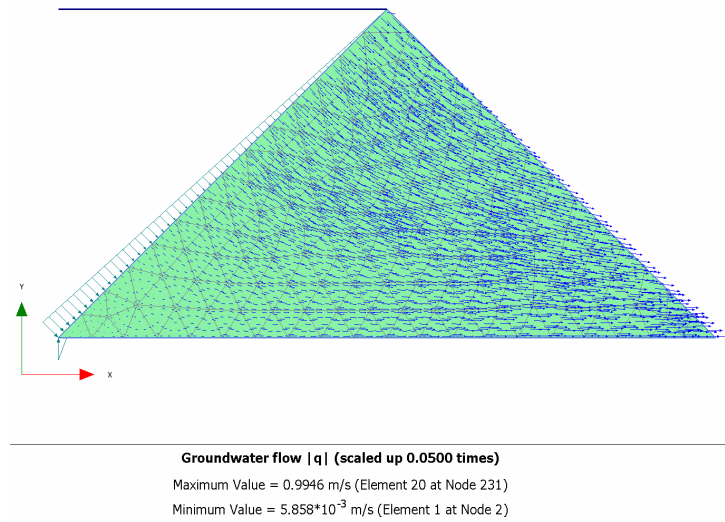
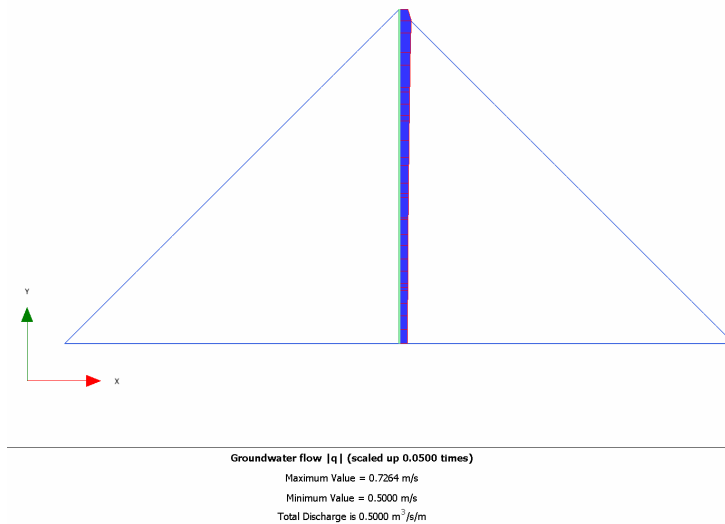
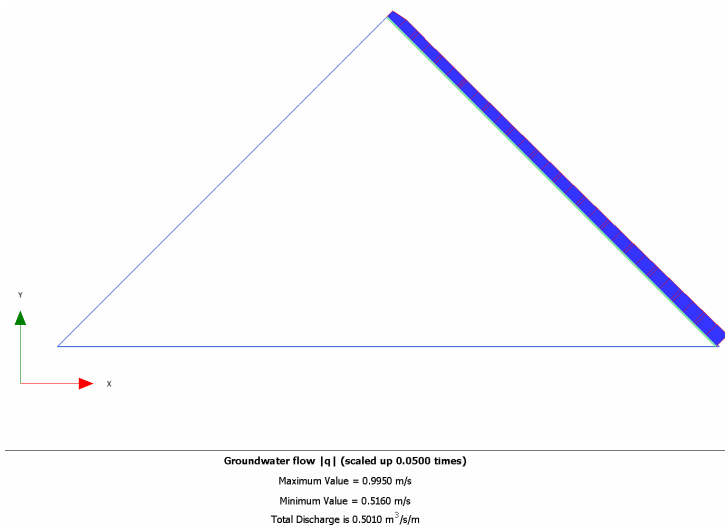
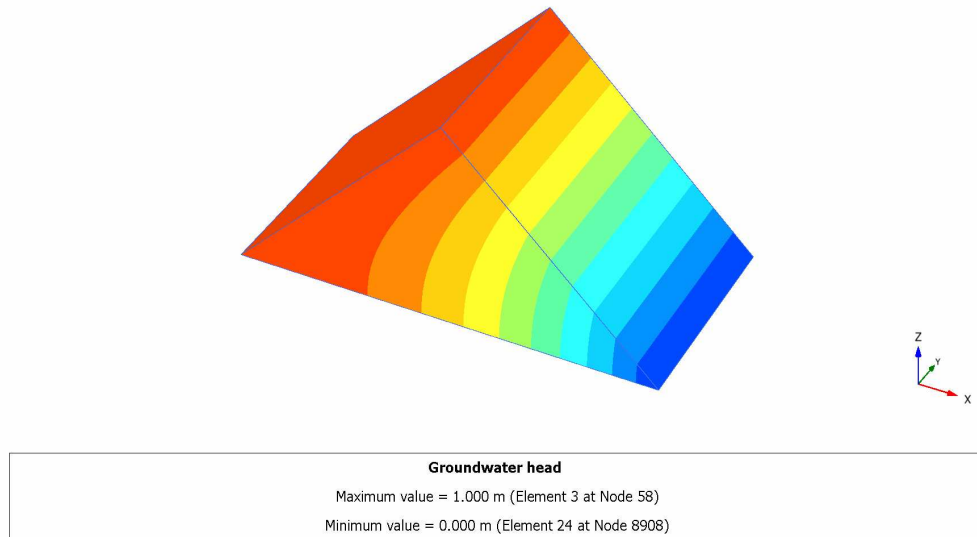
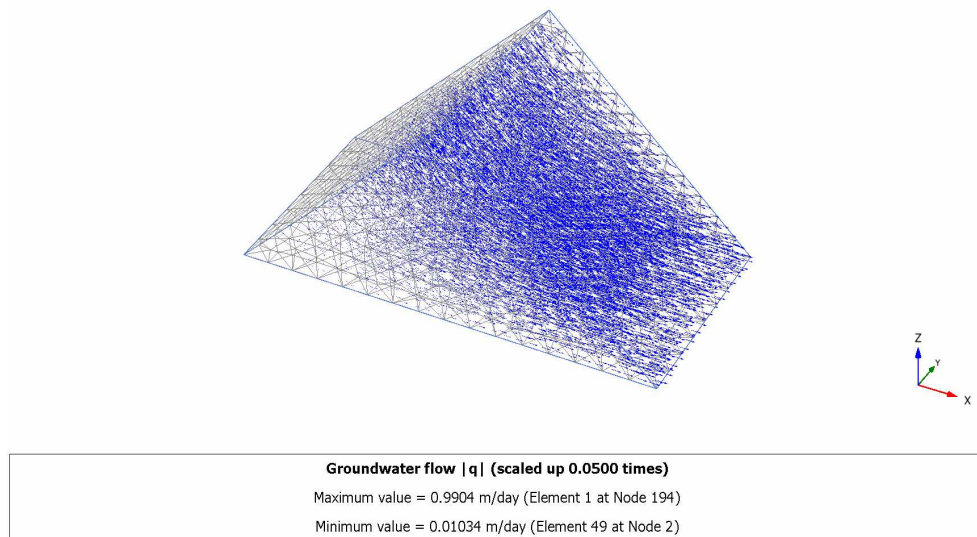
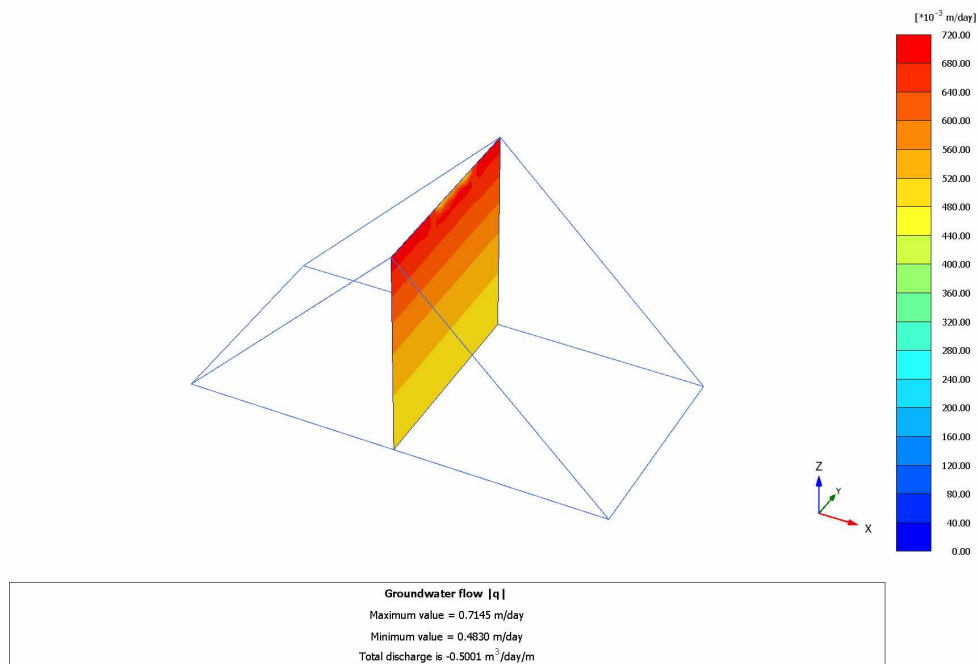


Fig. G2.3.2D: Groundwater head (PLAXIS 2D)

**Fig. G2.4.2D:** Groundwater flow field (PLAXIS 2D)**Fig. G2.5.2D:** Total discharge at cross section A-A: $Q=0.5000 \text{ m}^3/\text{day}/\text{m}$ (PLAXIS 2D)**Fig. G2.6.2D:** Total discharge at cross section B-B: $Q=0.5010 \text{ m}^3/\text{day}/\text{m}$ (PLAXIS 2D)

**Fig. G2.3.3D:** Groundwater head (PLAXIS 3D)**Fig. G2.4.3D:** Groundwater flow field (PLAXIS 3D)**Fig. G2.5.3D:** Total discharge at cross section A-A: $Q=0.5001$ m³/day/m (PLAXIS 3D)

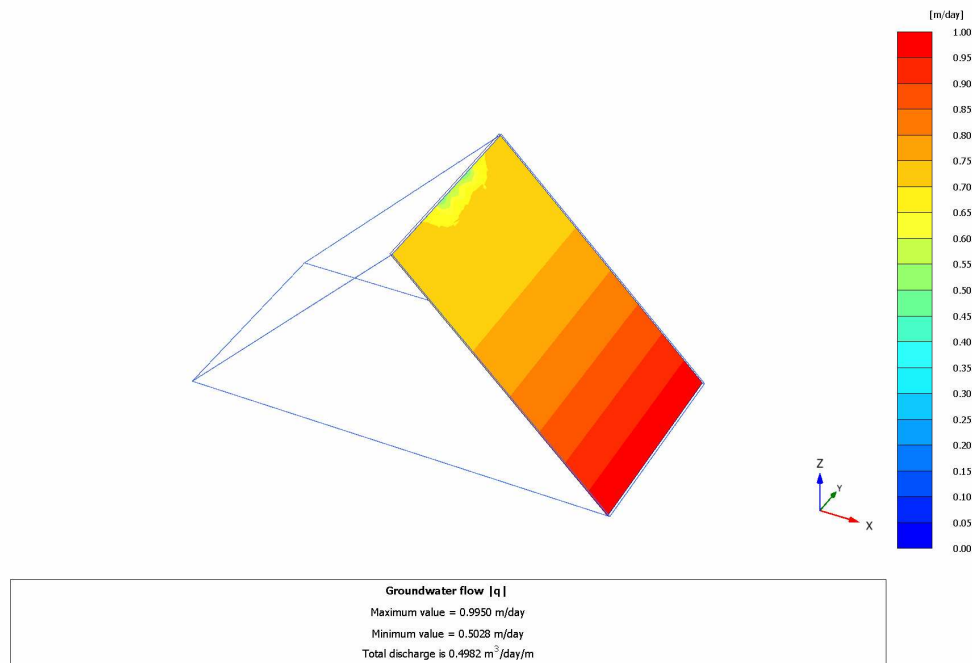


Fig. G2.6.3D: Total discharge at cross section B-B: $Q=0.4982$ m³/day/m (PLAXIS 3D)

To determine the total discharge in PLAXIS, two cross sections have been made (see Figure G2.1). The cross sections A-A and B-B are along CD and BC respectively. The total discharges in the cross sections A-A and B-B are given in Table G2.1 (see Figures G2.5 and G2.6):

Tab. G2.1: Total discharge

	Analytical	PLAXIS 2D (A-A)	PLAXIS 2D (B-B)	PLAXIS 3D (A-A)	PLAXIS 3D (B-B)
discharge	0.5000	0.5000	0.5010	0.5001	0.4982
error	0	0 %	0.2 %	0.02 %	0.36 %

Summary:

Apparently the results of both analytical and PLAXIS calculations are similar. It should be noted that some error may occur during numerical integration in output program.

8.3 Case G3: Confined Flow around a cutoff wall

The following example illustrates the problem of confined flow around an impermeable wall

Figure G3.1 shows the geometry and boundary conditions of the problem. As indicated in the figure there is a 10 m wide impermeable dam founded on a soil layer of 10m thick. The bottom of the soil layer is considered to be impermeable. A 5.0 m wall is placed under the dam. At the left side of the dam (as shown in figure) the water level is 15.0 m while at the right side the water level is 13.0 m. The wall is simulated by means of an impermeable interface. The element mesh is locally refined around the wall particularly at the tip of the wall. 6 noded and 15 noded elements are alternately used. The problem is also simulated with PlaxFlow to compare outputs. Permeability of soil is 1.0 m/day.

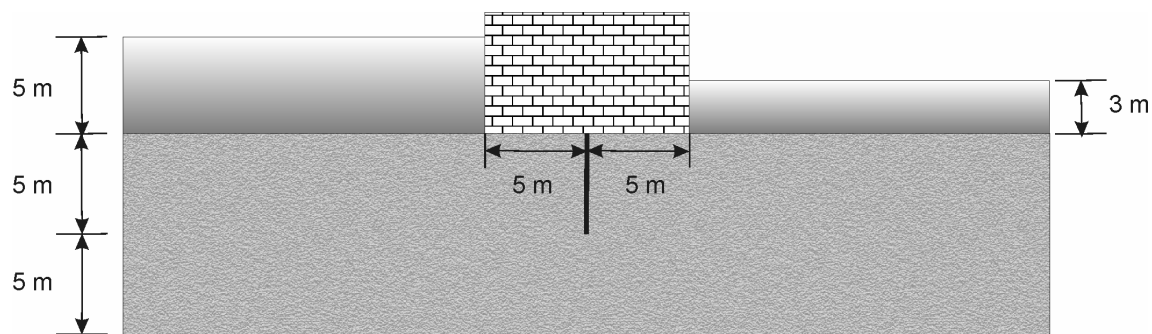


Fig. G3.1: Geometry of the problem

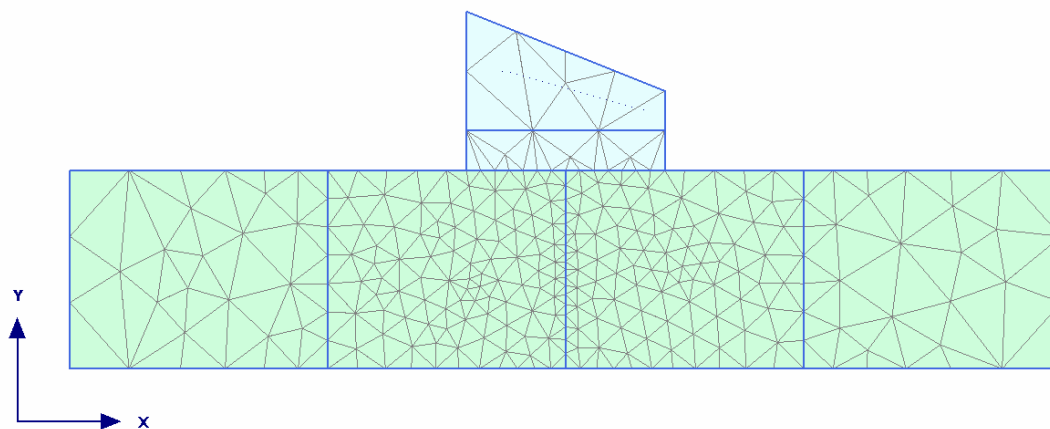


Fig. G3.2.2D: Finite element mesh (PLAXIS 2D)

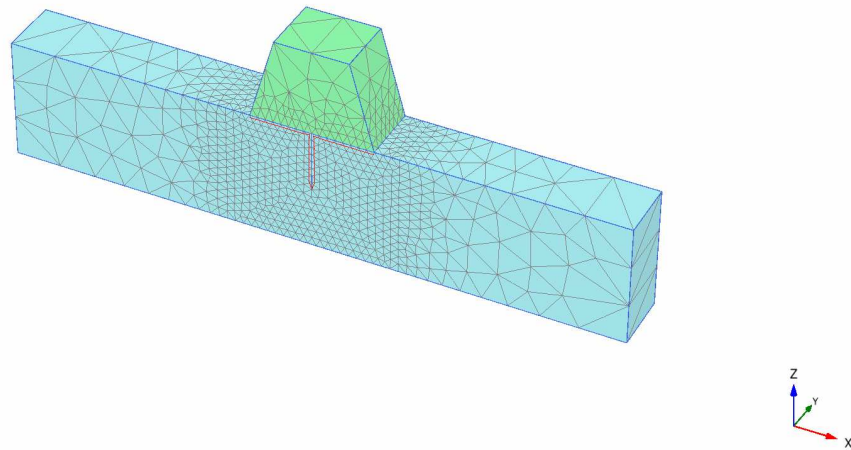


Fig. G3.2.3D: Finite element mesh (PLAXIS 3D)

Analytical solution: A closed form solution has been given for the discharge of the problem of confined flow around a wall for different geometrical ratios by Harr (1962). Figure G3.1 shows the closed form solution. In this situation ($s/T=0.5$ and $b/T=0.5$) the solution is:

$$\frac{Q}{k \Delta h} \approx 0.4$$

which gives a total discharge of roughly $0.8 \text{ m}^3/\text{day}/\text{m}$.

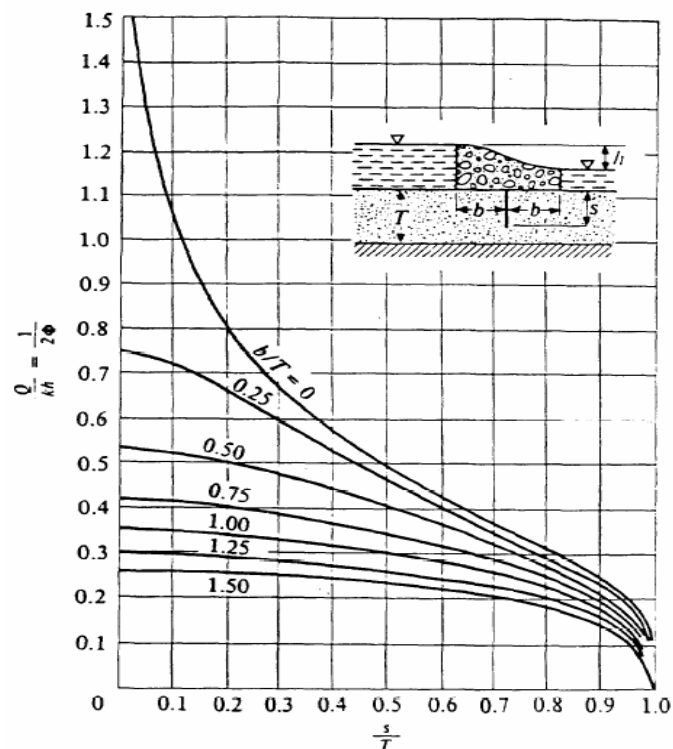


Fig. G3.3: Closed form solution

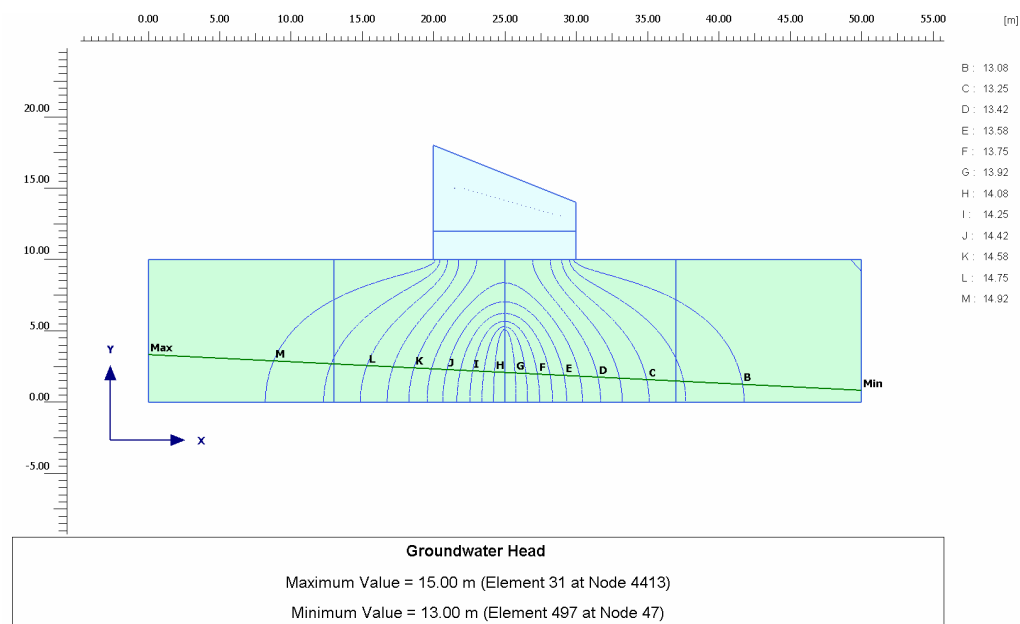


Fig. G3.4.2D: Groundwater head (PLAXIS 2D)

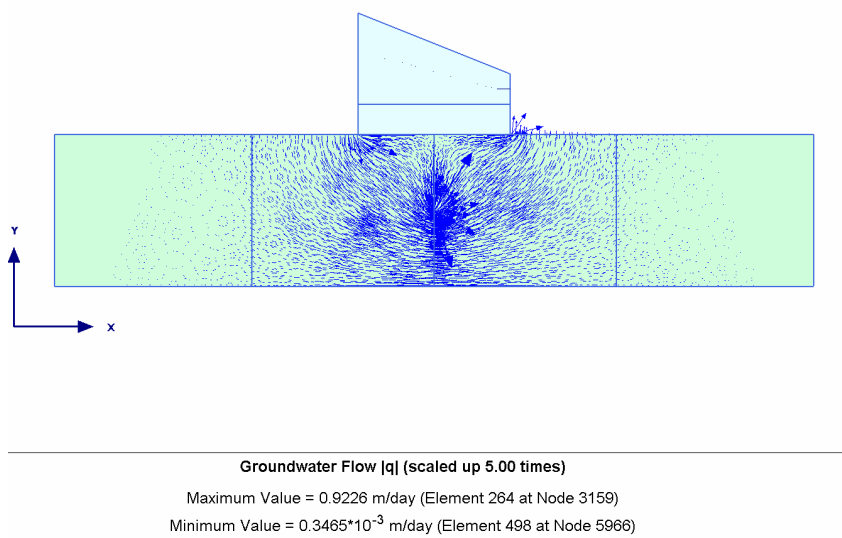


Fig. G3.5.2D: Flow field (PLAXIS 2D)

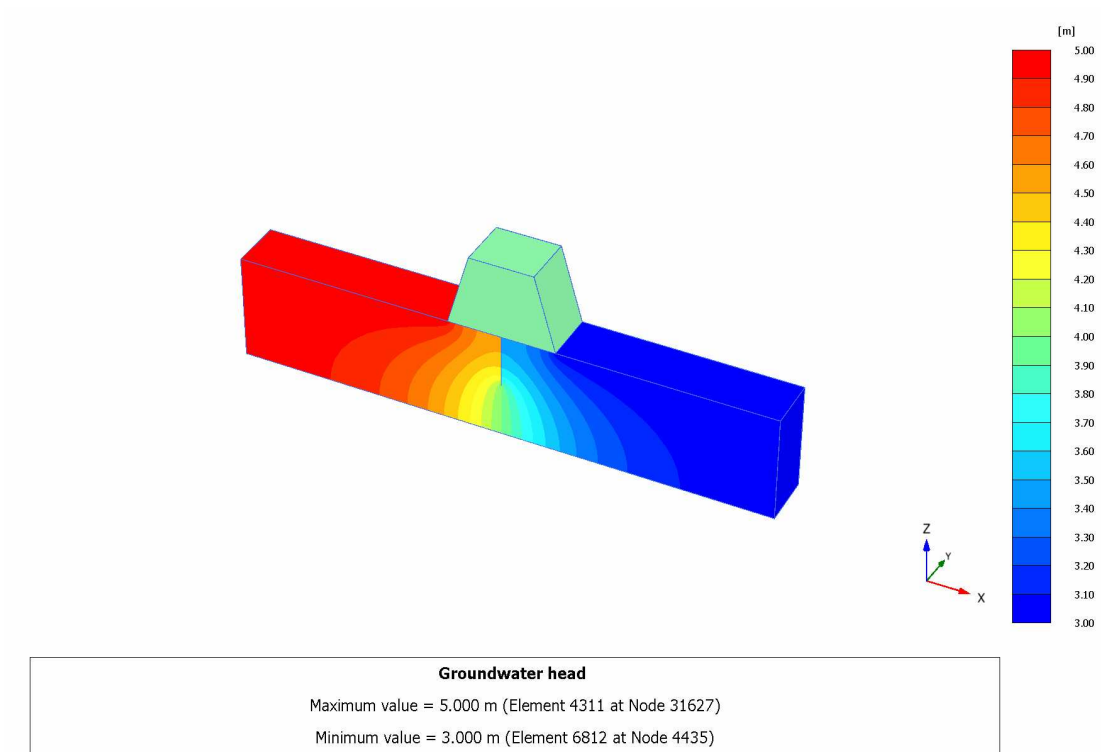


Fig. G3.4.3D: Groundwater head (PLAXIS 3D)

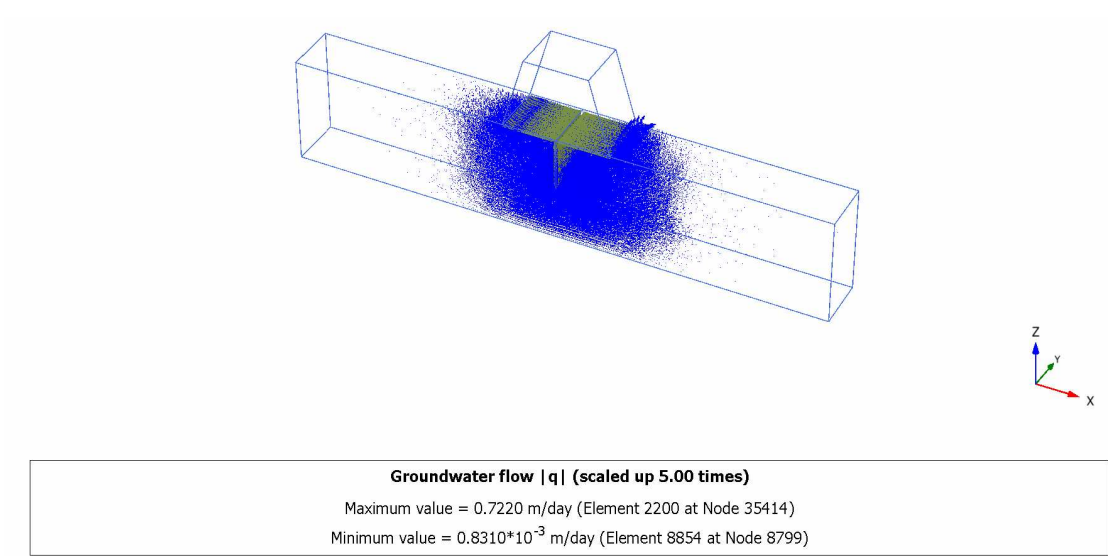


Fig. G3.5.3D: Flow filed (PLAXIS 3D)

Tab. G3.1: Total discharge

	Analytical	PlaxFlow	PLAXIS 2D 15 noded	PLAXIS 2D 6 noded	PLAXIS 3D 10 noded
discharge	0.800	0.818	0.815	0.822	0.819
error	0	2.25 %	1.87 %	2.75 %	2.32 %

Summary:

PLAXIS 2D with 15 noded elements produces the most accurate result. However, the accuracy can be improved by refining the mesh.

8.4 Case G4: Flow through a sand layer

This example illustrates leakage from a canal into a nearby river through a sand structure.

Figure G4.1 shows the geometry and finite element mesh for the problem. The thickness of the layer is 3.0 m and the length is 10.0 m. The bottom of the layer is impermeable. On the left hand side the groundwater head is prescribed 2.0 m and at the right hand side 1.0 m. The permeability is 1.0 m/day.

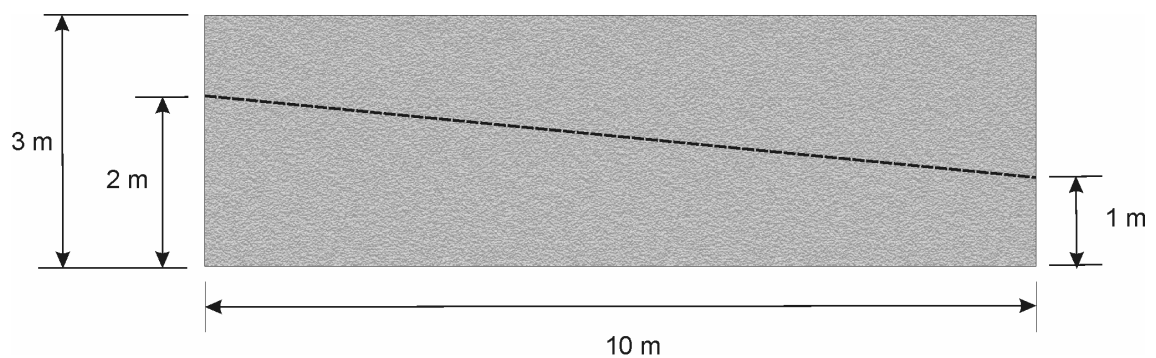


Fig. G4.1: Geometry of the problem

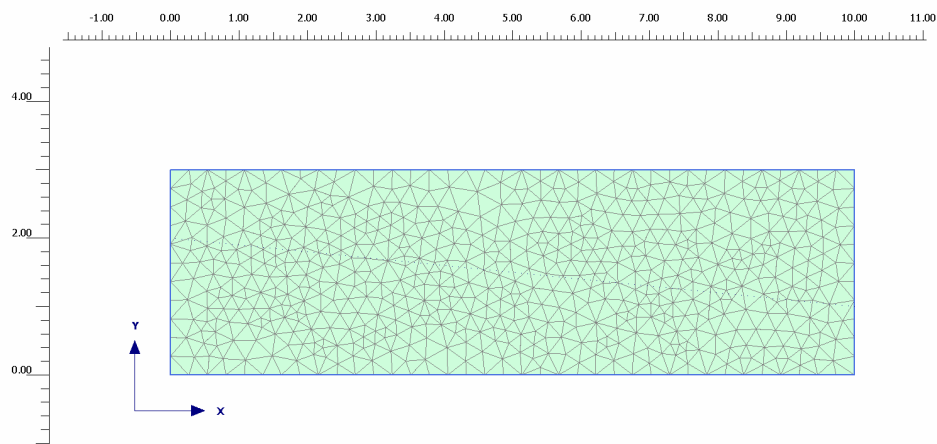


Fig. G4.2.2D: Finite element mesh (PLAXIS 2D)

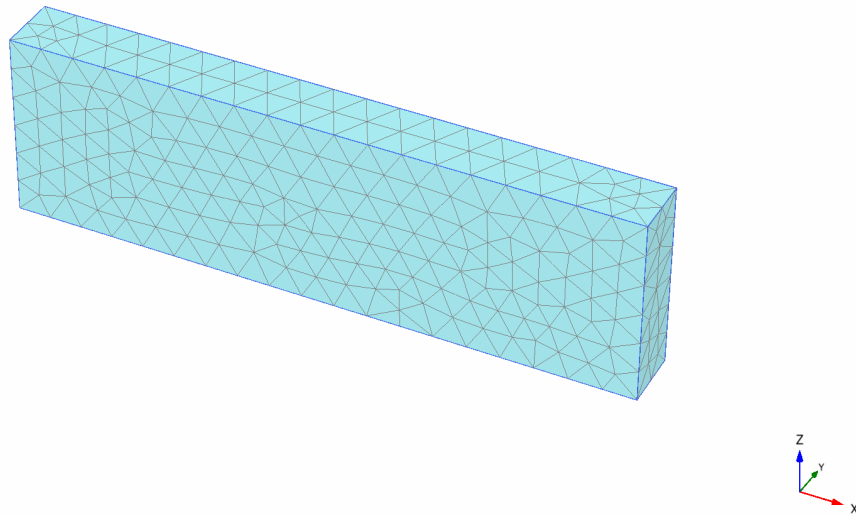


Fig. G4.2.3D: Finite element mesh (PLAXIS 3D)

Analytical solution: Under the assumption of a hydrostatic pore pressure distribution for each vertical cross-section the total discharge, Q , through the layer can be approximated with Dupuit's formula for unconfined flow:

$$Q = k \frac{\varphi_1^2 - \varphi_2^2}{2L}$$

where k is the permeability, L is the length of the layer and φ_1 and φ_2 are the ground water head at the left and right boundary, respectively. For the current situation this results in a theoretical solution of $0.150 \text{ m}^3/\text{day}/\text{m}$.

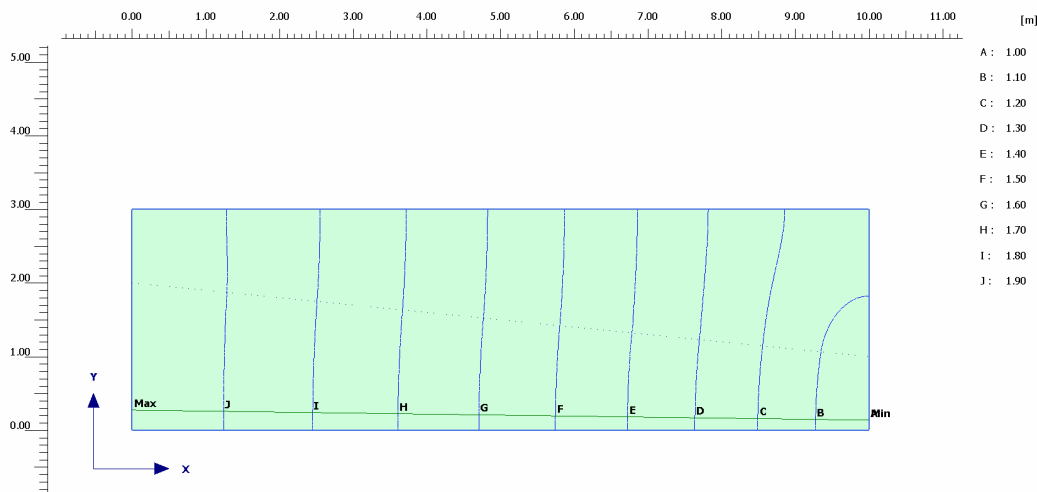


Fig. G4.3.2D: Groundwater head (PLAXIS 2D)

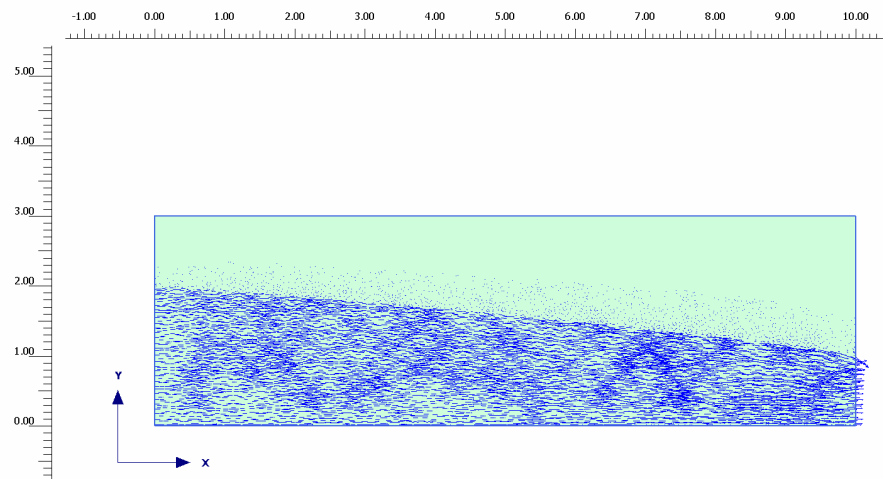


Fig. G4.4.2D: Flow field (PLAXIS 2D - 15 noded elements)



Fig. G4.5.2D: Total discharge $Q=0.1497 \text{ m}^3/\text{day}/\text{m}$ (PLAXIS 2D - 15 noded elements)

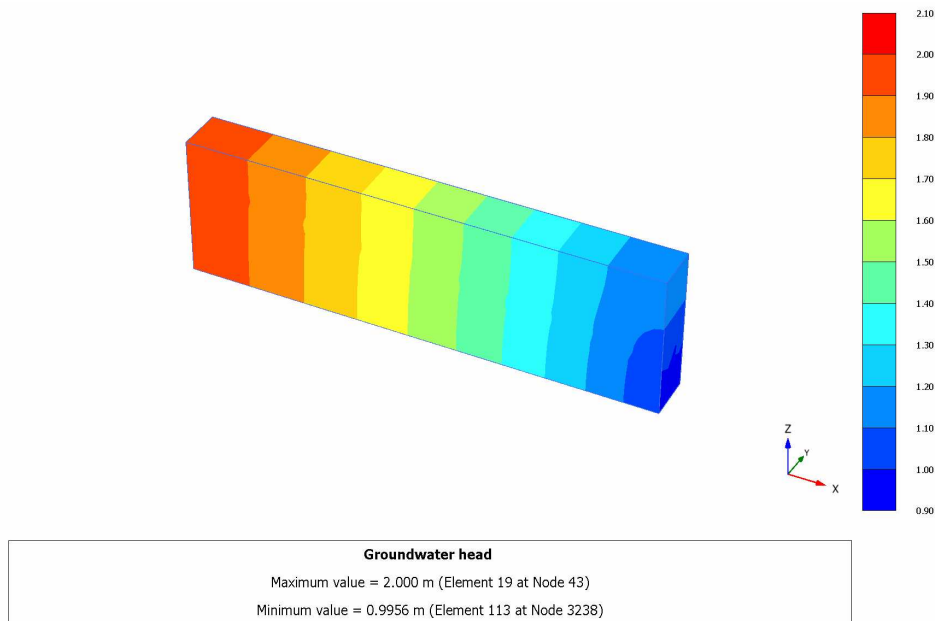


Fig. G4.3.3D: Groundwater head (PLAXIS 3D)

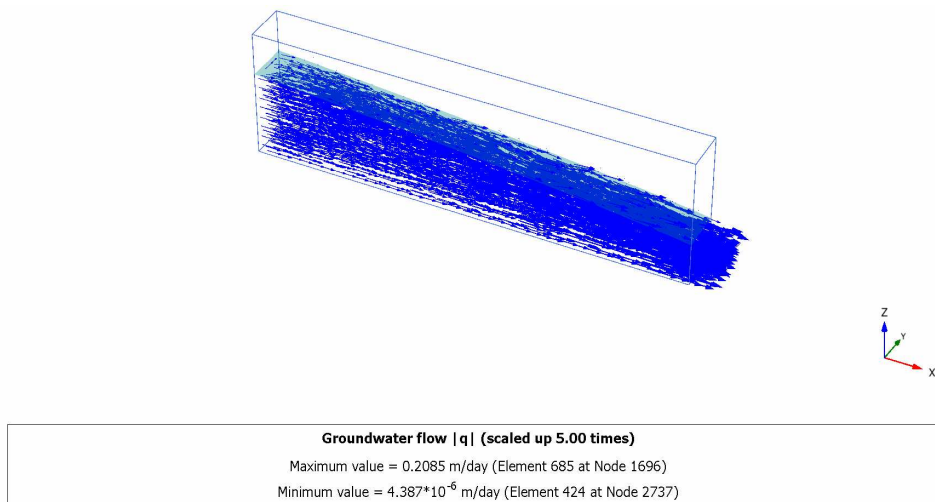


Fig. G4.4.3D: Flow field (PLAXIS 3D - 10 noded tetrahedral elements)

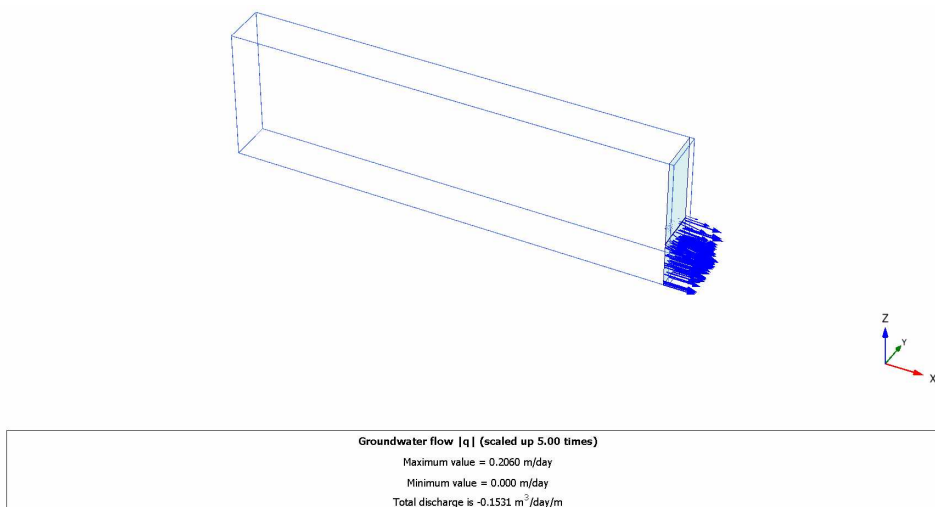


Fig. G4.5.3D: Total discharge $Q=0.1531 \text{ m}^3/\text{day}/\text{m}$ (PLAXIS 3D - 10 noded tetrahedral elements)

Tab. G4.1: Total discharge

	Analytical	PlaxFlow	PLAXIS 2D 15 noded	PLAXIS 2D 6 noded	PLAXIS 3D 10 noded
discharge	0.150	0.152	0.1497	0.1546	0.1531
error	0	1.3 %	0.2 %	3.0 %	2.06 %

Summary:

Since the total discharge is calculated in the output program which uses linear interpolation, the accuracy strongly depends on the size of elements. Therefore the results can be improved by refining the mesh.

8.5 Case G5: Seepage length

The purpose of this example is to determine the length of the seepage face, l , in an inclined river bank, knowing the location of a point P on the phreatic surface. The slope of the river bank is at an angle α . The location of point P is defined by the distances L and H , Fig G5.1.

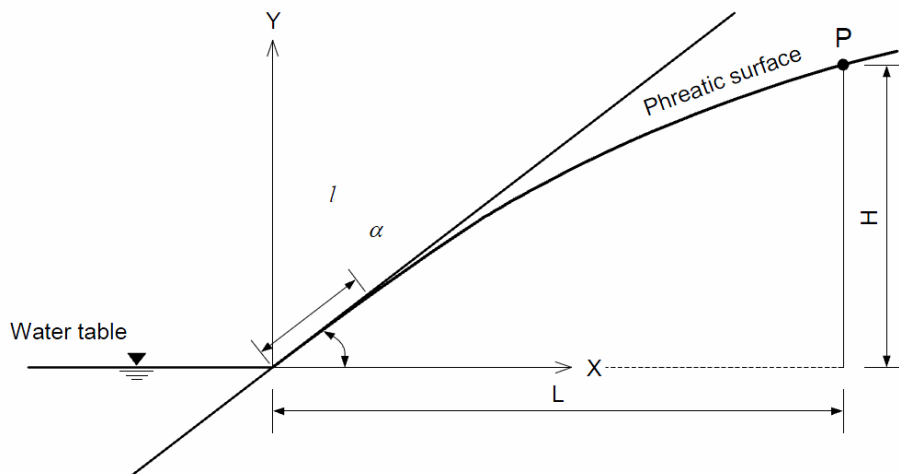


Fig. G5.1: Geometry of the problem

Analytical solution: A closed form solution of this problem is given by Strack and Asgari (1978) with the following assumptions:

1. The river bank is presented as an infinite slope at an angle α
2. Unconfined ground water flows from far away towards the river bank.
3. The flow is two dimensional, i.e., no flow occurs in the direction parallel to the river.
4. The permeability is homogeneous and isotropic.
5. Flow is steady
6. The soil is saturated below the phreatic surface and is dry above it.

The solution is presented in the form of a chart. This chart plots l/L as a function of H/L for different values of α . For this particular problem, $H/L = 0.5$ and $\alpha = 45^\circ$. Therefore $l/L = 0.255$.

The Finite element mesh and geometry of the problem is shown in Fig. G5.2. It is assumed that $L = 100$ m. Therefore the analytical length of seepage face is $l = 25.5$ m.

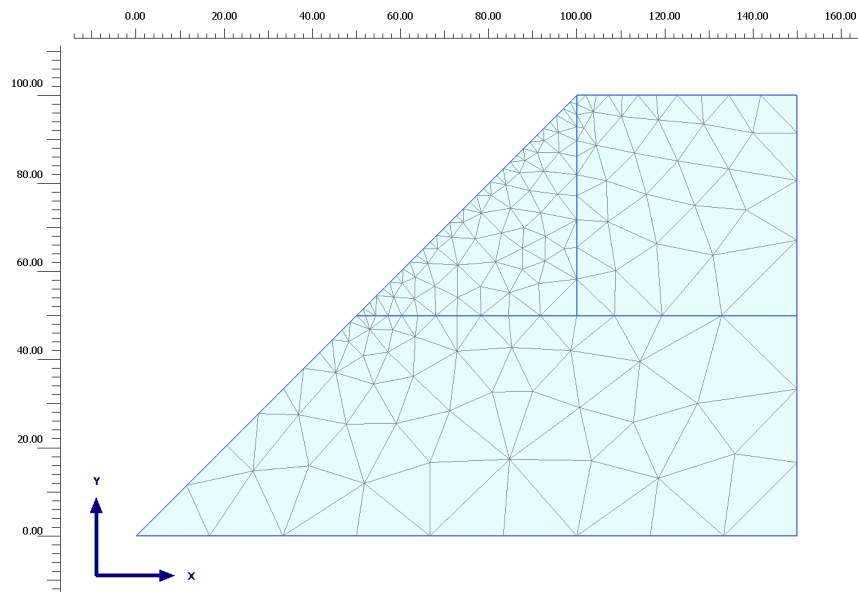


Fig. G5.2.2D: Finite element mesh (PLAXIS 2D - 15 noded elements)

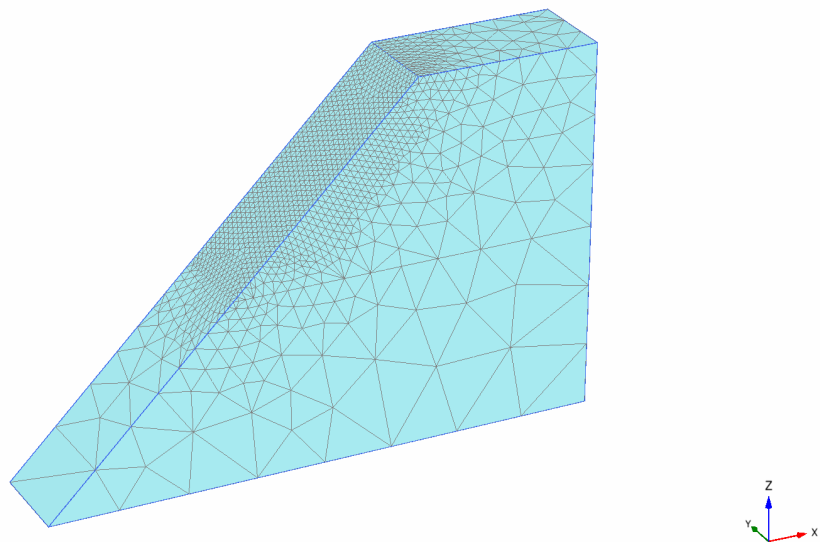


Fig. G5.2.3D: Finite element mesh (PLAXIS 3D - 10 noded tetrahedral elements)

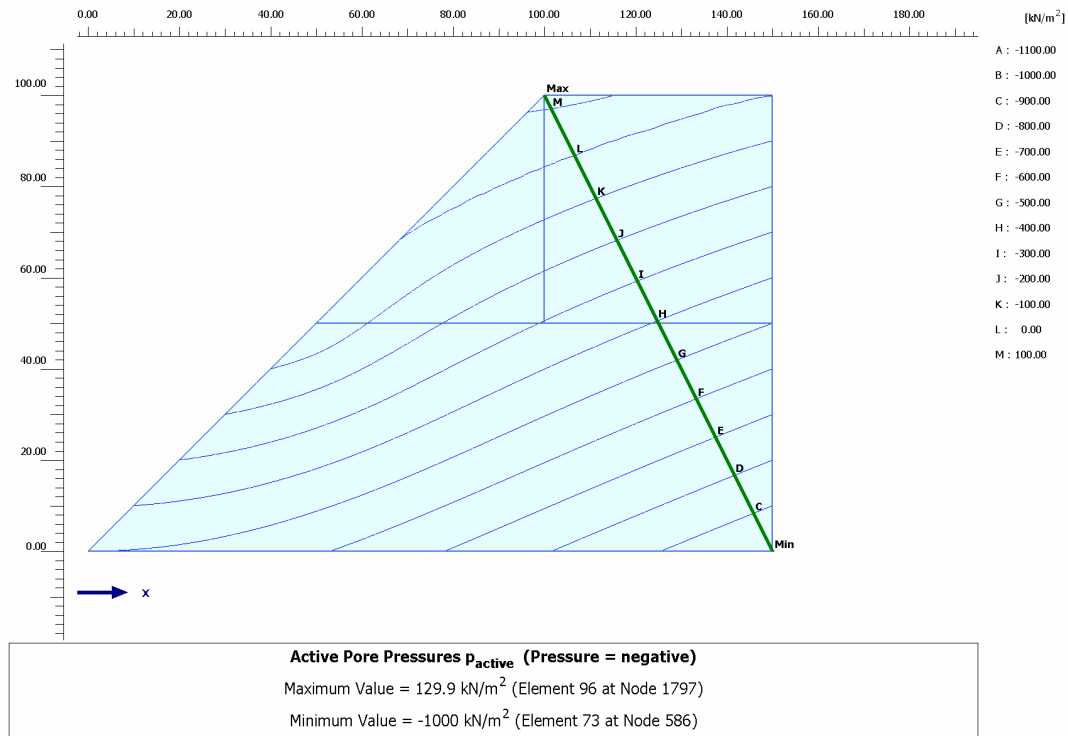


Fig. G5.3.2D: Active pore pressure (PLAXIS 2D)

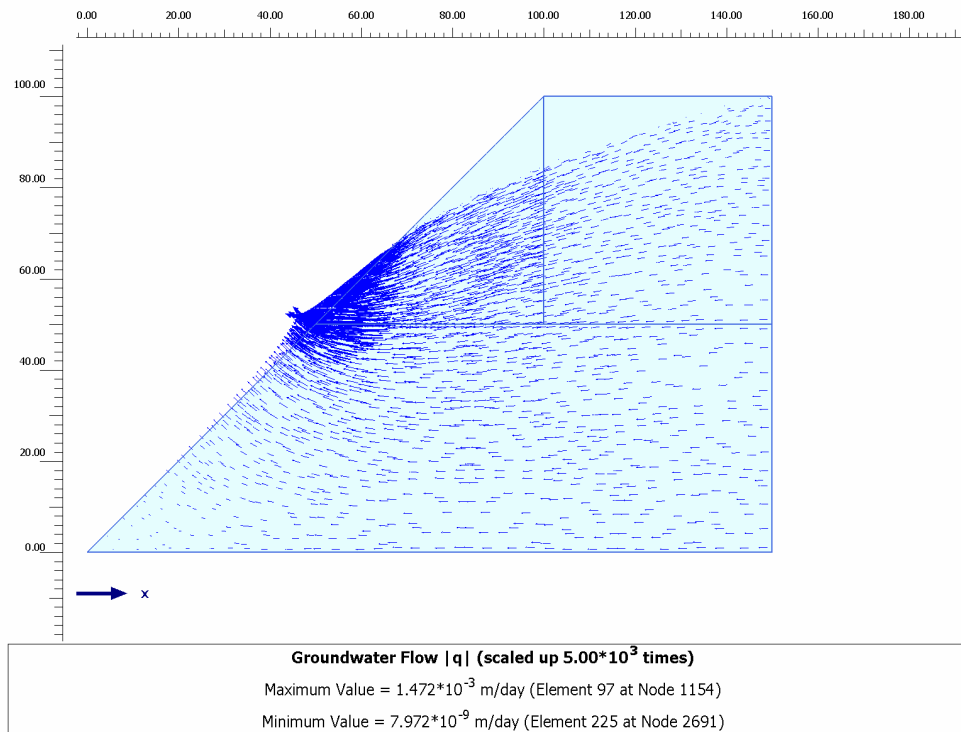


Fig. G5.4.2D: Flow field (PLAXIS 2D)

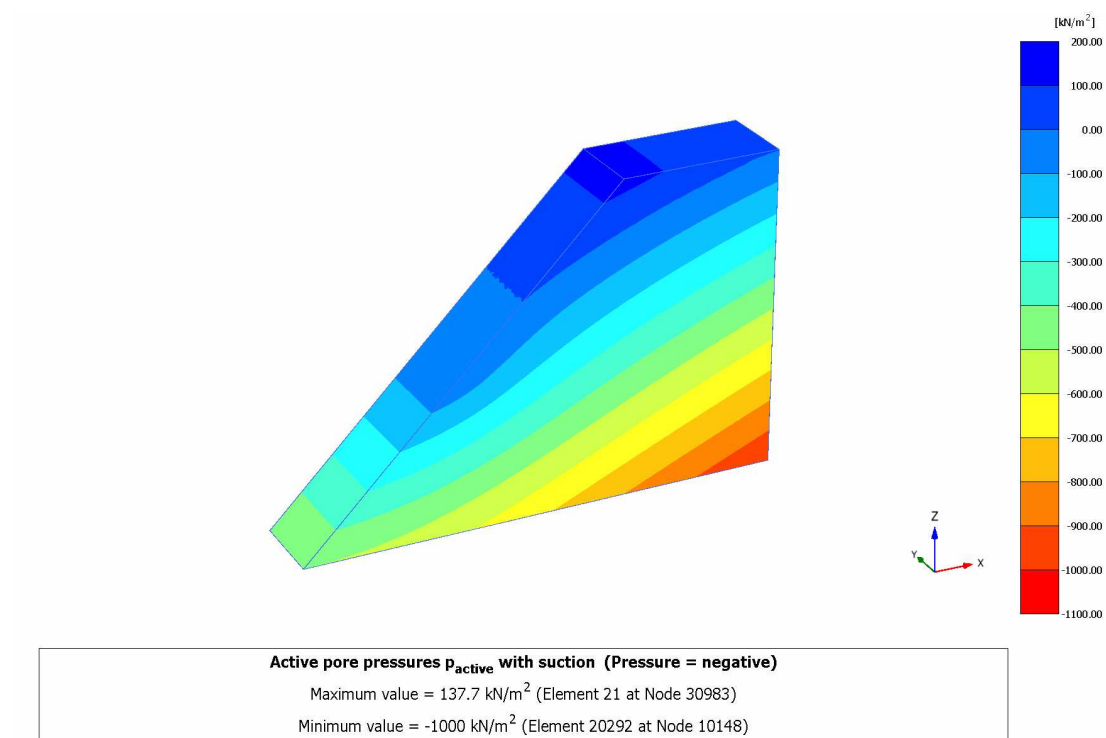


Fig. G5.3.3D: Active pore pressure (PLAXIS 3D)

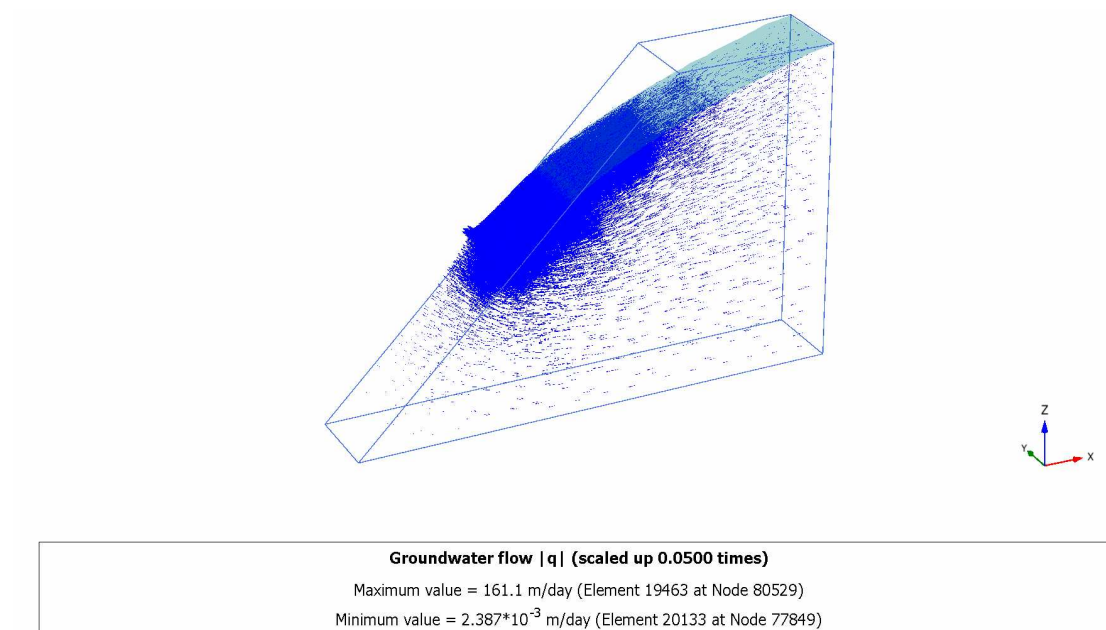


Fig. G5.4.3D: Flow field (PLAXIS 3D)

Tab. G5.1: Seepage length

	Analytical	PLAXIS 2D 15 noded	PLAXIS 3D 10 noded
Seepage length	25.5 m	25.73 m	25.74 m
error	0	0.9 %	0.94 %

Summary:

PLAXIS 2D with 15 noded elements produces the most accurate result. However, the accuracy can be improved by refining the mesh.

8.6 Case G6: Muskat problem (Dam with vertical faces)

In this example a vertical cross section of an unconfined groundwater flow system in a homogeneous earth dam underlain by an impervious base is considered (Fig. G6.1). Such a problem is commonly known as the Muskat problem where the free phreatic surface and the seepage face are unknown, leading thus to a set of nonlinear equations. Permeability of soil is 1.00 m/day.

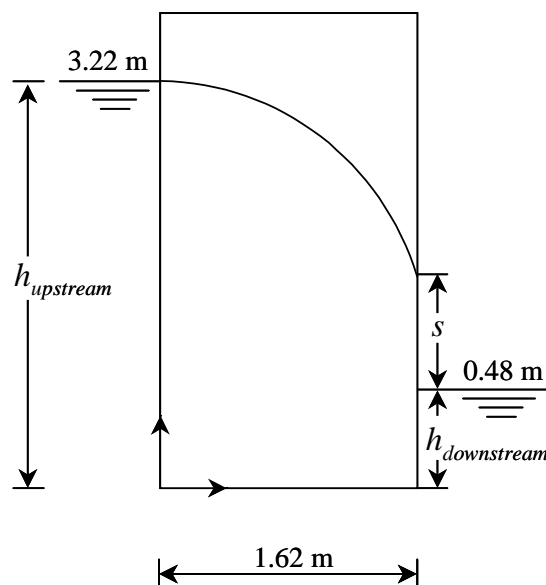


Fig. G6.1: Geometry of the problem

In this section the solution of the Muskat equation for the seepage face (s) has been compared with the non-linear solution of PLAXIS.

Analytical solution: For Muskat equations, monographs which describe the relationship between the geometry of the structure, the heads and the length of the seepage face have been presented by many researchers. Here, the monograph presented by Kang-Kun Lee and Darrell I. Leap, 1997 (Figure G6.2) has been used.

The geometry and boundary conditions of the problem illustrated in Figure G6.1 are simulated by PLAXIS as shown in Figure G6.3. The Finite element mesh consists of 699 15 noded elements with a fourth order of integration. The groundwater flow field and the active pore pressures and seepage surface are shown in Figure G6.4 and Figure G6.5, respectively.

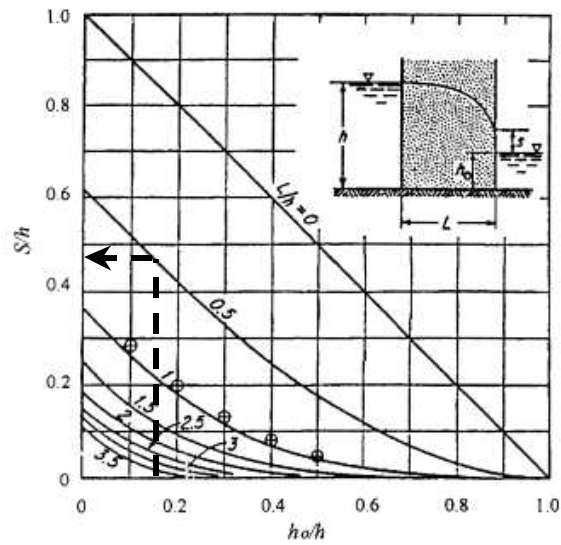


Fig. G6.2: Monograph for Muskat problem (Kang-Kun Lee and Darrell I. Leap, 1997)

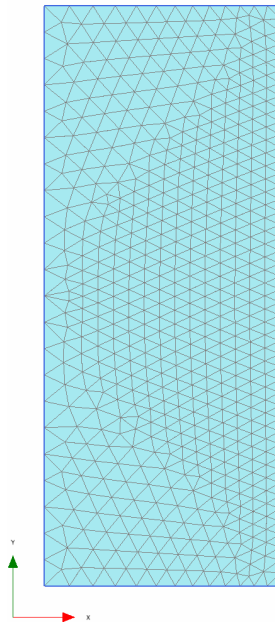


Fig. G6.3.2D: Finite element mesh (PLAXIS 2D - 15 noded elements)

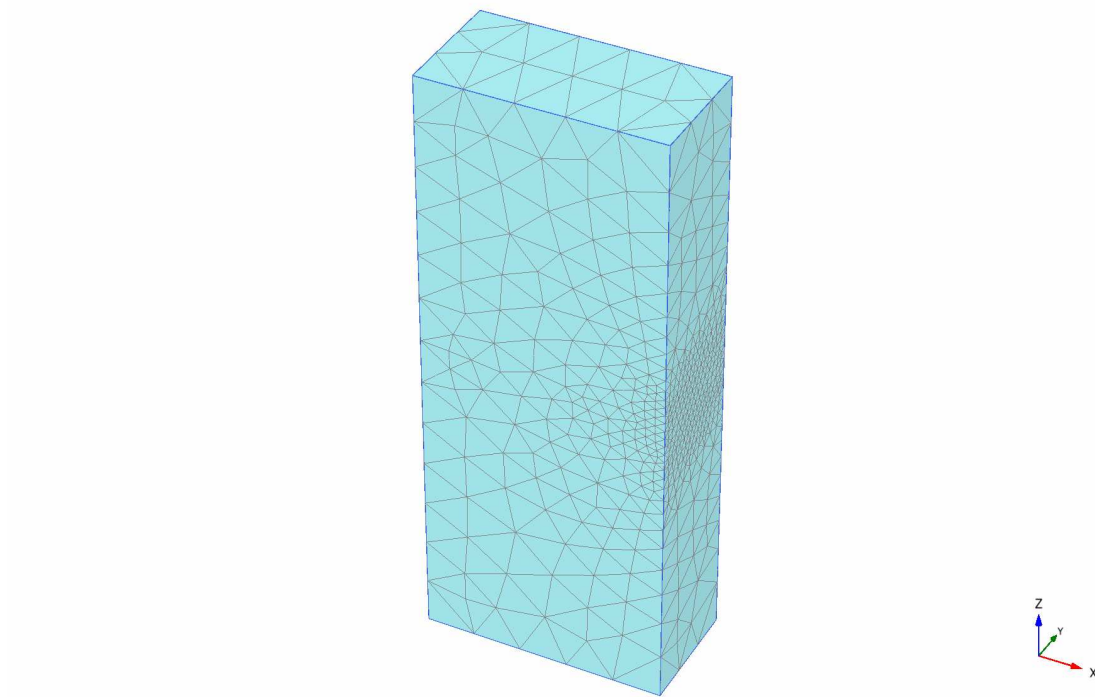


Fig. G6.3.3D: Finite element mesh (PLAXIS 3D - 10 noded tetrahedral elements)

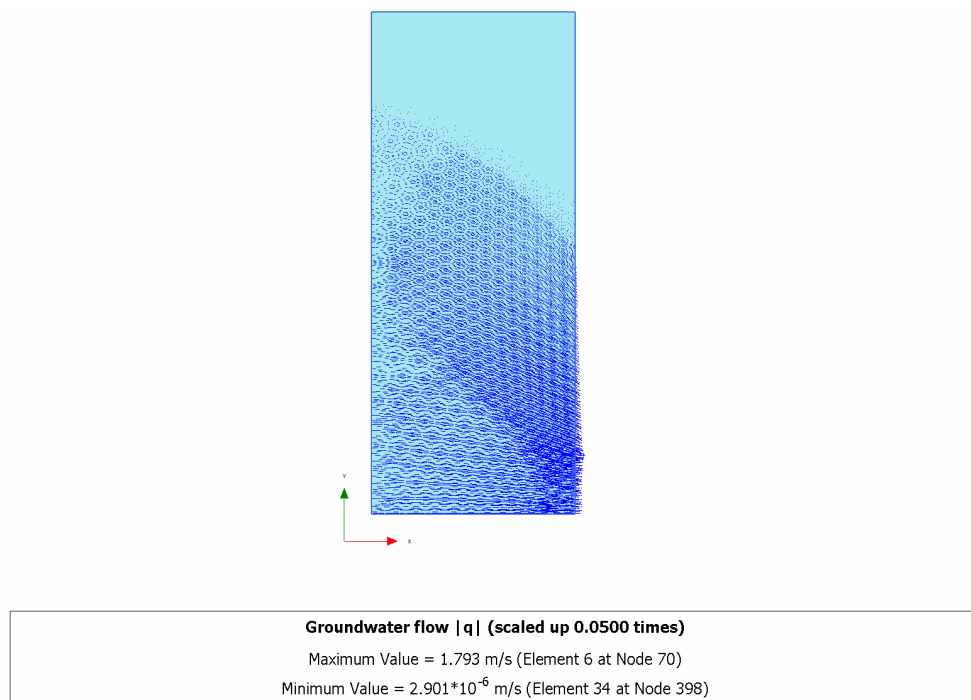


Fig. G6.4.2D: Flow field (PLAXIS 2D)

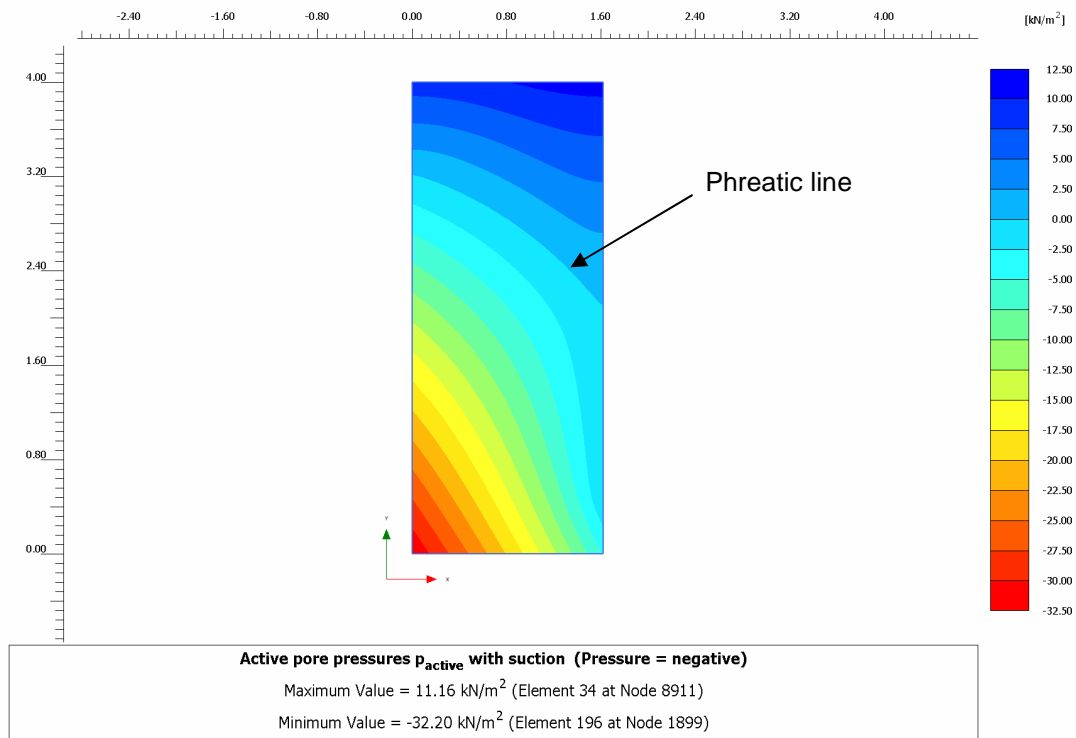


Fig. G5.3.2D: Active pore pressure (PLAXIS 2D)

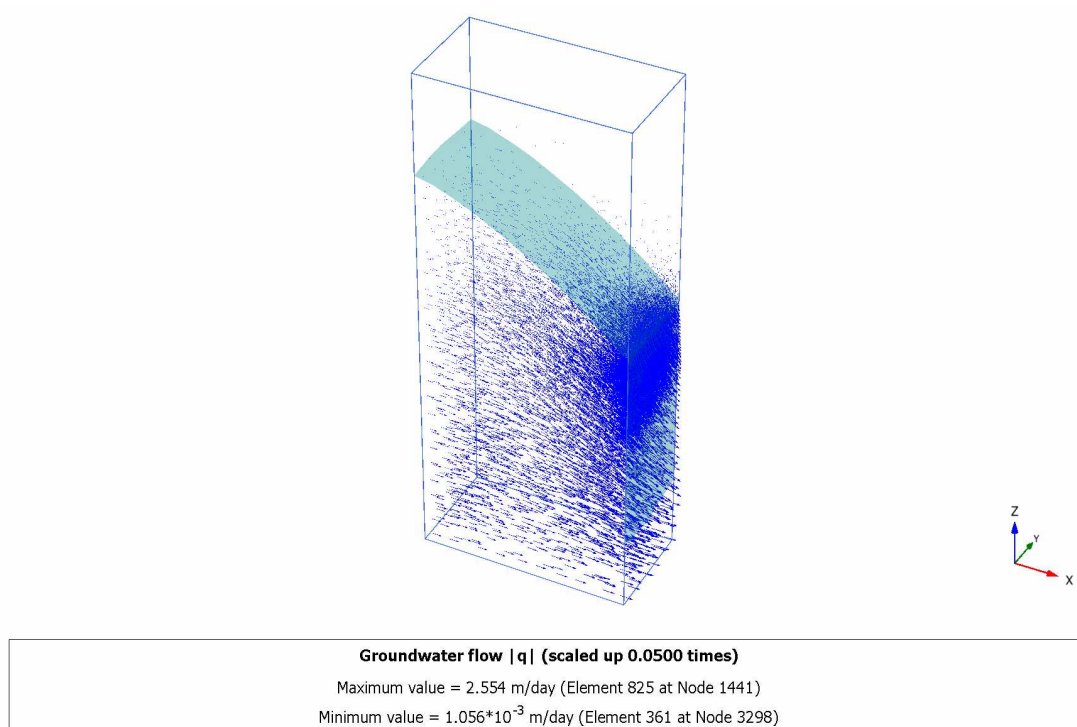
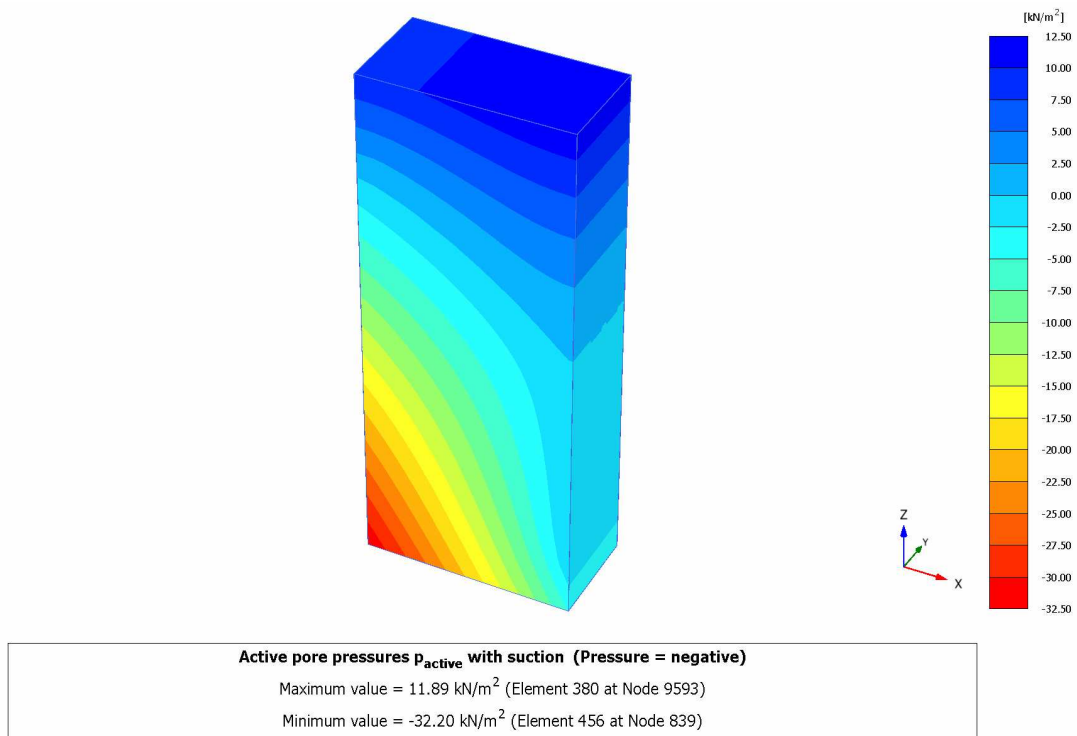


Fig. G6.4.3D: Flow field and phreatic surface (PLAXIS 3D)

**Fig. G5.3.3D:** Active pore pressure (PLAXIS 3D)**Tab. G5.1:** Seepage length

	Analytical	PlaxFlow	PLAXIS 2D 15 noded	PLAXIS 3D 10 noded
Seepage length	1.54 m	1.68 m	1.63 m	1.69 m
error	0	9.1 %	4.6 %	9.7 %

Summary:

As seen the deviation from the analytical solution is pretty high in all cases. Calculation of seepage face is usually affected by the element size of seepage boundaries. In this example, where the seepage boundary is vertical, the effect of the element size is higher.

8.7 Case G7: Well

In this example a column of soil with a well inside is simulated. Geometry of the problem and the finite element mesh is shown in Figure G7.1. Phreatic line is at the top boundary to generate fully saturated soil. The side and the bottom boundaries are closed for flow, therefore inflow or outflow can only occur through the top boundary. The total discharge of well is consider $1 \text{ m}^3/\text{day}$. This example is calculated in PLAXIS 2D (plane strain and axi-symmetric) and in PLAXIS 3D.

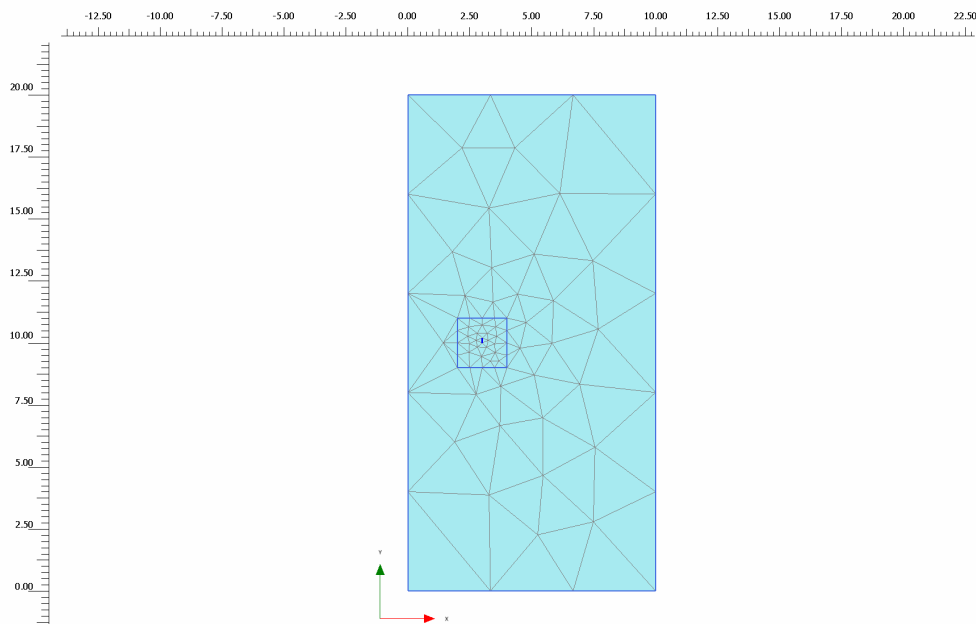


Fig. G7.1.2D: Geometry and FE mesh (PLAXIS 2D)

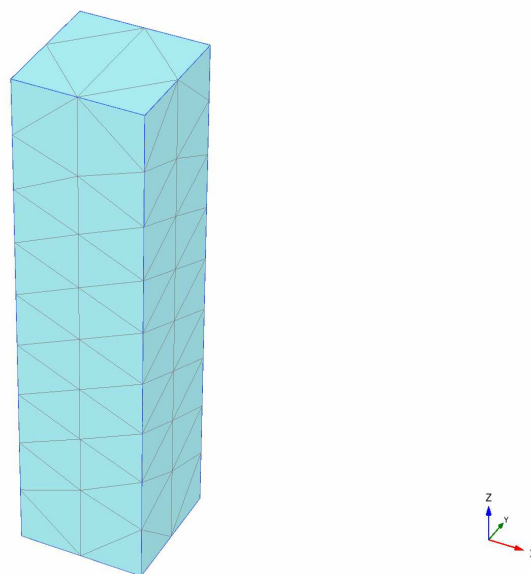


Fig. G7.1.3D: Geometry and FE mesh (PLAXIS 3D)

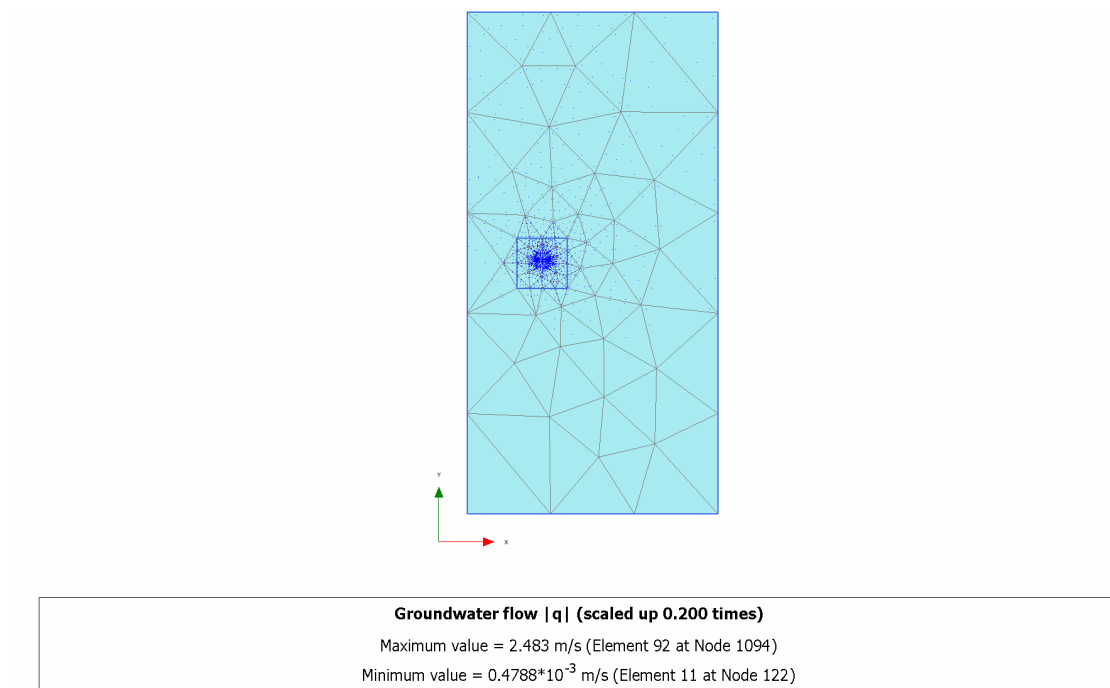


Fig. G7.2.2D.1: Flow field (PLAXIS 2D – plane strain)

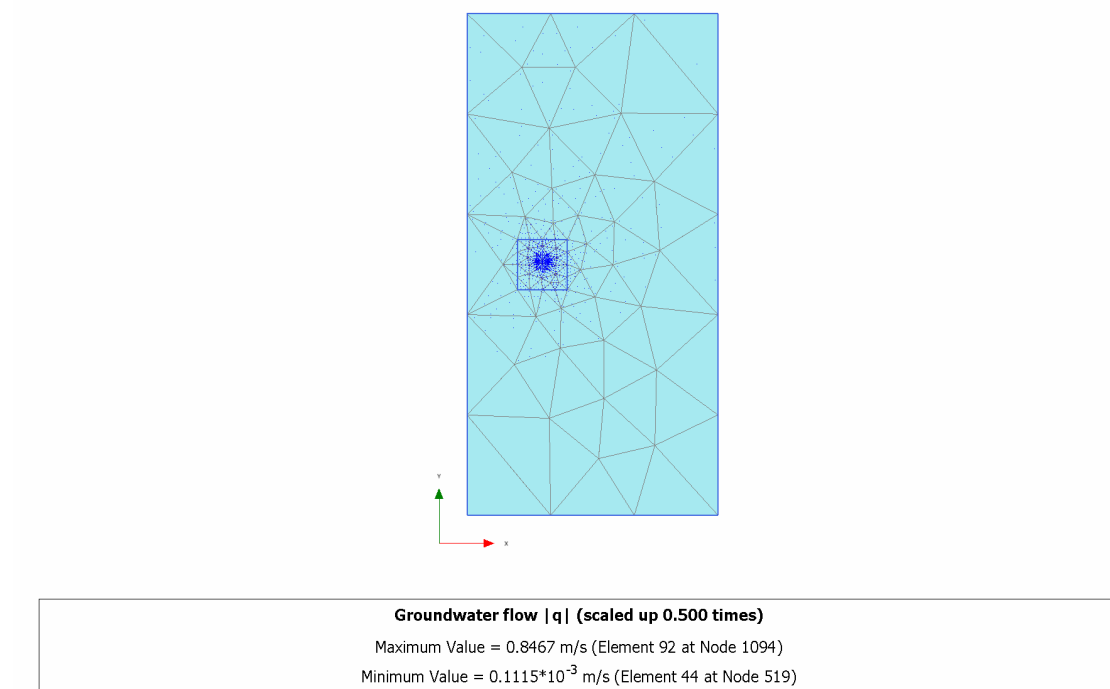


Fig. G7.2.2D.2: Flow field (PLAXIS 2D – axis-symmetric)

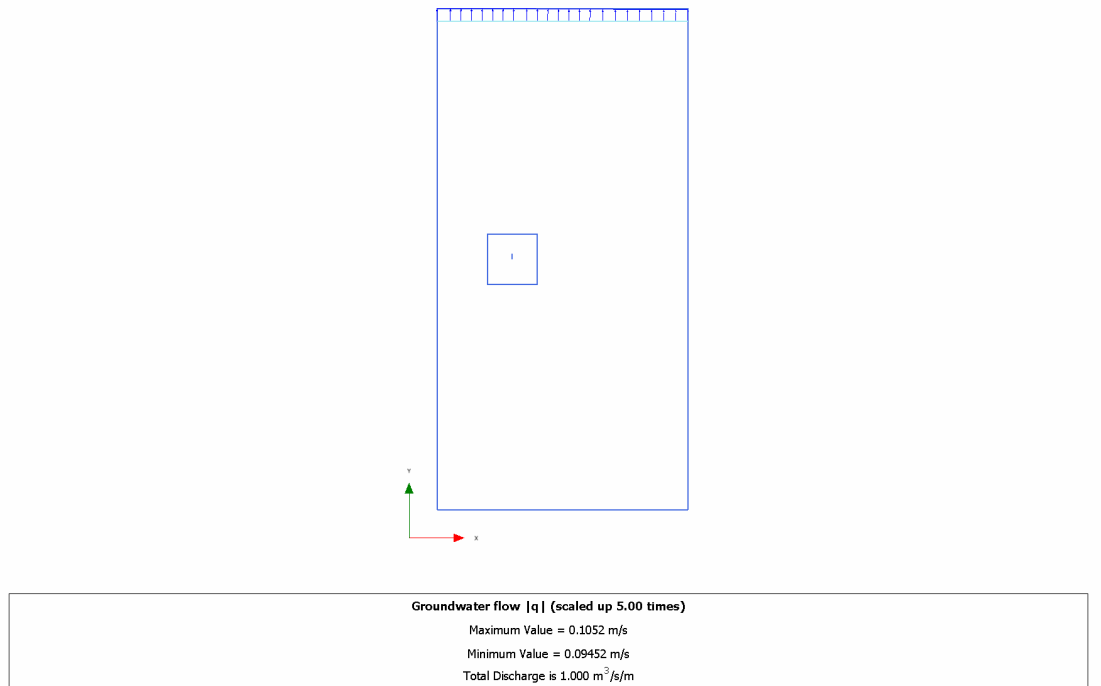


Fig. G7.3.2D.1: Total discharge leaving the domain; $Q=1.0 \text{ m}^3/\text{day}/\text{m}$ (PLAXIS 2D – plane strain)

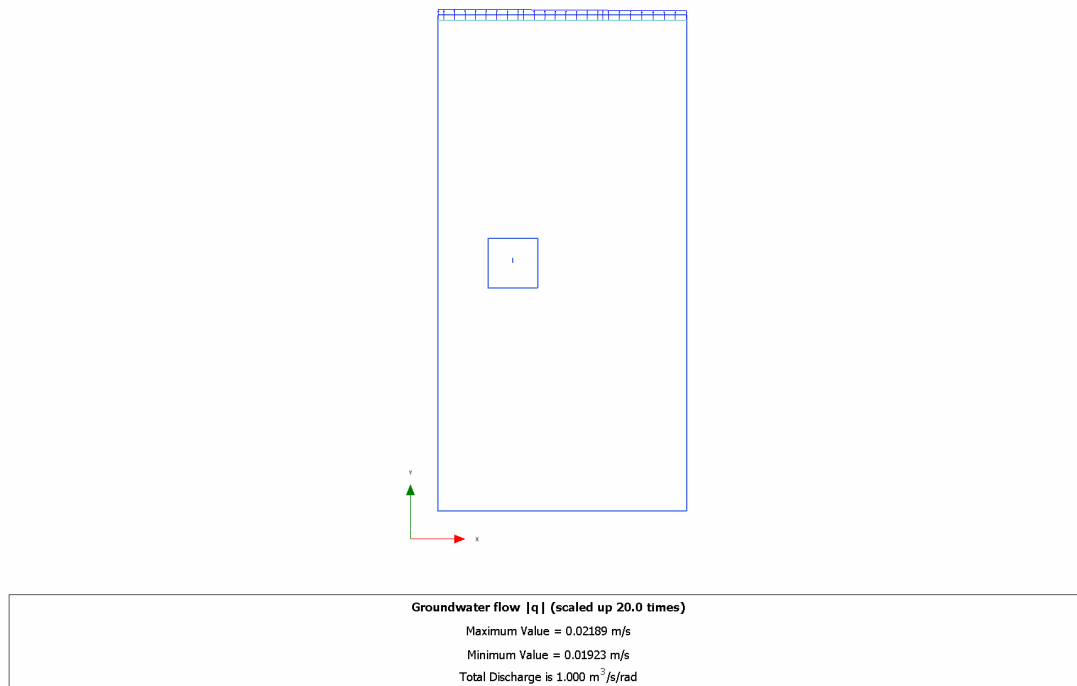


Fig. G7.3.2D.2: Total discharge leaving the domain; $Q=1.0 \text{ m}^3/\text{day}/\text{rad}$ (PLAXIS 2D – axis-symmetric)

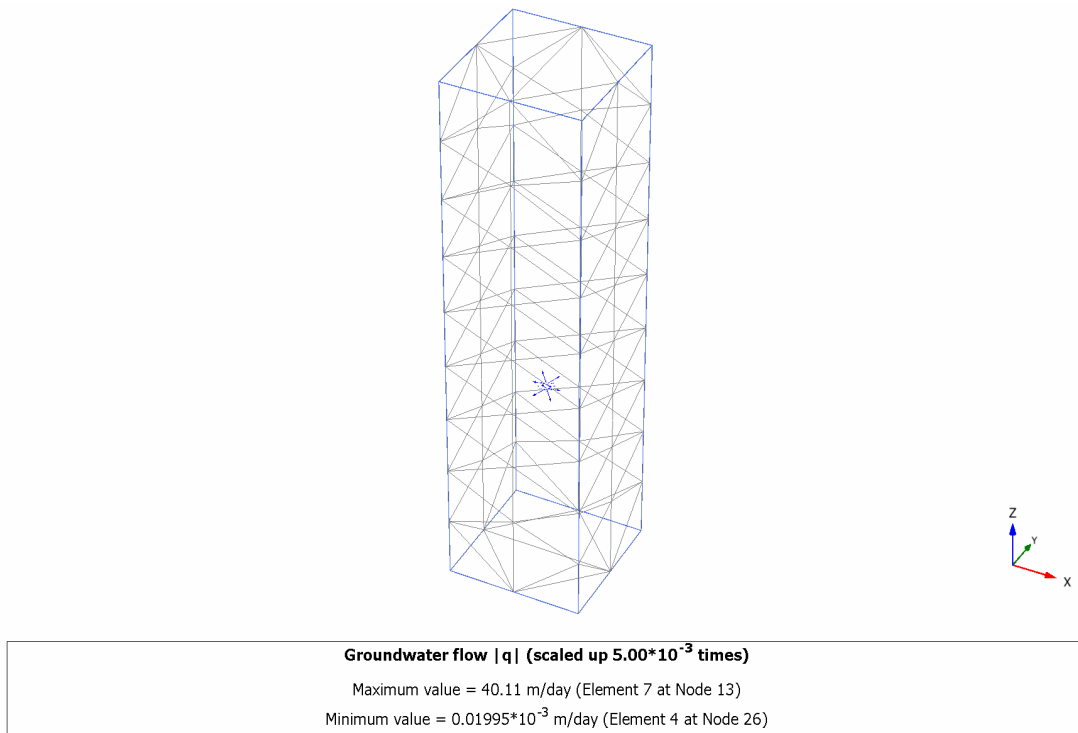
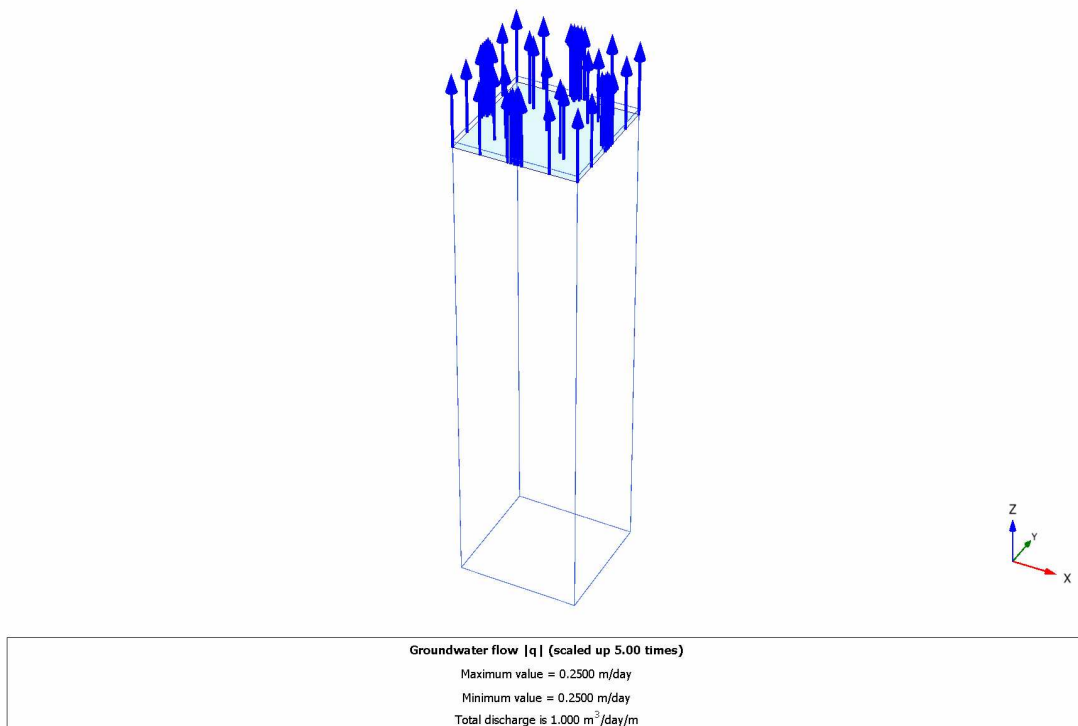
**Fig. G7.2.3D:** Flow field (PLAXIS 3D)**Fig. G7.3.3D:** Total discharge leaving the domain; $Q=1.0 \text{ m}^3/\text{day}$ (PLAXIS 3D)*Summary:*

Figure G7.2 and Figure G7.3 show flow field and total discharge after activation of the well. As seen the total discharge is exactly the same as total discharge imposed in the well.

8.8 Case G8: Drain

In this example a block of soil with a drain inside is simulated with PLAXIS 2D and PLAXIS 3D. Geometry of the problem and the finite element mesh is shown in Figure G8.1. The block is 50 m long, 20 m high (and 10 m wide in case of 3D) and the drain is exactly in the middle. The initial water level is at 18 m. Permeability of soil is 1 m/day and coarse material (from standard data set) is used for retention curve. Steady state type of calculation is used. The minimum head of drain is 10 m.

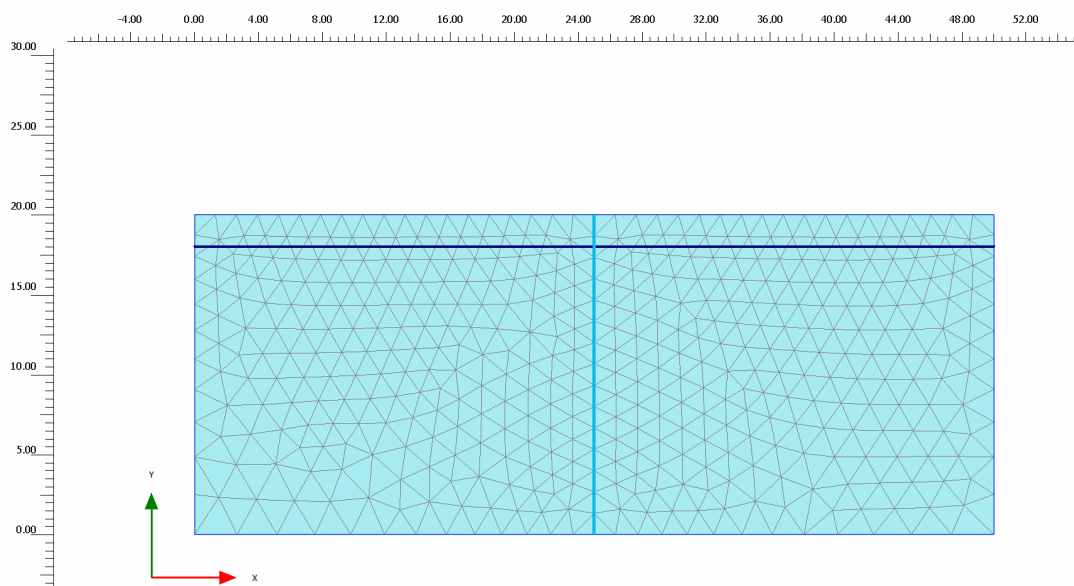


Fig. G8.1.2D: Geometry and FE mesh (PLAXIS 2D)

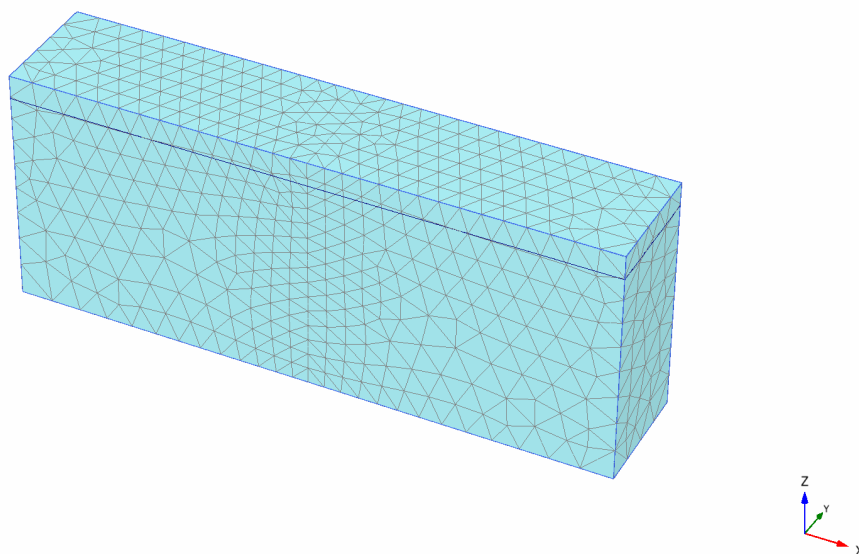
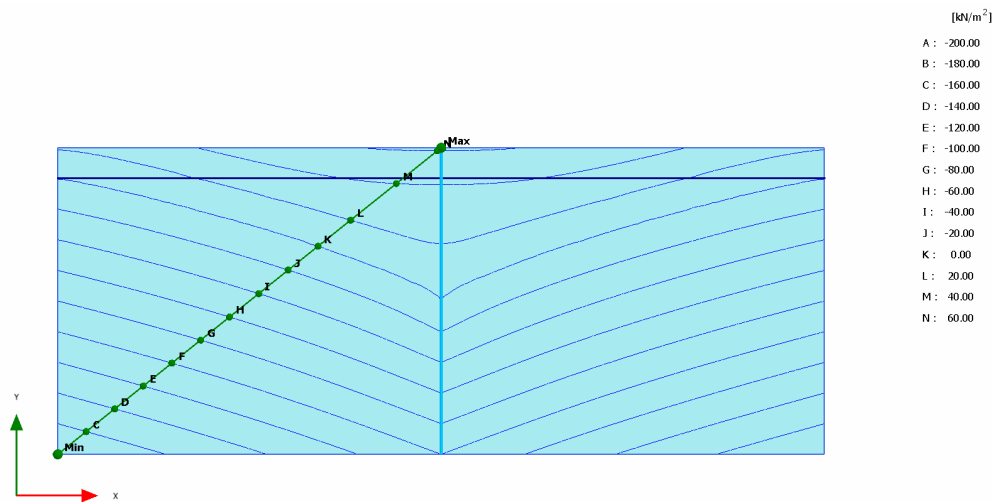
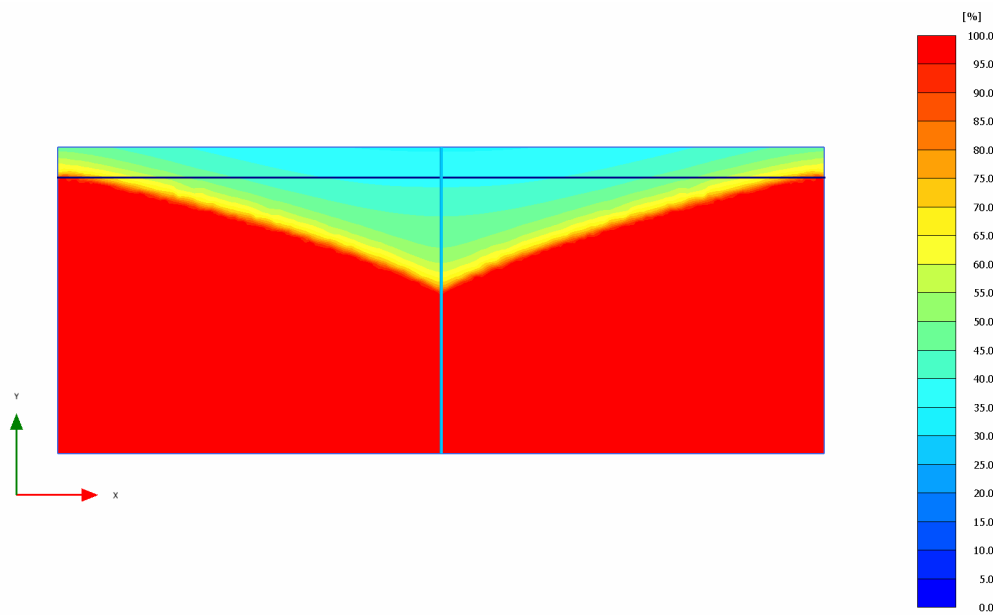


Fig. G8.1.3D: Geometry and FE mesh (PLAXIS 3D)



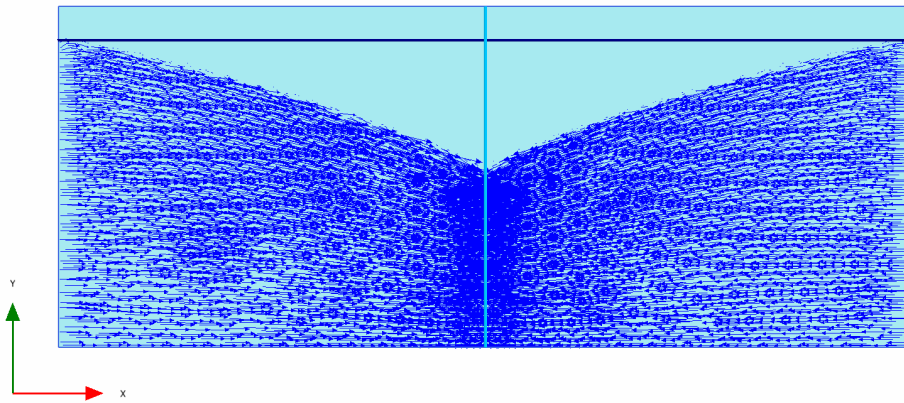
Active pore pressures p_{active} with suction (Pressure = negative)
Maximum value = 61.97 kN/m² (Element 4 at Node 3805)
Minimum value = -180.0 kN/m² (Element 412 at Node 578)

Fig. G8.2.2D: Active pore pressure (PLAXIS 2D)



Saturation
Maximum value = 100.0 % (Element 1 at Node 3015)
Minimum value = 34.49 % (Element 4 at Node 3805)

Fig. G8.3.2D: Degree of saturation (PLAXIS 2D)

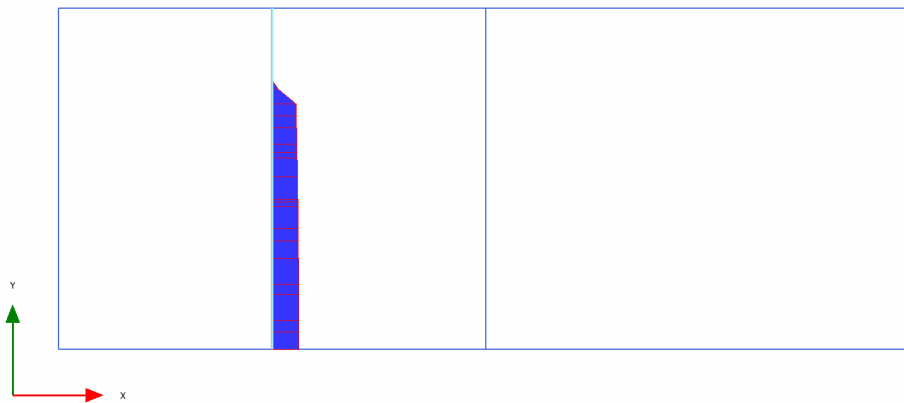


Groundwater flow $|q|$ (scaled up 5.00 times)

Maximum value = 0.9323 m/day (Element 31 at Node 369)

Minimum value = $0.5022 \cdot 10^{-6}$ m/day (Element 438 at Node 5247)

Fig. G8.4.2D: Flow field (PLAXIS 2D)



Groundwater flow $|q|$ (scaled up 5.00 times)

Maximum value = 0.3137 m/day

Minimum value = 0.000 m/day

Total discharge is $4.473 \text{ m}^3/\text{day/m}$

Fig. G8.5.2D: Total discharge in soil; $Q=4.473 \text{ m}^3/\text{day/m}$ (PLAXIS 2D)

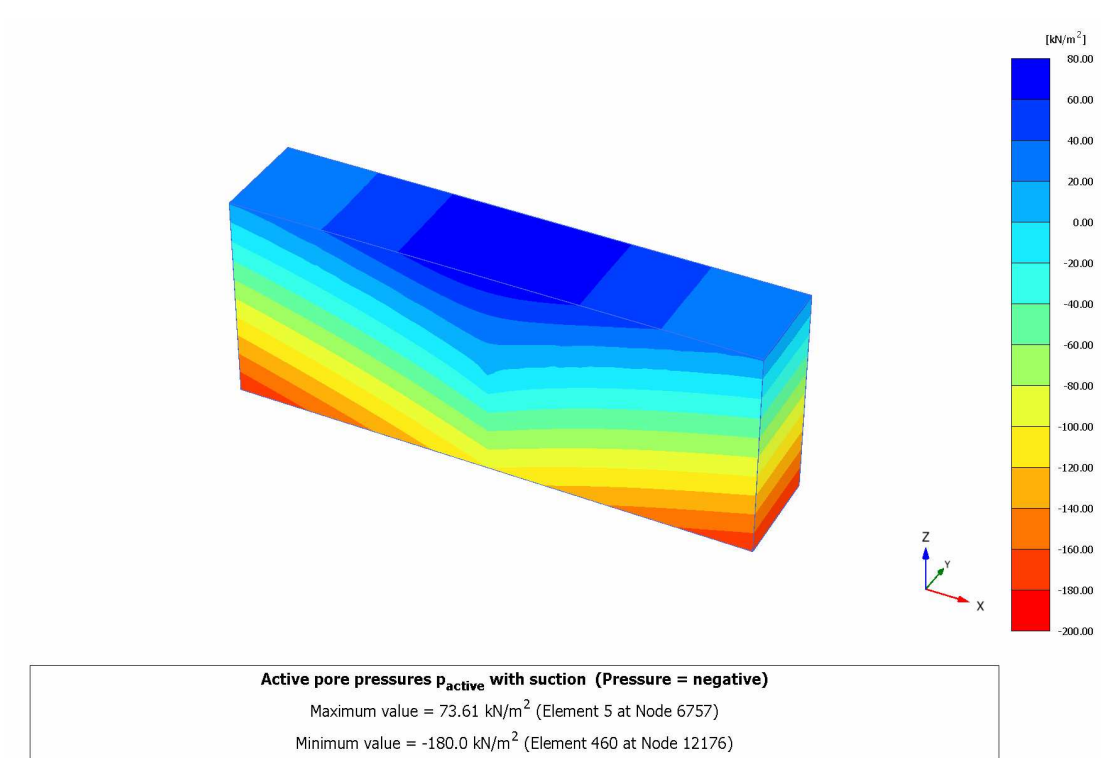


Fig. G8.2.3D: Active pore pressure (PLAXIS 3D)

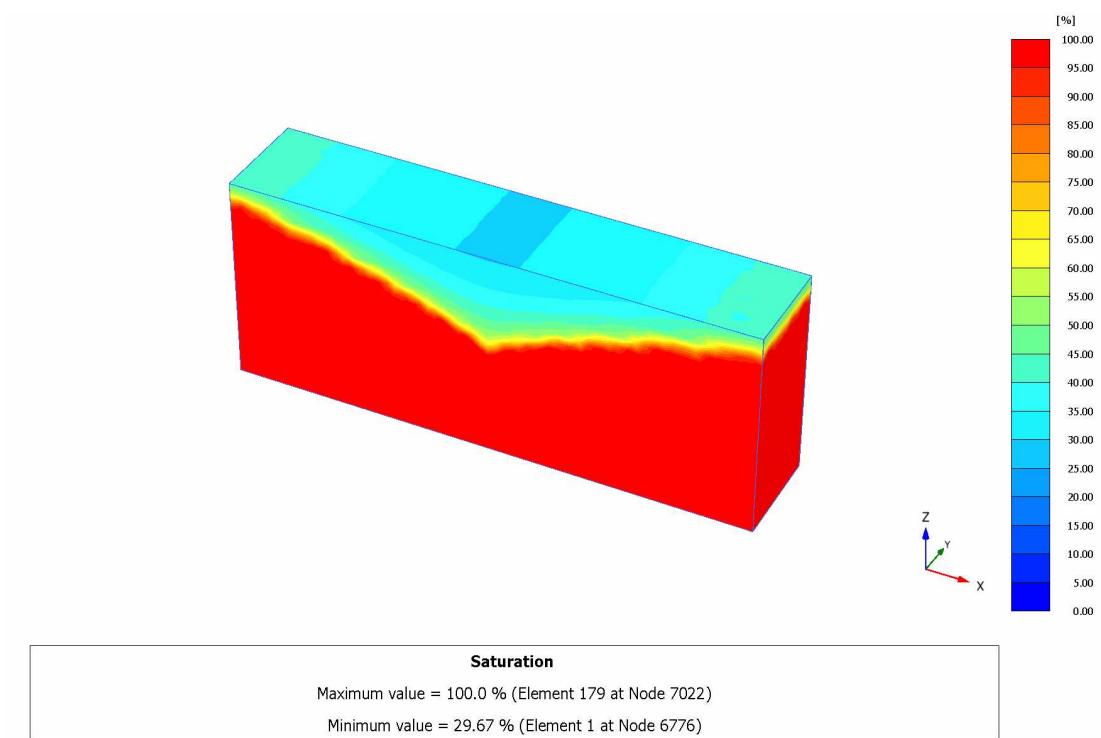


Fig. G8.3.3D: Degree of saturation (PLAXIS 3D)

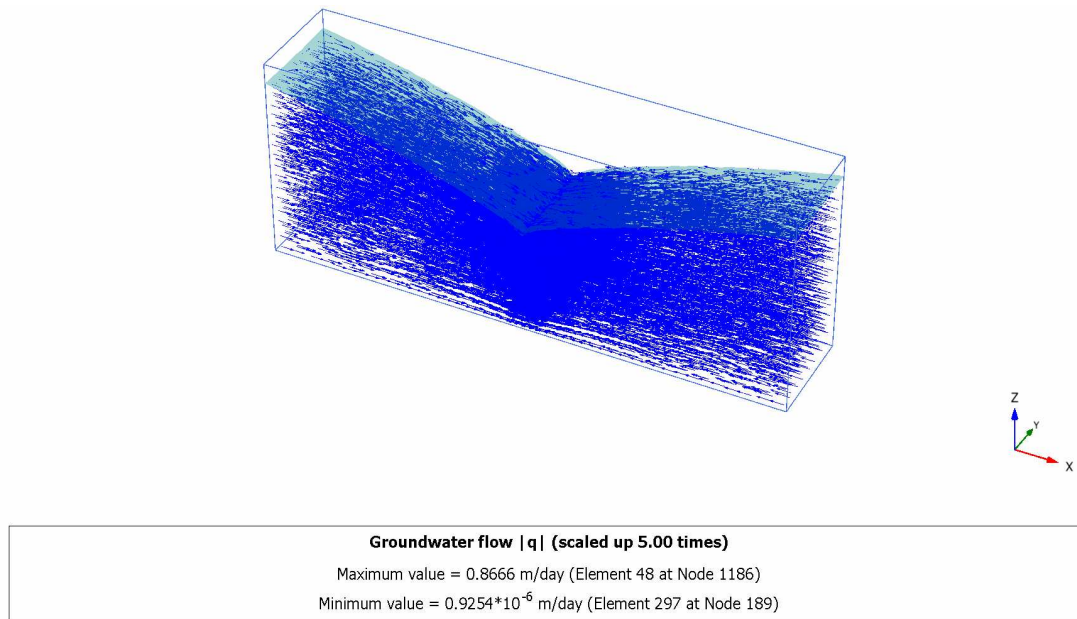


Fig. G8.4.3D: Flow field (PLAXIS 3D)

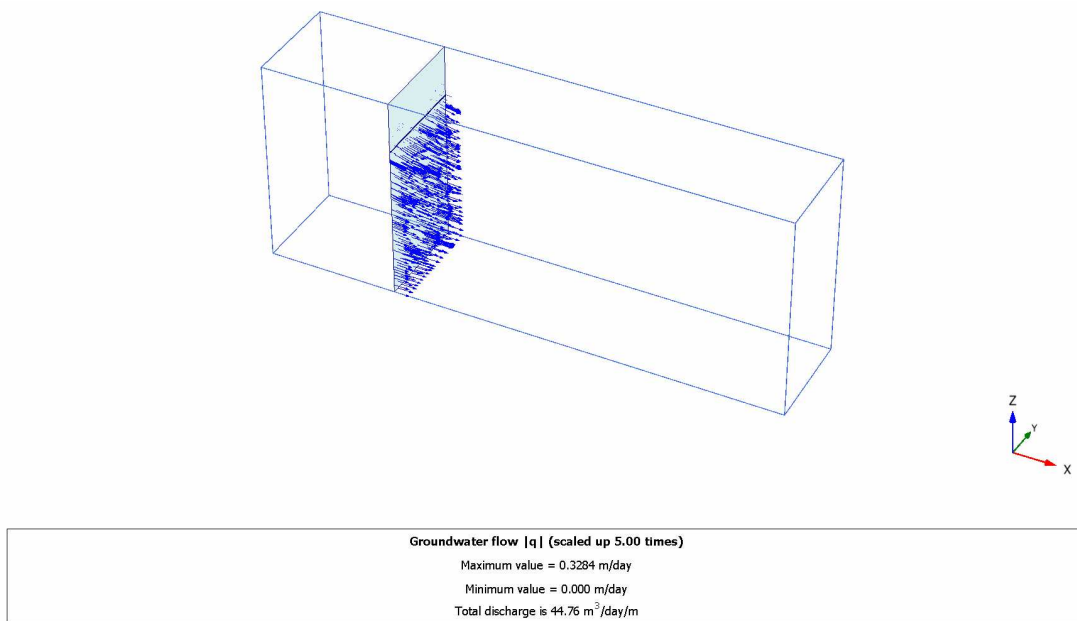


Fig. G8.5.3D: Total discharge in soil; $Q=4.476 \text{ m}^3/\text{day}/\text{m}$ (PLAXIS 3D)

Analytical solution: Under the assumption of a hydrostatic pore pressure distribution for each vertical cross-section the total discharge, Q , through the layer can be approximated with Dupuit's formula for unconfined flow:

$$Q = k \frac{\varphi_1^2 - \varphi_2^2}{2L}$$

where k is the permeability, L is the distance between the left boundary (or the right boundary) and the drain and φ_1 and φ_2 are the ground water head at the left (or right) and at the drain boundary, respectively. For the current situation this

results in a theoretical solution of $4.48 \text{ m}^3/\text{day}/\text{m}$. Therefore the total amount of water leaving from the drain is $8.96 \text{ m}^3/\text{day}/\text{m}$. The comparison between the total discharges simulated with PLAXIS 2D and 3D and the analytical solution are given in Table G8.1.

Tab. G8.1: Total discharge

	Analytical	PLAXIS 2D 15 noded	PLAXIS 3D 10 noded
In soil	4.48	4.473 (0.16 % error)	4.476 (0.09 % error)
drain	8.96	8.975 (0.17 % error)	8.966 (0.07 % error)

Summary:

It can be seen that both PLAXIS 2D and PLAXIS 3D are capable of simulating drains with a given head. The errors in the total discharge leaving the domain are quite low in both 2D and 3D simulations.

8.9 Case G9: Flow through an earth dam

The following problem illustrates water seepage through an earth dam with a toe drain. Due to the unknown phreatic level and the unknown size of the seepage surface the flow is an unconfined flow. The flow net technique can be used to solve this problem.

The water level on the upstream side is at a level of 12.2 m while on the down stream side the water level is at the surface level. The coefficient of permeability of the soil is 1.52×10^{-5} m/sec. Figure G9.1 shows the geometry of the problem. The material for drainage at the toe is simulated by a relatively high coefficient of permeability, 0.3048 m/sec. The saturated model is used to describe the hydraulic behavior of the soil.

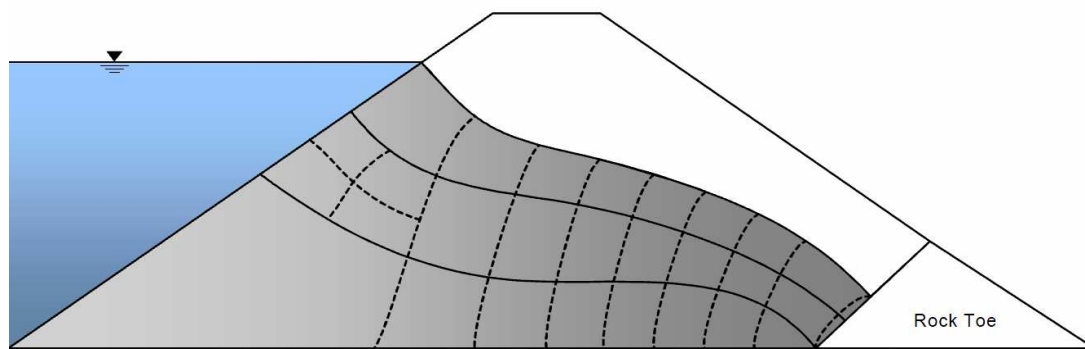


Fig. G9.1: Geometry of the problem

Analytical solution: The total discharge as calculated by the flow net is $Q = 4.708 \text{ m}^3/\text{day}/\text{m}$.

The geometry and finite element mesh used for the calculation in PLAXIS is shown in Figure G9.2. The model is 10 m wide in the 3D simulations. In 2D calculations both 6 noded and 15 noded elements are used. Figures G9.3 to G9.4 show the active pore pressures and the total discharge at the middle of the dam for 2D (6-noded and 15 noded elements) and 3D simulations.

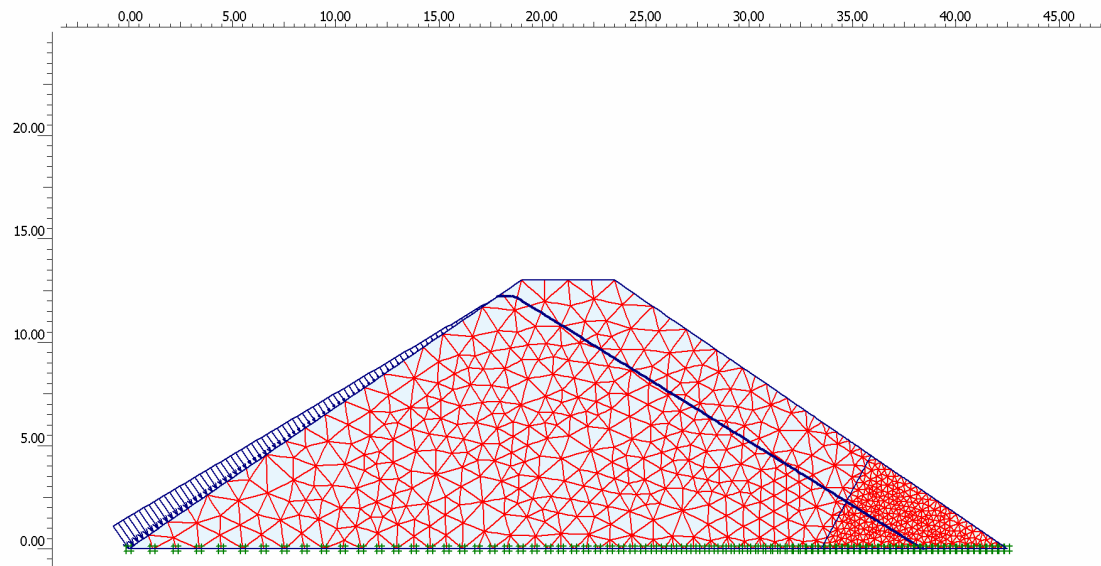


Fig. G9.2.2D: Geometry and FE mesh (PLAXIS 2D)

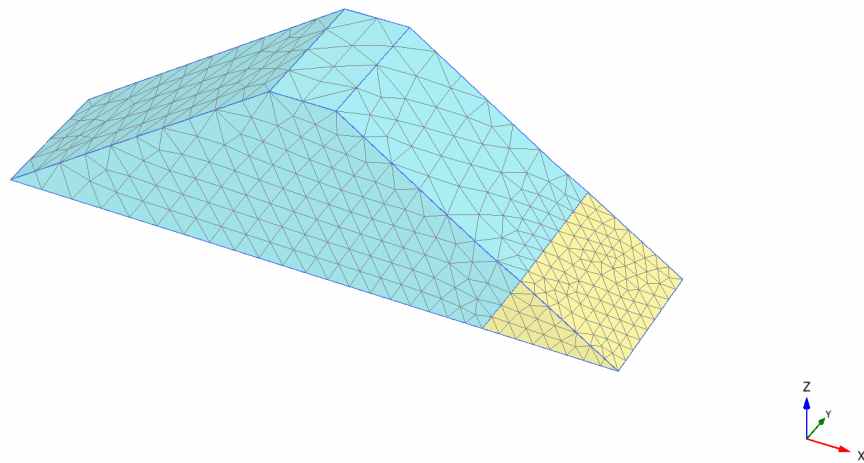


Fig. G9.2.3D: Geometry and FE mesh (PLAXIS 3D)

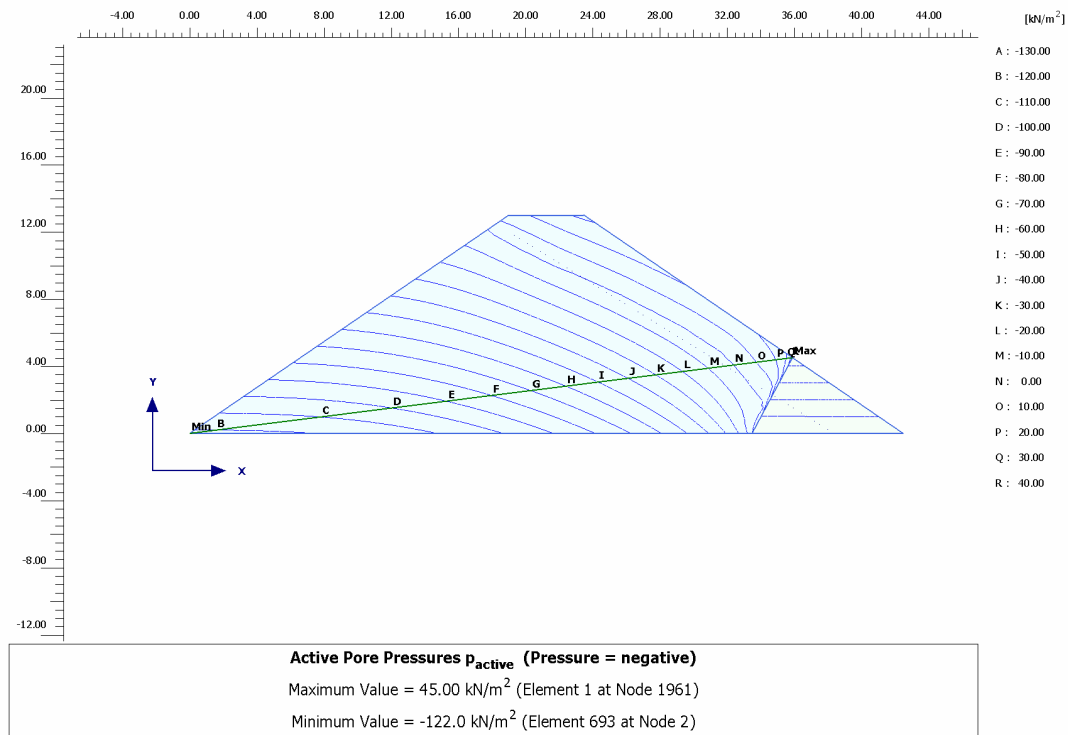


Fig. G9.3.2D6: Active pore pressures (6-noded elements)

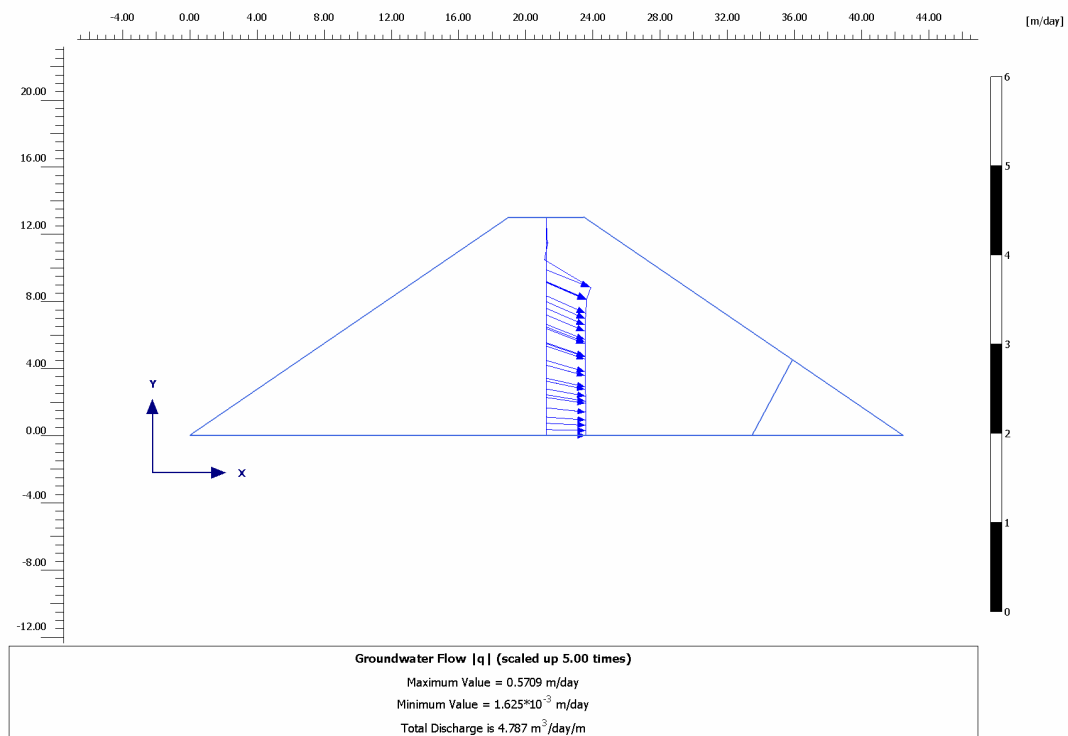


Fig. G9.4.2D6: Total discharge at the middle of the earth dam for 6-noded elements mesh ($Q = 4.787 \text{ m}^3/\text{day}/\text{m}$)

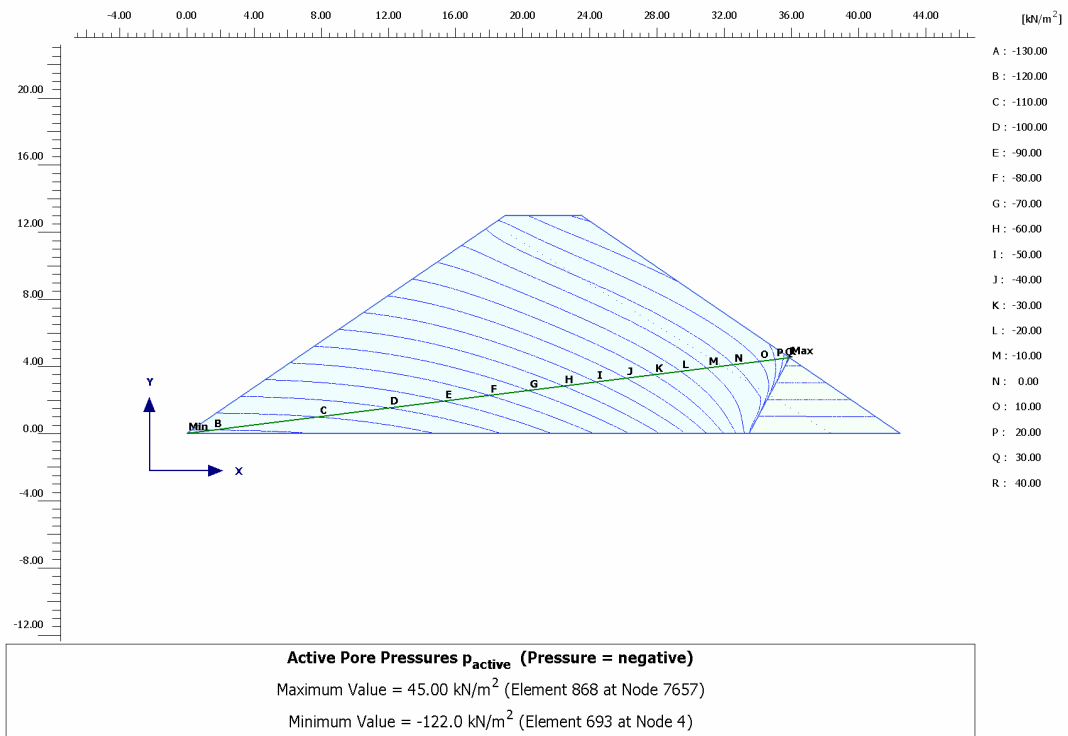


Fig. G9.3.2D15: Active pore pressures (15-noded elements)

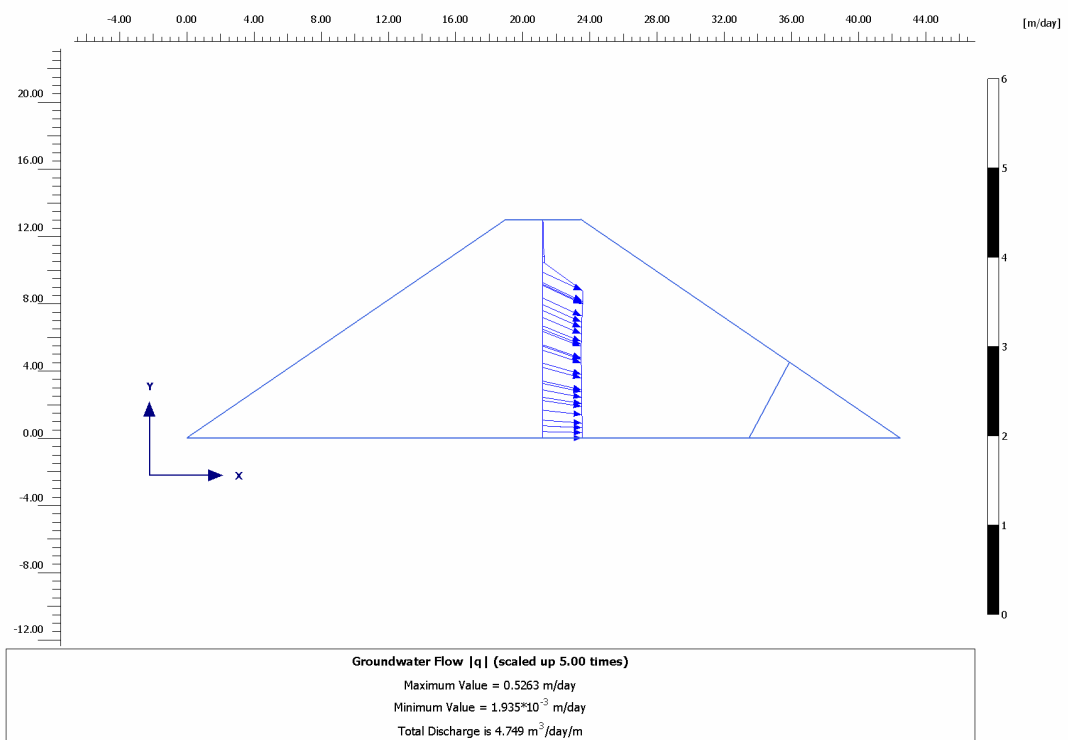


Fig. G9.4.2D15: Total discharge at the middle of the earth dam for 15-noded elements mesh ($Q = 4.749 \text{ m}^3/\text{day/m}$)

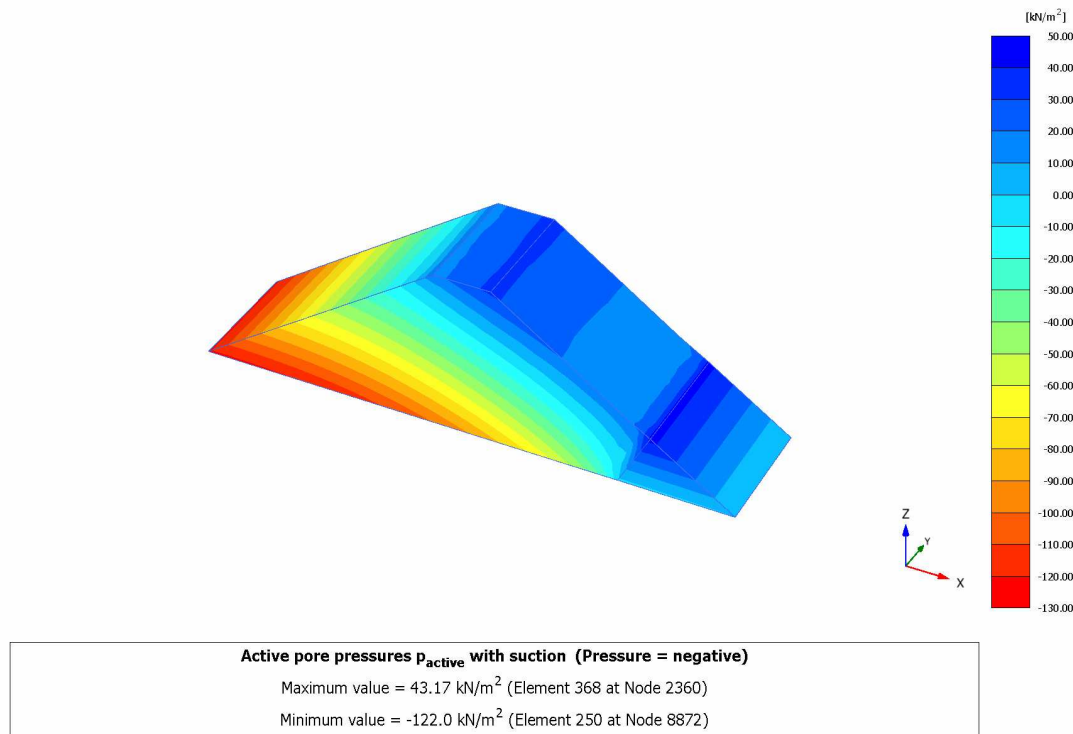


Fig. G9.3.3D: Active pore pressures (15-noded elements)

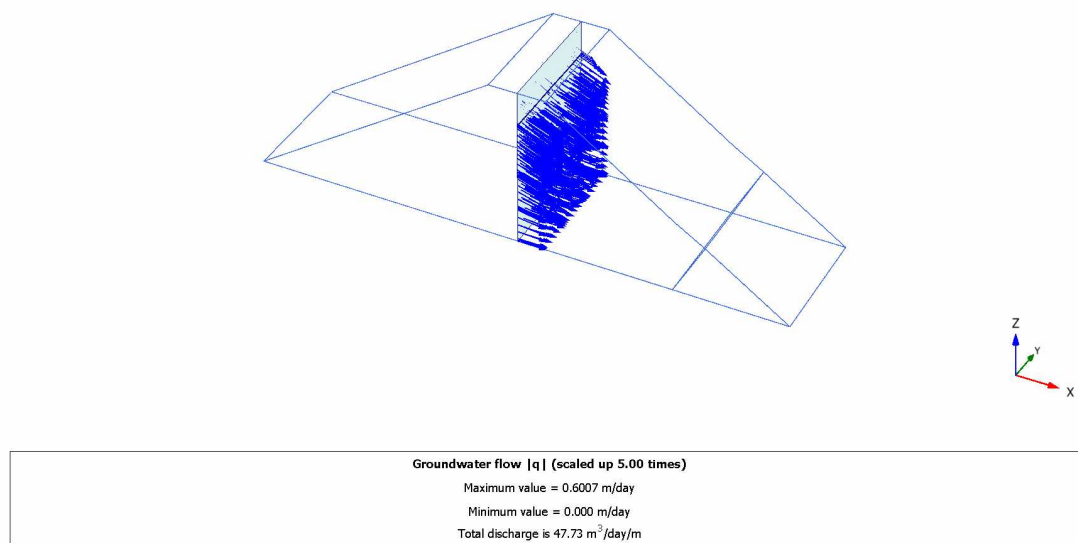
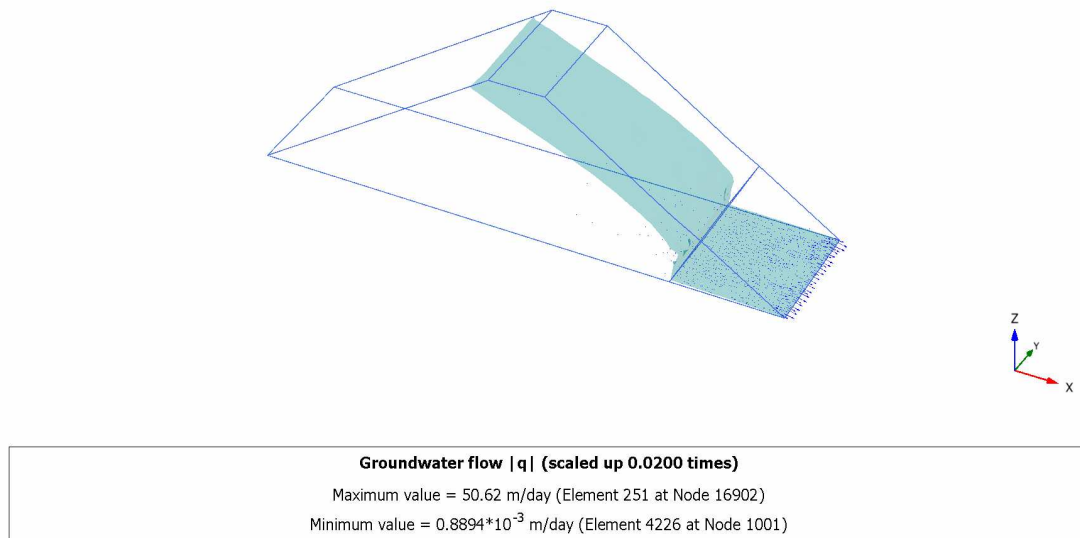


Fig. G9.4.3D: Total discharge at the middle of the earth dam; $Q = 4.773$ m³/day/m (PLAXIS 3D)

**Fig. G9.5.3D:** Flow field and calculated phreatic surface (PLAXIS 3D)**Tab. G9.1:** Total discharge

	Analytical	PLAXIS 2D 6 noded	PLAXIS 2D 15 noded	PLAXIS 3D 10 noded
Total discharge	4.708 $\text{m}^3/\text{day}/\text{m}$	4.787 $\text{m}^3/\text{day}/\text{m}$	4.749 $\text{m}^3/\text{day}/\text{m}$	4.773 $\text{m}^3/\text{day}/\text{m}$
error	0	1.68 %	0.87 %	1.38 %

Summary:

Apparently the results of both analytical and PLAXIS calculations are similar.

8.10 Case G10: Non-homogeneous rectangular dam

This is an example used by different researchers to show the capability of the groundwater flow codes to solve unconfined problems (e.g. Oden and Kikuchi (1980); Lacy and Prevost (1987); Borja and Kishnani (1991); Bardet and Tobita (2002)). Figure G10.1 shows the geometry of the problem which is 5 m wide and 10 m high (and 2.5 m thick in 3D). This dam consists of two blocks with different saturated permeability. Permeability of soil is 1.0 m/day for the left block and 10.0 m/day for the right block. The left, top and the right boundaries are considered as seepage boundary and the bottom is closed for flow.

To investigate the effect of retention curve on the results, four cases have been considered, namely fully saturated, starting set (sand O1), Hypres coarse top soil and USDA sand, see the PlaxFlow manual. The Van Genuchten parameters are given in Table G10.1.

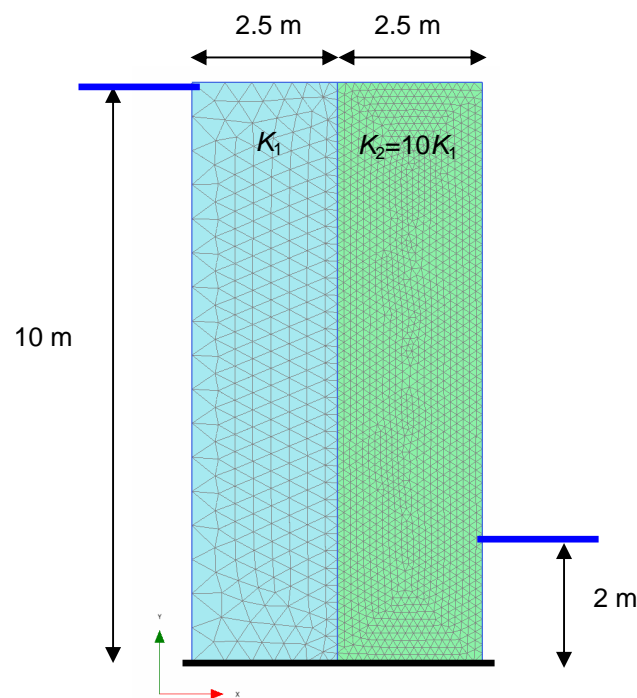


Fig. G10.1.2D: Geometry, boundary conditions and FE mesh (6 noded elements)

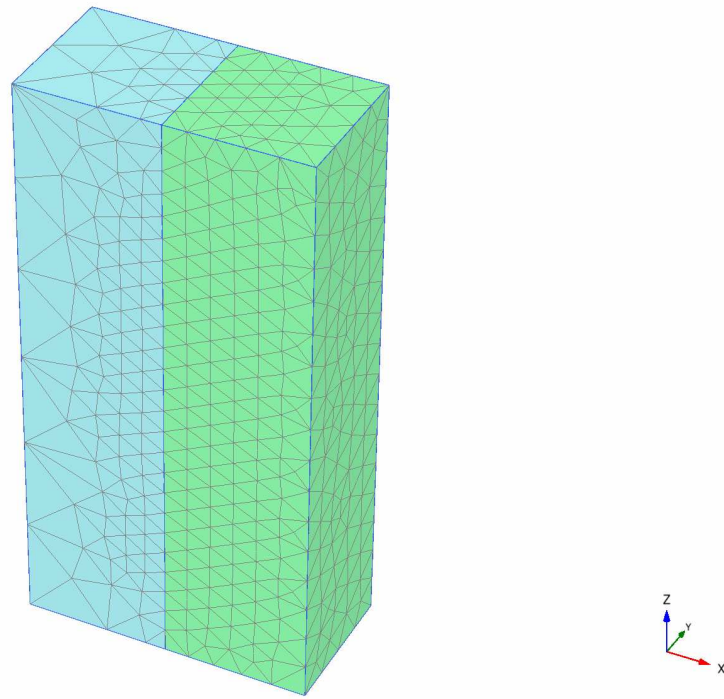


Fig. G10.1.3D: FE mesh (PLAXIS 3D 10 noded elements)

Tab. G10.1: Van Genuchten parameters

Data set	S_{sat} [-]	S_{res} [-]	g_a [m ⁻¹]	g_l [-]	g_n [-]
Staring (O1)	1.0	0.02	2.240	0.000	2.286
Hypres (coarse-top soil)	1.0	0.02	3.830	1.250	1.3774
USDA (sand)	1.0	0.02	14.500	0.500	2.680

Figure G10.2 shows a comparison of the calculated phreatic levels for the problem from different codes (Bardet & Tobita, 2002).

The location of phreatic level calculated with PLAXIS 2D is shown in Figure G10.3 and G10.4 for different types of material. As seen the shape of the phreatic line (or surface) is affected by the type of material used for the soils. The phreatic levels in Figure G10.3b and G10.3d are similar to the results of Bardet & Tobita (2002) and Oden and Kikuchi (1980) while by using Staring sand (O1) material, PLAXIS 2D provides results similar to the results of Borja & Kishnani (1991).

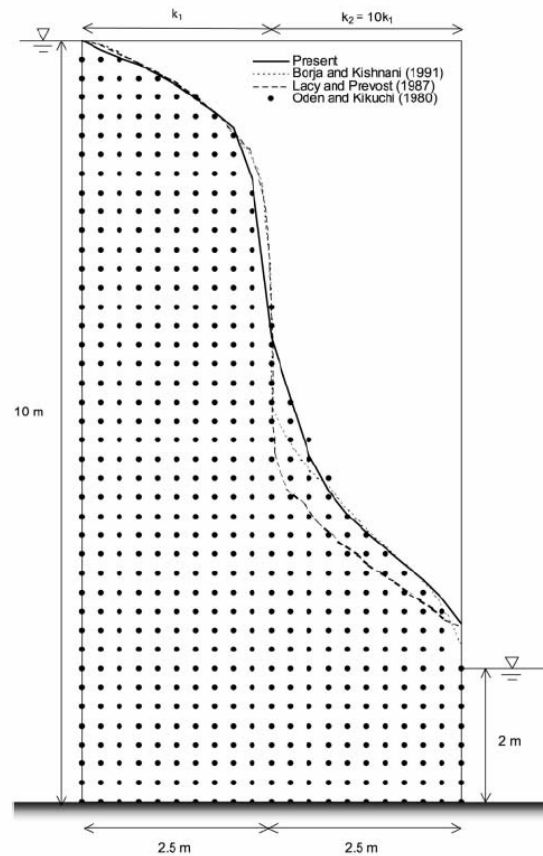


Fig. G10.2: Comparison of phreatic level for non-homogeneous rectangular dam made by Bardet & Tobita (2002)

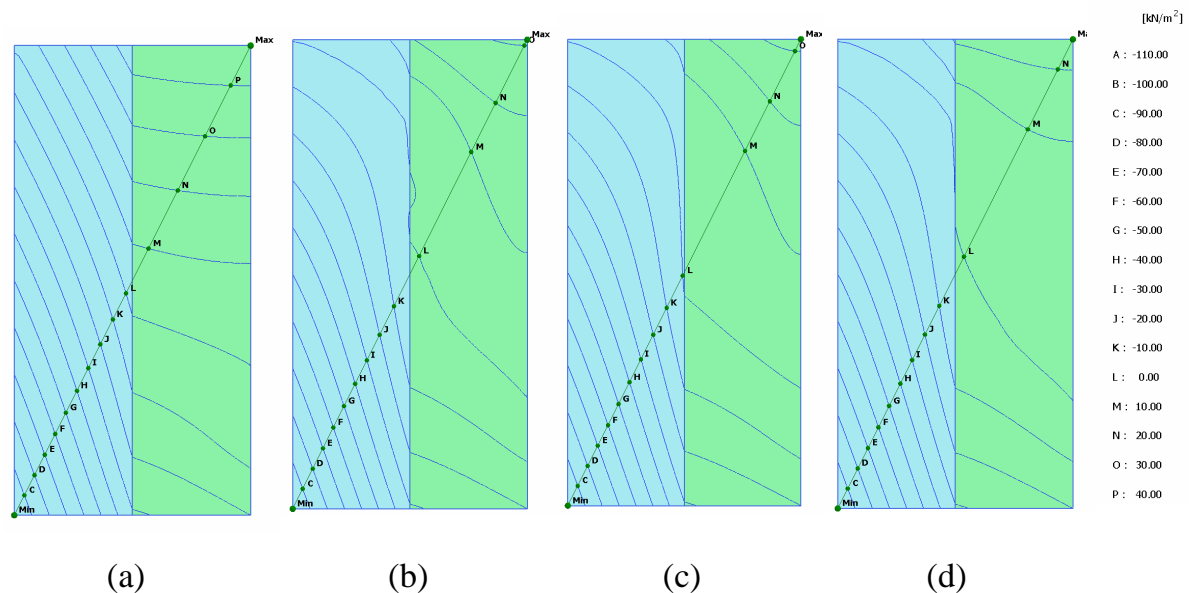


Fig. G10.3.2D: Active pore pressures calculated with PLAXIS 2D. In all cases line L is the phreatic line; (a) fully saturated; (b) Hypres coarse top soil; (c) Staring sand (O1); (d) USDA sand

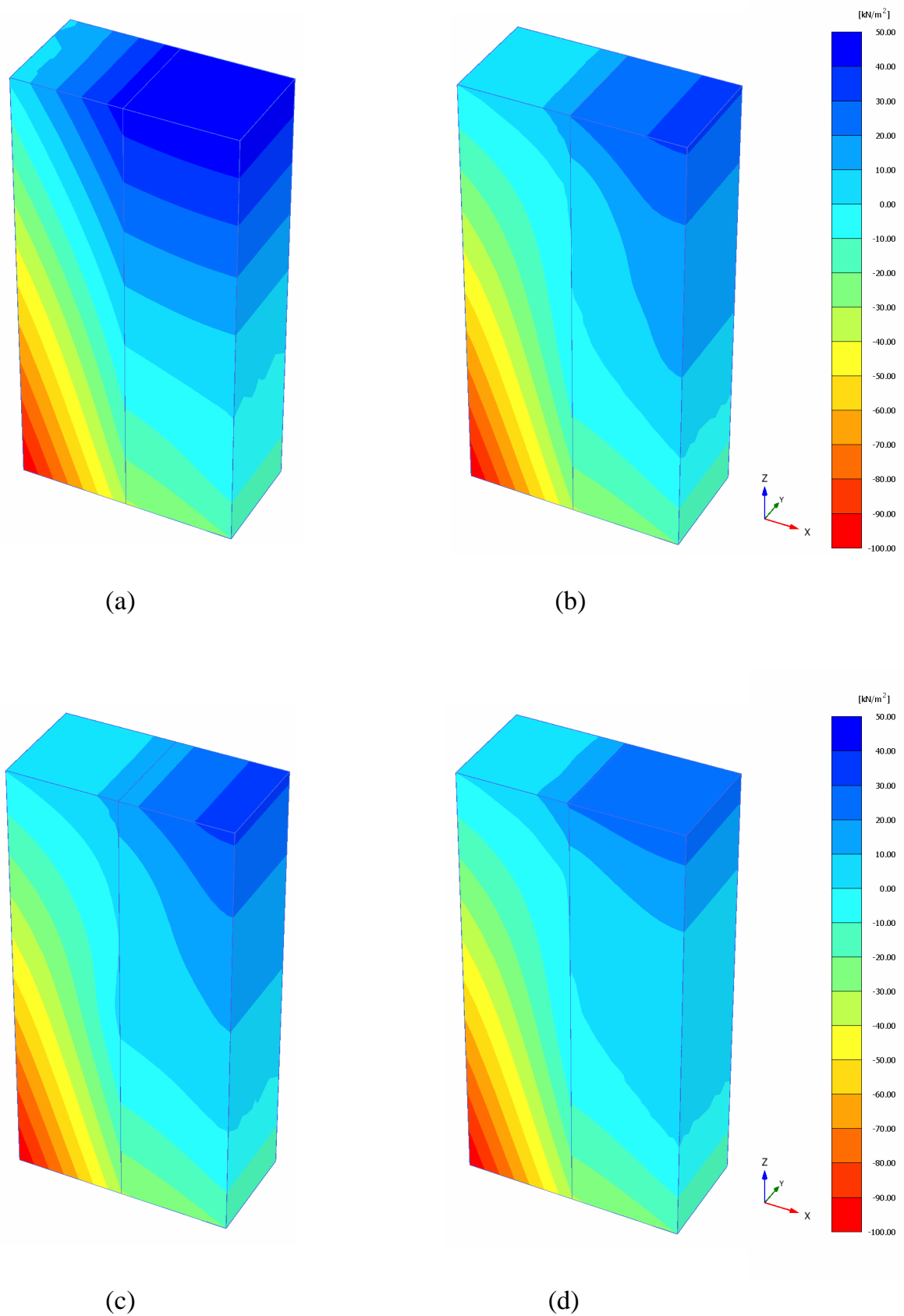
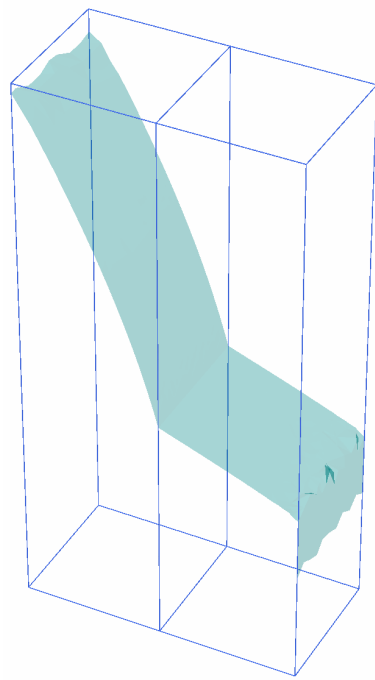
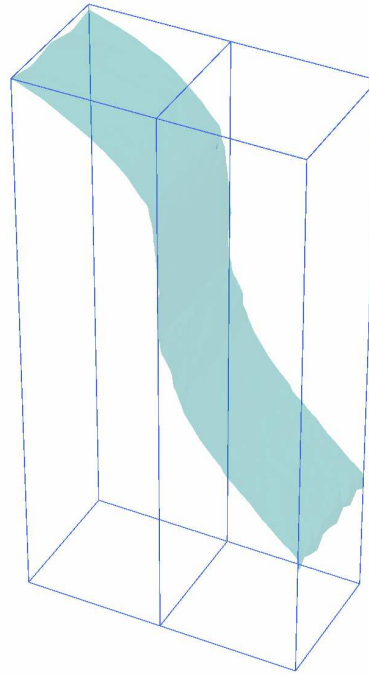


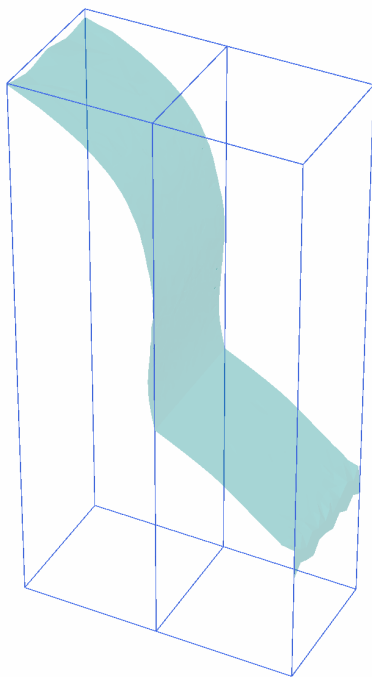
Fig. G10.3.3D: Active pore pressures calculated with PLAXIS 3D; (a) fully saturated; (b) Hypres coarse top soil; (c) Staring sand (O1); (d) USDA sand



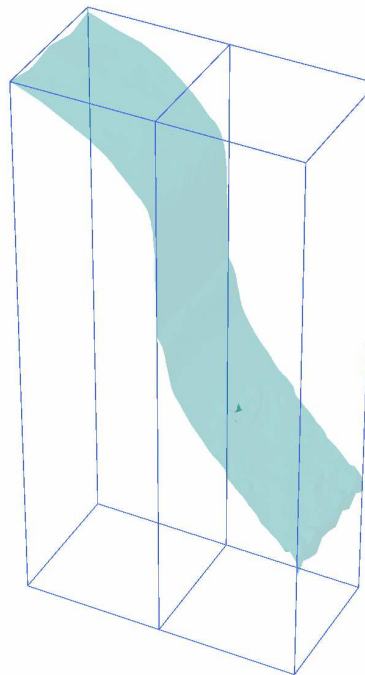
(a)



(b)



(c)



(d)

Fig. G10.4.3D: Phreatic surface calculated with PLAXIS 3D; (a) fully saturated; (b) Hypres coarse top soil; (c) Staring sand (O1); (d) USDA sand

8.11 Conclusions

Results of 10 two and three dimensional flow problems, solved by the new PLAXIS 2D and 3D kernels, are shown in this chapter and most of them are compared with analytical solutions or PlaxFlow results.

The following features have been tested:

1. *Boundary conditions.* Almost all boundary conditions have been tested in the chapter of one dimensional groundwater flow. However, seepage boundary condition, inflow, precipitation and well are tested here.
2. *Steady state and transient calculation.* Both steady state and transient types of calculations have been tested.
3. *Confined and unconfined groundwater flow calculations.* Confined groundwater flow calculations are linear and unconfined groundwater flow calculations are usually nonlinear. It has been shown that PLAXIS is capable of calculating both types of calculations.
4. *Seepage face calculation.* Calculation of seepage face is highly nonlinear and needs additional procedures. In the case of higher order elements, as used in PLAXIS, the problem is more difficult due to irregular distribution of discharge at nodes. As shown in several problems, PLAXIS is capable of calculating seepage face with a reasonable accuracy.
5. *Drain.* The kind of boundary condition has been tested and validated with PLAXIS 2D and 3D.
6. *Element types.* Both types of elements, namely 15 noded with a fourth order of integration for pore pressure and 6-noded with a second order of integration for pore pressure can be used for groundwater flow calculation.

9 Verification of coupled flow – deformation analysis

This chapter presents the results of 5 two dimensional and three dimensional coupled flow - deformation calculations and one calculation of gravity loading based on Bishop stress. In the case of one dimensional consolidation, the results are compared with analytical solutions but for the rest the results are compared with other codes like combination of PLAXIS with PlaxFlow (semi-coupled) and PLAXIS 3D Foundation (recently developed for fully saturated consolidation based on total pore pressure approach by John Van Esch from Deltares). As the same flow boundary conditions are used for the groundwater flow and coupled calculations, here it is not necessary to test all boundary conditions for flow. It is intended to demonstrate that the coupled flow-deformation analysis is stable and accurate.

9.1 Case CA1: Bishop effective stress

As Bishop effective stress is used in PLAXIS when unsaturated behaviour of soil is simulated, this example shows the capability of the code to calculate Bishop effective stress. Figure CA1.1 shows the geometry of the problem. This picture presents the initial boundary conditions from which a steady state flow situation is calculated. Imposing a head of -1.0 m at the bottom of the model and 1.0 m at the top generates unsaturated starting conditions. This condition leads to have a constant suction of 10 kPa in entire the domain. The corresponding degree of saturation is 0.3398.

Table CA1.1 gives the input parameters used for the calculation.

The following steps are performed in this case:

1. *Steady state*: Steady state groundwater flow calculation to generate initial pore pressure, (suction pore pressure of 10 kPa in the entire column).
2. *Gravity loading*: To generate initial stress

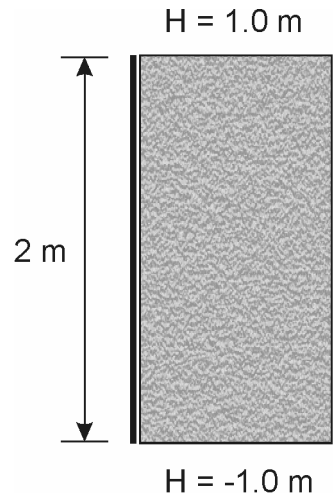


Fig. CA1.1: Geometry of case CA1

Verification:

Bishop stress reads:

$$\sigma = \sigma' + m(S p_w) \quad (1.12)$$

The vertical total stress at the bottom is:

$$\sigma = h \cdot \gamma = -2 \times 20 = -40 \text{ kPa}$$

As the degree of saturation is constant in entire the model and is equal to 0.3398, Bishop effective stresses at the top and bottom are:

$$\sigma'_{top} = \sigma_{top} - S \cdot p_w = 0 - 0.3398 \times 10 = -3.398 \text{ kPa}$$

$$\sigma'_{bottom} = \sigma_{bottom} - S \cdot p_w = -40 - 0.3398 \times 10 = -43.398 \text{ kPa}$$

Figure CA1.2 shows the effective stresses calculated by PLAXIS 2D and 3D. As seen the maximum and minimum effective stresses are -3.398 kPa and -43.40 kPa which are very close to the analytical solution.

Tab. CA1.1: Input data (Linear elastic model)

Description	Symbol	Unit	Value
Elastic modulus	E^{ref}	[kN/m ²]	10000
Poisson's ratio	ν	[-]	0.2
initial void ratio	e_{init}	[-]	0.5625
Saturated saturation	S_{sat}	[-]	1.0
Residual saturation	S_{res}	[-]	0.02
Van Genuchten	g_n	[-]	2.286
Van Genuchten	g_a	[m ⁻¹]	2.24
Van Genuchten	g_l	[-]	0
Water weight	γ_w	[kN/m ³]	10.0
Soil weight (sat)	γ_{sat}	[kN/m ³]	20.0
Soil weight (dry)	γ_{unsat}	[kN/m ³]	20.0

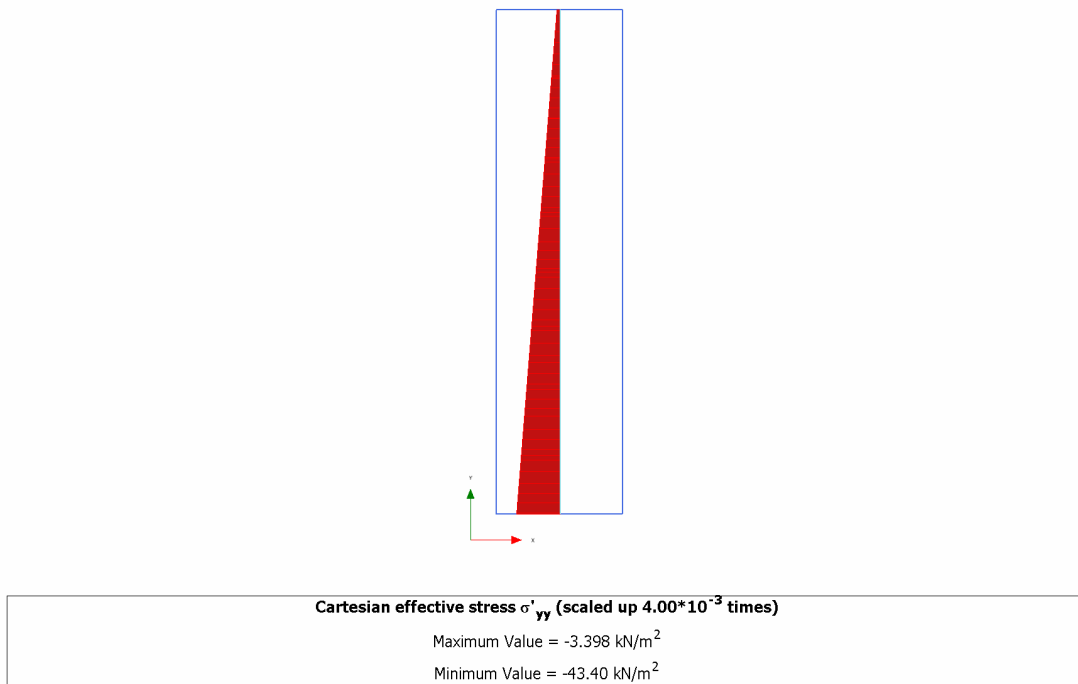


Fig. CA1.2.2D: Vertical effective stresses (PLAXIS 2D)

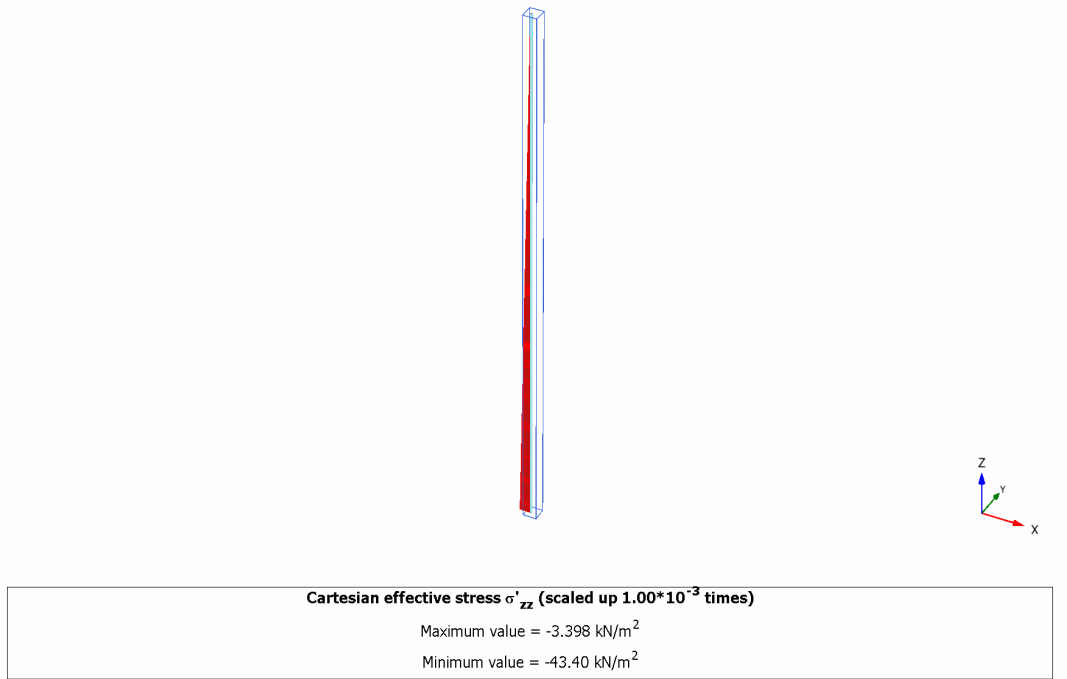


Fig. CA1.2.3D: Vertical effective stresses (PLAXIS 3D)

The horizontal effective stresses are shown in Figure CA1.3. As linear elastic model is used, the lateral stresses can be obtained from:

$$\sigma'_{xx} = \left(\frac{\nu'}{1-\nu'} \right) \sigma'_{yy}$$

which provides -0.8495 kPa for the top and -10.85 for the bottom.

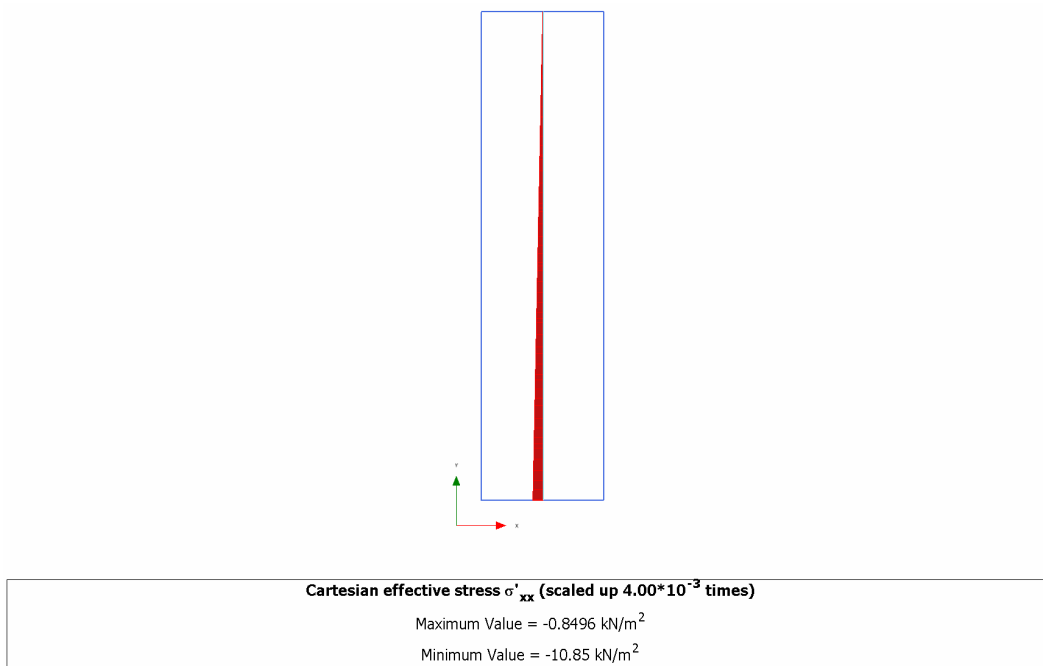


Fig. CA1.3.2D: Horizontal effective stresses (PLAXIS 2D)

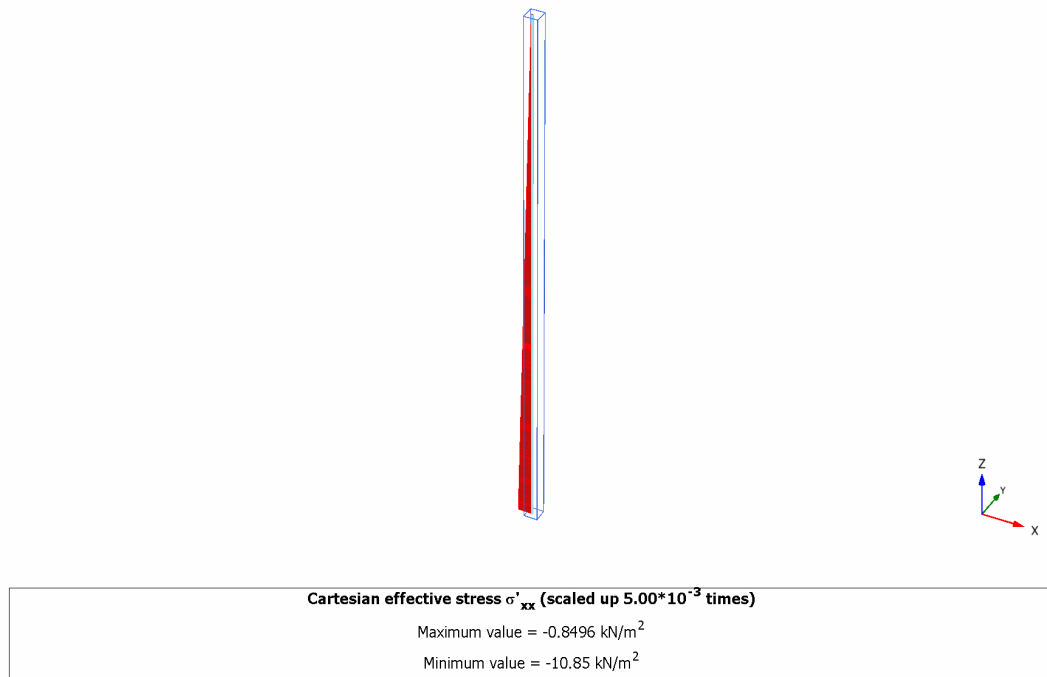


Fig. CA1.3.3D: Horizontal effective stresses (PLAXIS 3D)

Figure CA1.4 shows the vertical total stresses calculated by the output program of PLAXIS. The minimum and maximum vertical total stresses should be 0 kPa and -40 kPa. As seen the results are very close to the analytical solution. The horizontal total stresses are plotted in Figure CA1.5.

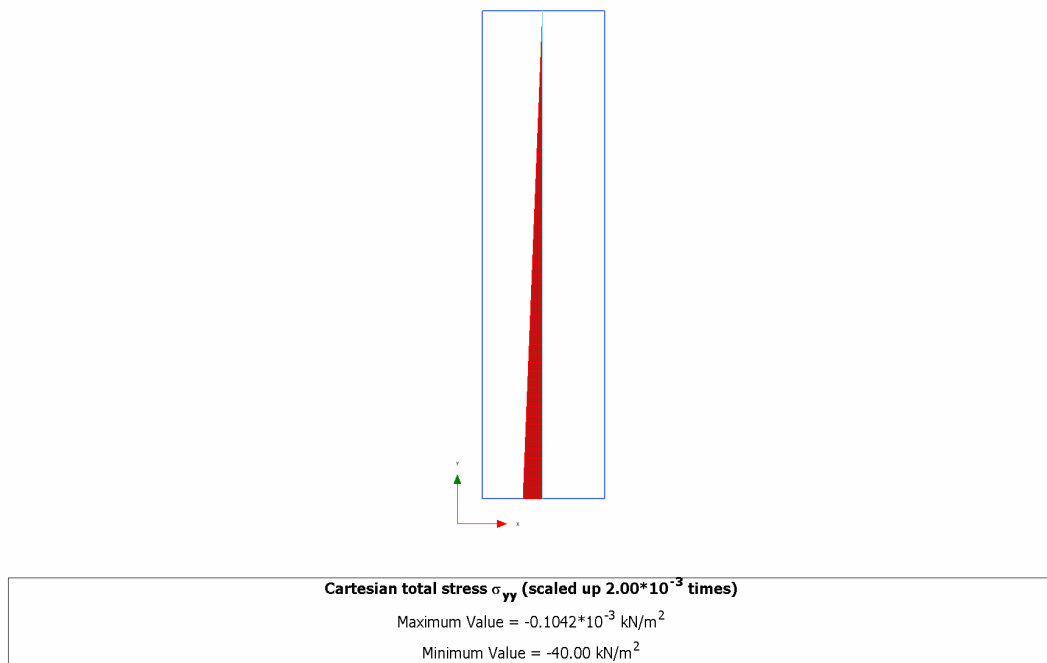
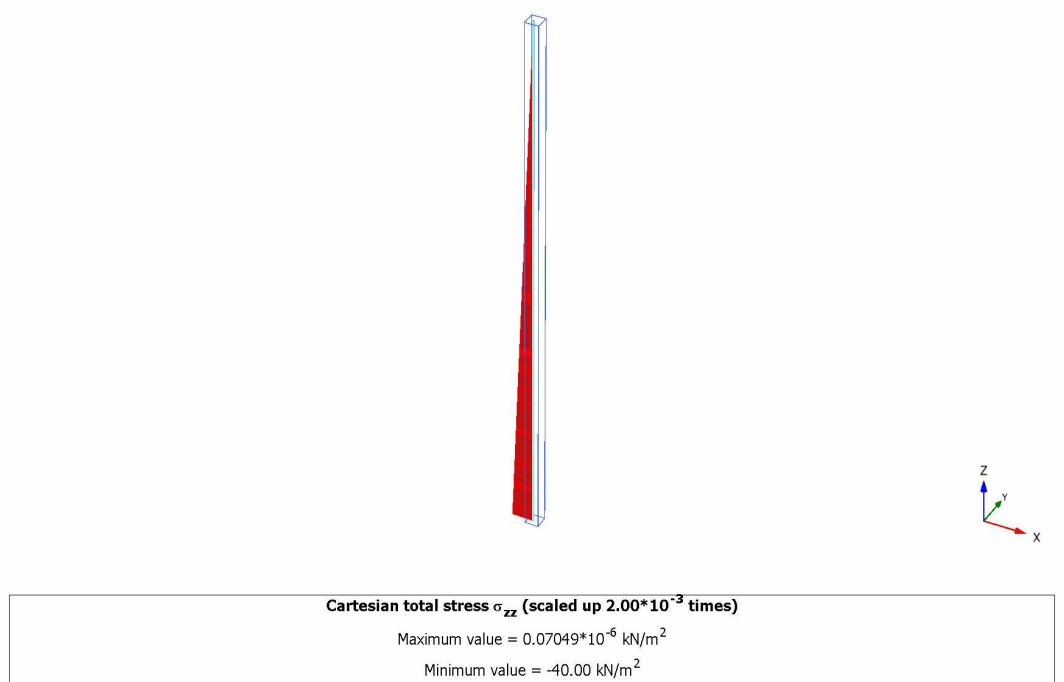
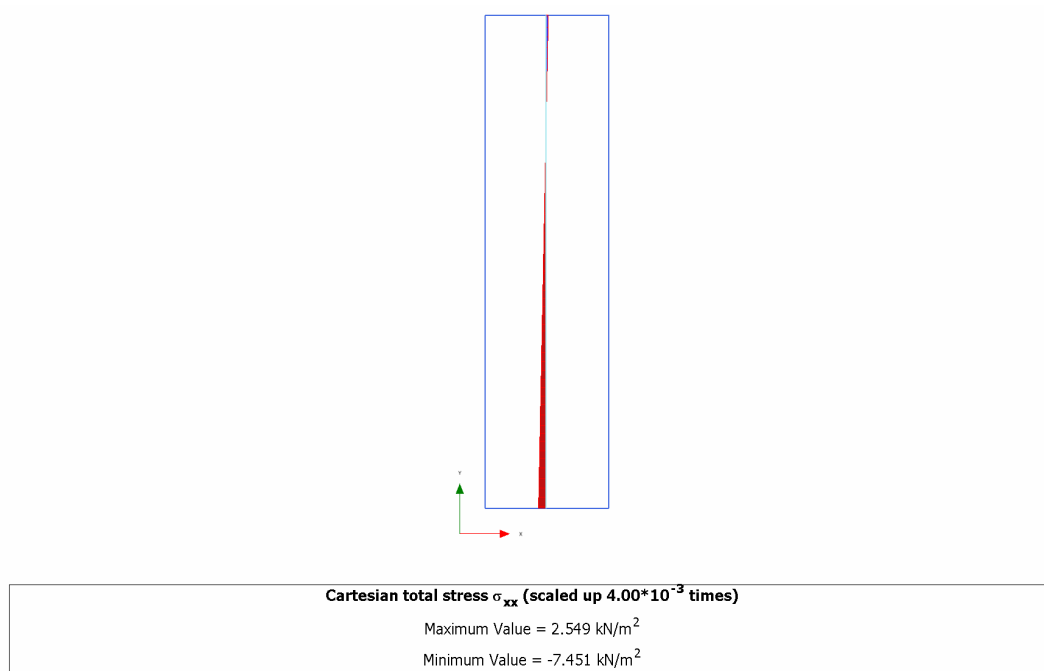


Fig. CA1.4.2D: Vertical total stresses (PLAXIS 2D)

**Fig. CA1.4.3D:** Vertical total stresses (PLAXIS 3D)**Fig. CA1.4.2D:** Horizontal total stresses (PLAXIS 2D)

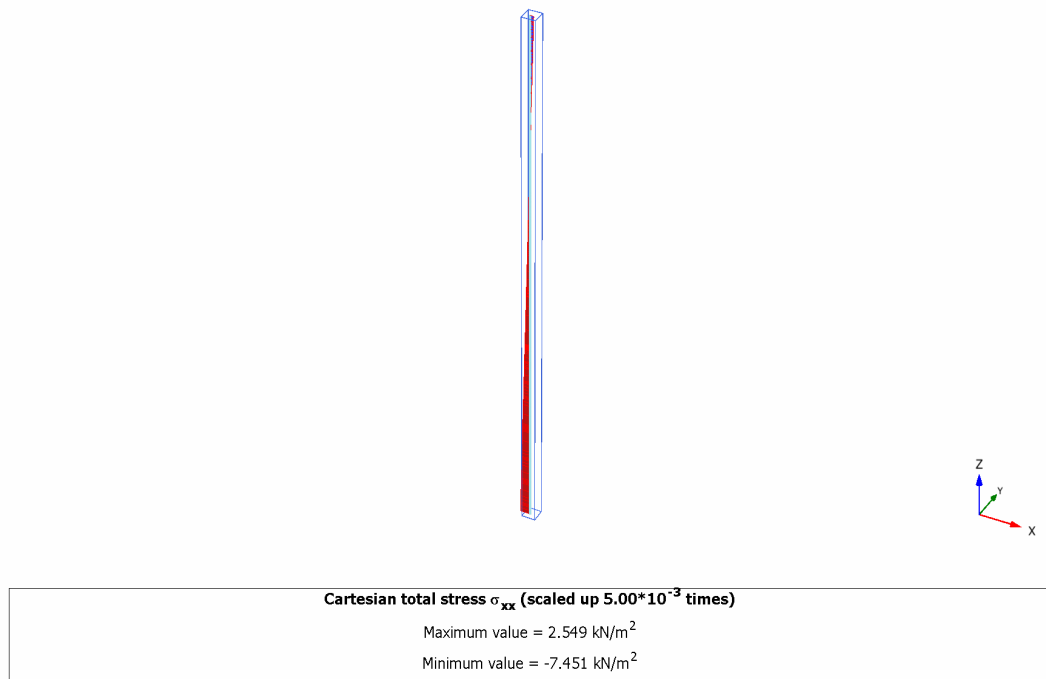


Fig. CA1.4.3D: Horizontal total stresses (PLAXIS 3D)

Summary:

As seen the results from PLAXIS 2D and 3D kernels and the output (total stresses) are correct.

9.2 Case CA2: One dimensional consolidation in saturated soil

Input: Figure CA2.1 shows PLAXIS finite element mesh for one dimensional consolidation problem. The side and the bottom are kept undrained by applying closed boundary condition while the top surface is allowed to drain. Initial effective stresses and initial pore pressures are not generated. To generate an excess pore pressure, p_o , an external load P_o is applied on the upper surface in the first phase (plastic calculation) followed by seven consolidation analyses of ultimate times 0.1, 0.5, 1.0, 2.0, 5.0, 10.0 and 50 days respectively which were performed with the coupled flow deformation formulation in PLAXIS 2D and 3D (based on Total Pore Pressure). Note: Phreatic line is on the top of the model to generate fully saturated soil.

The following steps are performed in this case:

1. *Gravity loading:* To generate initial active pore pressure and Bishop effective stresses.
2. *Plastic calculation:* 10 kPa is applied on the top of the model to generate additional pore pressure in the model.
3. *Consolidation:* Consolidation phases with different time intervals are performed (ultimate times 0.1, 0.5, 1.0, 2.0, 5.0, 10.0 and 50 days).

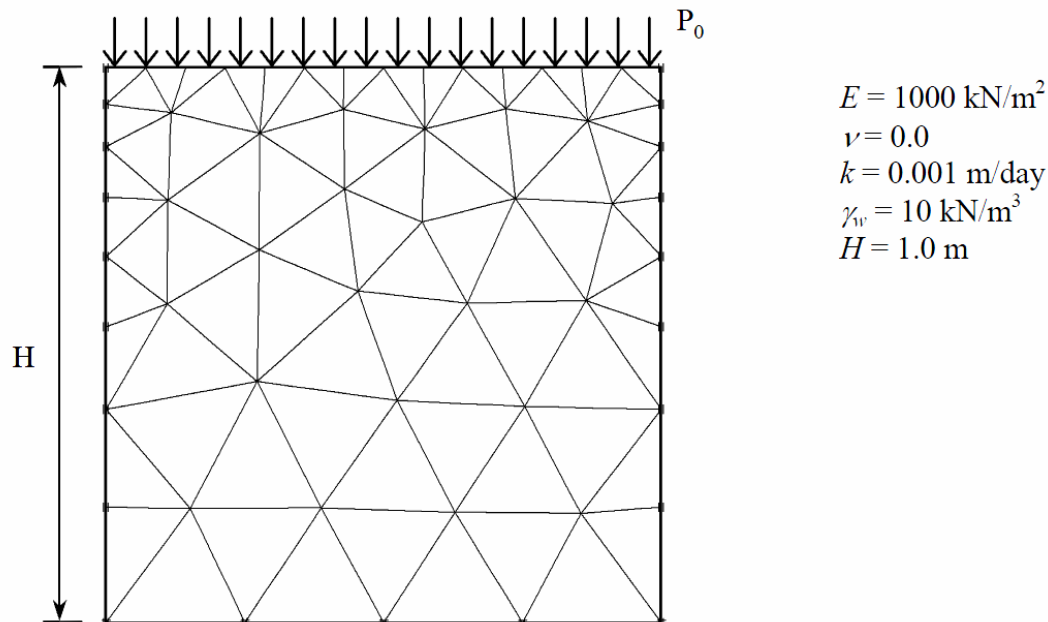


Fig. CA2.1: Geometry and finite element mesh of case CA2

Verification: The problem of one dimensional consolidation can be formulated by a differential equation (Terzaghi, 1923):

$$\frac{\partial p}{\partial t} = c_v \frac{\partial^2 p}{\partial z^2} \quad (9.1)$$

$$c_v = \frac{kE_{oed}}{\gamma_w}; \quad E_{oed} = \frac{(1-\nu)E}{(1+\nu)(1-2\nu)}; \quad z = h - y \quad (9.2)$$

$$\frac{p}{p_0}(z, t) = \frac{4}{\pi} \sum_{j=1}^{\infty} \frac{(-1)^{j-1}}{2j-1} \cos\left((2j-1)\frac{\pi}{2} \frac{y}{H}\right) \exp\left(-(2j-1)^2 \frac{\pi^2}{4} \frac{c_v t}{H^2}\right) \quad (9.3)$$

$$T = \frac{c_v t}{H^2} \quad (9.4)$$

The consolidation phenomenon will be practically finished when the argument of the exponential function is about 4 or 5 (Verruijt, 1993). This will be the case when $T \approx 2$.

This analytical solution is indicated along with the PLAXIS finite element calculation results in Figures CA2.3. As seen, the results from consolidation based on total pore pressure are more accurate compared to the EPP results. For saturated soils, the formulations of both types of calculations are the same. The reason is only due to selecting smaller time steps in the TPP analysis which leads to calculate pore pressure more accurate.

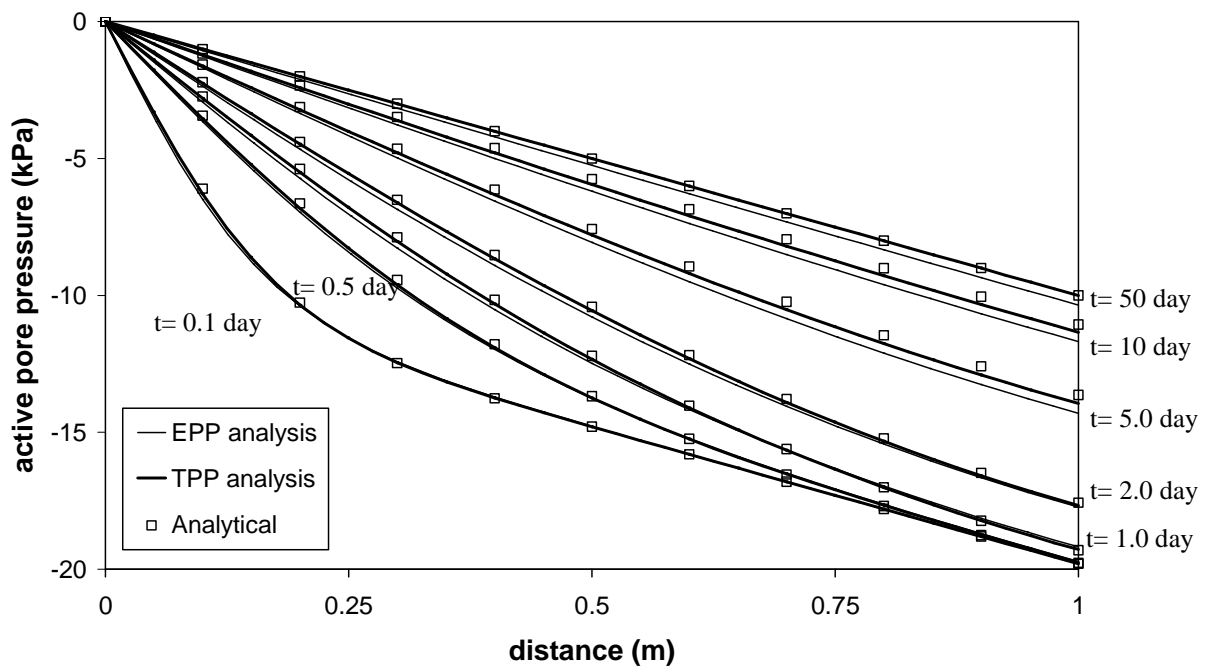


Fig. A1.2: Active pore pressure vs height

9.3 Case CA3: One dimensional varying mechanical loading

This example involves two cases, in which on the top of a column, the mechanical loads are varying. Different situations have been considered. Figure CA3.1 shows the geometry and boundary conditions for the problem. The column is 1 m high. In case 1a, the top boundary is open for flow and in case 1b the top boundary is closed for flow. In both cases the side boundaries are closed for flow. The material data are given in Table CA3.1.

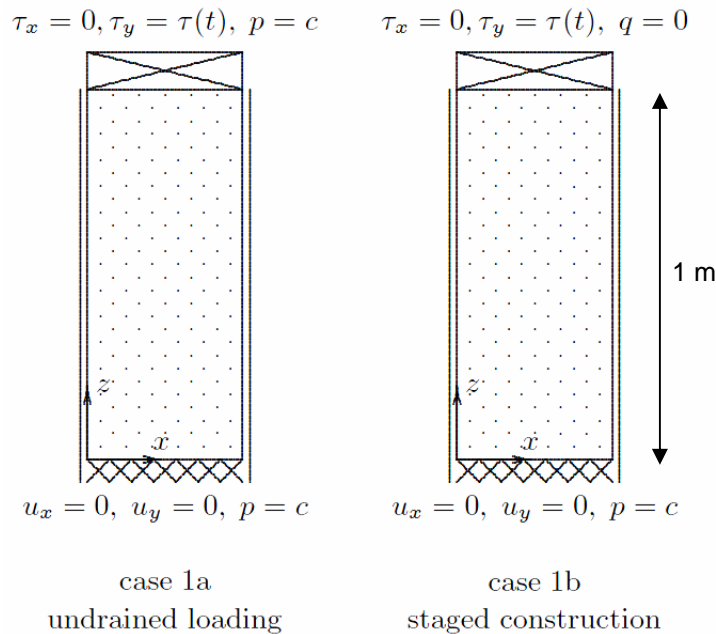


Fig. CA3.1: Geometry boundary conditions for problem CA3

Tab. CA3.1: Input data

Description	Symbol	Unit	Value
Young's modulus	E	[kN/m ²]	10000
Poisson's ratio	ν	[-]	0
Soil weight (sat)	γ_{sat}	[kN/m ³]	10
Soil weight (dry)	γ_{unsat}	[kN/m ³]	0
Permeability	k_x, k_y, k_z	[m/day]	0.001
initial void ratio	e_{init}	[-]	0.5
Elastic storage	$K_{w,ref}/n$	[kN/m ²]	4.95×10^5

The mechanical loading is applied according to the following function (Figure CA3.F):

$$\tau_c = \begin{cases} \tau^0 + (\tau^1 - \tau^0)t/t^1 & \text{if } t < t^1 \\ \tau^1 & \text{if } t \geq t^1 \end{cases} \quad (9.5)$$

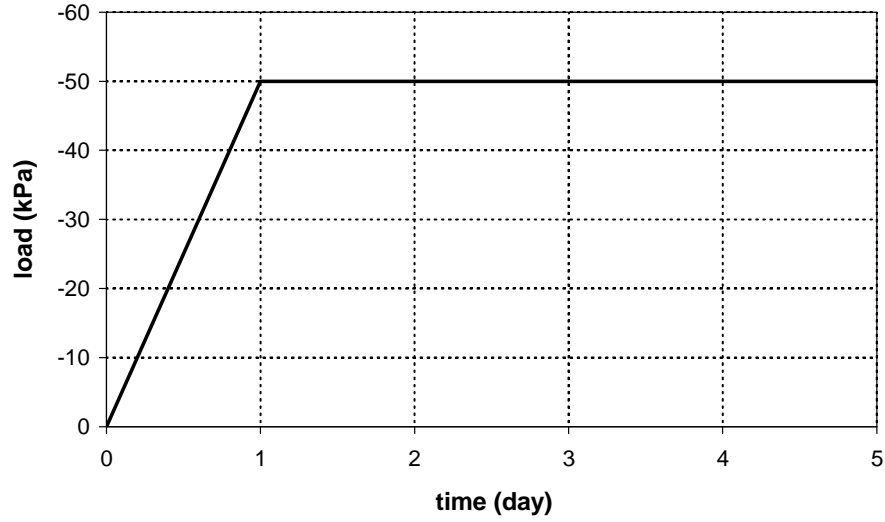


Fig. CA3.F: Applied load vs time in problem CA3

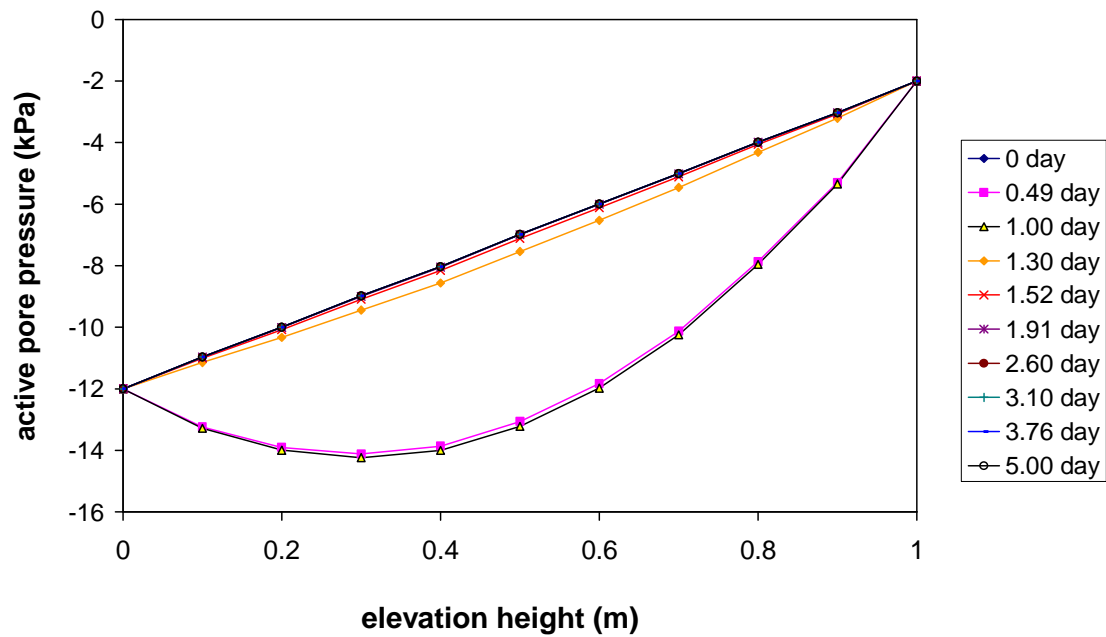
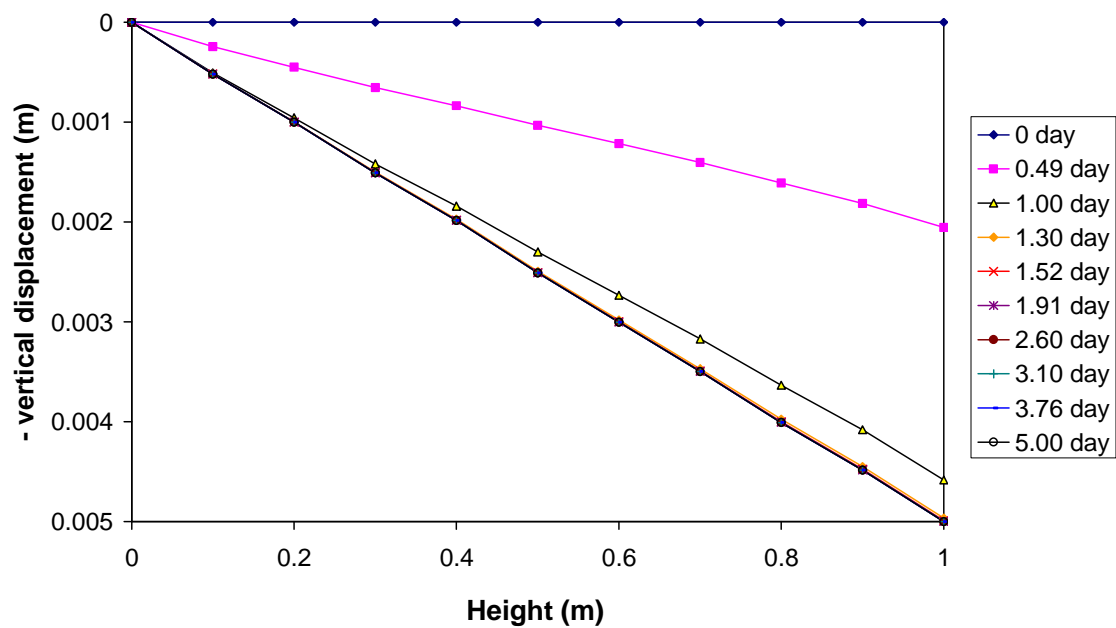
Case 1a:

$$\left\{ \begin{array}{l} t^1 = 1 \text{ day} \\ \tau^0 = 0 \text{ kPa} \\ \tau^1 = -50 \text{ kPa} \\ \text{top boundary open} \end{array} \right.$$

Case 1b:

$$\left\{ \begin{array}{l} t^1 = 1 \text{ day} \\ \tau^0 = 0 \text{ kPa} \\ \tau^1 = -50 \text{ kPa} \\ \text{top boundary closed} \end{array} \right.$$

This example has also been calculated with PLAXIS 3D Foundation by John Van Esch. Here the results of all calculations are given.

Results of case 1a:**Fig. CA3.2:** Active pore pressure for case 1a (PLAXIS 2D)**Fig. CA3.3:** Vertical displacement for case 1a (PLAXIS 2D)

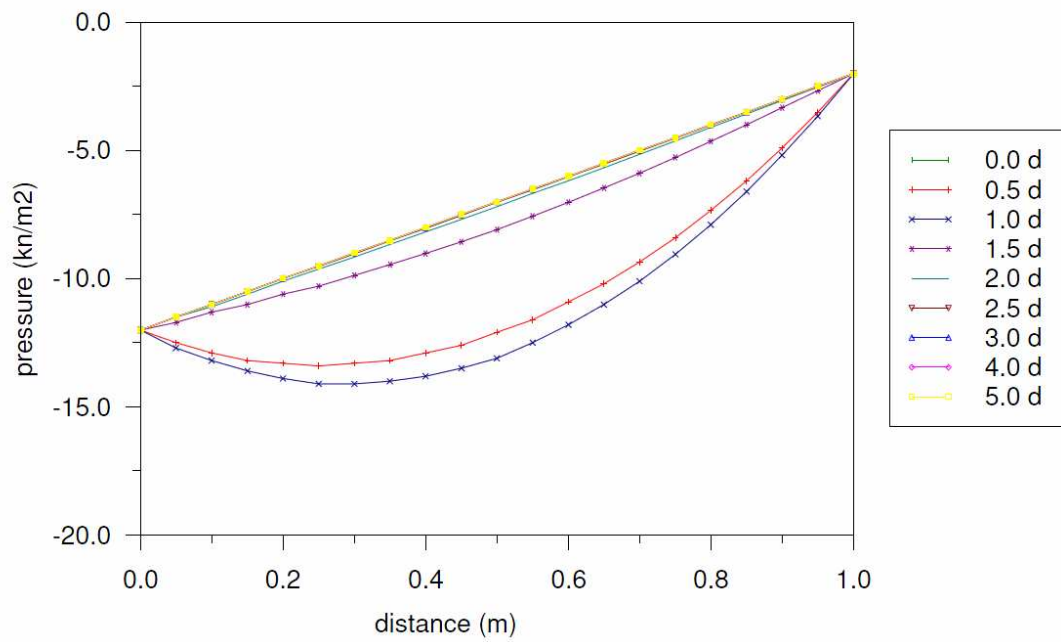


Fig. CA3.4: Active pore pressure for case 1a (PLAXIS 3D Foundation)

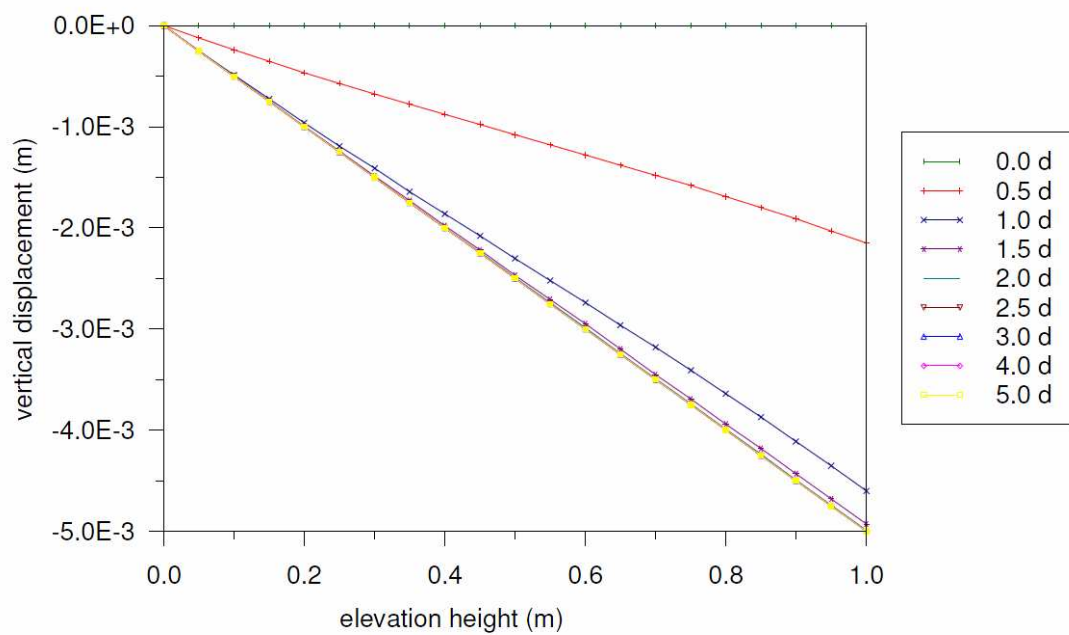


Fig. CA3.5: Vertical displacement for case 1a (PLAXIS 3D Foundation)

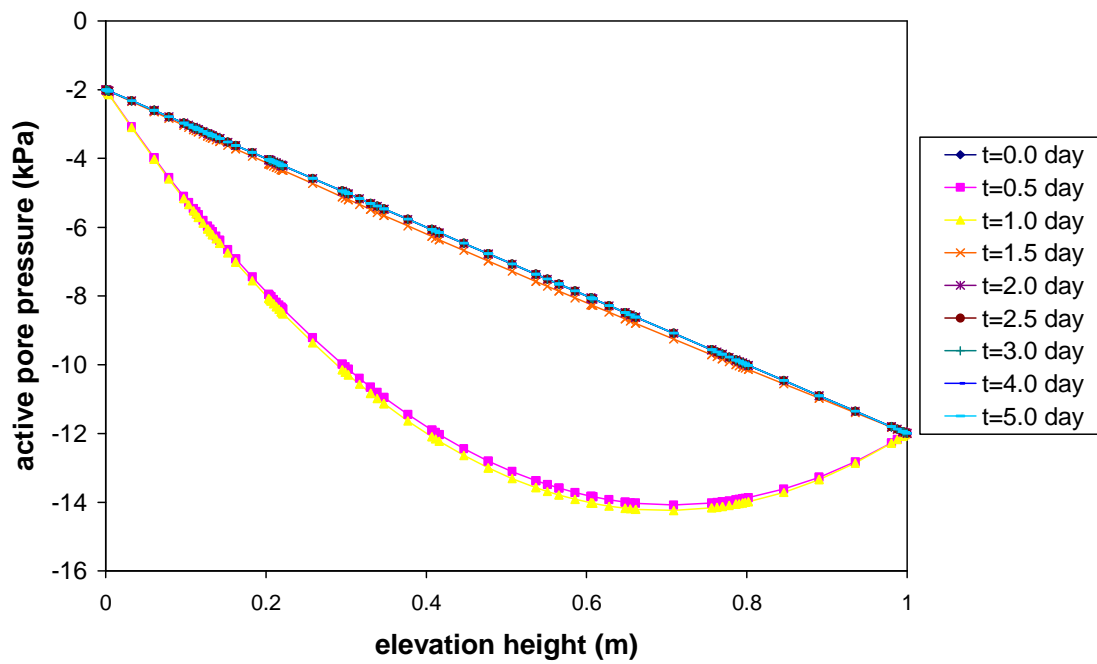


Fig. CA3.6: Active pore pressure for case 1a (PLAXIS 3D)

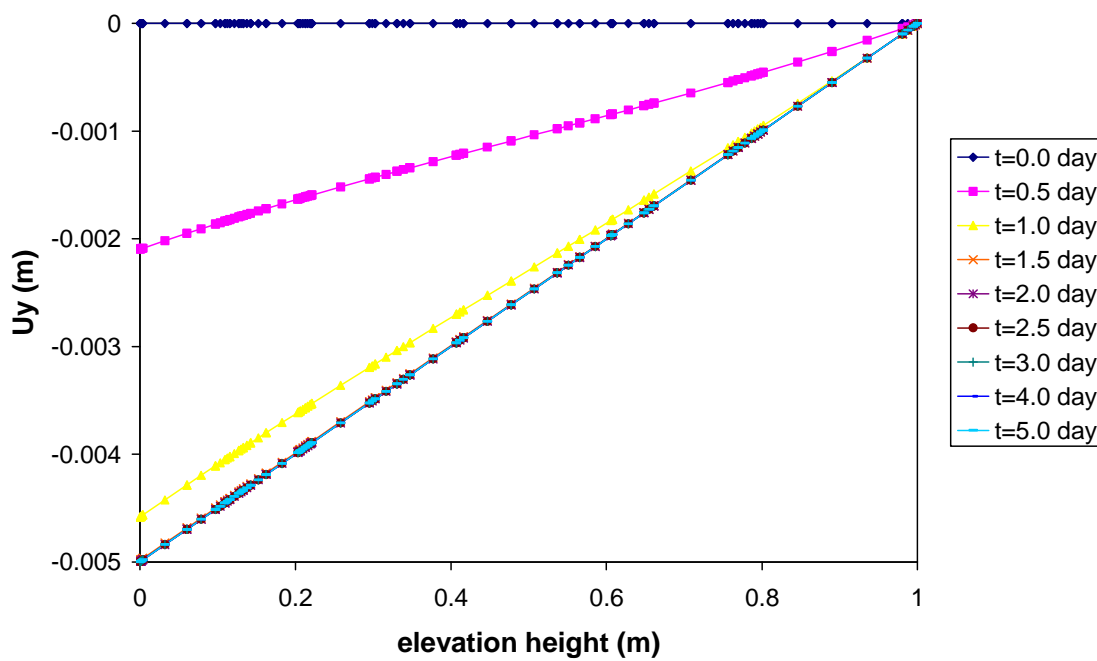
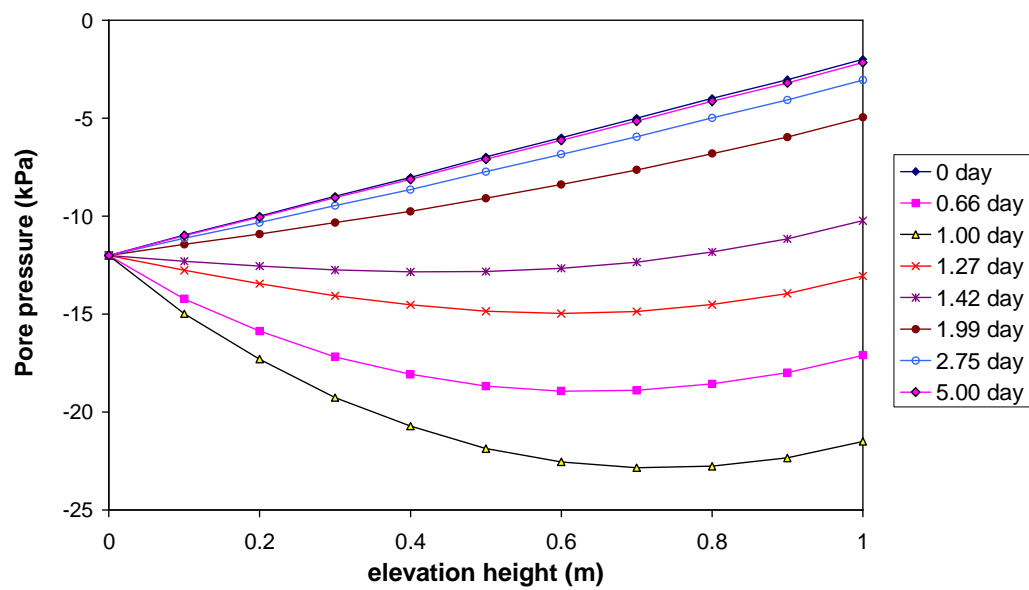
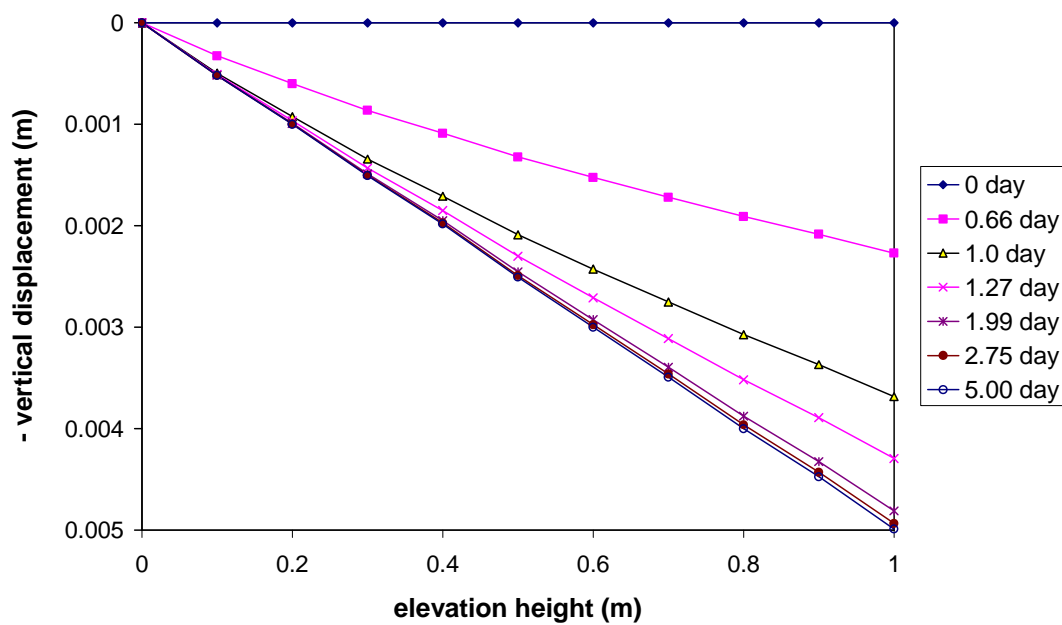


Fig. CA3.7: Vertical displacement for case 1a (PLAXIS 3D)

Results of case 1b:**Fig. CA3.8:** Active pore pressure for case 1b (PLAXIS 2D)**Fig. CA3.9:** Vertical displacement for case 1b (PLAXIS 2D)

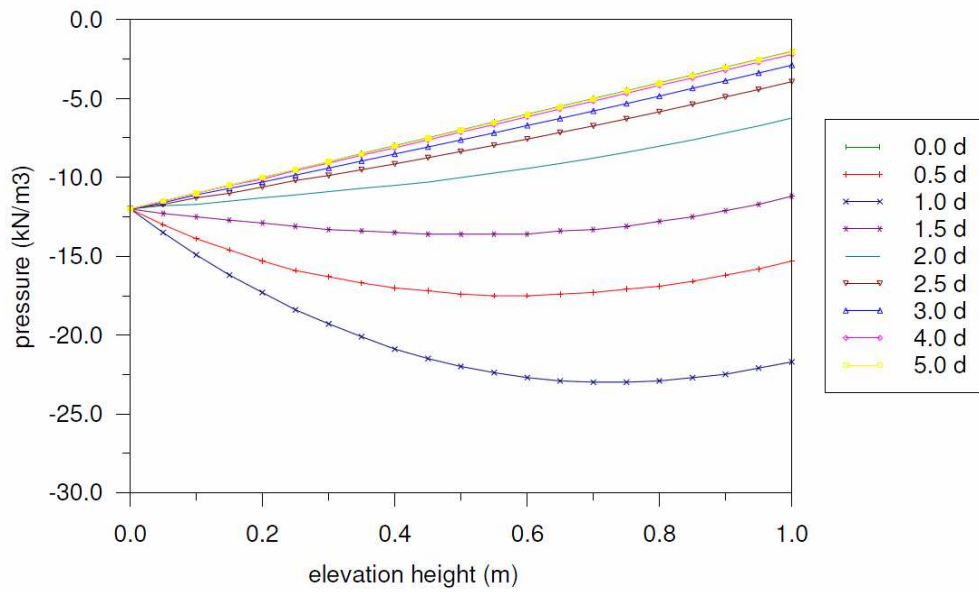


Fig. CA3.10: Active pore pressure for case 1b (PLAXIS 3D Foundation)

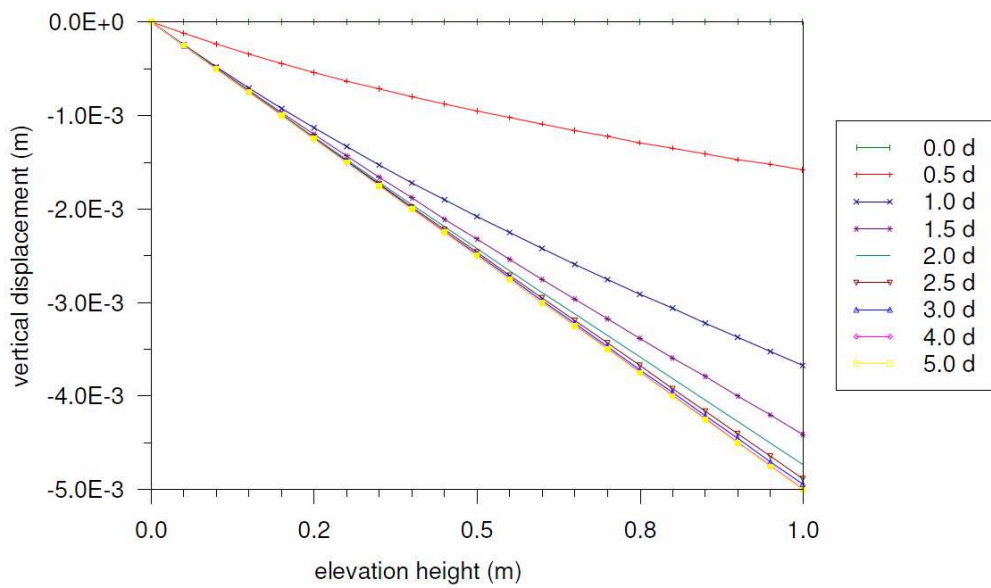


Fig. CA3.11: Vertical displacement for case 1b (PLAXIS 3D Foundation)

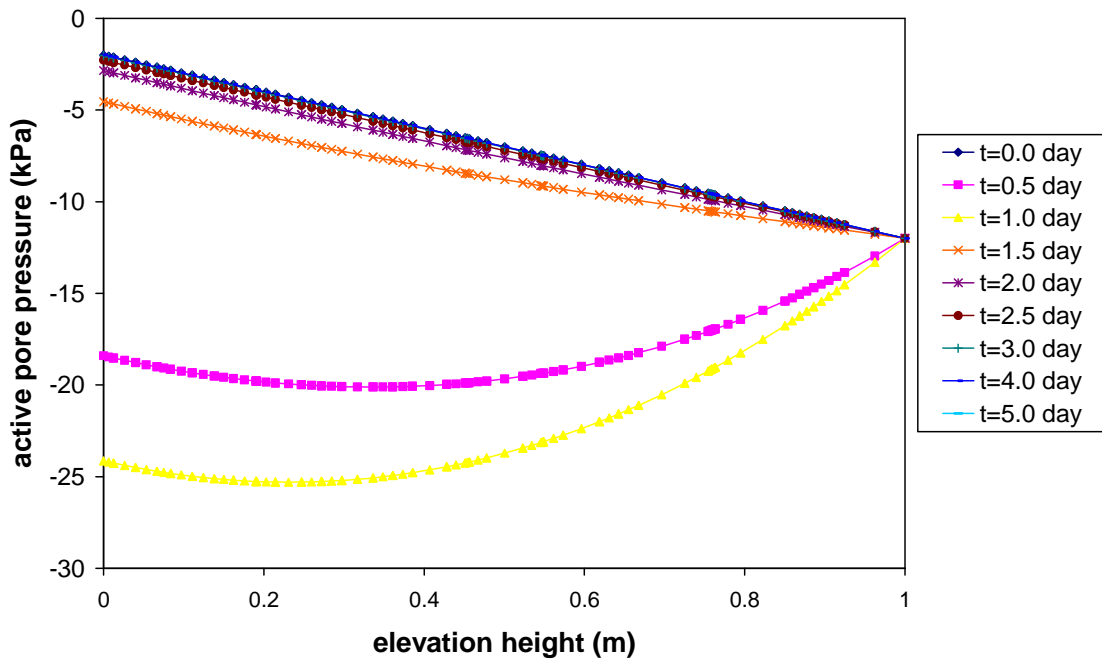


Fig. CA3.12: Active pore pressure for case 1b (PLAXIS 3D)

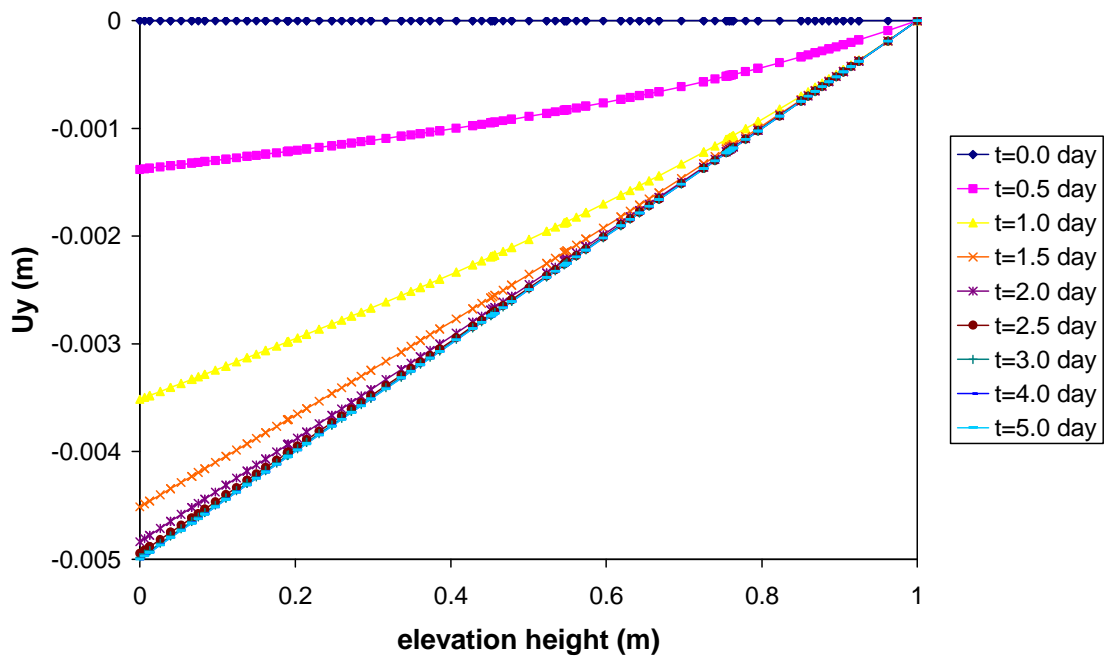


Fig. CA3.13: Vertical displacement for case 1b (PLAXIS 3D)

Summary:

As seen the results from PLAXIS 2D kernel and PLAXIS 3D are similar. The differences are due to the different time steps used during the calculations.

9.4 Case CA4: One dimensional varying hydraulic loading

This example involves two cases, in which on the top of a column, the hydraulic loads are varying. Different situations have been considered. Figure CA4.1 shows the geometry and boundary conditions for the problem. The column is 1 m high. In case 1a, the top boundary is open for flow and in case 1b the top boundary is closed. In both cases the side boundaries are closed for flow. The material data are given in Table CA4.1.

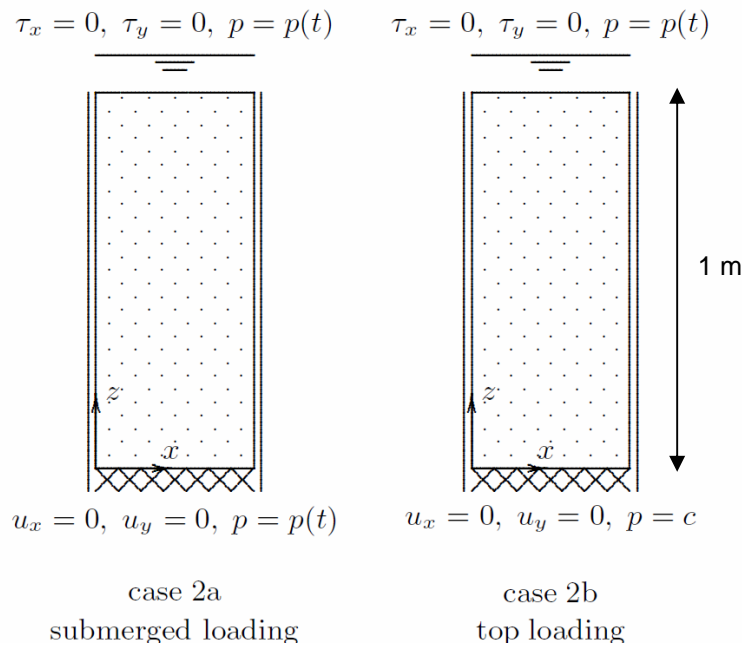


Fig. CA4.1: Geometry boundary conditions for problem CA4

Tab. G1.1: Input data

Description	Symbol	Unit	Value
Young's modulus	E	[kN/m ²]	10000
Poisson's ratio	ν	[-]	0
Soil weight (sat)	γ_{sat}	[kN/m ³]	10
Soil weight (dry)	γ_{unsat}	[kN/m ³]	0
Permeability	k_x, k_y, k_z	[m/day]	0.001
initial void ratio	e_{init}	[-]	0.5
Elastic storage	$K_{w,ref}/n$	[kN/m ²]	4.95×10^5

The hydraulic loading is applied according to the following function. It should be noted that the following loading is applied after 0.1 day (see Figure CA4.F):

$$p_c = \begin{cases} p^0 + (p^1 - p^0)t/t^1 & \text{if } t < t^1 \\ p^1 & \text{if } t \geq t^1 \end{cases} \quad (9.6)$$

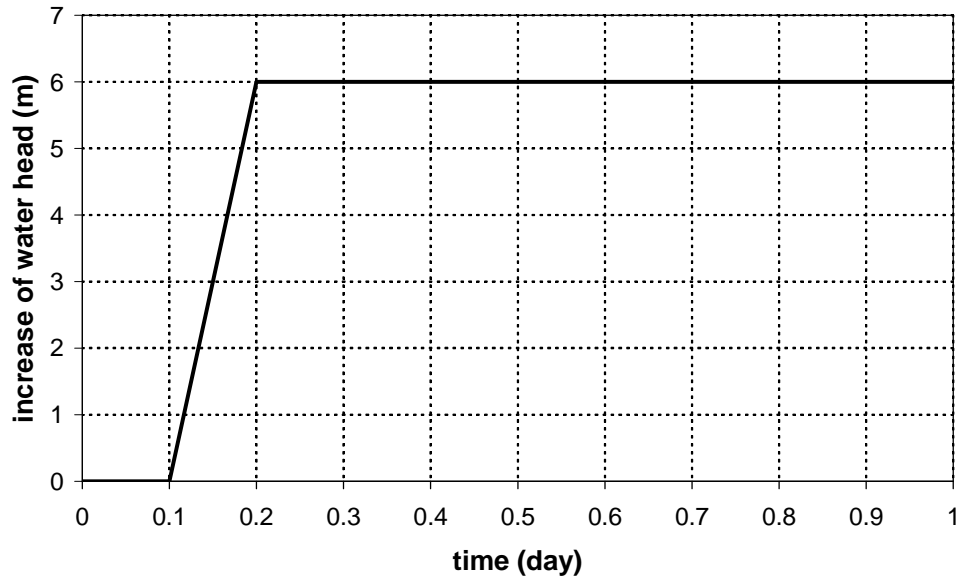


Fig. CA4.F: Increase of water head as a function of time in problem CA4

Case 2a: Increase of water head on the top and bottom boundary.

$$t^1 = 0.2 \text{ day}$$

$$p_{top}^0 = -2.0 \text{ kPa}$$

$$p_{bottom}^0 = -12.0 \text{ kPa}$$

$$p_{top}^1 = -52.0 \text{ kPa}$$

$$p_{bottom}^1 = -62.0 \text{ kPa}$$

Case 2b: Increase of water head on the top boundary.

$$t^1 = 0.2 \text{ day}$$

$$p_{top}^0 = -2.0 \text{ kPa}$$

$$p_{bottom}^0 = -12.0 \text{ kPa}$$

$$p_{top}^1 = -52.0 \text{ kPa}$$

This example has also been calculated with PLAXIS 3D by John Van Esch. Here the results of both calculations are given.

Results of case 2a:

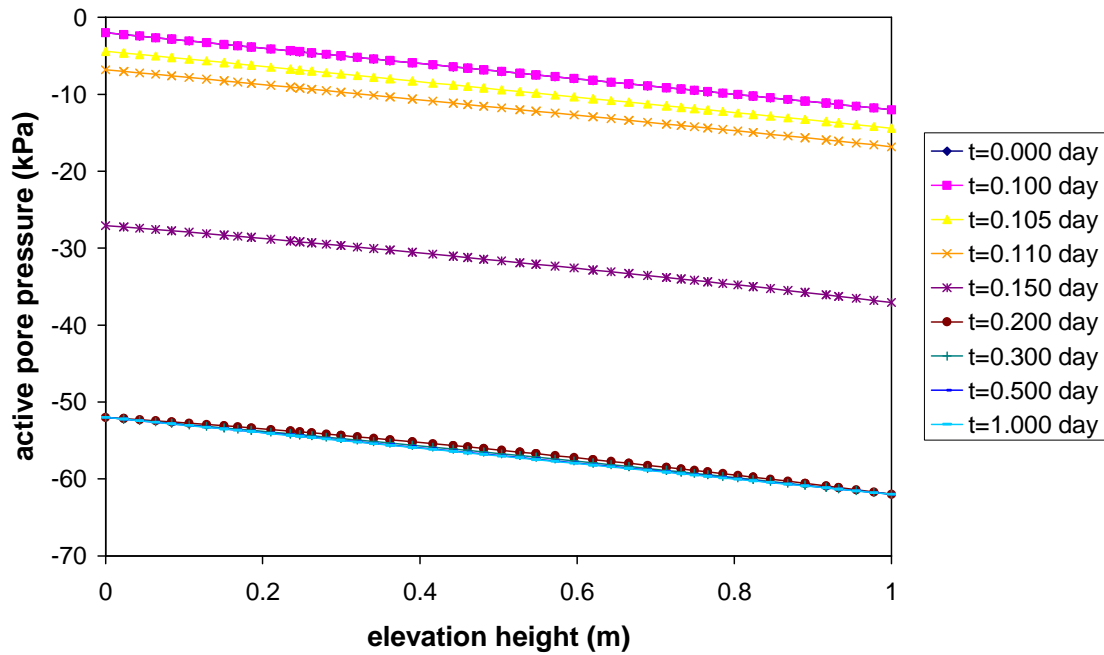


Fig. CA4.2: Active pore pressure for case 2a (PLAXIS 2D)

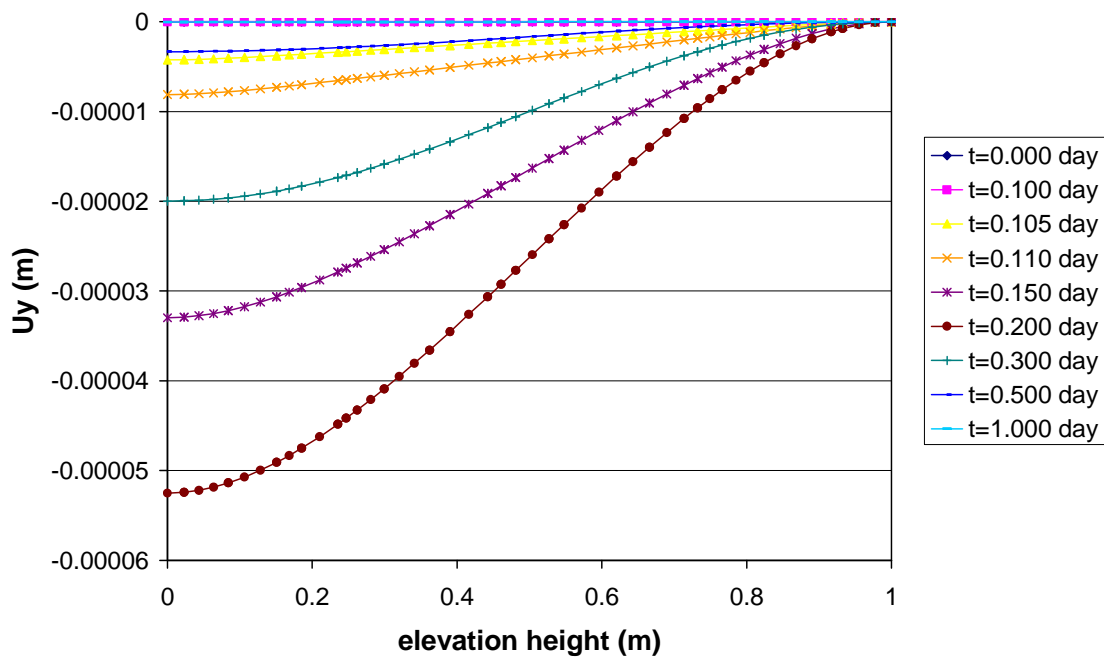


Fig. CA4.3: Vertical displacement for case 2a (PLAXIS 2D)

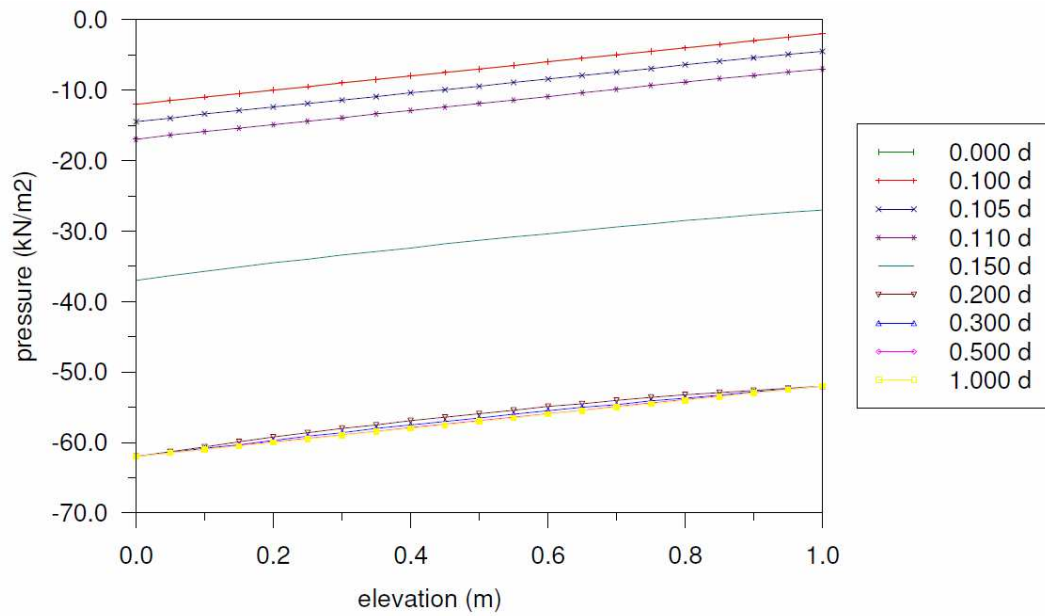


Fig. CA4.4: Active pore pressure for case 2a (PLAXIS 3D Foundation)

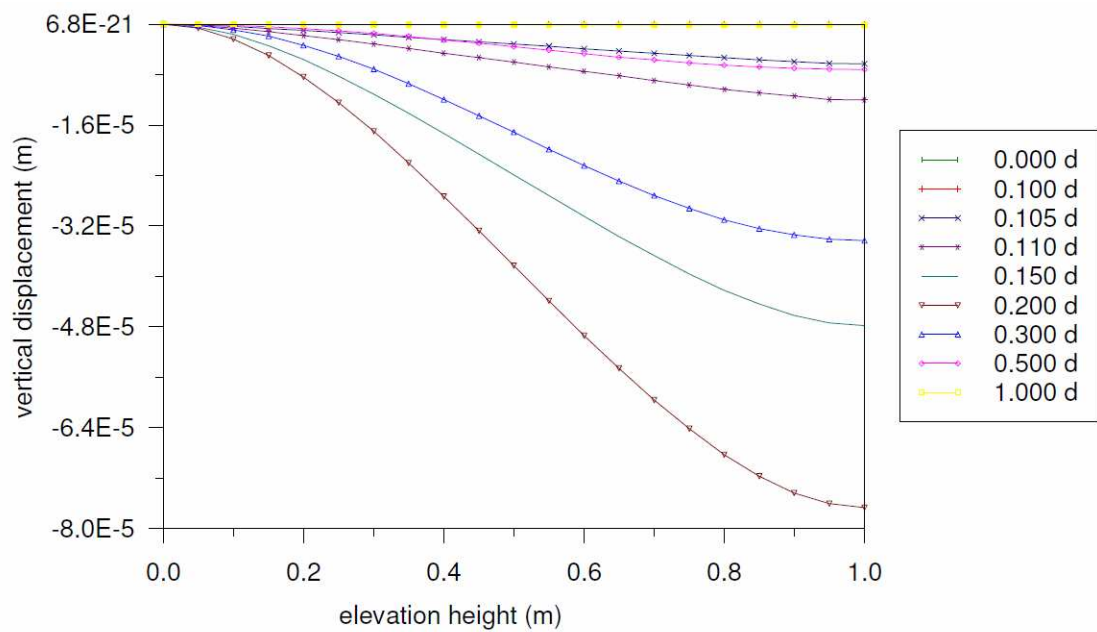


Fig. CA4.5: Vertical displacement for case 2a (PLAXIS 3D Foundation)

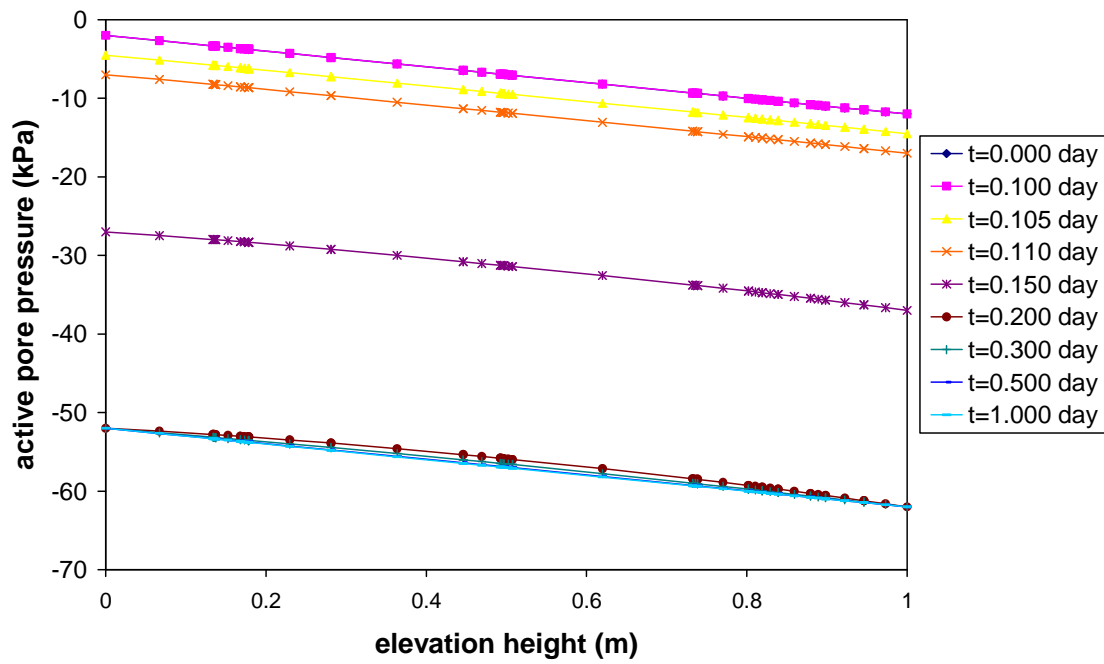


Fig. CA4.6: Active pore pressure for case 2a (PLAXIS 3D)

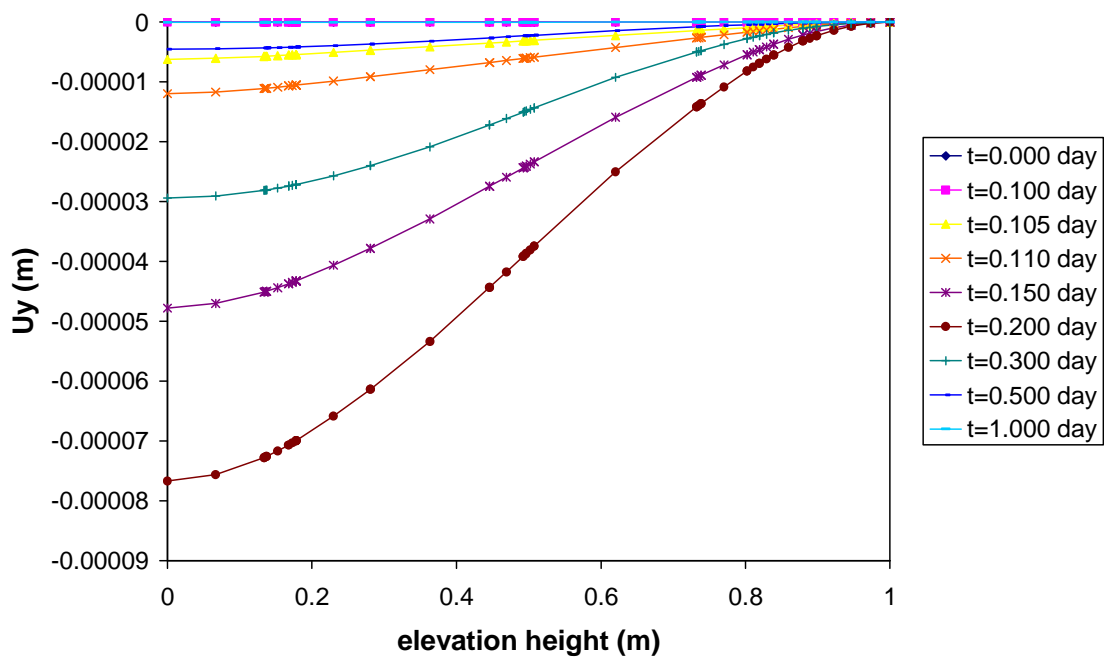
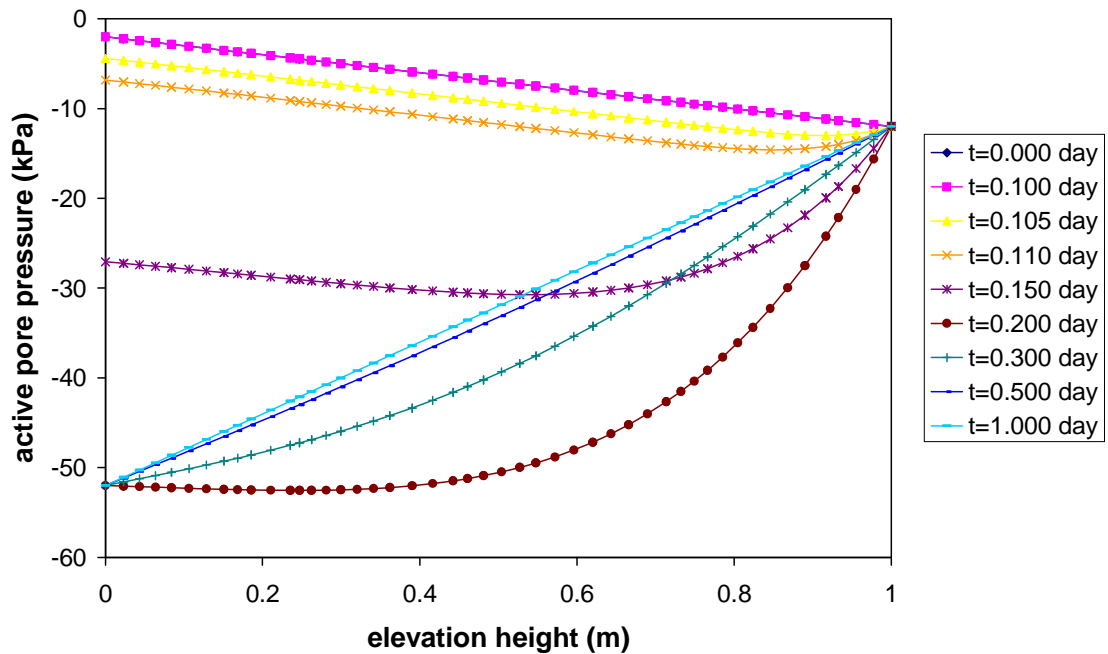
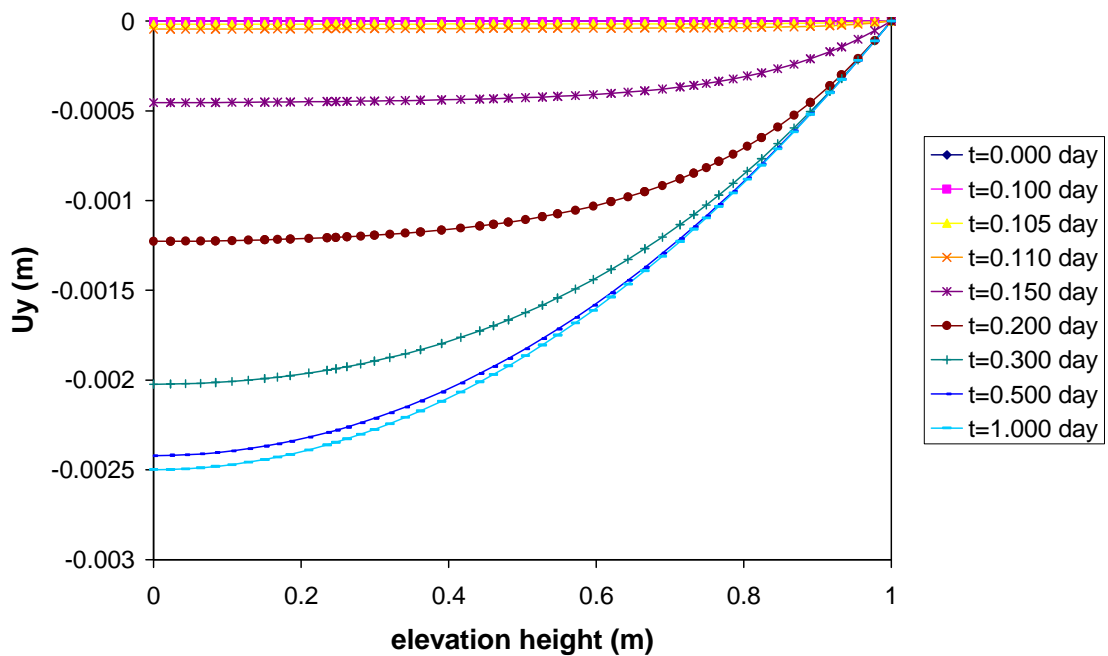


Fig. CA4.7: Vertical displacement for case 2a (PLAXIS 3D Foundation)

Results of case 2b:**Fig. CA4.8:** Active pore pressure for case 2b (PLAXIS 2D)**Fig. CA3.9:** Vertical displacement for case 2b (PLAXIS 2D)

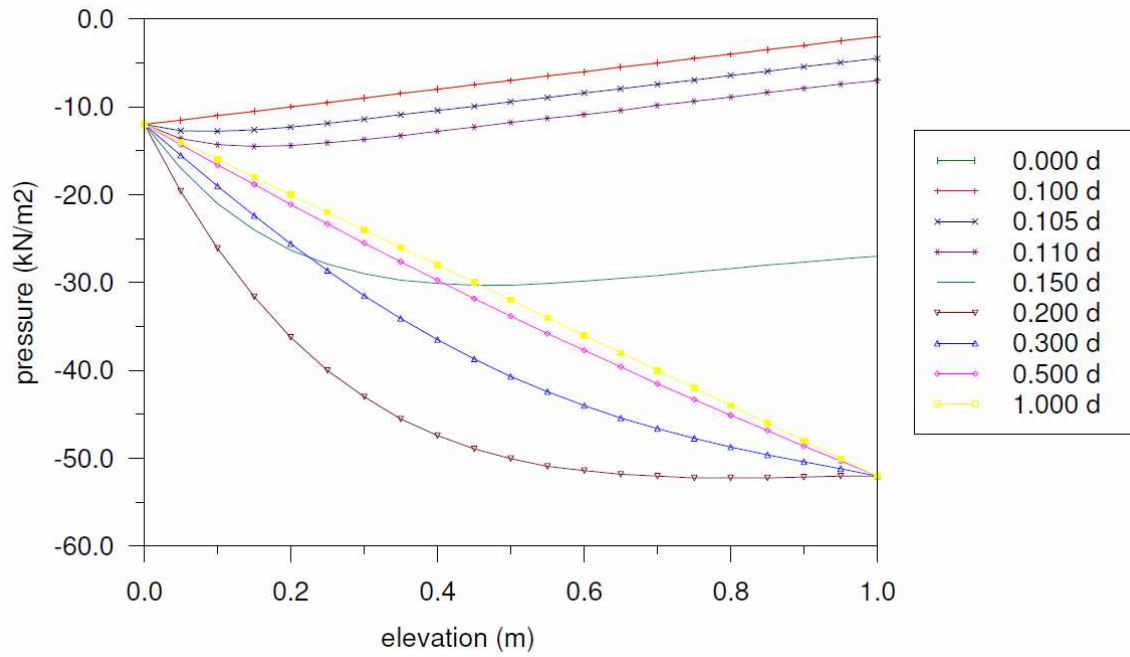


Fig. CA4.10: Active pore pressure for case 2b (PLAXIS 3D Foundation)

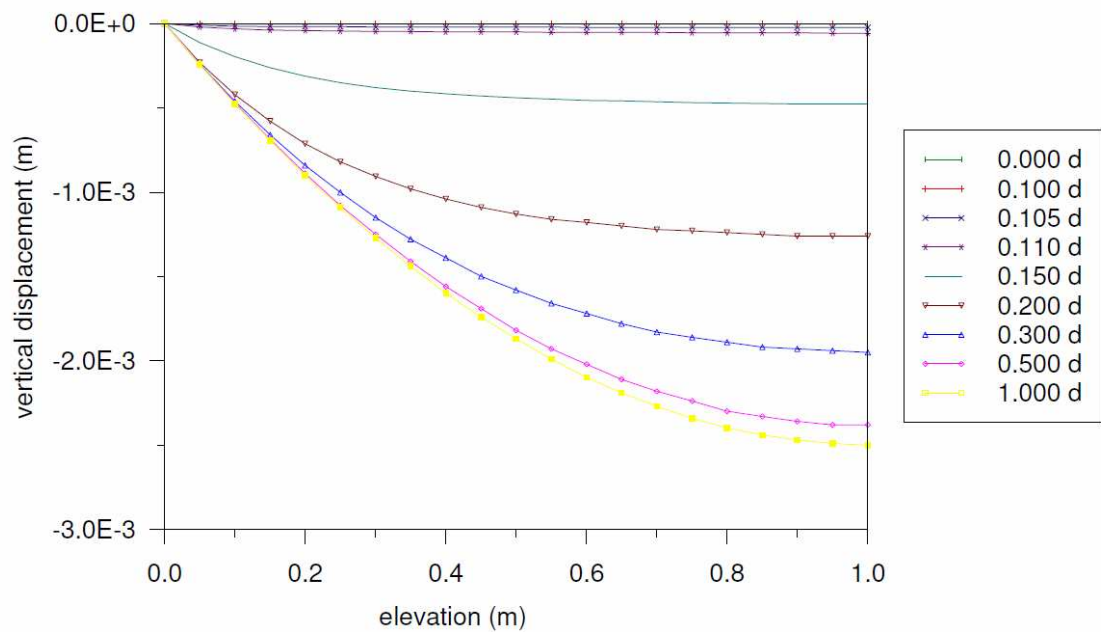


Fig. CA4.11: Vertical displacement for case 2b (PLAXIS 3D Foundation)

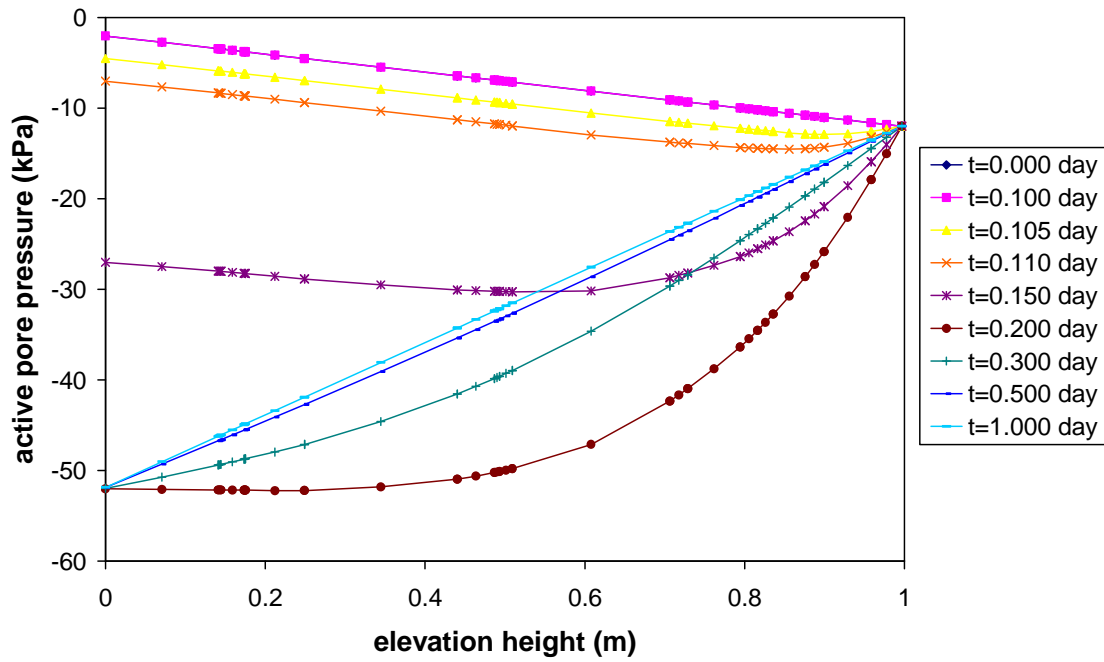


Fig. CA4.12: Active pore pressure for case 2b (PLAXIS 3D)

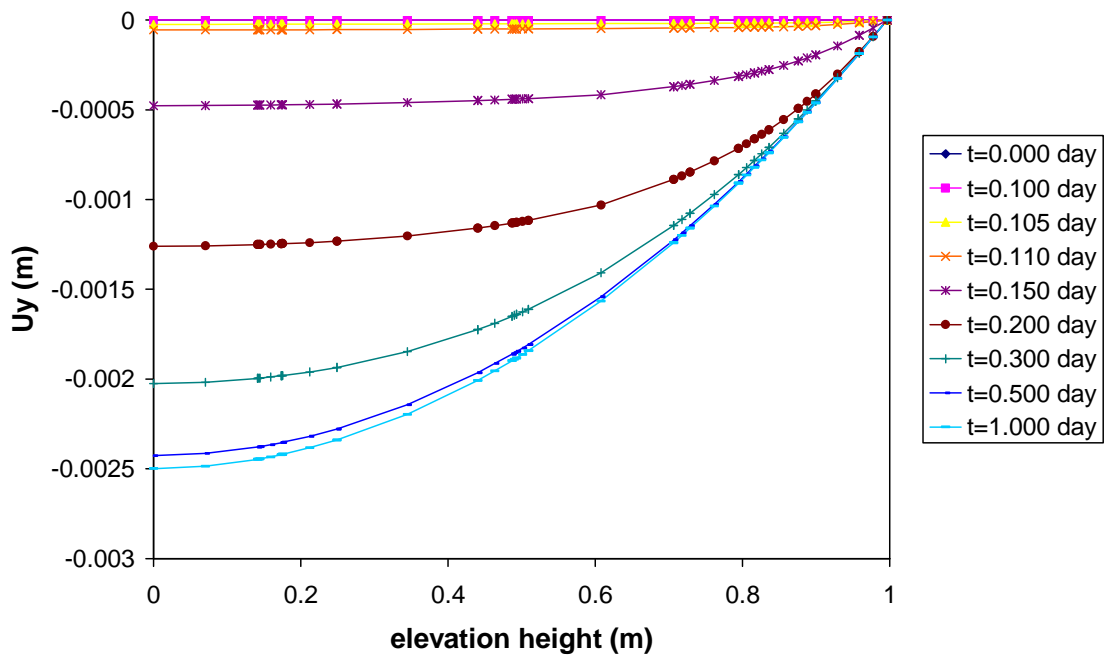


Fig. CA4.13: Vertical displacement for case 2b (PLAXIS 3D)

Summary:

As seen the results from PLAXIS 2D and 3D kernels are similar. The differences are due to different time steps used during the calculations.

9.5 Case CA5: Potato field moisture

The example of Potato field which is calculated by transient calculation, is chosen for fully coupled flow-deformation analysis (example G1). This lesson demonstrates the applicability of PLAXIS to agricultural problems. The potato field lesson involves a loam layer on top of a sandy base. Regional conditions prescribe a water level at the position of the material interface. The water level in the ditches remains unchanged. The precipitation may vary on a daily basis due to weather conditions. The calculation aims to predict the variation of the water content in the loam layer in time as a result of time-dependent boundary conditions.

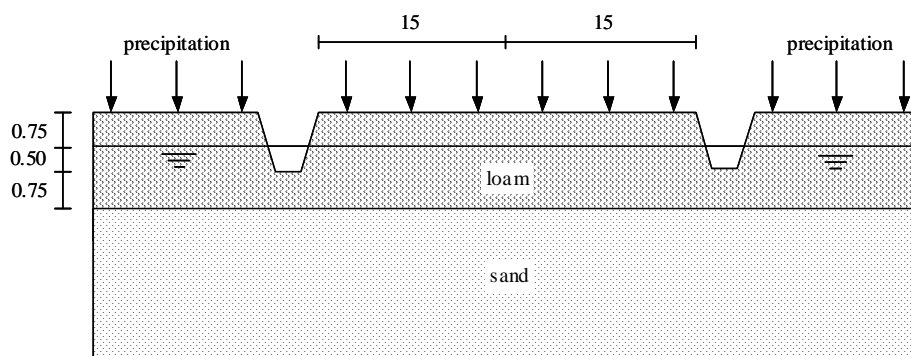


Fig. CA5.1: Potato field geometry

Starting series B9 and O2 represent the top and the bottom layers. The parameters are given in Table CA5.1 and CA5.2, respectively.

Tab. CA5.1: Input data for loam layer (B9)

Description	Symbol	Unit	Value
Permeability	k_x, k_y, k_z	[m/day]	0.0154
initial void ratio	e_{init}	[-]	0.754
Elastic storage	$K_{w,ref}/n$	[kN/m ²]	4.875×10^5
Saturation (saturated)	S_{sat}	[-]	1.0
Saturation (residual)	S_{res}	[-]	0.06831
Van Genuchten	g_n	[-]	1.325
Van Genuchten	g_a	[m ⁻¹]	0.650
Van Genuchten	g_l	[-]	-2.161
Young's modulus	E	[kN/m ²]	20000
Poisson's ratio	ν	[-]	0.2
Soil weight (sat)	γ_{sat}	[kN/m ³]	19
Soil weight (dry)	γ_{unsat}	[kN/m ³]	17

Tab. CA5.1: Input data for sand layer (O2)

Description	Symbol	Unit	Value
Permeability	k_x, k_y, k_z	[m/day]	0.1270
initial void ratio	e_{init}	[-]	0.62
Elastic storage	$K_{w,ref}/n$	[kN/m ²]	4.875×10^5
Saturation (saturated)	S_{sat}	[-]	1.0
Saturation (residual)	S_{res}	[-]	0.06203
Van Genuchten	g_n	[-]	1.951
Van Genuchten	g_a	[m ⁻¹]	2.13
Van Genuchten	g_l	[-]	0.168
Young's modulus	E	[kN/m ²]	13000
Poisson's ratio	ν	[-]	0.2
Soil weight (sat)	γ_{sat}	[kN/m ³]	19
Soil weight (dry)	γ_{unsat}	[kN/m ³]	17

The precipitation fluxes are given in Table CA5.3. The threshold values for ponding and precipitation (evapotranspiration) are chosen as 1 m and 0 at the top of the boundary, respectively.

Tab. CA5.3: Prescribed flux ($\varphi_{min} = 0$ and $\varphi_{max} = 1$ m)

Time (day)	Q (m/day)
0	0
1	0
1	0.01
2	0.01
2	0.03
3	0.03
3	0
4	0
4	0.03
5	0.03
5	0
6	0
6	0.01
8	0.01
8	0
9	0

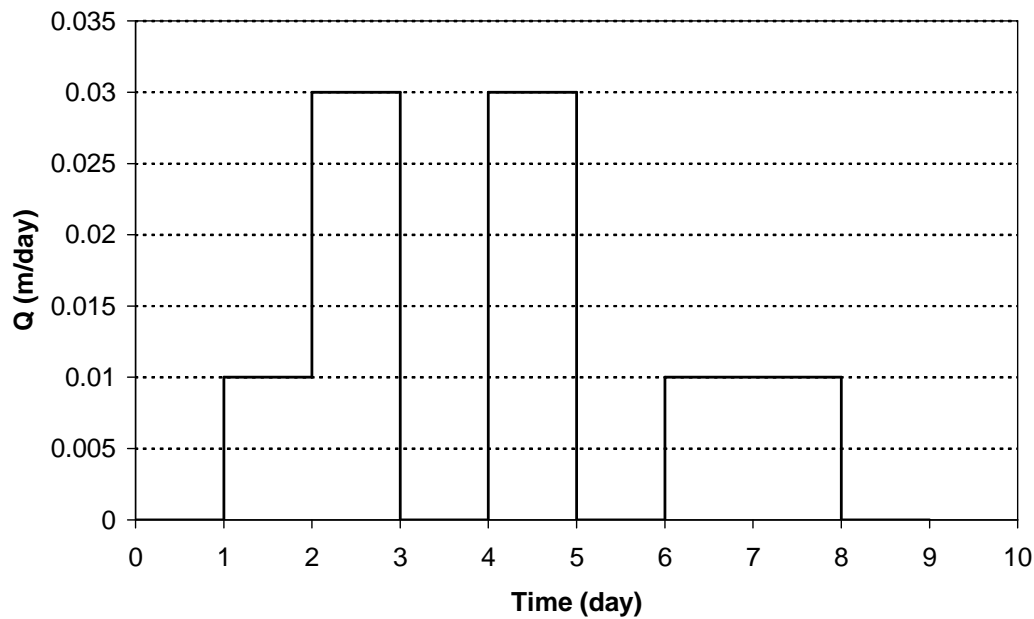


Fig. CA5.2: Prescribed flux

Due to the symmetry of the problem, it is sufficient to simulate a strip with a width of 15.0 m, as indicated in Figure CA5.3. The thickness of the loam layer is 2.0 m and the sand layer is 3.0 m deep.

The finite element mesh used for the calculation is depicted in Figure CA5.3. The mesh consists of 735 15-noded elements in case of 2D and 20648 10 noded tetrahedral elements in case of 3D.

The following steps are performed in this case:

1. *Gravity loading*: Gravity loading is performed to generate initial stresses.
2. *Steady state + Plastic drained*: a Steady state calculation followed by a plastic drained to obtain equilibrium (the bottom head is imposed to 3 m). The initial displacement is set to zero.
3. *Coupled analysis*: The top boundary head is set to influx. The initial displacement is set to zero.

Active pore pressure, degree of saturation and flow fields are shown in the following for steady state, after 5 and after 9 days.

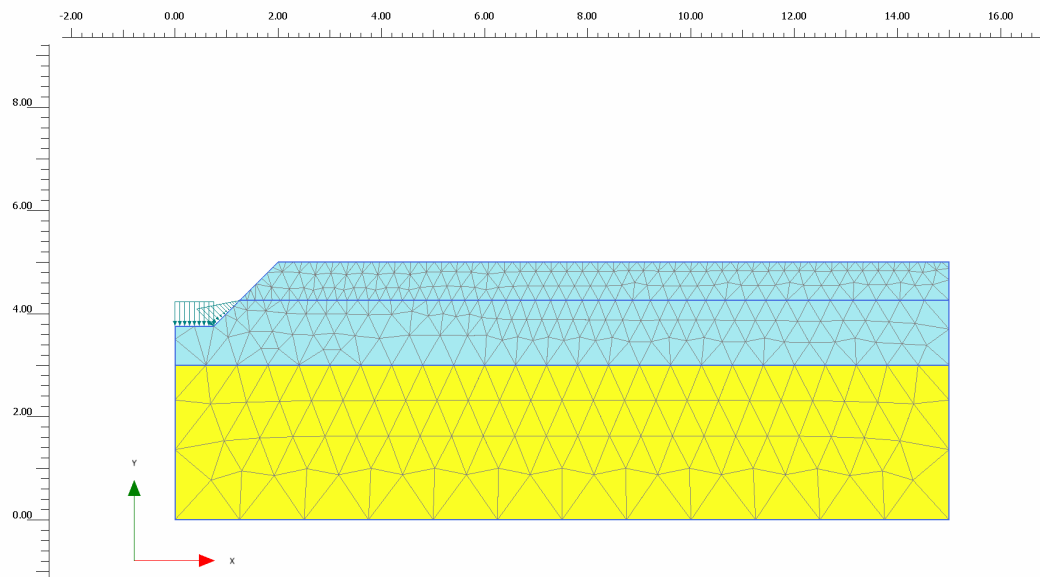


Fig. CA5.3.2D: Finite element mesh (15 noded elements)

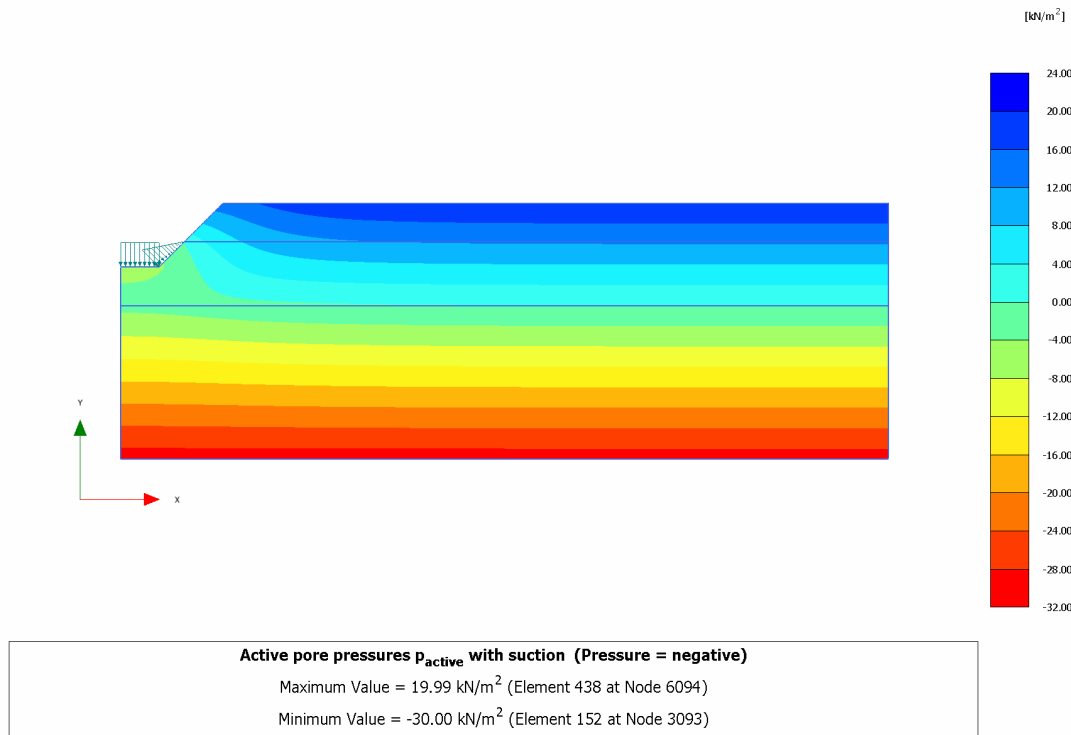


Fig. CA5.4.2D: Active pore pressure after steady state phase (imposing head)

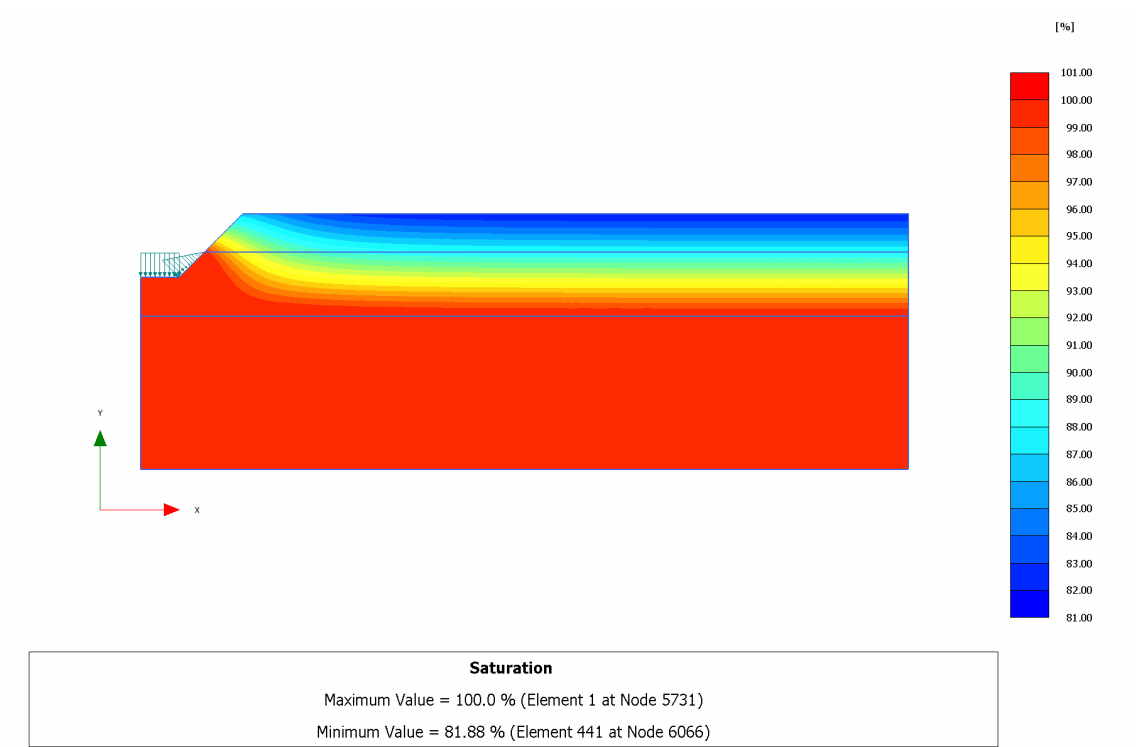


Fig. CA5.5.2D: Degree of saturation after steady state phase (imposing head)

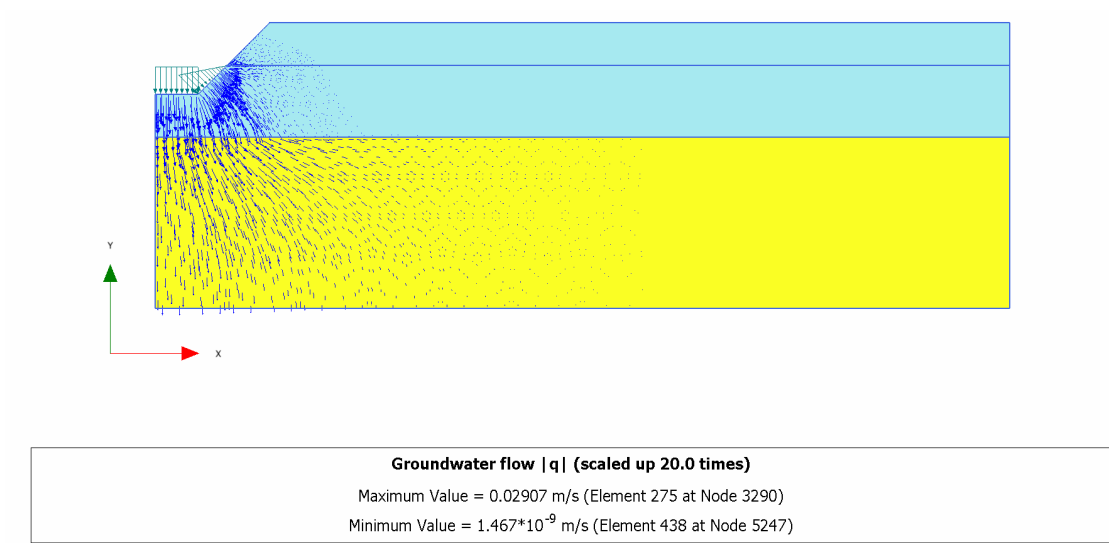


Fig. CA5.6.2D: Flow field after steady state phase (imposing head)

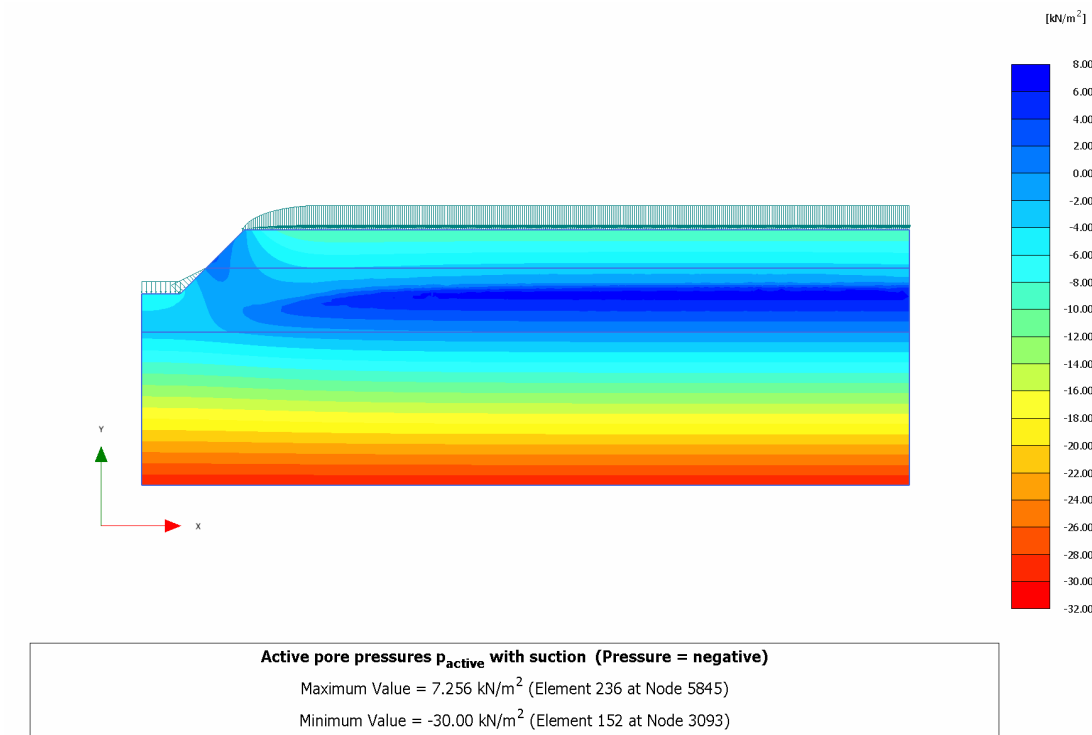


Fig. CA5.7.2D: Active pore pressure and external water load after 5 days

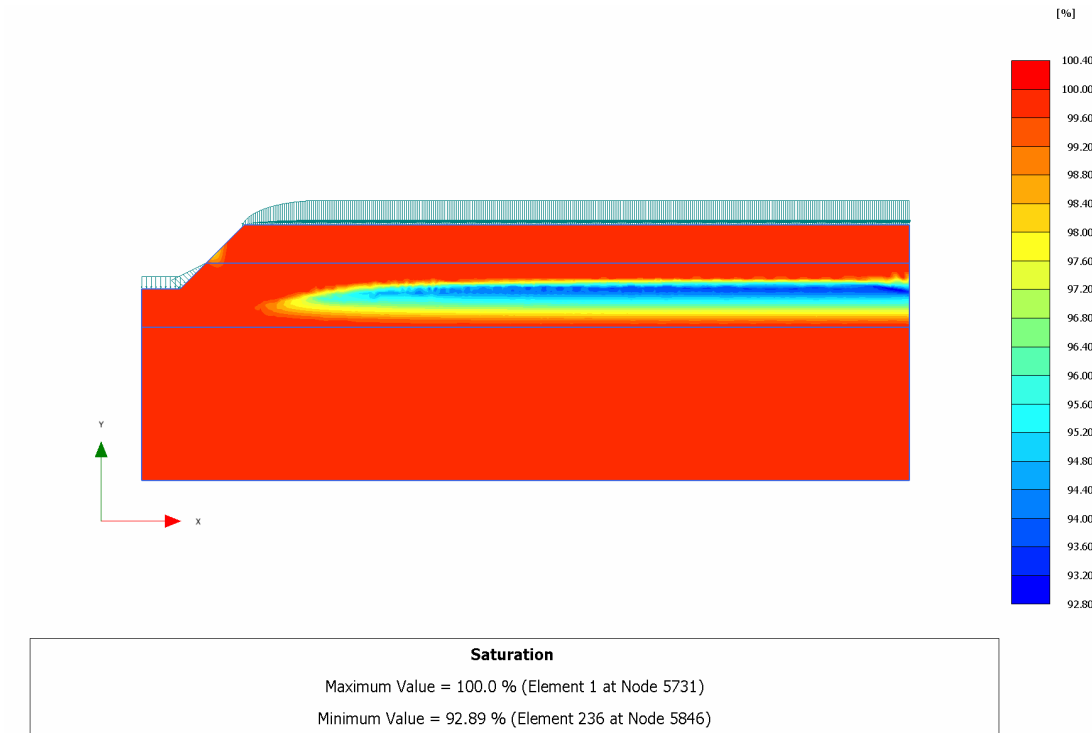


Fig. CA5.8.2D: Degree of saturation after 5 days

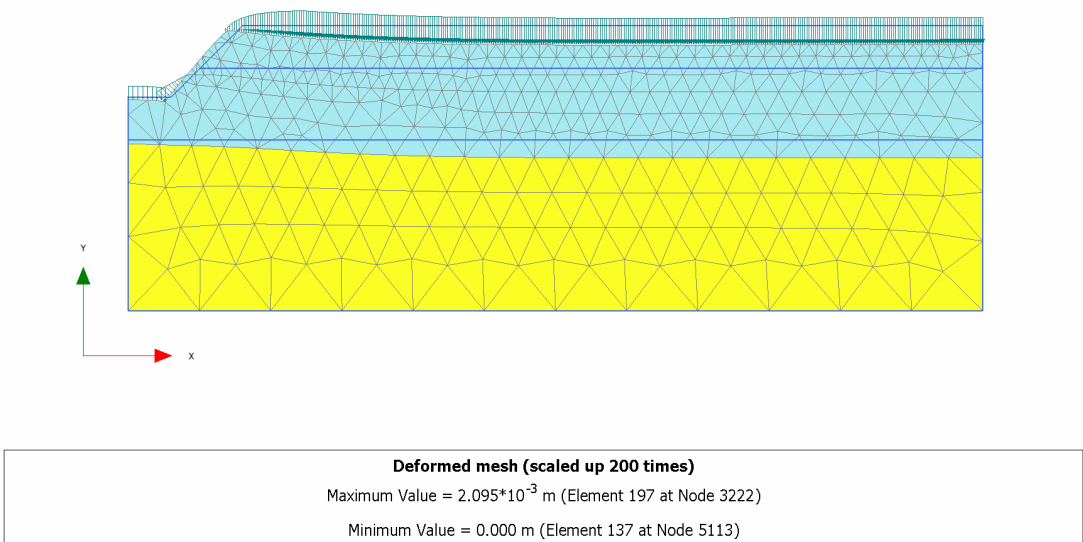


Fig. CA5.9.2D: Deformed mesh after 5 days

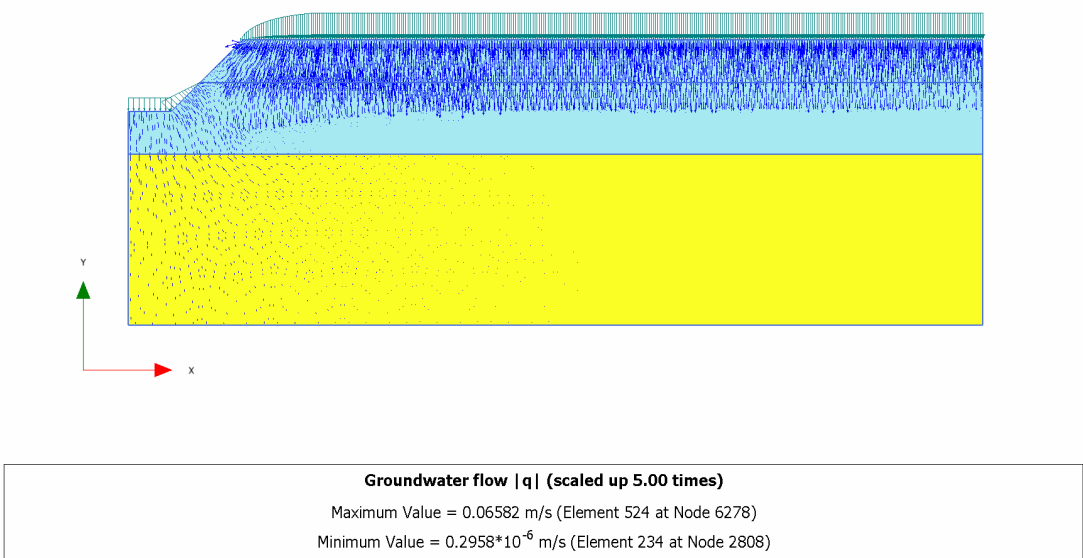


Fig. CA5.10.2D: Flow field after 5 days

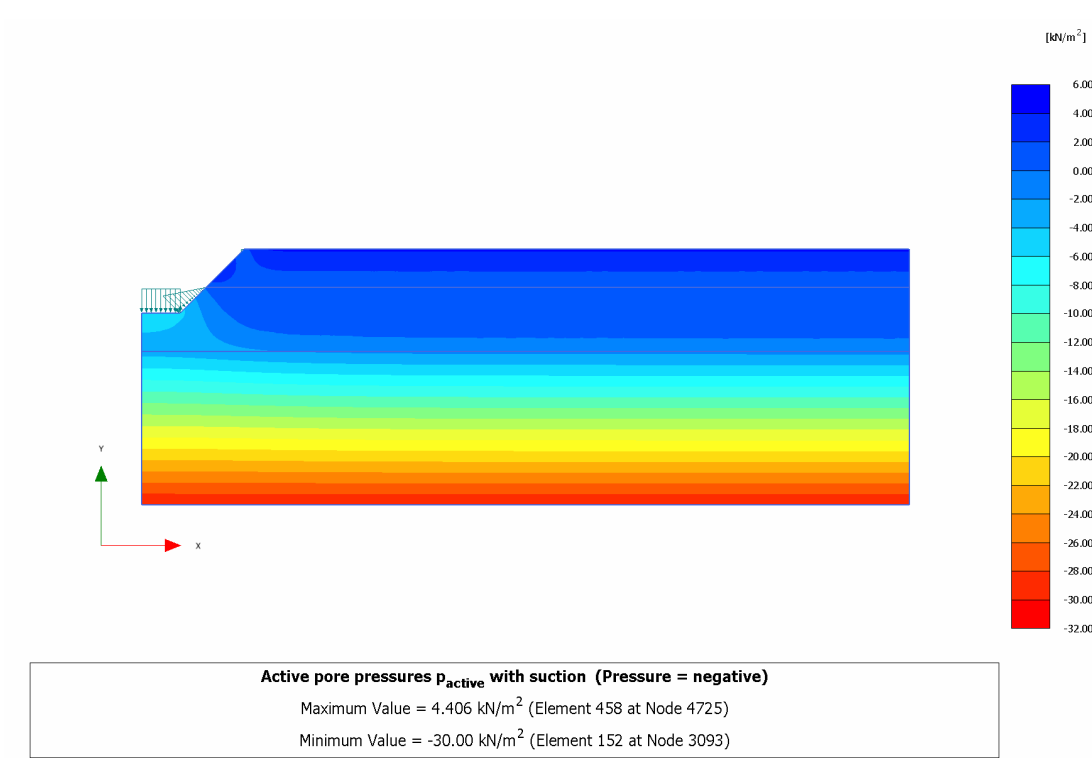


Fig. CA5.11.2D: Active pore pressure after 9 days

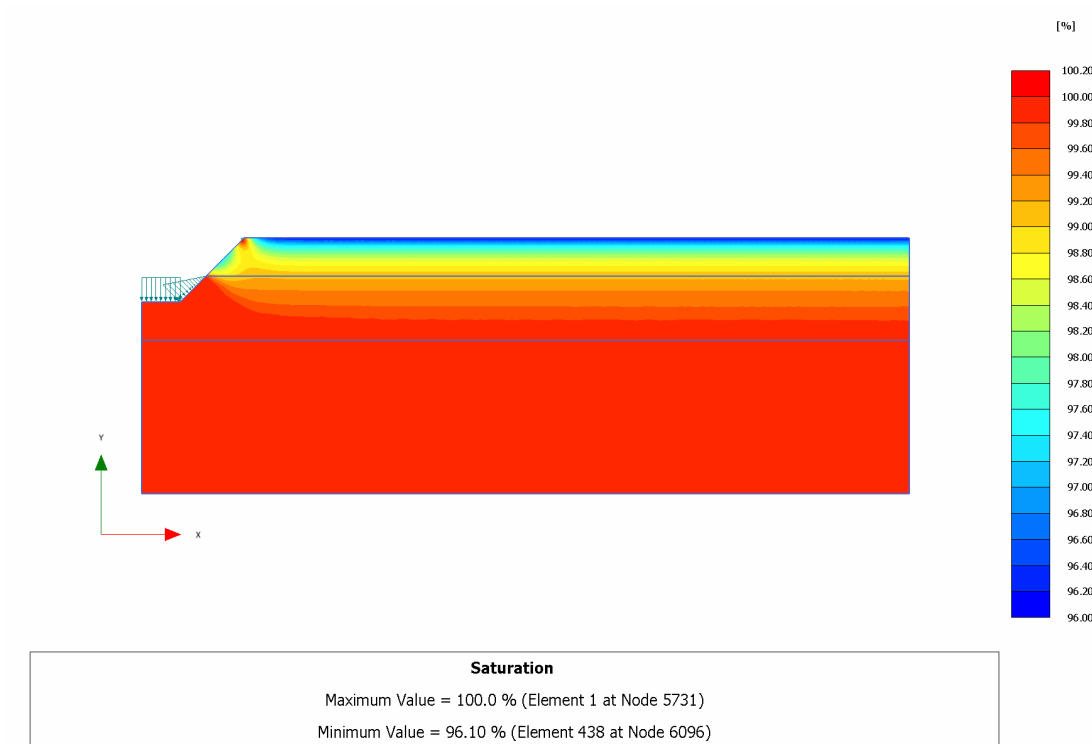


Fig. CA5.12.2D: Degree of saturation after 9 days

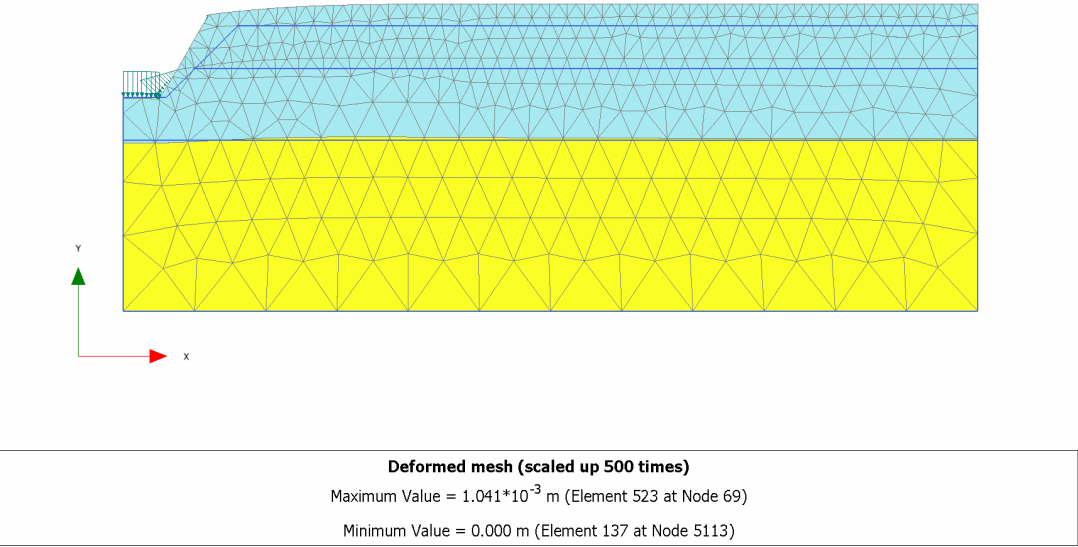


Fig. CA5.13.2D: Deformed mesh after 9 days

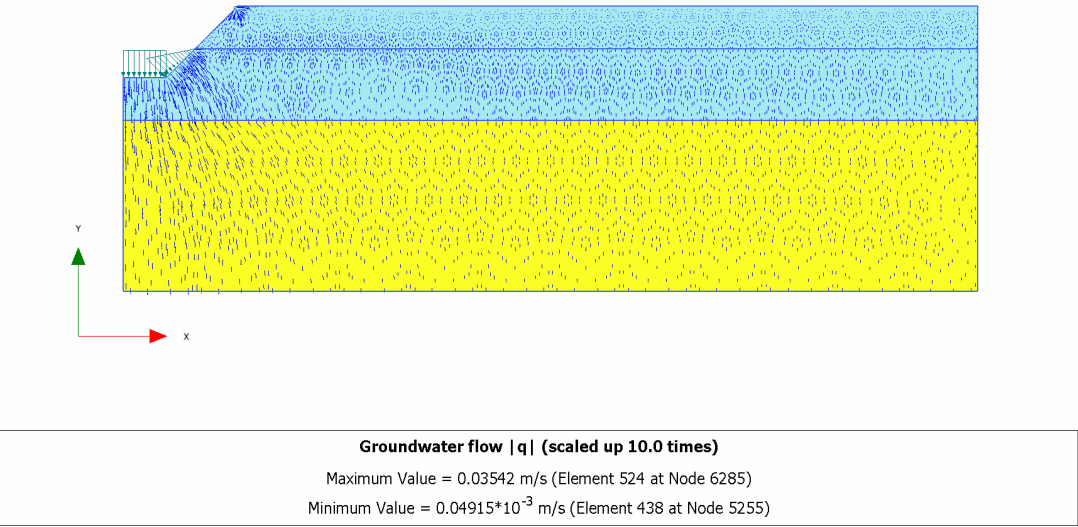


Fig. CA5.14.2D: Flow field after 9 days

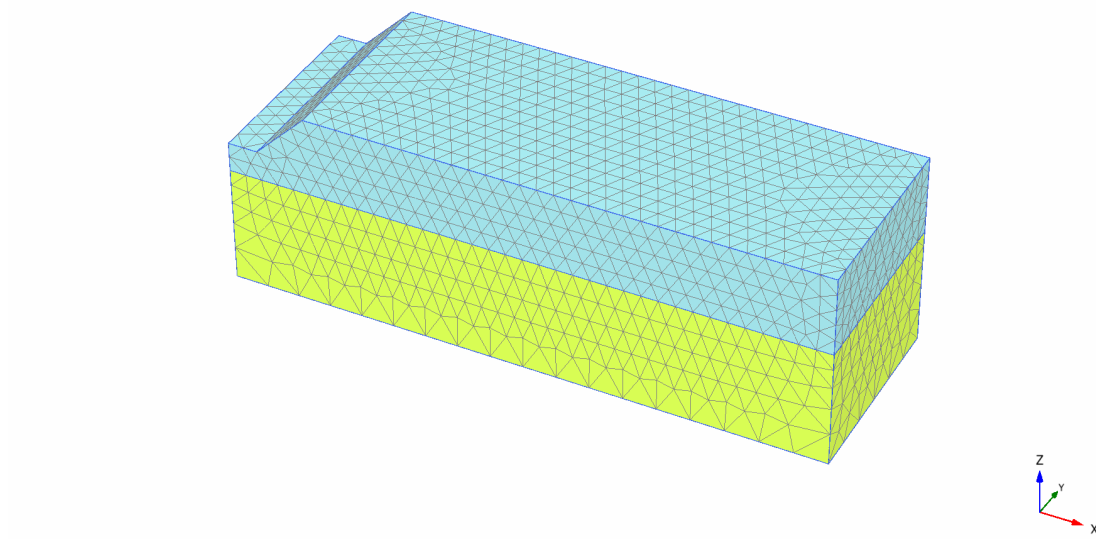


Fig. CA5.3.3D: Finite element mesh (10 noded elements)

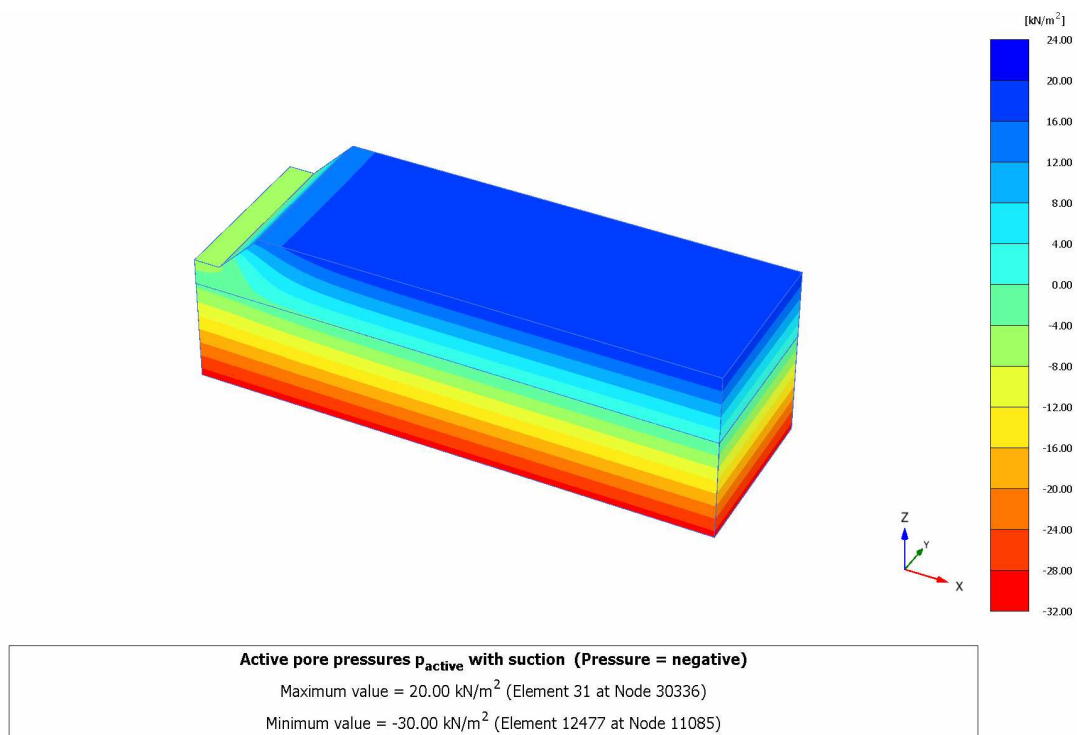


Fig. CA5.4.3D: Active pore pressure after steady state phase (imposing head)

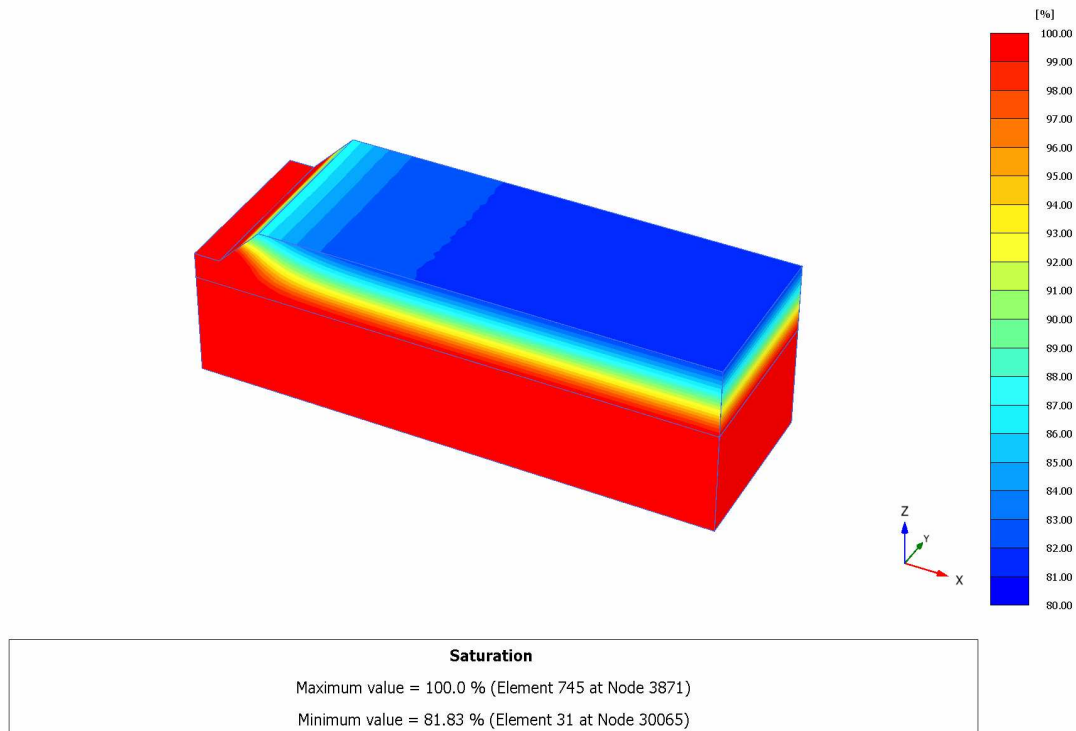


Fig. CA5.5.3D: Degree of saturation after steady state phase (imposing head)

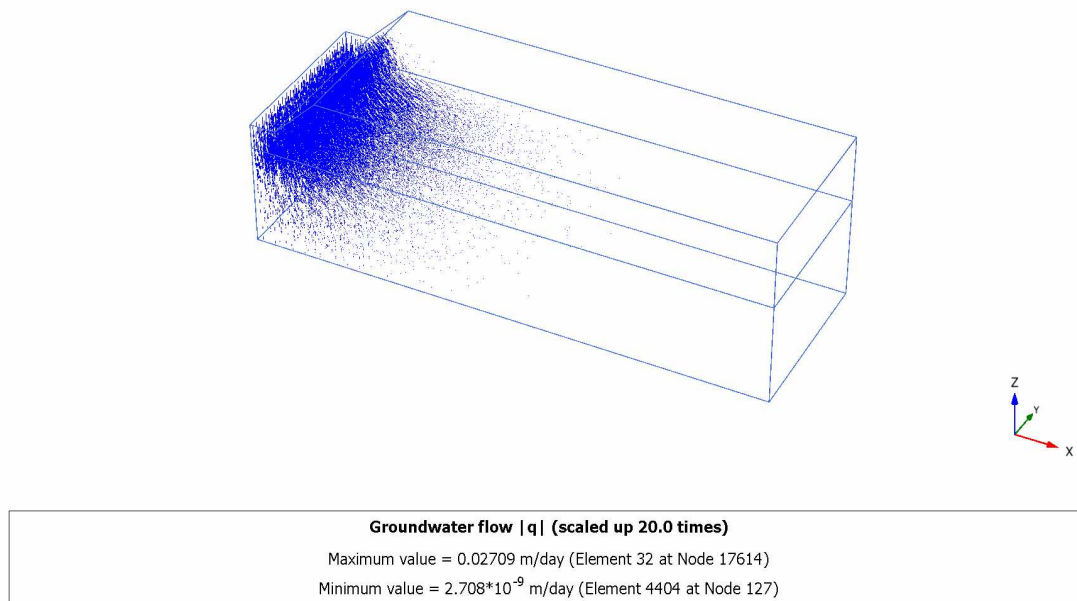


Fig. CA5.6.3D: Flow field after steady state phase (imposing head)

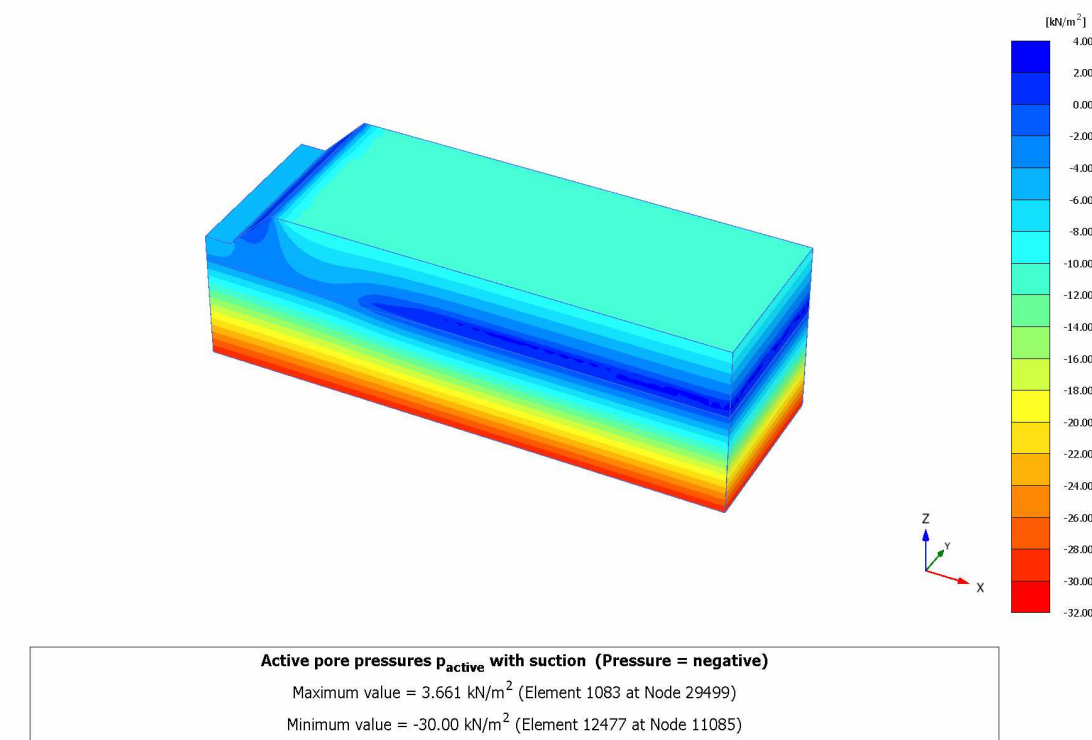


Fig. CA5.7.3D: Active pore pressure and external water load after 5 days

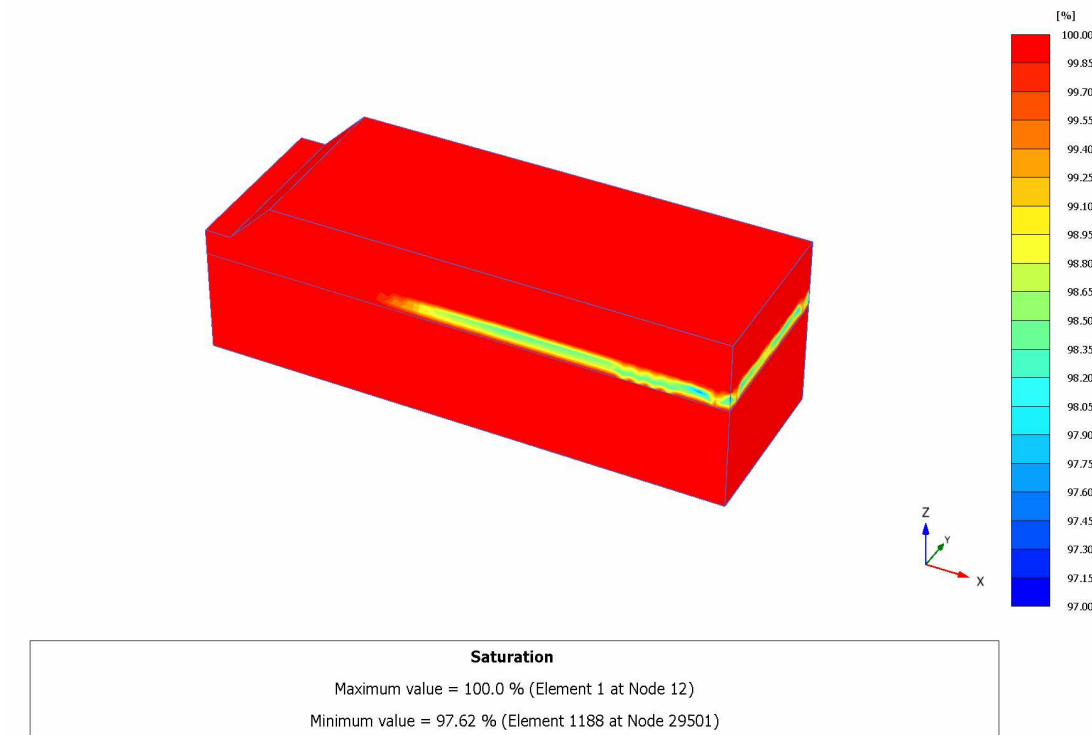


Fig. CA5.8.3D: Degree of saturation after 5 days

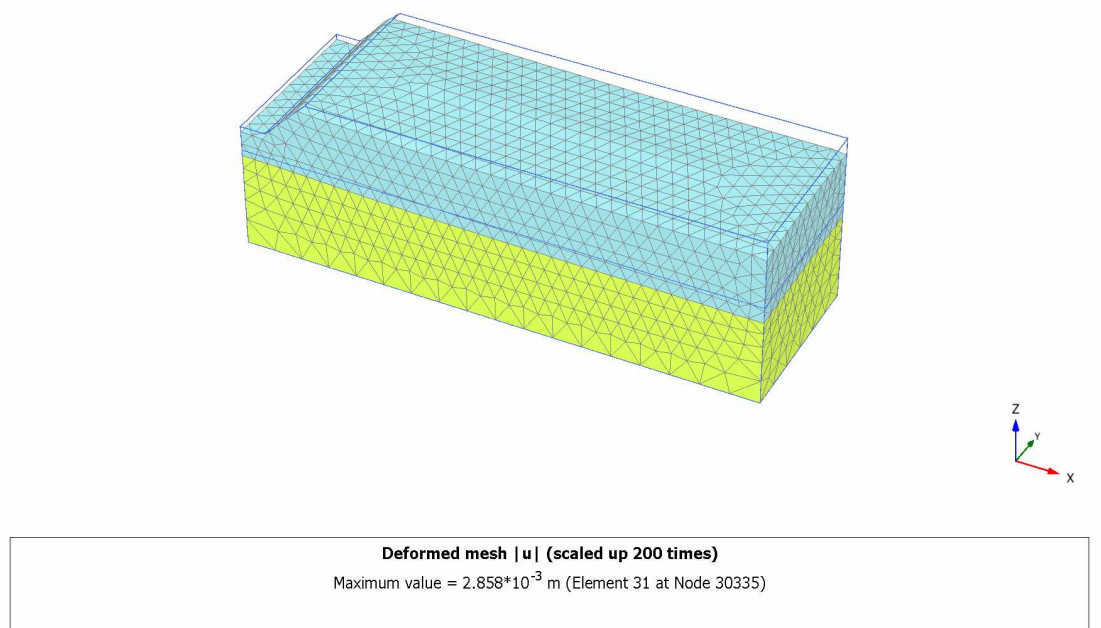


Fig. CA5.9.3D: Deformed mesh after 5 days

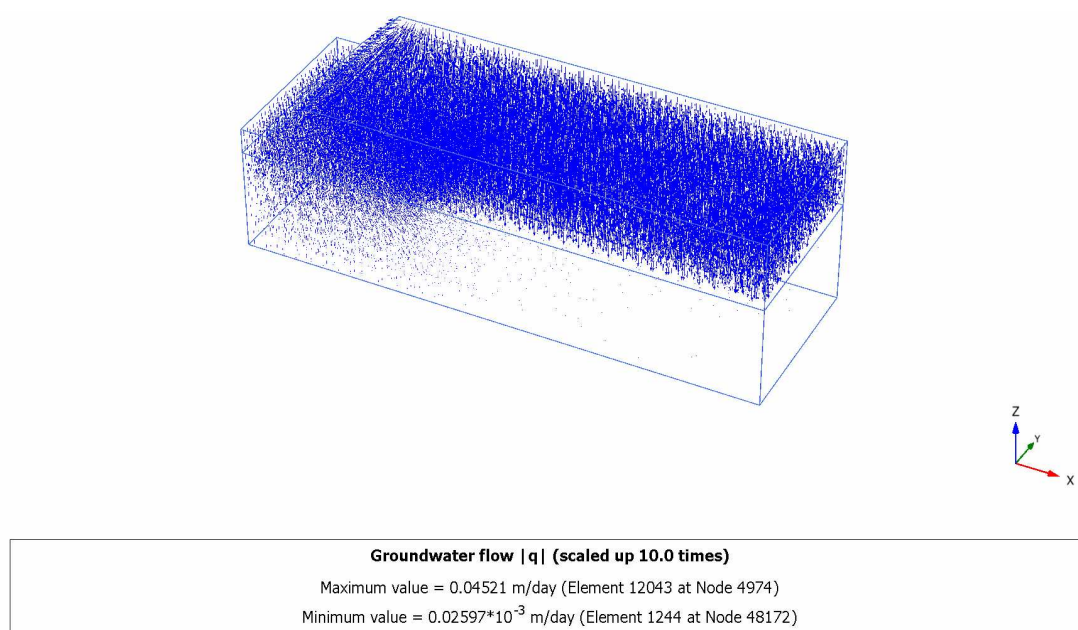


Fig. CA5.10.3D: Flow field after 5 days

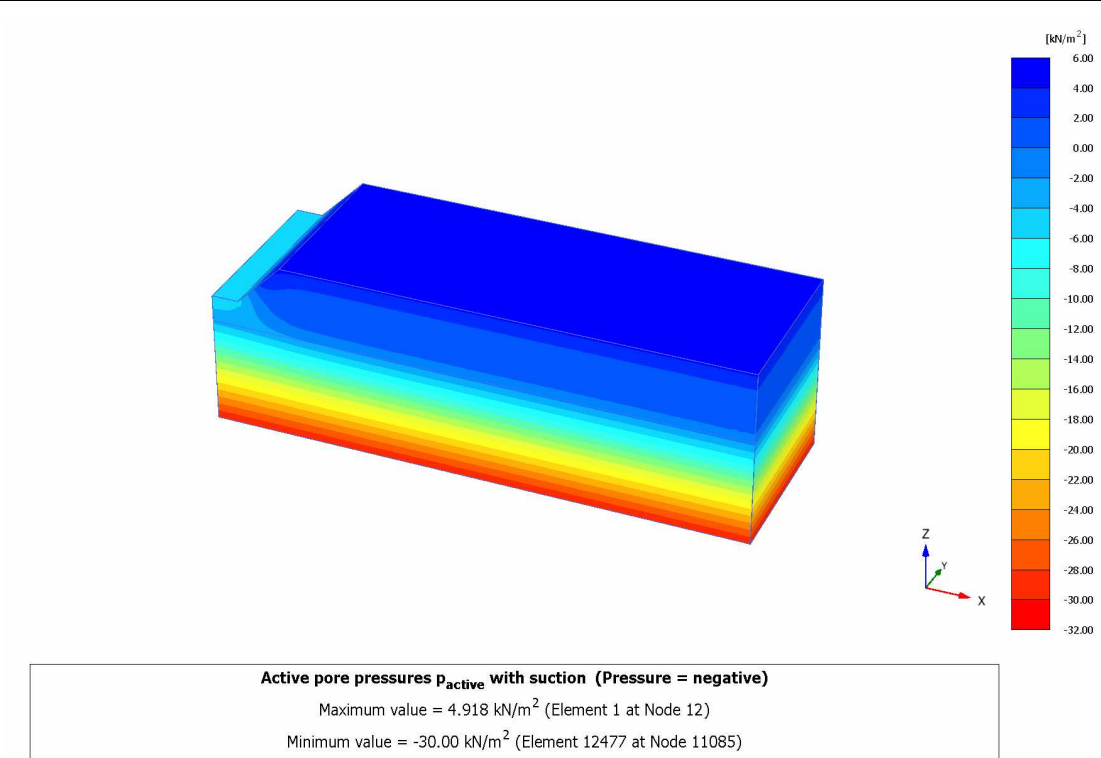


Fig. CA5.11.3D: Active pore pressure after 9 days

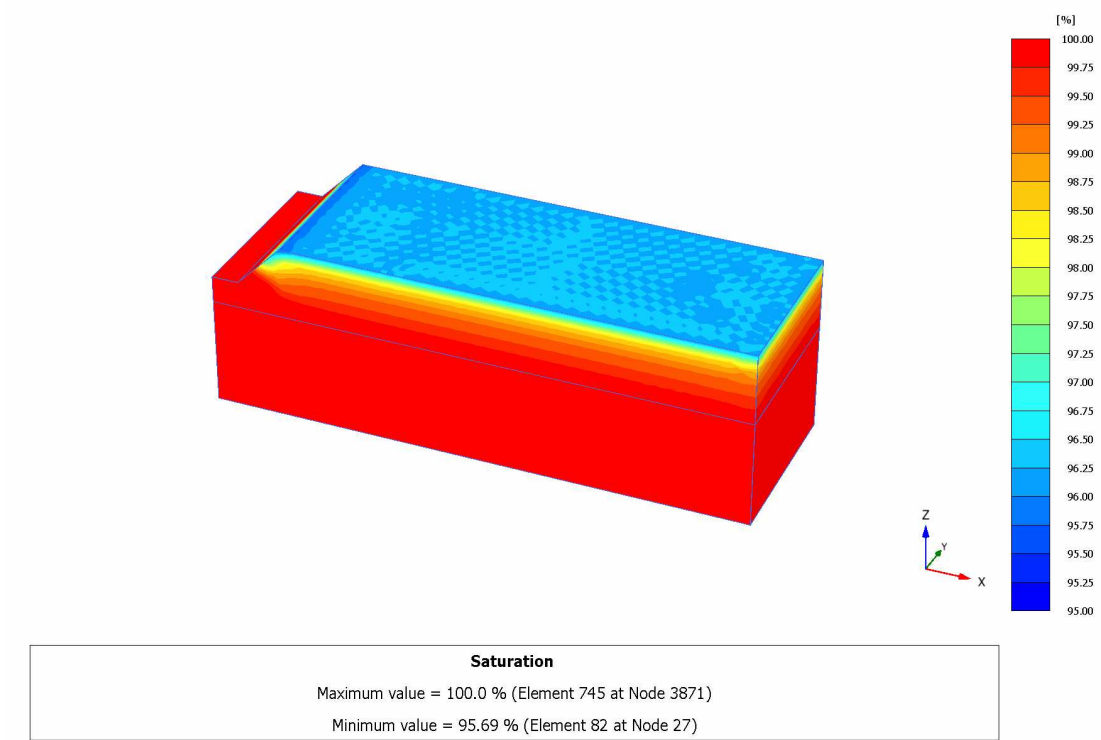


Fig. CA5.12.3D: Degree of saturation after 9 days

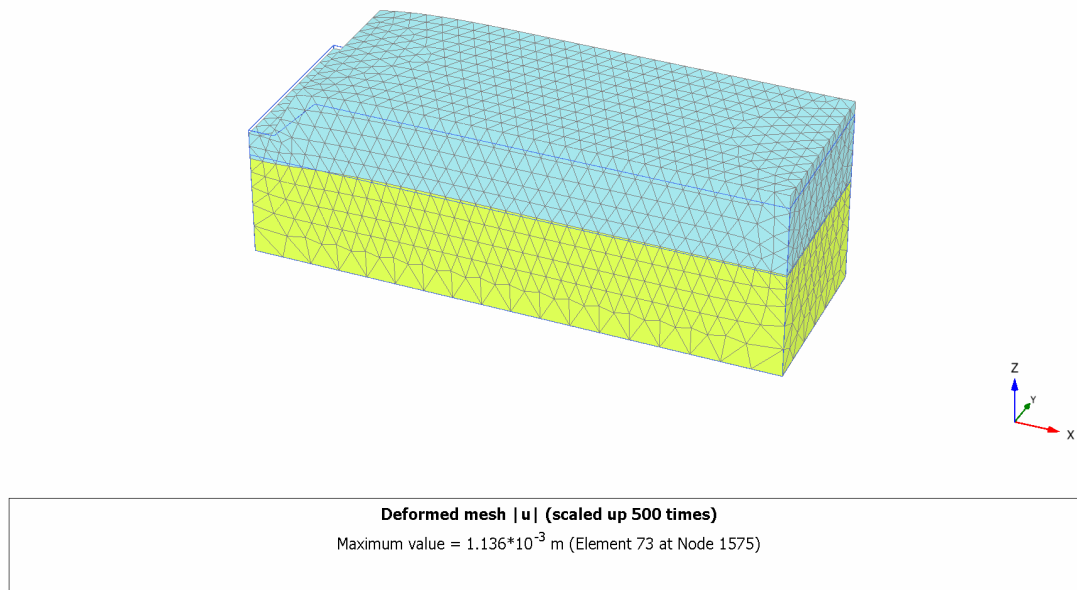


Fig. CA5.13.3D: Deformed mesh after 9 days

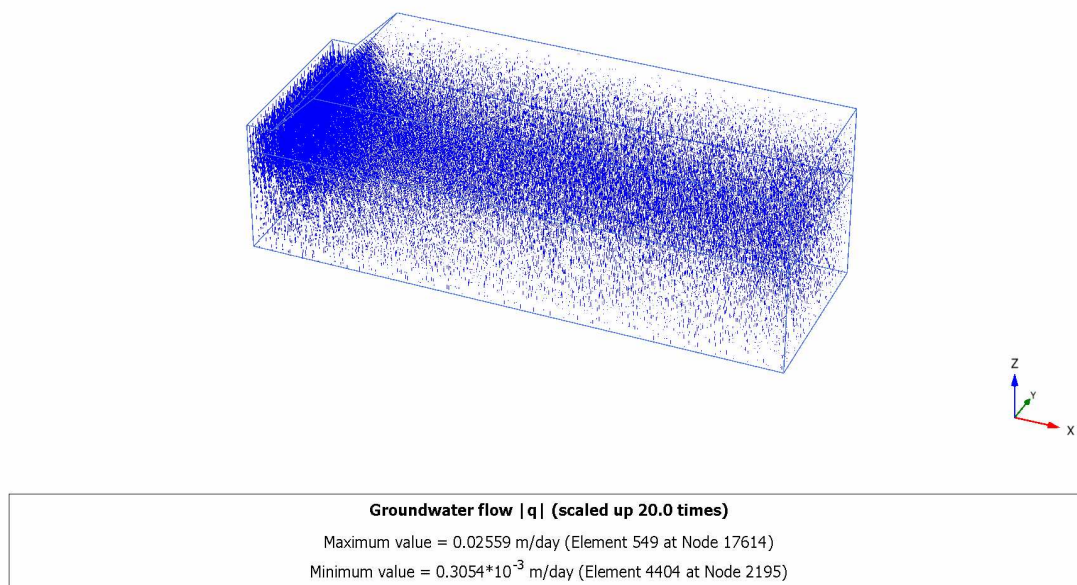


Fig. CA5.14.3D: Flow field after 9 days

Summary:

This example cannot be verified. However by comparing the flow results, it can be seen that the flow response is similar to what calculated with transient calculation. As displacements are set to zero in the beginning of each phase, the deformation is only due to change in water pore pressure in the phase. In the third phase, heave can be seen which is because of raining that leads to decrease suction and consequently to decrease Bishop effective stress. Results from PLAXIS 2D and 3D are similar.

9.6 Case CA6: Rapid draw down

This example concerns the stability of a reservoir dam under conditions of drawn down. Fast reduction of the reservoir level may lead to instability of the dam due to high pore water pressures that remain inside the dam. To analyse such a situation using the finite element method, a coupled flow – deformation calculation is required. This example demonstrates how coupled flow – deformation analysis and stability analysis can interactively be performed in PLAXIS.

Input:

The dam to be considered is 30 m high and the width is 167.5 m at the base and 5 m at the top. The dam consists of a clay core with a well graded fill to both sides. The geometry of the dam is depicted in Fig. CA6. The normal water level behind the dam is 25 m high. A situation is considered where the water level drops to only 5 m. The normal phreatic level at the right hand side of the dam is 10 m below ground surface.

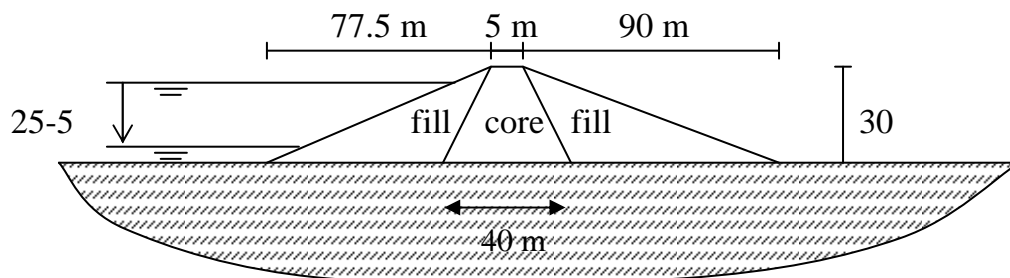


Fig. CA6.1: Geometry of the dam

The sub-soil consists of overconsolidated silty sand. The data of the dam materials and the sub-soil are given in Table CA6.1

Geometry Model:

The situation can be modelled with a geometry model in which the sub-soil is modelled to a depth of 30 m. The left hand boundary can be taken 50 m left of the dam toe and the right hand boundary can be taken 37.5 m right of the other dam toe. The proposed geometry model is presented in Figure CA6.2 for both 2D and 3D calculations. For 3D calculations the width of the geometry is taken 50 m.

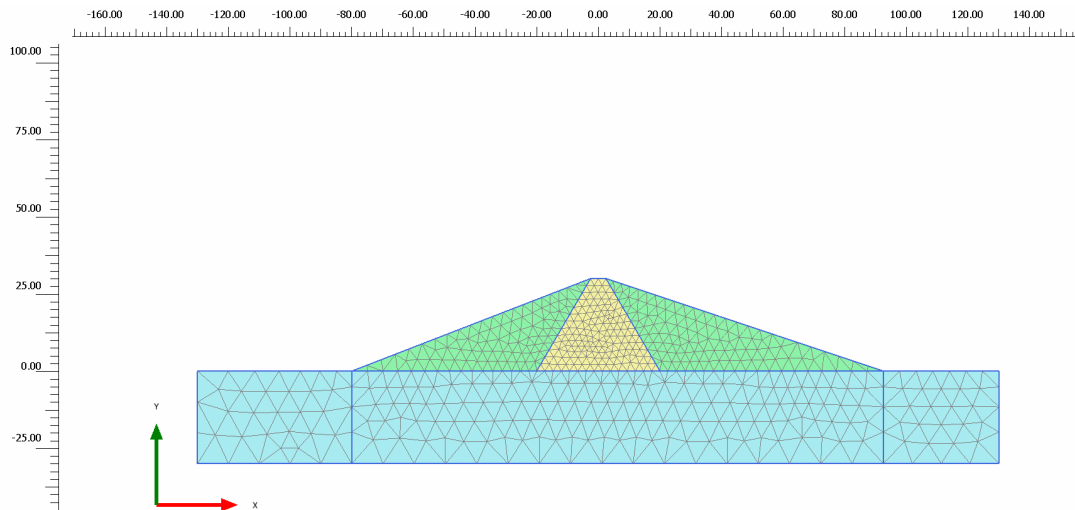


Fig. CA6.2.2D: Geometry and finite element mesh of the dam and sub-soil (PLAXIS 2D – 6 noded elements)

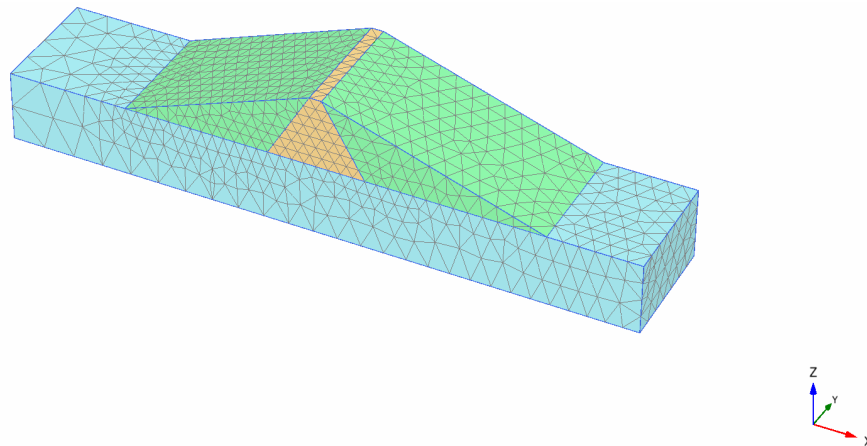


Fig. CA6.2.3D: Geometry and finite element mesh of the dam and sub-soil (PLAXIS 3D)

The calculation consists of nine phases. In the first phase the dam is constructed. In the second phase the reservoir is filled up, bringing the water level to the standard level of 25m. For this situation the water pressure distribution is calculated using a steady-state groundwater flow calculation. The third and fourth phase both start from this standard situation (i.e. a dam with a reservoir level at 25 m) and the water level is lowered to 5 m. A distinction is made in the time interval at which this is done (i.e. different speeds of water level reduction; rapid drawdown and slow drawdown). In both cases the water pressure distribution is calculated using a coupled flow – deformation calculation. The fifth calculation phase also starts from the second phase and considers the long-term behaviour of the dam at the low reservoir level of 5 m, which involves a steady-state groundwater flow calculation to calculate the water pressure distribution.

Finally, for all four water pressure situations the safety factor of the dam is calculated by means of phi-c reduction. This leads to the following cases being considered:

- water level remains at 25m.
- water level drops quickly from 25 to 5m.
- water level drops slowly from 25 to 5m.
- water level drops extremely slowly to 5m and remains there.

Material properties:

The material data sets of the clay core, the fill material and the sub-soil are shown in table CA6.1.

Tab. CA6.1: Dam and soil properties (Mohr-Coulomb model)

Parameter	Symbol	Core	Fill	Sub-soil	Unit
Material model	Model	Mohr-Coulomb	Mohr-Coulomb	Mohr-Coulomb	-
Type of behaviour	Type	Undrained	Undrained	Undrained	-
Unsaturated weight	γ_{unsat}	16.0	16.0	17.0	kN/m ³
Saturated weight	γ_{sat}	20.0	20.0	21.0	kN/m ³
Permeability	k_x, k_y, k_z	$1.0 \cdot 10^{-4}$	0.25	0.02	m/d
Young's modulus	E	8000	20000	50000	kN/m ²
Poisson's ratio	ν	0.35	0.33	0.3	-
Cohesion	c'	5.0	5.0	10.0	kN/m ²
Friction angle	ϕ'	25.0	30.0	32.0	°
Dilatancy angle	ψ	0.0	0.0	0.0	°
Void ratio	e_{init}	0.5	0.5	0.5	-
Flow data set		Standard (very fine)	Standard (coarse)	Standard (Medium)	
Lateral earth pressure	K_0	n/a	n/a	0.47	-

Calculation phases:

Phase 1: Steady state groundwater flow calculation.

- Create a closed flow boundary at the bottom of the model
- Generate groundwater head conditions at the other model boundaries by creating a general water level. The left head must be at a level of 25 m above the ground surface and the right boundary at a level of 10 m below the ground surface.

Phase 2: Gravity loading

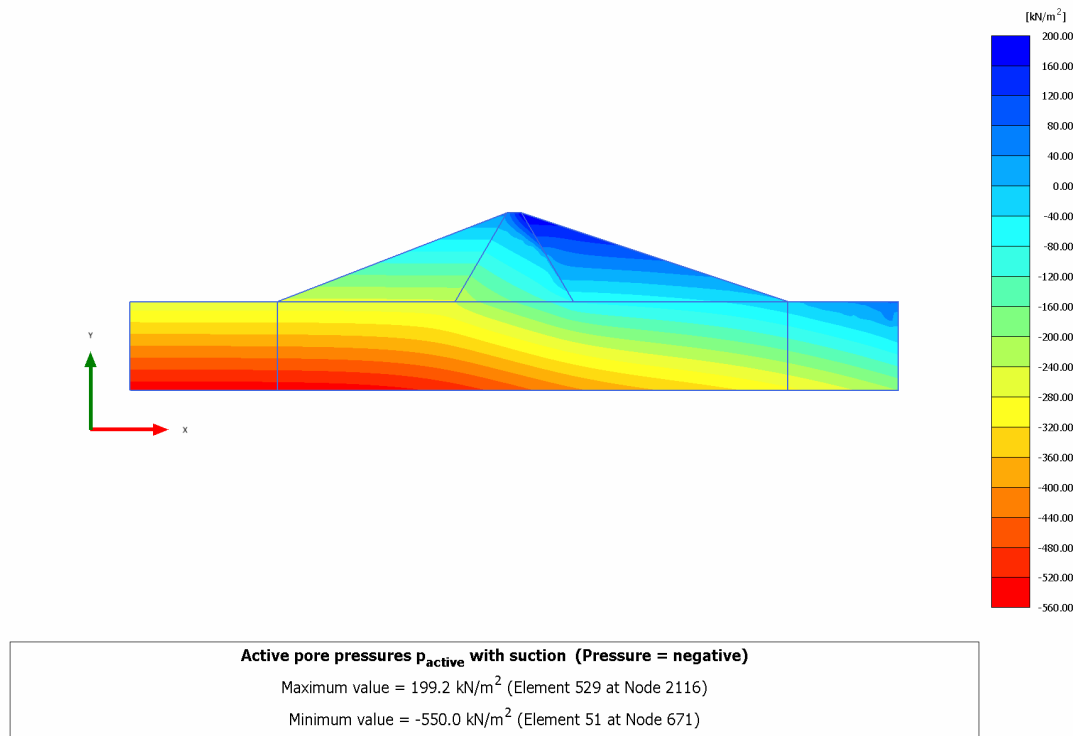


Fig. CA6.3.2D: Steady-state pore pressure for high reservoir level (PLAXIS 2D)

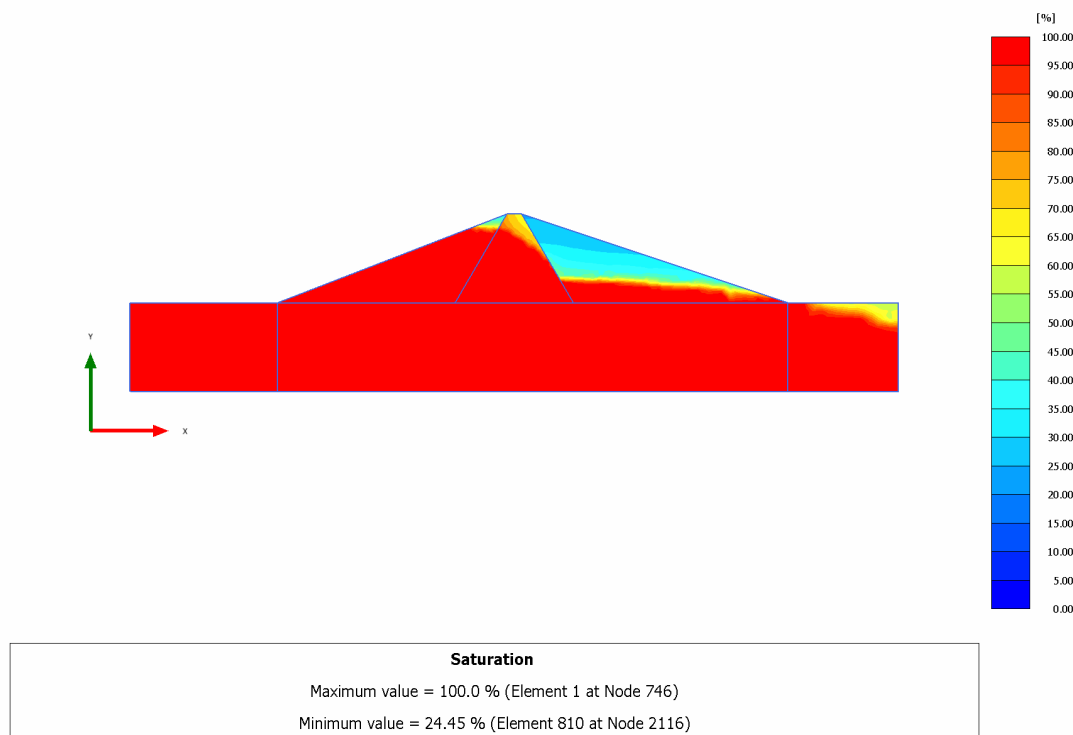


Fig. CA6.4.2D: Degree of saturation for high reservoir level (PLAXIS 2D)

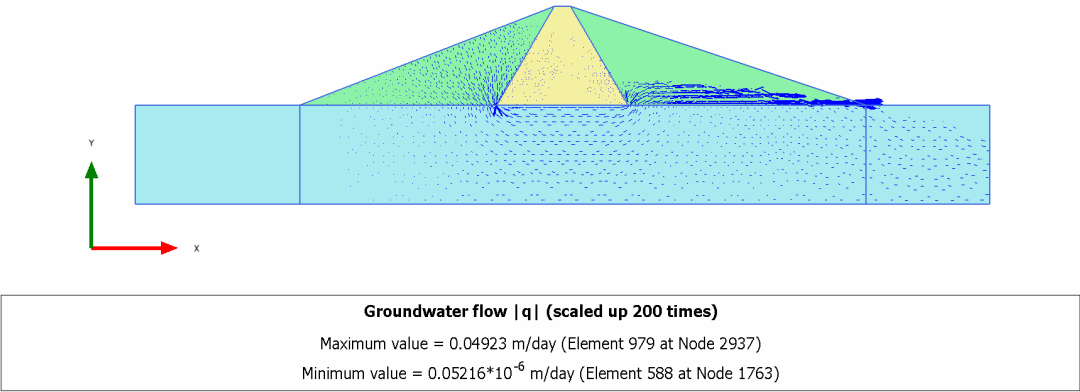


Fig. CA6.5.2D: Flow field for high reservoir level (PLAXIS 2D)

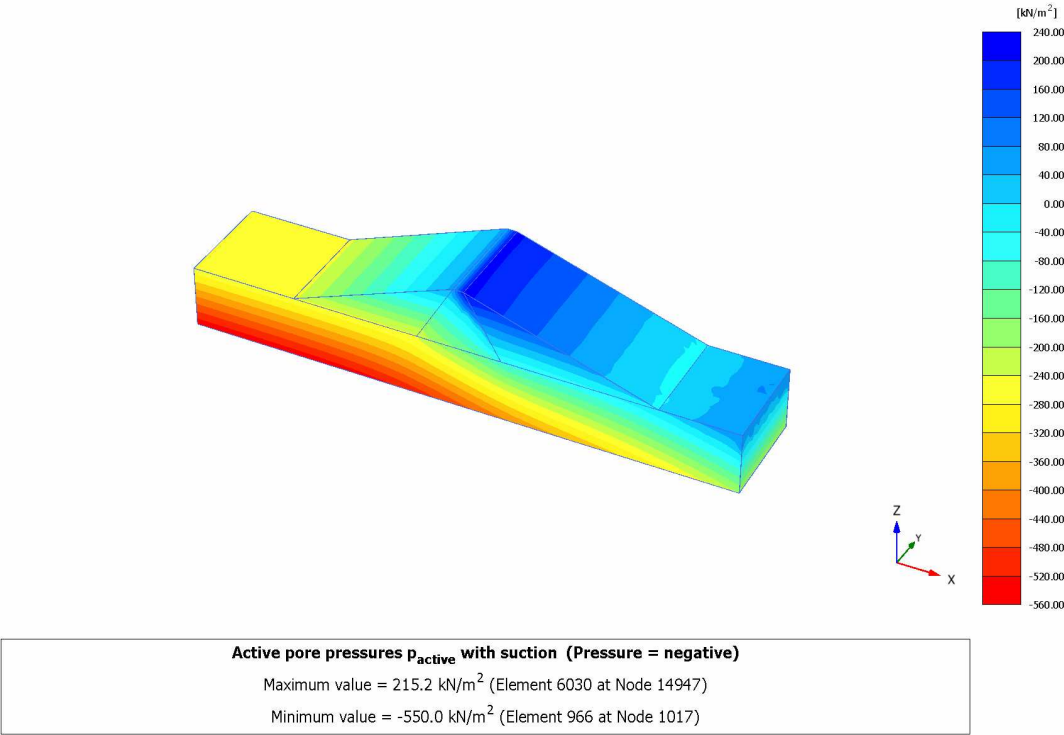


Fig. CA6.3.3D: Steady-state pore pressure for high reservoir level (PLAXIS 3D)

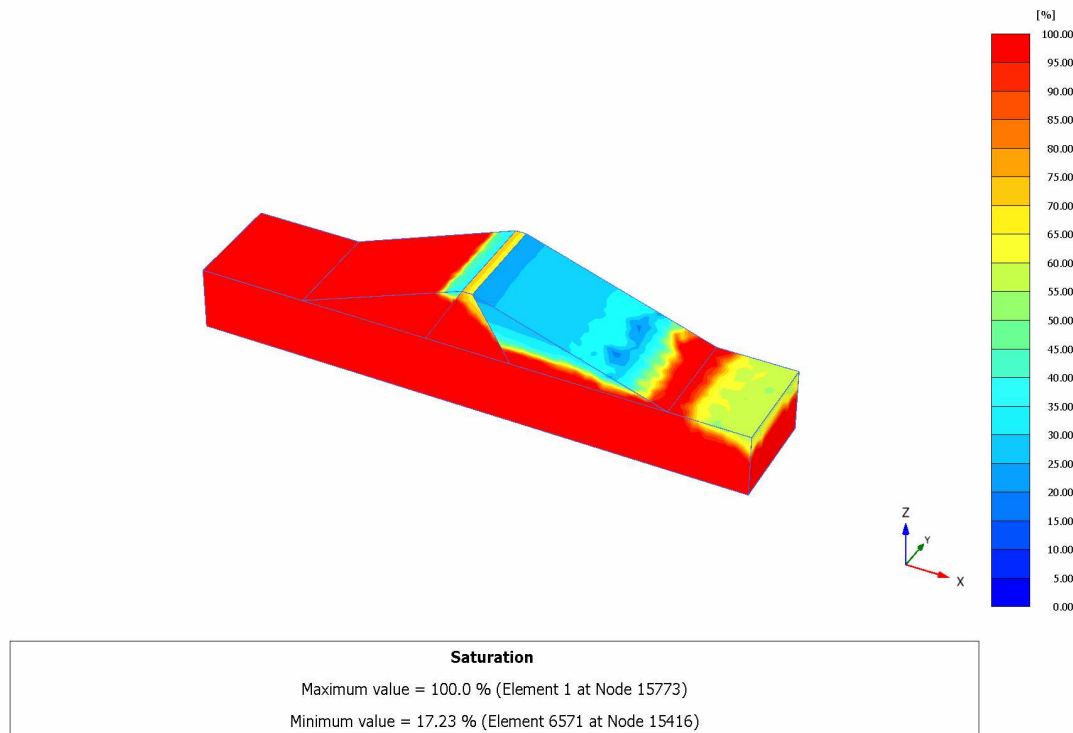


Fig. CA6.4.3D: Degree of saturation for high reservoir level (PLAXIS 3D)

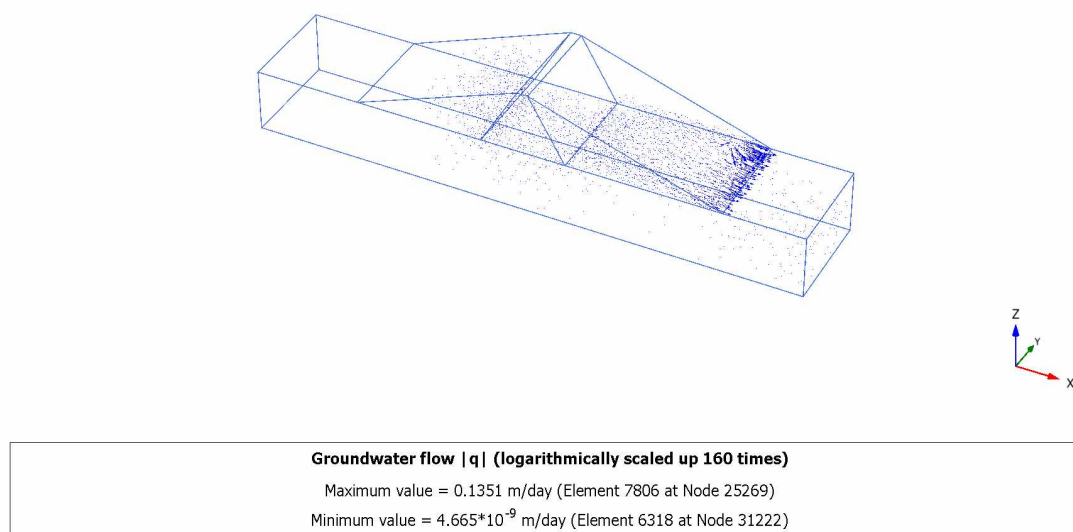


Fig. CA6.5.3D: Flow field for high reservoir level (PLAXIS 2D)

Phase 3: Rapid drawdown:

In this phase rapid drawdown of the reservoir level is considered.

- In the *Parameters* tab, select *Reset displacements to zero* and set the *Loading input* to *Stage construction*. Enter a value of 5 days for the *Time interval*.

Figure CA6.4 shows active pore pressures. It can be seen that, although the reservoir level has dropped down to 5 m, there are still high pore pressures in the dam, especially in the clay core. Other output options may be used to view the groundwater head, the degree of saturation and the flow field. The development

of various quantities in time may be viewed using the Animation option or the Curves option in the view menu.

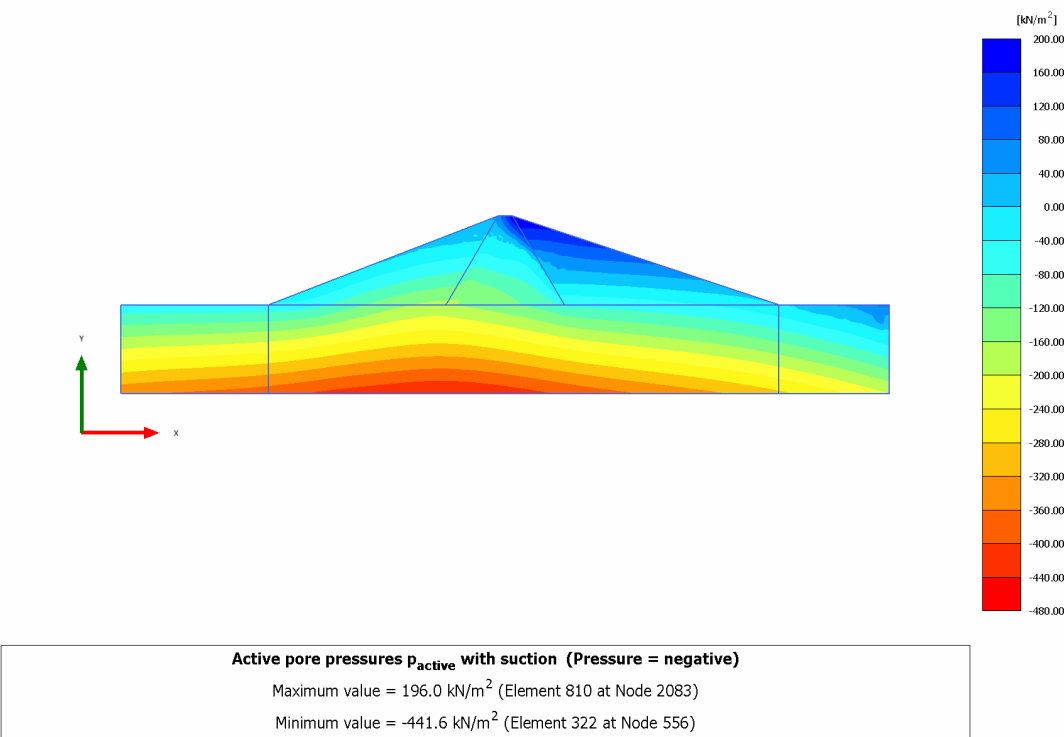


Fig. CA6.6.2D: Active pore pressure after rapid drawdown (PLAXIS 2D)

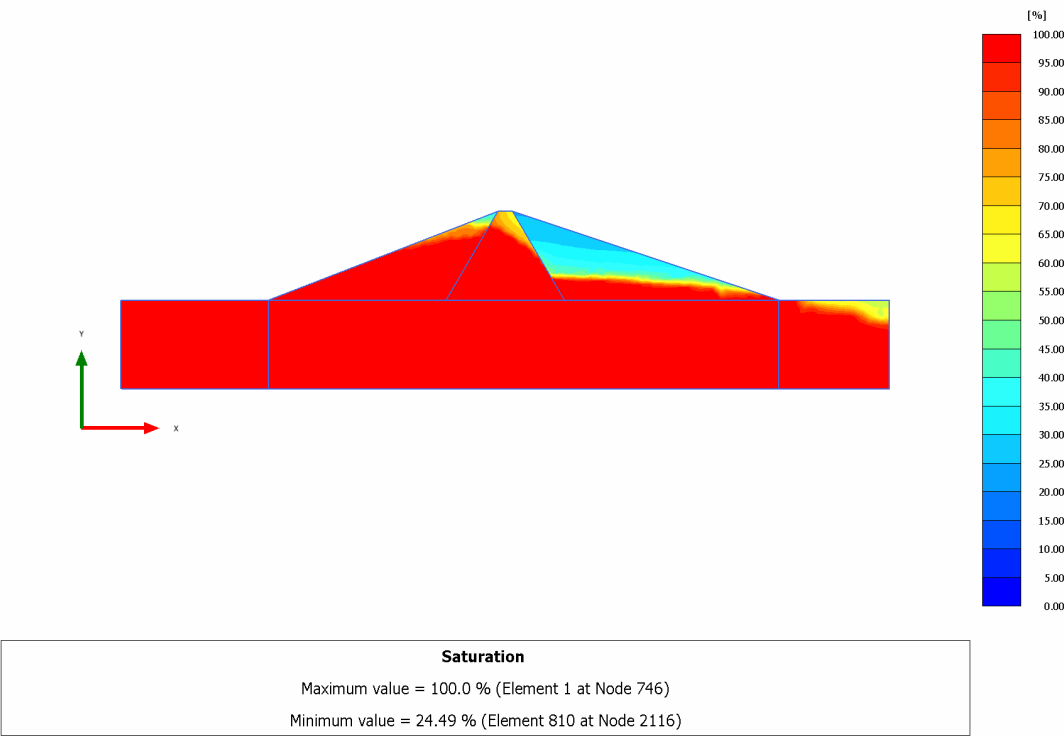


Fig. CA6.7.2D: Degree of saturation after rapid drawdown (PLAXIS 2D)

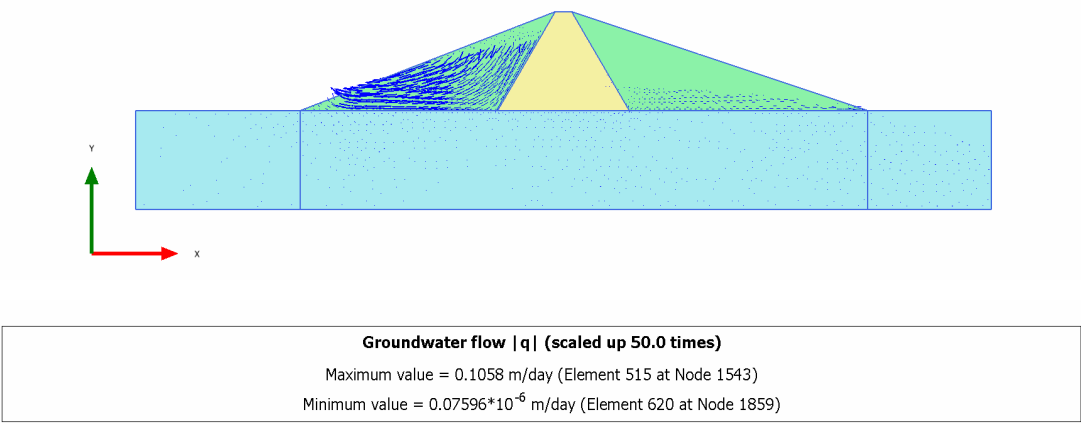


Fig. CA6.8.2D: Flow field after rapid drawdown (PLAXIS 2D)

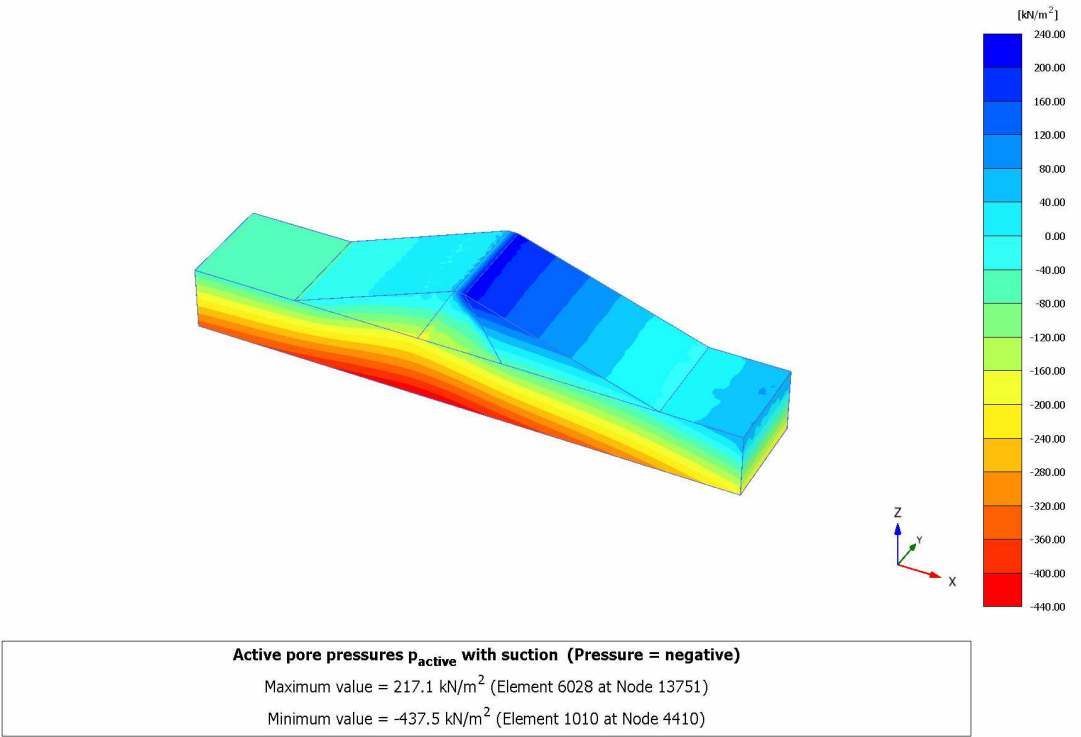


Fig. CA6.6.3D: Active pore pressure after rapid drawdown (PLAXIS 3D)

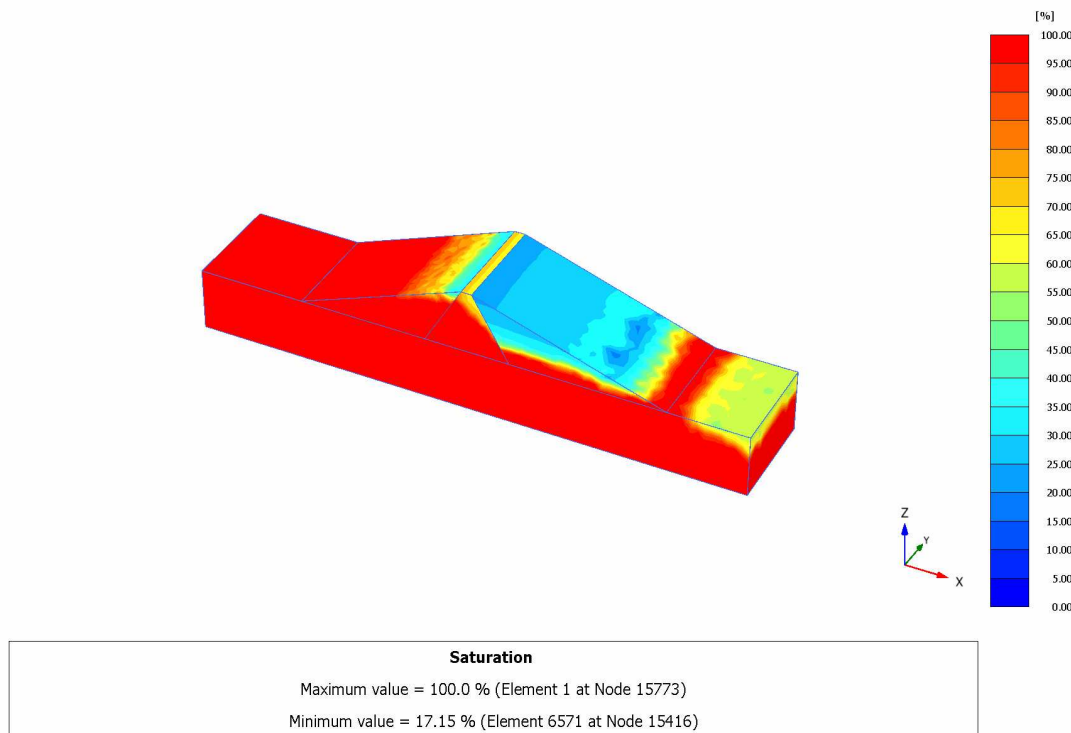


Fig. CA6.7.3D: Degree of saturation after rapid drawdown (PLAXIS 3D)

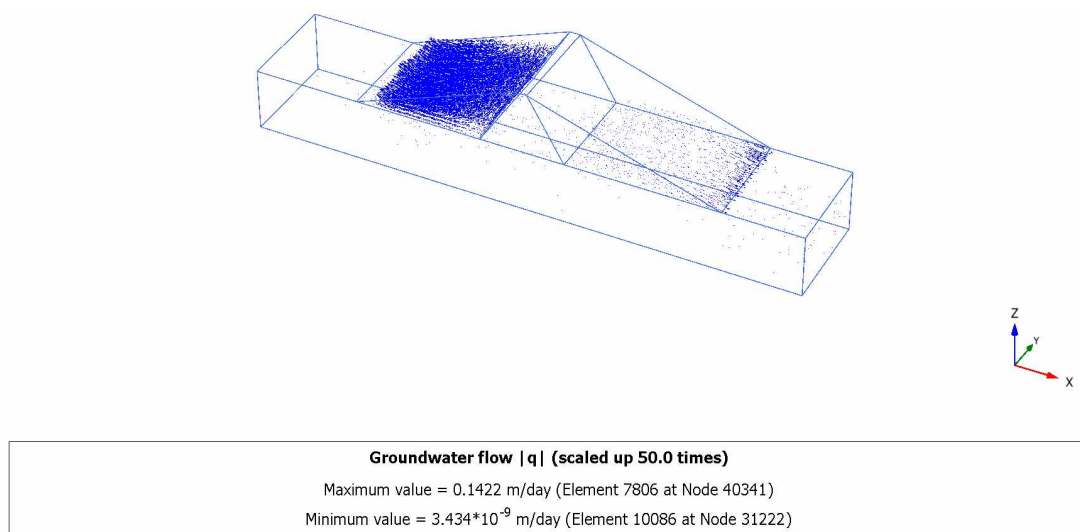


Fig. CA6.8.3D: Flow field after rapid drawdown (PLAXIS 3D)

Phase 3: Slow drawdown:

In this phase slow draw down of the reservoir level is considered.

- Set the *Start from phase* parameter to Phase 1.
- In the *Parameters* tab, select *Reset displacements to zero* and set the *Loading input* to *Stage construction*. Enter a value of 50 days for the *Time interval*.

Figure CA6.5 shows active pore pressures.

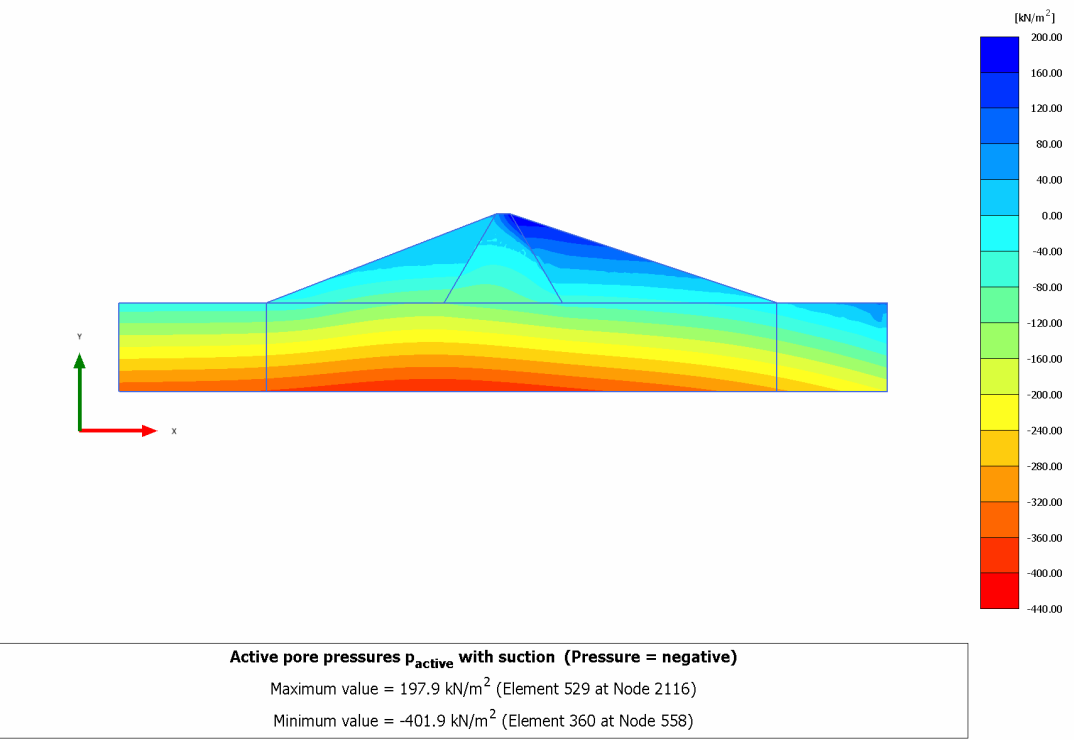


Fig. CA6.9.2D: Active pore pressure after slow drawdown (PLAXIS 2D)

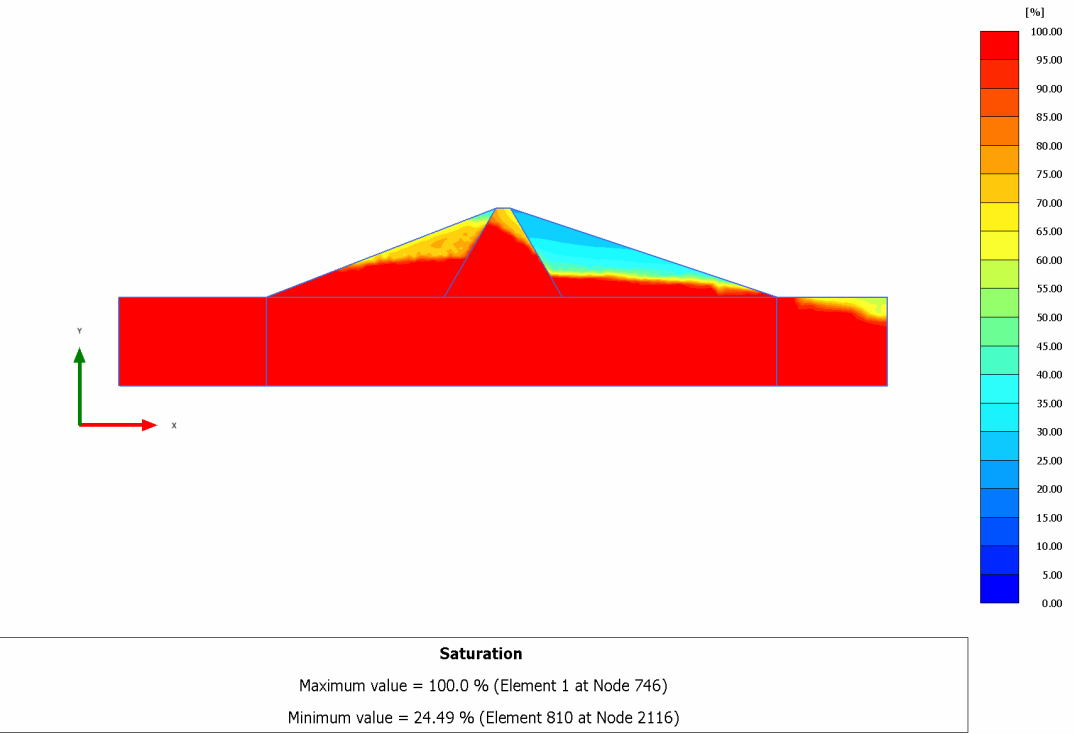


Fig. CA6.10.2D: Degree of saturation after slow drawdown (PLAXIS 2D)

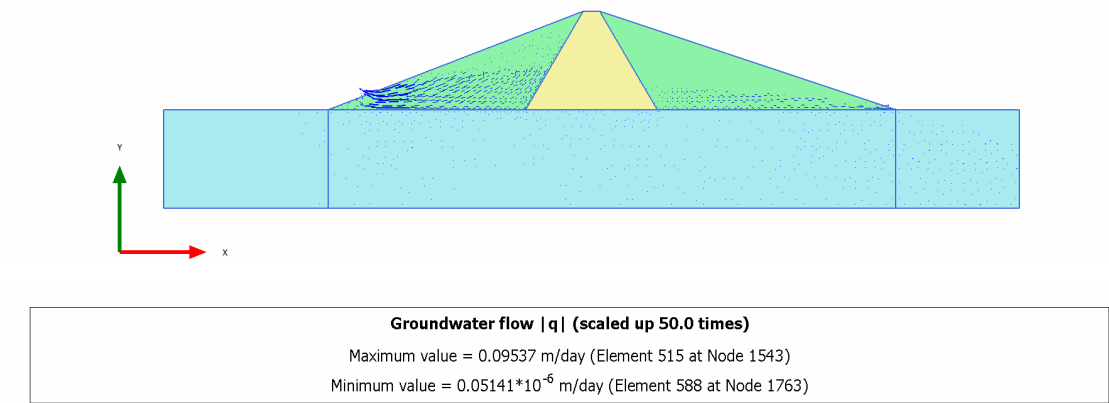


Fig. CA6.11.2D: Flow field after slow drawdown (PLAXIS 2D)

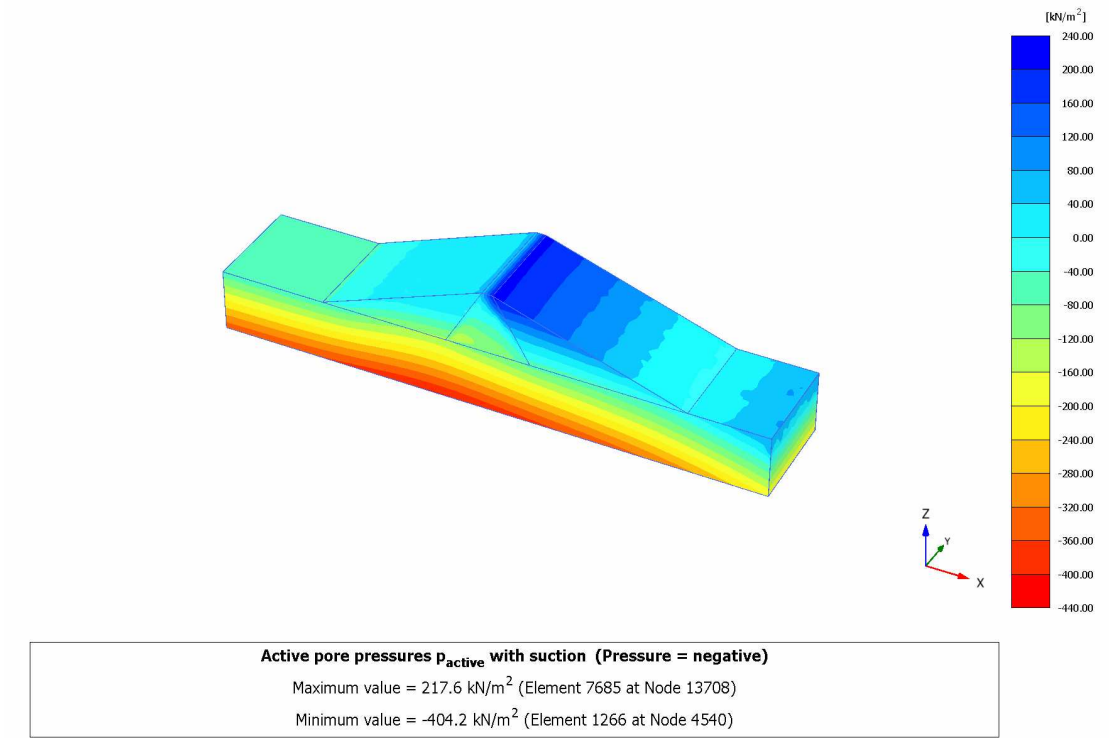


Fig. CA6.9.3D: Active pore pressure after slow drawdown (PLAXIS 3D)

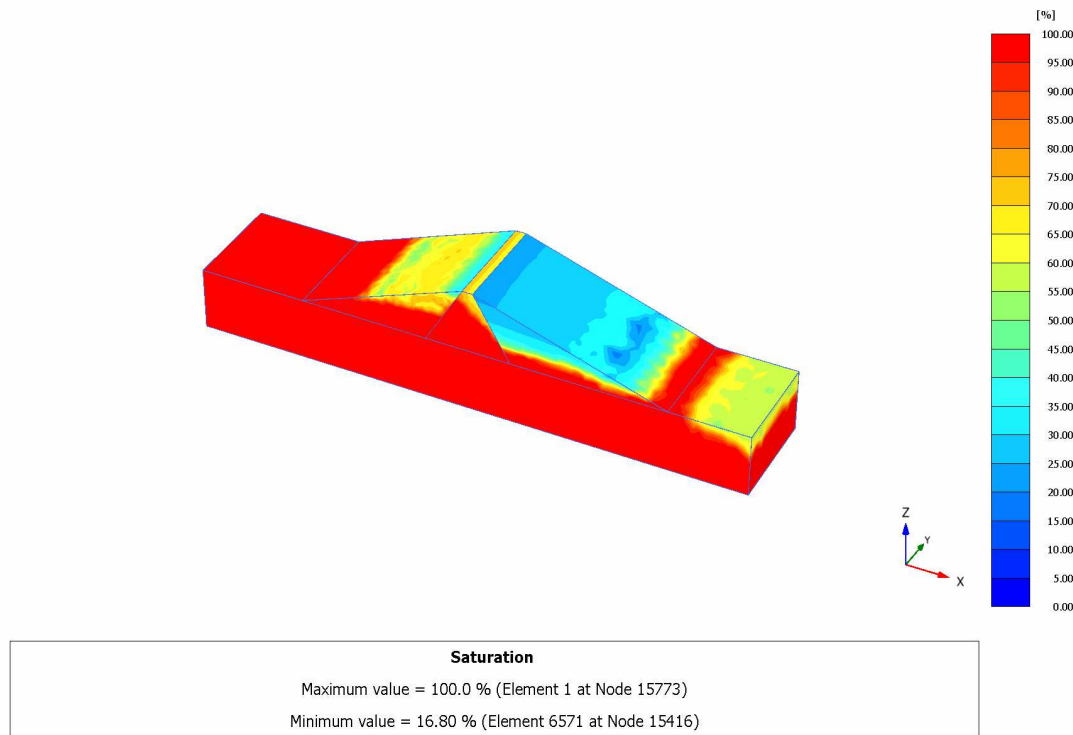


Fig. CA6.10.3D: Degree of saturation after slow drawdown (PLAXIS 3D)

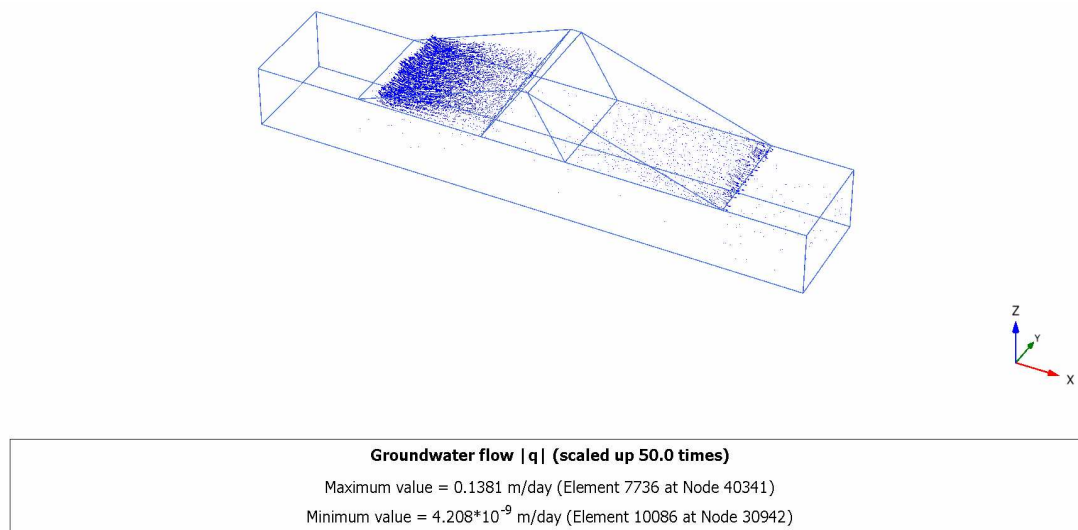


Fig. CA6.11.3D: Flow field after slow drawdown (PLAXIS 3D)

Phase 4: Steady state calculation:

This phase considers the steady-state situation of a low reservoir level.

- Set the *Start from phase* parameter to Phase 1.
- In the staged construction mode, switch to the water conditions mode. Generate proper boundary conditions for a steady-state groundwater flow calculation in the following way:
- Make sure that the bottom of the model is still closed.

- Generate groundwater head conditions at the other model boundaries by creating a new general water level. The very left side at a level of 5 m above the ground surface and the right boundary at a level of 10 m below the ground surface.

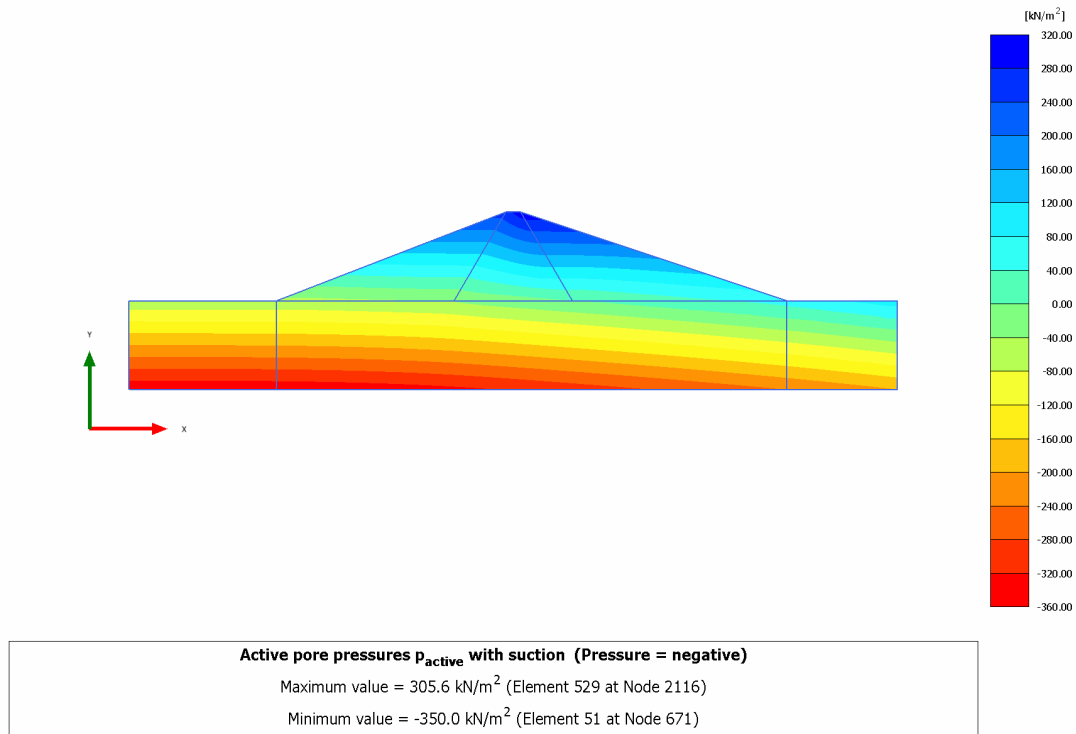


Fig. CA6.12.2D: Steady-state pore pressure for low reservoir level (PLAXIS 2D)

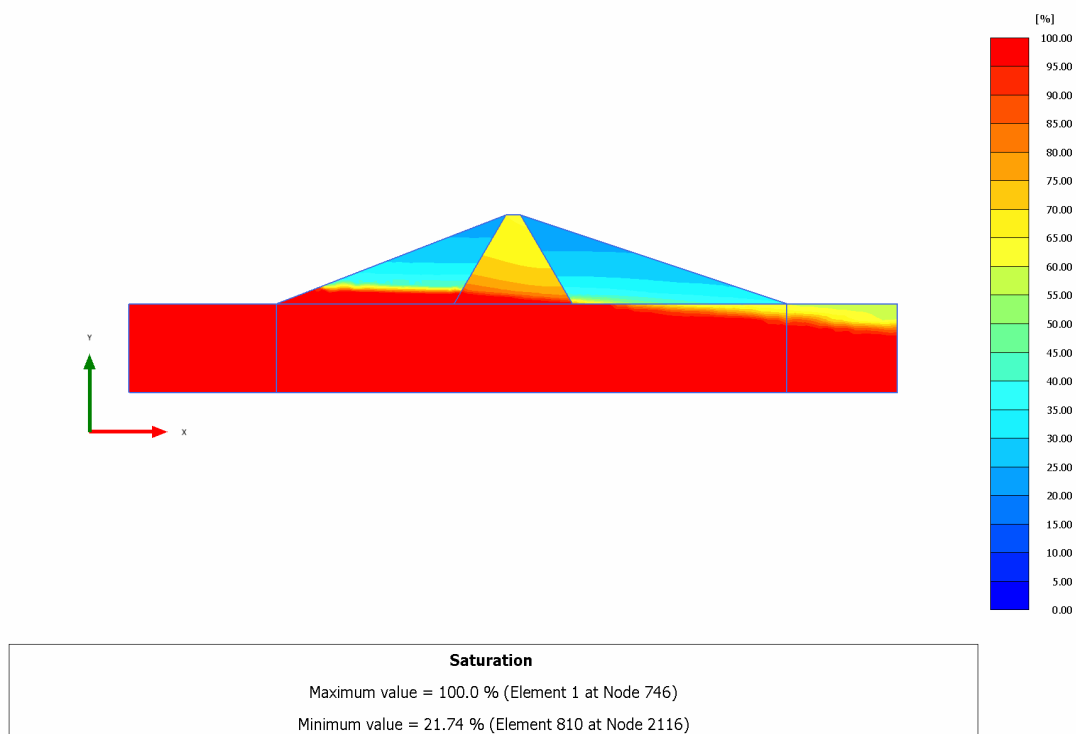


Fig. CA6.13.2D: Degree of saturation for low reservoir level (PLAXIS 2D)

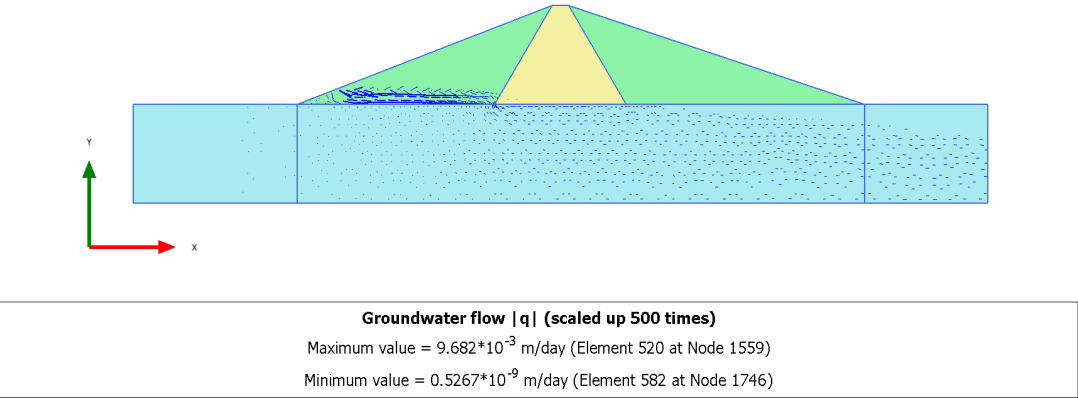


Fig. CA6.14.2D: Flow field for low reservoir level (PLAXIS 2D)

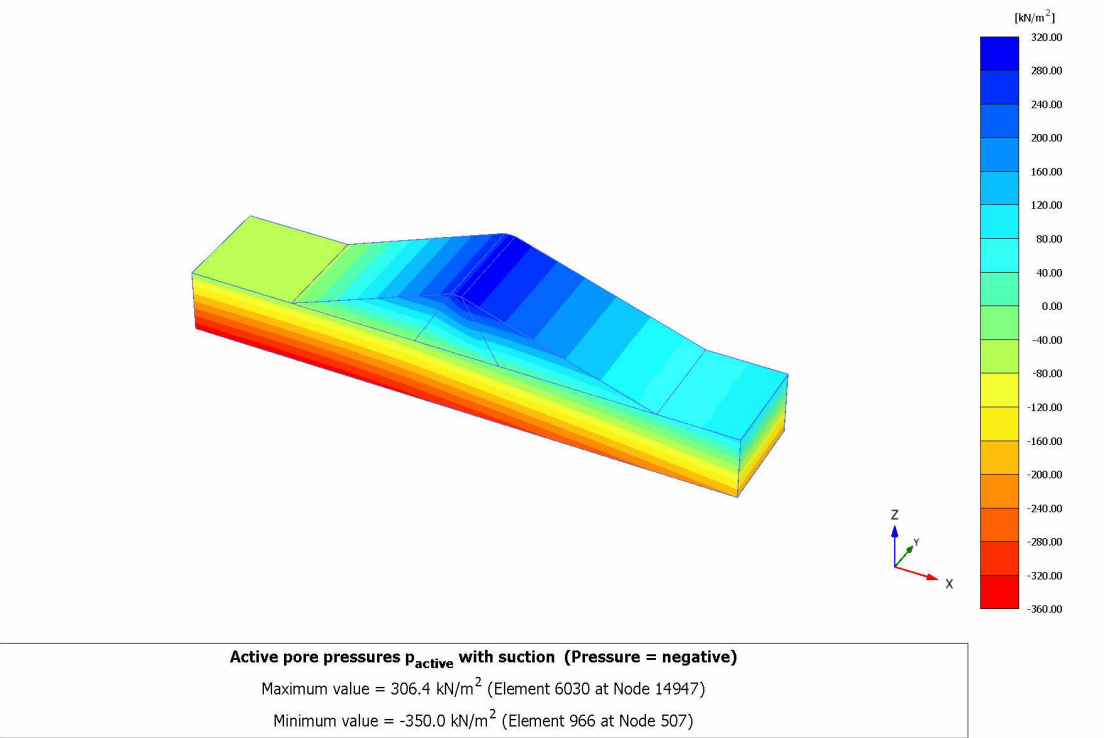


Fig. CA6.12.3D: Steady-state pore pressure for low reservoir level (PLAXIS 3D)

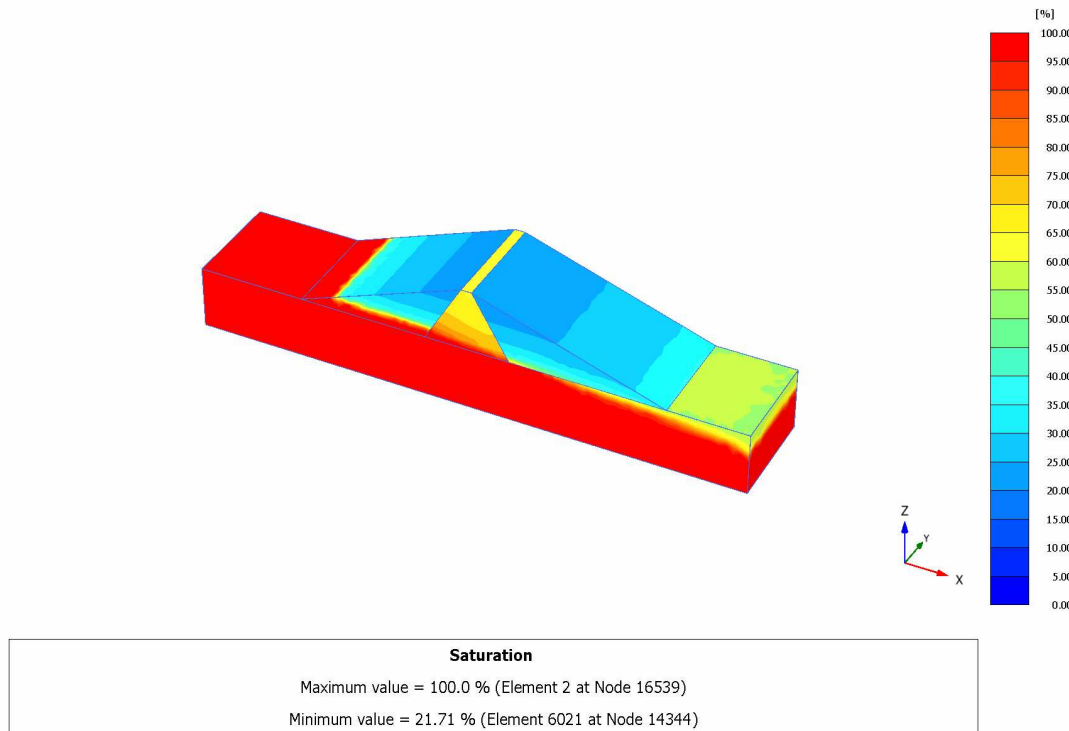


Fig. CA6.13.3D: Degree of saturation for low reservoir level (PLAXIS 3D)

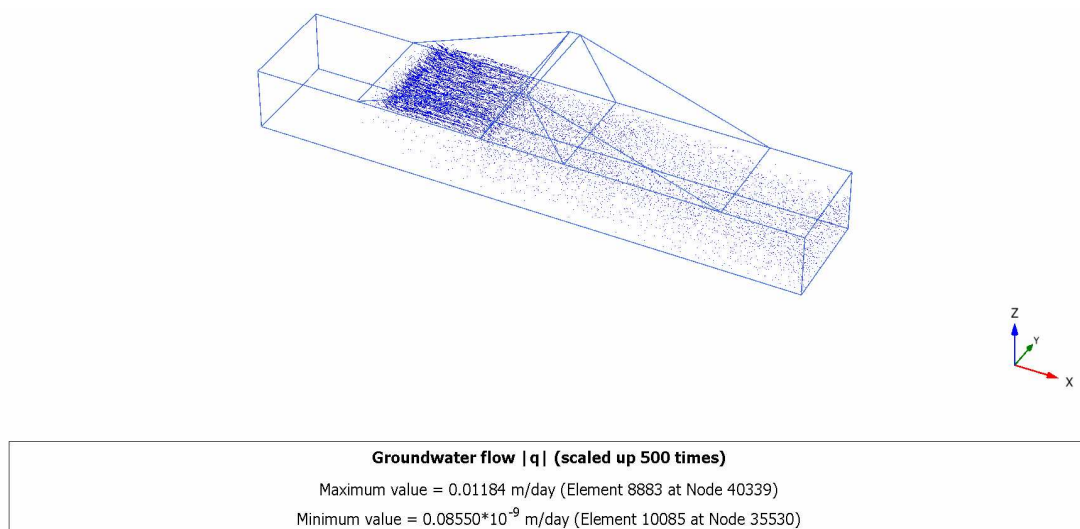


Fig. CA6.14.3D: Flow field for low reservoir level (PLAXIS 3D)

Phase 5 to 8: Stability calculations:

In Phases 5 to 8 stability calculations are defined for the phases 1 to 4 respectively. Therefore, select the corresponding phase in the *Start from phase* parameter and set the Calculation type to *Phi-c reduction*. In the Parameter tab set the number of additional steps to 50 and select *Reset displacement to zero*.

Output:

The results of the four groundwater flow calculations in terms of pore pressure distribution have been shown in previous figures. Four different situations were considered:

1. The steady-state situation with a high (standard) reservoir level.
2. The coupled analysis after rapid drawdown of the reservoir level.
3. The coupled analysis after slow drawdown of the reservoir level.
4. The steady-state situation with a low reservoir level.

When the change of pore pressure is taken into account in a deformation analysis, some additional deformation of the dam will occur. These deformations and the effective stress distribution can be viewed on the basis of the results of phases 1 to 4. Here, attention is focused on the variation of the safety factor of the dam for the different situations. Therefore, the development of ΣM_{sf} is plotted for the phases 5 to 8 as a function of the displacement of the dam crest point (see Fig. CA6.15.2D and CA6.15.3D).

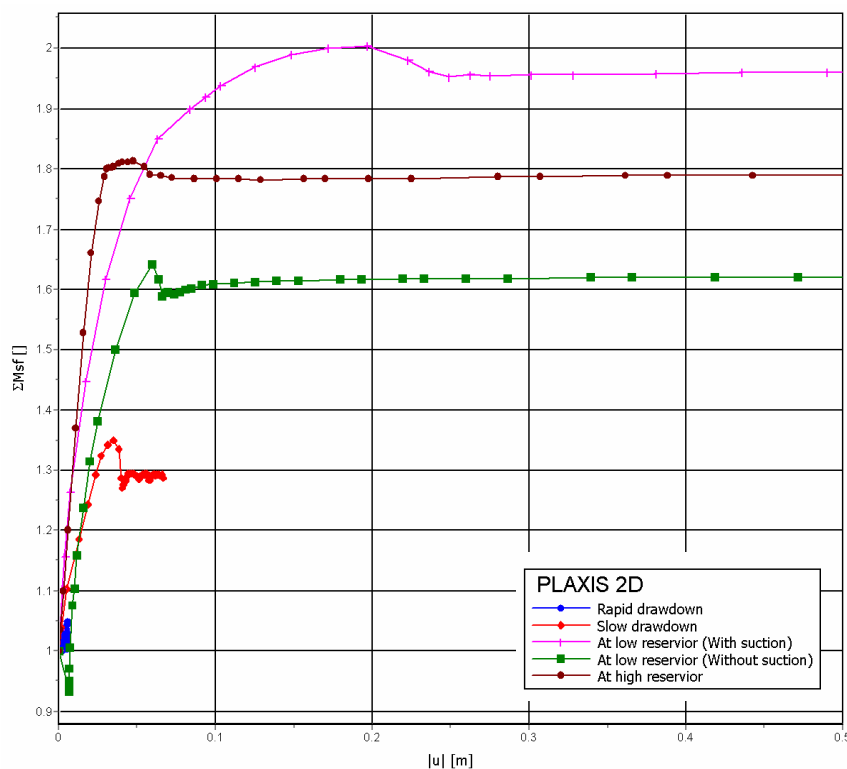


Fig. CA6.15.2D: Safety factors for different situations (PLAXIS 2D)

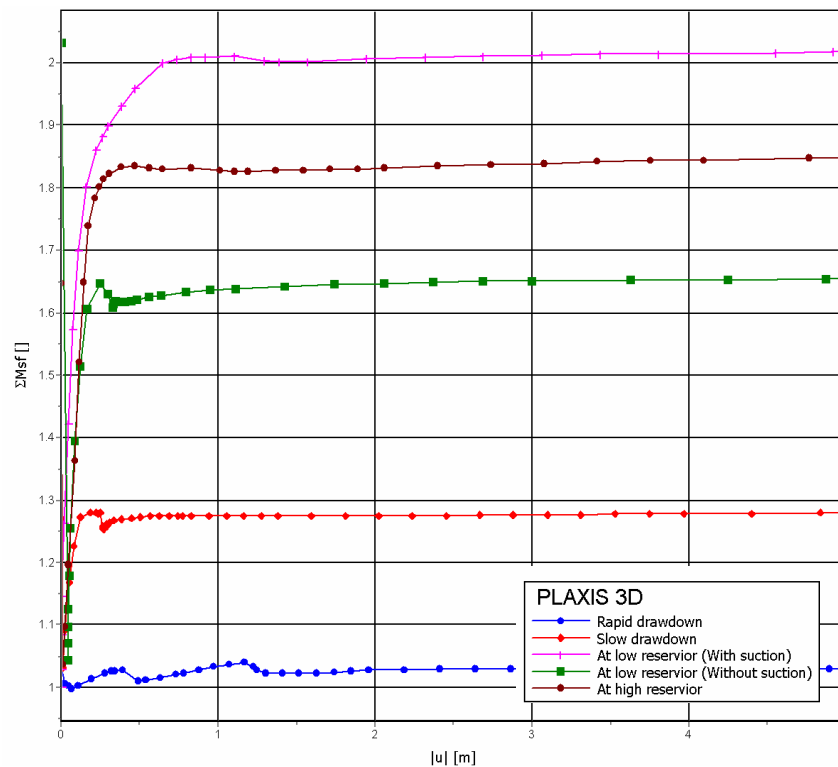


Fig. CA6.15.3D: Safety factors for different situations (PLAXIS 3D)

Summary:

Rapid drawdown of a reservoir level can reduce the stability of a dam significantly. It follows from Figure CA6.6 that using suction and Bishop stress may increase factor of safety significantly. It has been shown that if Terzaghi stress without suction is used, factor of safety in case of reservoir at low level is around 1.6 while this factor is 2.0 if Bishop stress is utilised. It should be noted that the difference between these two factors of safety is mainly dependent on the soil water characteristic curve used for the soil layers. As seen in Figures CA6.12 and CA6.13 (both 2D and 3D) the minimum degree of saturation in the core is around 60% and the maximum suction is around 300 kPa which means that in case of Bishop stress, the effective stress in this layer is about 180 kPa ($300\text{kPa} \times 0.60$) more than the corresponding Terzaghi stress. This additional stress makes the embankment more stable. It follows from the formulation of Bishop stress (degree of saturation is used in the formulation) that the factor of safety might be significantly dependent on the SWCC utilised for the unsaturated soil layers.

In the following groundwater flow results of PlaxFlow are given:

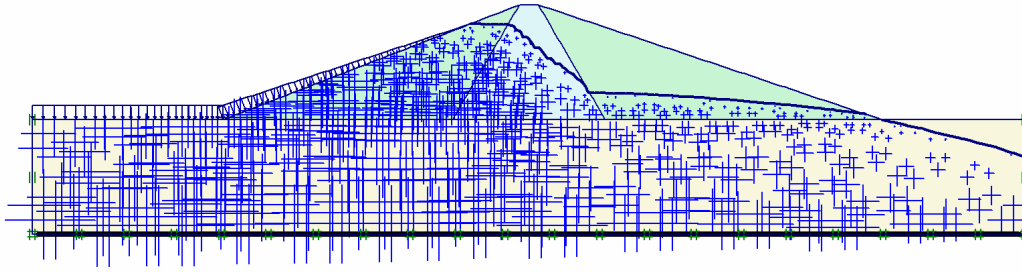


Fig. CA6.16.PF: Steady-state pore pressure distribution for high reservoir level (PlaxFlow)

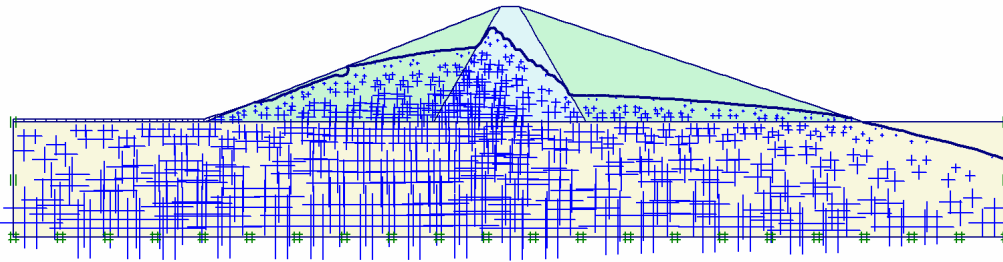


Fig. CA6.17.PF: Pore pressure distribution after rapid draw down (PlaxFlow)

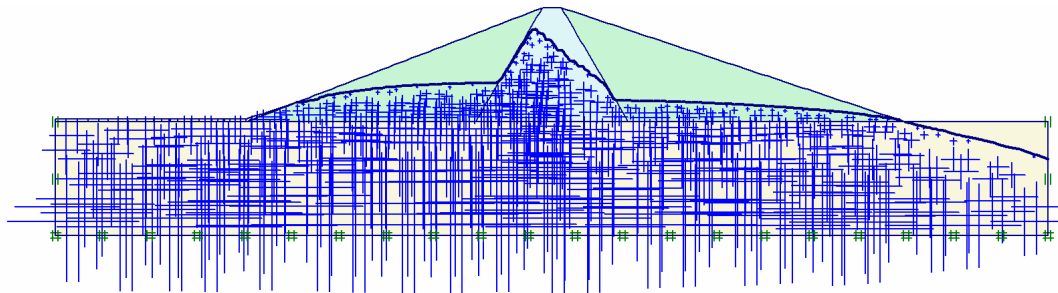


Fig. CA6.18.PF: Pore pressure distribution after slower draw down (PlaxFlow)

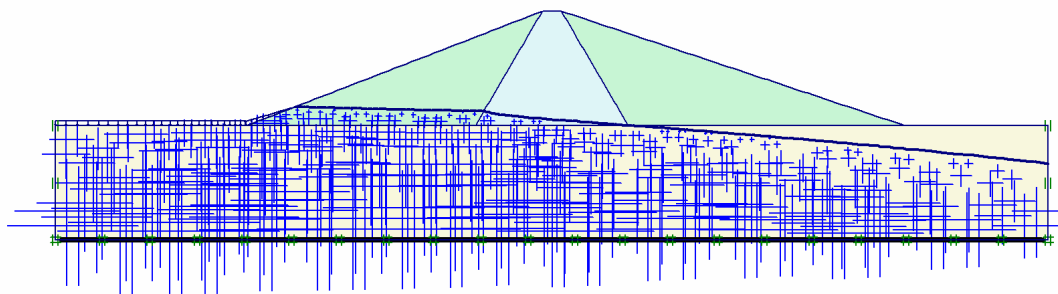


Fig. CA6.19.PF: Steady-state pore pressure distribution for low reservoir level (PlaxFlow)

9.7 Conclusions

Results of 5 coupled flow – deformation analyses and one gravity loading with Bishop stress, solved by the new PLAXIS 2D and 3D kernels, are shown in this chapter. Some of them have been verified against analytical solution.

The following features have been tested:

1. *Boundary conditions.* All boundary conditions have been tested in the chapters of groundwater flow. However, seepage boundary condition, inflow, precipitation are tested here.
2. *Bishop stress:* Bishop effective stress has been tested in this chapter and it has been shown that PLAXIS is capable of calculating Bishop effective stress.
3. *One dimensional consolidation.* Results of one-dimensional consolidation are very close to the analytical ones
4. *Safety factor with suction.* It has been shown that if Bishop stress is used, the factor of safety might be higher than the factor of safety if Terzaghi stress without suction is used. **For practical application, this should be changed and suction should not be considered in ϕ/c reduction!** For transient from Bishop to Terzaghi, a nil phase may be needed because of the out of balance force.

10 Verification of unsaturated soil model

In this chapter two examples are presented to show the capability of the proposed formulations, which consists of the fully coupled flow-deformation analysis and the unsaturated soil model. At first some uncoupled numerical element tests using the Barcelona Basic Model are performed and then the capability of the coupled analysis and its algorithm is shown by numerical simulation of a footing problem.

10.1 Case USM1: Drained compression triaxial tests at different suctions

An example presented by Sheng et al. (2003) is used to show the capability of the constitutive soil model to simulate mechanical behaviour of unsaturated soils. As the unsaturated model used in the calculation is not the same as the model used by Sheng et al. (2003), the material data are calibrated. The material data are given in Table USM1.

To perform the test, the initially saturated soil is isotropically compressed to -24 kPa and unloaded to -20 kPa to produce an overconsolidated soil with OCR of 1.2, (point A in Figure USM1.1). Then suction is slowly increased such that the total axial and radial stresses are kept at 20 kPa, (point B in Figure USM1.1). Three different values are applied for suction, namely 0, 100 and 200 kPa. After applying the suction, the axial stress is increased under undrained conditions (point C in Figure USM1.1). At this stage, the total confining stress and the suction are kept constant.

Results:

Figures USM1.2 to USM1.5 show the predicted curves for different amount of suction calculated with Plaxis 2D. The corresponding results provided by Gonzalez & Gens (2008) and Sheng et al. (2003) show in Figures USM1.6 To USM1.11.

Tab. USM1.1: Material properties used for triaxial tests (After Sheng et al., 2003)

Parameter	Unit	Value
ν	[-]	0.3
κ	[-]	0.05
λ_0	[-]	0.25
κ_s	[-]	0
k_s	[-]	0
M	[-]	0.772
e_0	[-]	1.21
P_r	[kPa]	1.0
P'_0	[kPa]	24
r	[kPa]	0.75
β	[kPa ⁻¹]	0.012
g_a	[m ⁻¹]	1.0
g_n	[-]	0.5
g_c	[-]	-1.0

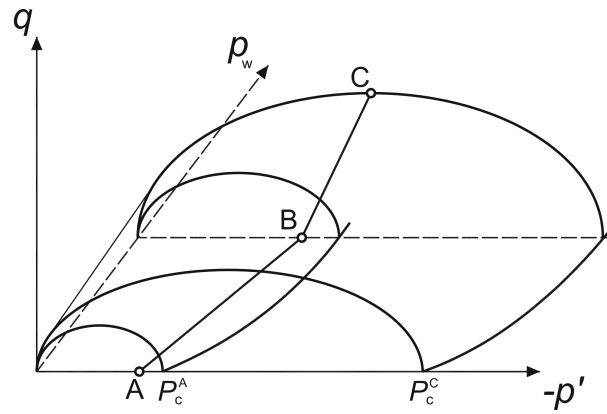


Fig. USM1.1: Stress path in triaxial compression test (After Sheng et al, 2003)

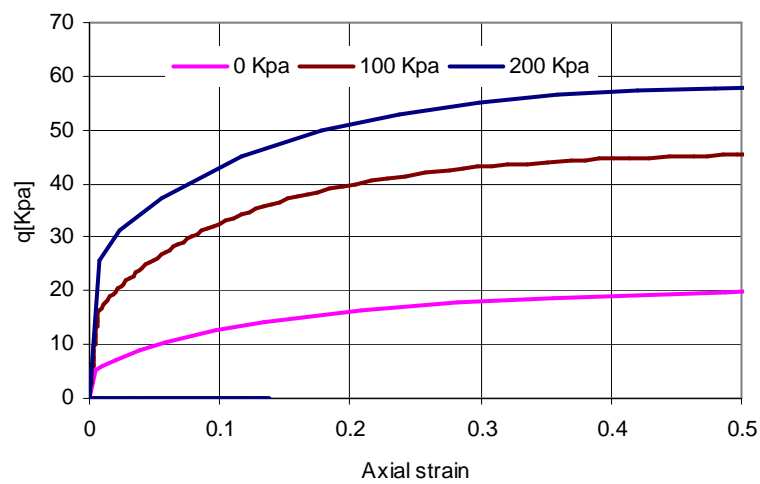


Fig. USM1.2: Shear stress versus axial strain for different suction (Plaxis)

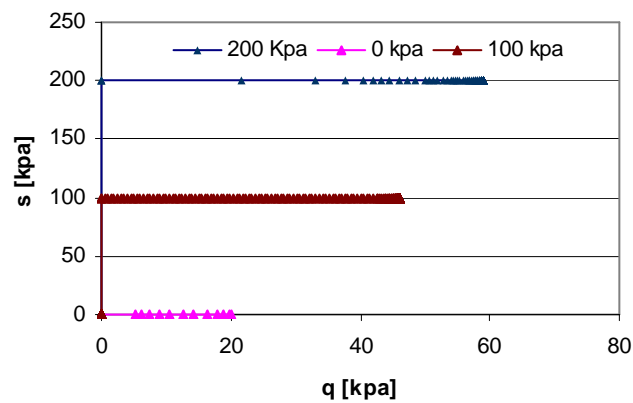


Fig. USM1.3: Suction versus deviatoric stress q (Plaxis)

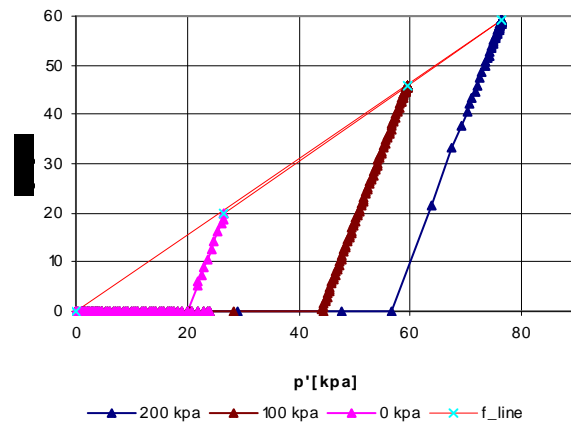


Fig. USM1.4: Stress path in p' - q space (Plaxis)

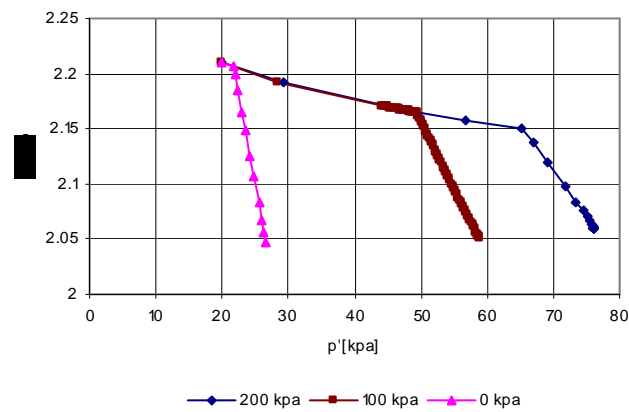


Fig. USM1.5: Specific volume versus mean effective stress p' (Plaxis)

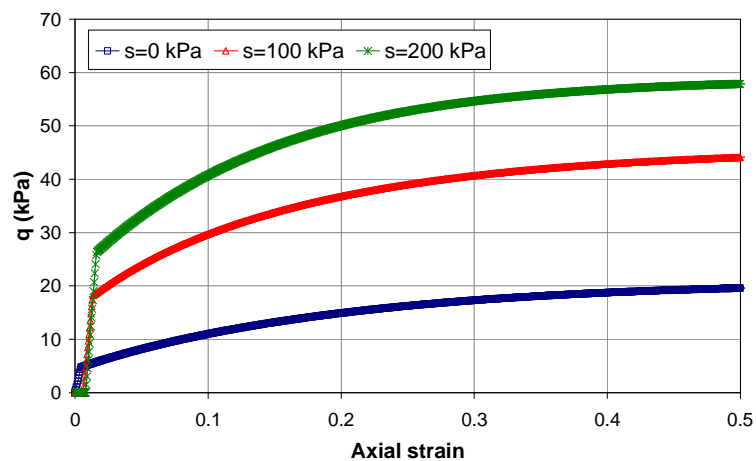


Fig. USM1.6: Shear stress versus axial strain for different suction (Gonzalez & Gens, 2008)

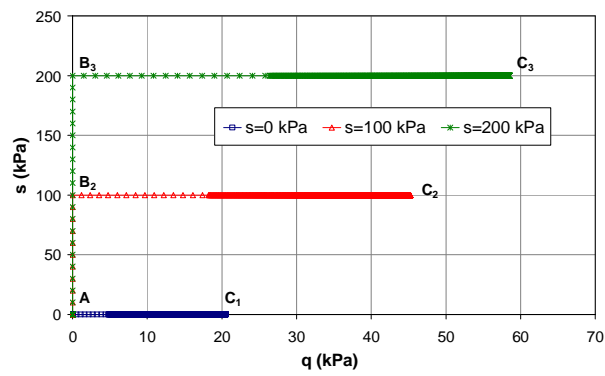


Fig. USM1.7: Suction versus deviatoric stress q (Gonzalez & Gens, 2008)

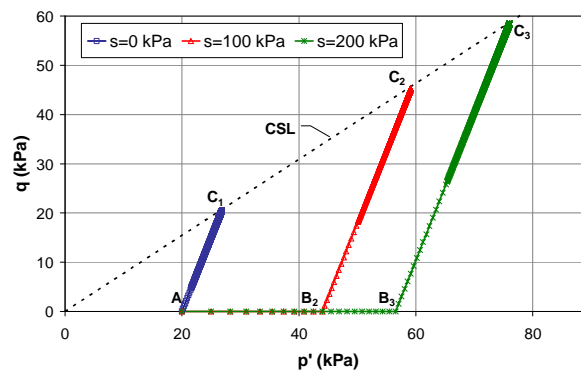


Fig. USM1.8: Stress path in p' - q space (Gonzalez & Gens, 2008)

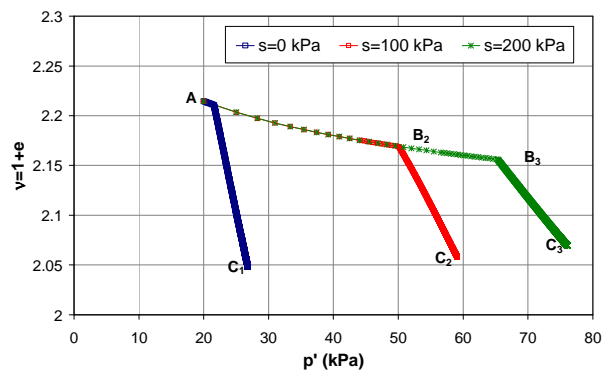


Fig. USM1.9: Specific volume versus mean effective stress p' (Gonzalez & Gens, 2008)

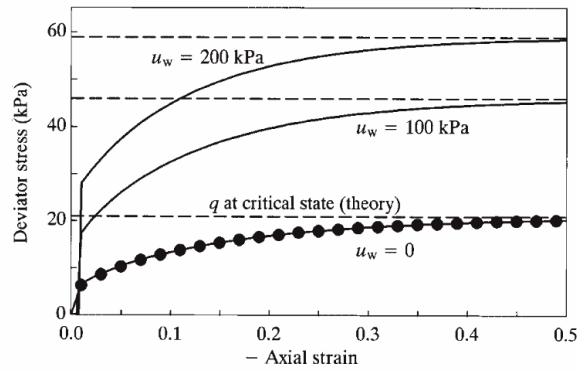


Fig. USM1.10: Shear stress versus axial strain for different suction (Sheng et al., 2003)

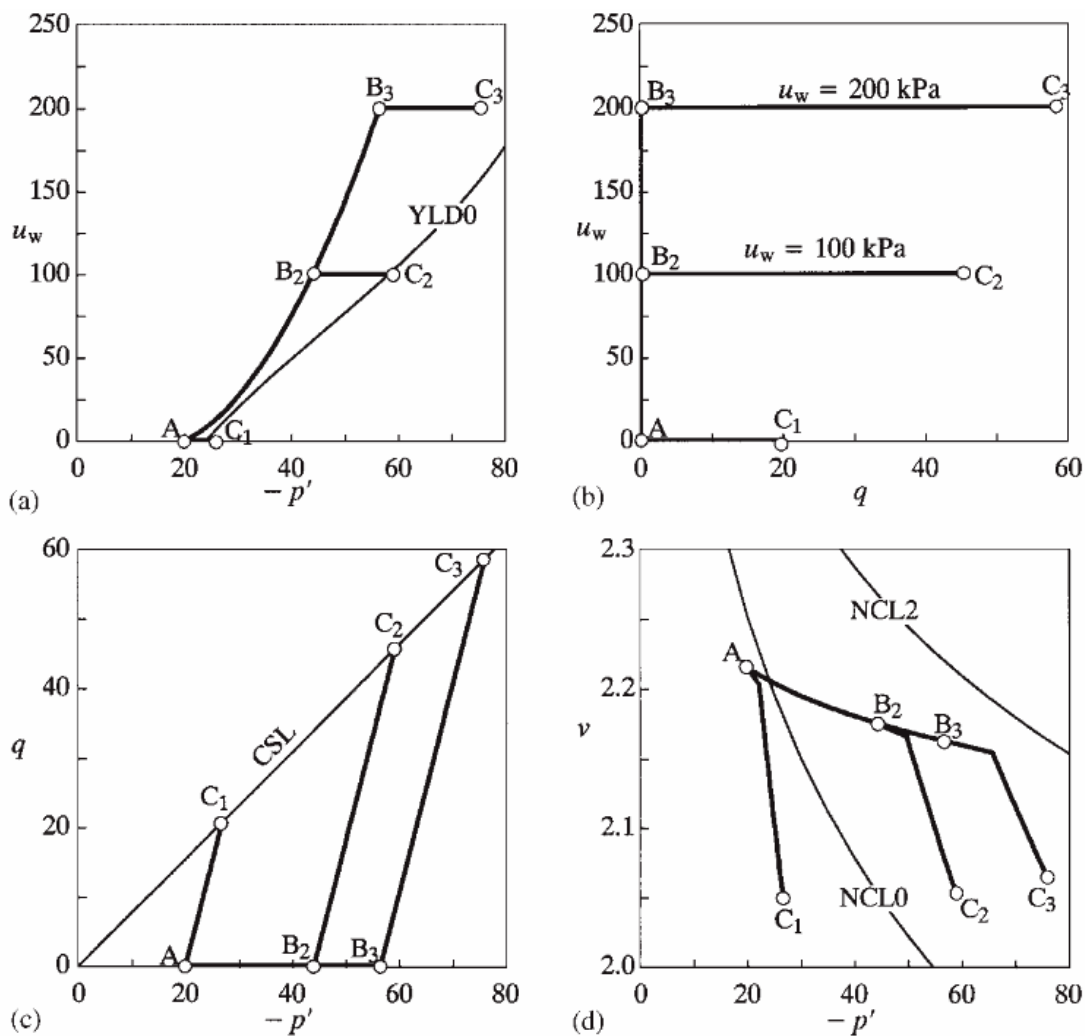


Fig. USM1.11: a) Suction versus mean effective stress p' ; b) suction versus deviatoric stress q ; c) stress path in p' - q space; d) specific volume versus mean effective stress p' (Sheng et al., 2003)

It follows from the figures that by increasing the suction, the deviatoric stress increases. The corresponding stress paths in the space p' - q are shown in Figure

USM1.2b. It follows from the figure that the stress paths reach the critical state line at the axial strain 50%.

Summary:

As seen, results from Plaxis are in agreement with the results provided by Gonzalez & Gens (2008) and Sheng et al. (2003).

10.2 Case USM2: Footing problem

In this section numerical simulation of a flexible footing on a partially saturated soil which collapses on wetting is presented. The fully coupled flow-deformation analysis is applied. Figure 3 shows the FE mesh and the boundary conditions used for the analysis. The mesh consists of 575 15-noded triangular elements with a fourth order interpolation for displacements and for pore pressures and 12 Gauss points (stress points) for each element. The width and height of the model are 10 m and a distributed load with width of 1 m is applied on top of the model. The initial position of phreatic line is at 5 m high. This level will be changed during drying and wetting processes.

In this example, soil is dried so that the suction reaches 100 kPa at the surface nodes and then the footing is vertically loaded to 100 kPa. After this loading phase, the soil is imposed to wetting. The top, left and right boundaries are closed for flow, and drying and wetting are only applied through the bottom boundary by linearly changing the water head in time (in drying phase, the head reduces from 5 m to 0 and in wetting phase the head increases to 5 m). All phases are performed slowly in order to maintain drained conditions (in 1000 days).

The material data of the soil is given in Table 2. For initialisation 100 kPa is assumed for preoverburden pressure (POP).

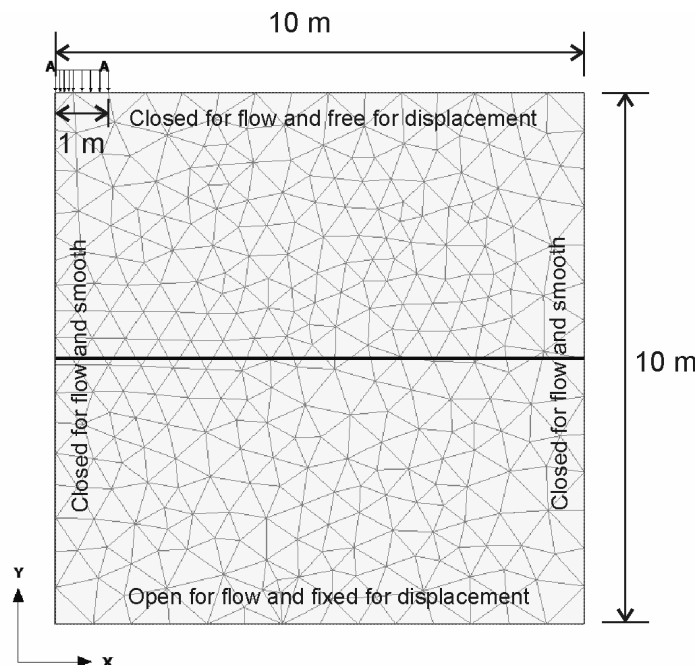


Fig. USM2.1: Geometry and FE mesh used for footing problem

The results of the fully coupled flow-deformation analysis are shown in Figure 4. The predicted settlements of the ground surface are plotted in Figure 4a. Figure 4b shows the amount of suction at the centre of the footing. During drying phase the ground surface settles roughly 9 cm. Applying the flexible footing (the distributed load) causes the centre of the footing settles 13.6 cm. Wetting of the soil leads to significantly increase the displacements of the nodes below the footing while the ground surface at $x=10$ m settles and rises a little. The maximum displacement occurs at the centre of the footing, 17 cm. Figure 5 shows the deformed mesh after the loading and wetting phases.

Tab. USM2.: Material properties used for triaxial tests (After Sheng et al., 2003)

Parameter	Unit	Value
γ_{sat}	[kN/m ³]	18.0
γ_{dry}	[kN/m ³]	16.0
k_x & k_y	[m/day]	0.086
ν	[-]	0.3
κ	[-]	0.02
λ_0	[-]	0.20
κ_s	[-]	0
k_s	[-]	0
M	[-]	0.984
e_0	[-]	1.17
P_r	[kPa]	1.0
P'_0	[kPa]	1.0
r	[kPa]	0.70
β	[kPa ⁻¹]	0.012
g_a	[m ⁻¹]	1.0
g_n	[-]	0.5
g_c	[-]	-1.0
g_l	[-]	0.0

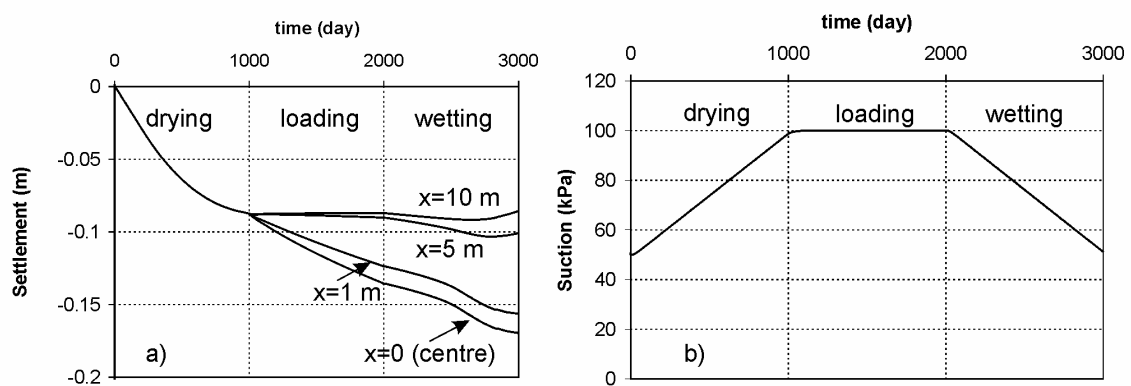


Fig. USM2.2: Footing problem: a) Settlement of the ground surface in time; b) Variation of suction at the centre of the footing

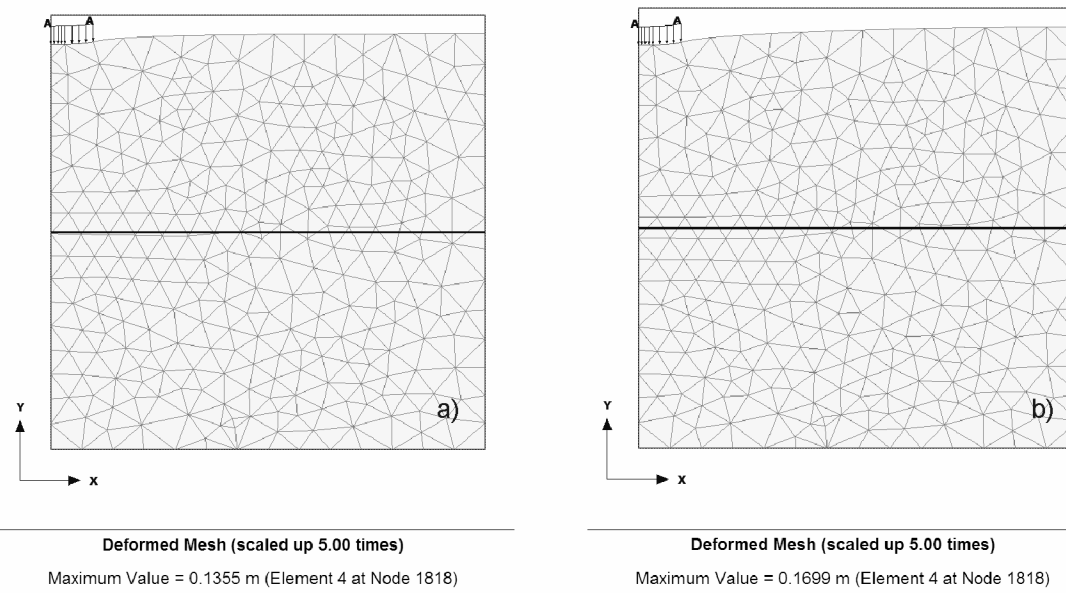


Fig. USM2.3: Deformed mesh; a) after loading phase; b) after wetting phase

10.3 Conclusions

Results of one plastic calculation and one coupled flow – deformation analysis using unsaturated soil model (Barcelona Basic Model), solved by the new Plaxis 2D kernel are shown in this chapter. The former one has been verified against numerical results provided by Gonzalez & Gens (2008) and Sheng et al. (2003).

The following features have been tested:

1. *Effect of suction.* The effect of suction has been investigated by numerical modelling of drained triaxial tests. As shown, results are very similar to the results of Gonzalez & Gens (2008) and Sheng et al. (2003).
2. *Drying and wetting:* Drying and wetting have been tested in the footing problem. It can be seen that the model is capable of simulating collapse upon wetting.
3. *Different calculation types.* The model has been tested with both plastic and fully coupled flow-deformation analyses.

11 Undrained analysis in PLAXIS

Numerical modelling of undrained response of soils as used in PLAXIS is described here. New features have been added to PLAXIS that may affect “undrained analysis” of soil, such as the new feature considered for unsaturated soil modelling. The main difference between the new and the previous versions of PLAXIS is using Bishop stress in the *advanced mode* (to describe partially saturated behaviour of soils) and changing water conditions (as groundwater flow calculation has been integrated in the calculation kernel the resulting pore pressures might be input pore pressures for the next phase).

Before describing the numerical modelling of undrained behaviour, the calculation modes in the new version of PLAXIS should be defined.

11.1 Calculation modes

Three modes have been implemented in PLAXIS which enables the user to perform particular types of calculations. The calculations modes are as follows:

1. *Classical mode*: This mode uses Terzaghi’s stress and is very similar to the old PLAXIS. The idea is to offer a mode in which old projects can be modelled. Pore pressures are divided into steady state and excess pore pressures. Steady state pore pressures are input data, i.e. generated based on phreatic levels or groundwater flow. Excess pore pressures are generated during plastic or consolidation calculations. The weight of soil is calculated according to the position of the phreatic level. Saturated weight of soil γ_{wet} is utilised for below the phreatic level and unsaturated weight of soil γ_{unsat} for above the phreatic level.

The types of calculations which can be done in this mode are:

- Plastic undrained
 - Plastic drained
 - Consolidation based on Excess Pore Pressure (EPP)
 - Dynamics
 - Free vibration
 - Phi/C reduction
2. *Advanced mode*: This mode uses Bishop’s stress and is suitable for calculating unsaturated response of soils and for performing fully coupled hydro-mechanical behaviour of soils. Bishop’s stress is defined by:

$$\sigma = \sigma' + m(\chi p_w) \quad (1)$$

χ is an effective stress parameter called matric suction coefficient and varies from 0 to 1 covering the range from dry to fully saturated

conditions. The matric suction coefficient χ is generally determined experimentally. This parameter depends on the degree of saturation, porosity and on the matric suction ($p_a - p_w$). In the current version of PLAXIS, this parameter is assumed to be equal to the effective saturation, i.e.:

$$\sigma = \sigma' + m(S_e p_w) \quad (2)$$

in which S_e is the effective saturation which is a function of the suction pore pressure. This relationship (i.e. relation between degree of saturation and suction) is known as Soil Water Characteristic Curve (SWCC). PLAXIS uses, Van Genuchten, simplified Van Genuchten and user defined relationships. It follows from the above statements that in the partially saturated zone, effective stresses may change by changing SWCC parameters. This causes that the results from the *advanced mode* are different from the *classical mode*, if the user calculates the same example in the above mentioned modes.

To calculate the weight of soil, the following formula is utilised to calculate the weight of soil:

$$\gamma = (1 - S_e)\gamma_{unsat} + S_e\gamma_{wet} \quad (3)$$

The types of calculations which can be done in this mode are as follows:

- Plastic undrained
 - Plastic drained
 - Consolidation based on Total Pore Pressure (TPP)
 - Dynamics
 - Free vibration
 - Phi/C reduction
3. *Flow mode*: This mode is for calculating pure groundwater flow calculations.

The types of calculations in this mode are:

- Steady state groundwater flow
- Transient groundwater flow

11.2 Undrained and drained behaviour

To generate proper excess pore water pressure in the advanced mode of PLAXIS, different bulk moduli of water are used depending on the type of material and on the type of calculation. In the following those cases are discussed.

During the undrained analysis, the changes in pore water pressure, dp_w is calculated based on the equivalent bulk modulus of pore fluid according to:

$$dp_w = K_e \cdot d\varepsilon_{vol} \quad (4)$$

K_e is the equivalent bulk modulus of pore fluid and is derived from:

$$K_e = \frac{K_w}{n} = K_u - K' = \frac{2 \cdot G}{3} \left(\frac{1 + \nu_u}{1 - 2\nu_u} - \frac{1 + \nu'}{1 - 2\nu'} \right) \quad (5)$$

where K_u and K' denote the undrained and drained bulk moduli of the soil respectively. G is the elastic shear modulus, ν' is the drained Poisson's ratio and ν_u is the undrained Poisson's. n is porosity of the soil.

In PLAXIS, it is possible to use effective parameters for undrained calculations. The undrained elastic moduli of soil can be related to the effective parameters according to

$$E_u = 2G(1 + \nu_u) \quad (6.1)$$

$$K_u = \frac{E_u}{3(1 - 2\nu_u)} \quad (6.2)$$

$$E_{oed,u} = \frac{(1 - \nu_u)E_u}{(1 - 2\nu_u)(1 + \nu_u)} \quad (6.3)$$

in which

$$\nu_u = \frac{\nu' + \mu(1 + \nu')}{1 + 2\mu(1 + \nu')} \quad (7)$$

with

$$\mu = \frac{1}{3 \cdot n} \cdot \frac{K_w}{K'} \quad (8)$$

$$K' = \frac{E'}{3(1 - 2\nu')} \quad (9)$$

Eq. (7) shows the relationship between the undrained Poisson's ratio, the effective Poisson's ratio, the bulk modulus of water, the bulk modulus of soil skeleton and porosity of the soil. It follows from Eq. (7) that if water is assumed to be incompressible ($K_w \rightarrow \infty$), then ($\nu_u \rightarrow 0.5$) which leads to singularity of stiffness matrix. Therefore it is assumed ν_u to be 0.495 for fully saturated. In reality, the bulk modulus of water is very large, but not infinite. The bulk modulus of pure water (without bubbles of air) is $K_w^0 = 2 \times 10^6$ kPa).

The generation of excess pore water pressure can be studied by means of the Skempton B -parameter which is defined as the ratio of excess pore water pressure increment to the mean total stress increment:

$$B = \frac{dp_w}{dp} \quad (10)$$

By substituting (4) into (10), we have

$$B = \frac{K_w d\epsilon_{vol}}{n \cdot dp} \quad (11)$$

and the mean total stress is

$$dp = K_u d\epsilon_{vol} \quad (12)$$

where K_u is the undrained bulk modulus of soil which can be obtained from

$$K_u = \frac{2G(1+\nu_u)}{3(1-2\nu_u)} \quad (13)$$

By substituting (13) and (5) in (11) the Skempton B -parameter as a function of the undrained Poisson's ratio (or the undrained Poisson's ratio as a function of the Skempton B -parameter) can be obtained:

$$B = \frac{K_w}{nK_u} = 1 - \frac{(1+\nu') (1-2\nu_u)}{(1+\nu_u) (1-2\nu')} \quad (14)$$

or

$$\nu_u = \frac{3\nu' + B(1-2\nu')}{3 - B(1-2\nu')} \quad (15)$$

As seen, B varies between 1 (for fully saturated conditions) and 0 (for fully dry condition) when $\nu_u=0.5$ and $\nu_u=\nu'$, respectively. Experimental data show that the parameter B decreases by decreasing the degree of saturation (Figure 1).

In the advanced mode of PLAXIS, the value of Skempton's B -parameter is unknown but the degree of saturation is known. Therefore the bulk modulus of water is estimated from:

$$K_w^{unsat} = \frac{K_w^{sat} K_{air}}{SK_{air} + (1-S)K_w^{sat}} \quad (16)$$

in which K_{air} is the bulk modulus of air which is about 100 kPa under atmospheric pressure. In PLAXIS, it is assumed that p_a (air pore pressure) is equal to 0 for practical application and therefore an artificial and small value (1 kPa) is used for the bulk modulus of air. K_w^{sat} and K_w^{unsat} are bulk moduli of water in saturated and unsaturated conditions, respectively. K_w^{sat} is calculated

based on v_u which is equal to 0.495 when the standard setting is being used. PLAXIS always checks the value of K_w^{sat} to ensure that K_w^{sat} is less than the bulk modulus of pure water ($K_w^0 = 2 \times 10^6$).

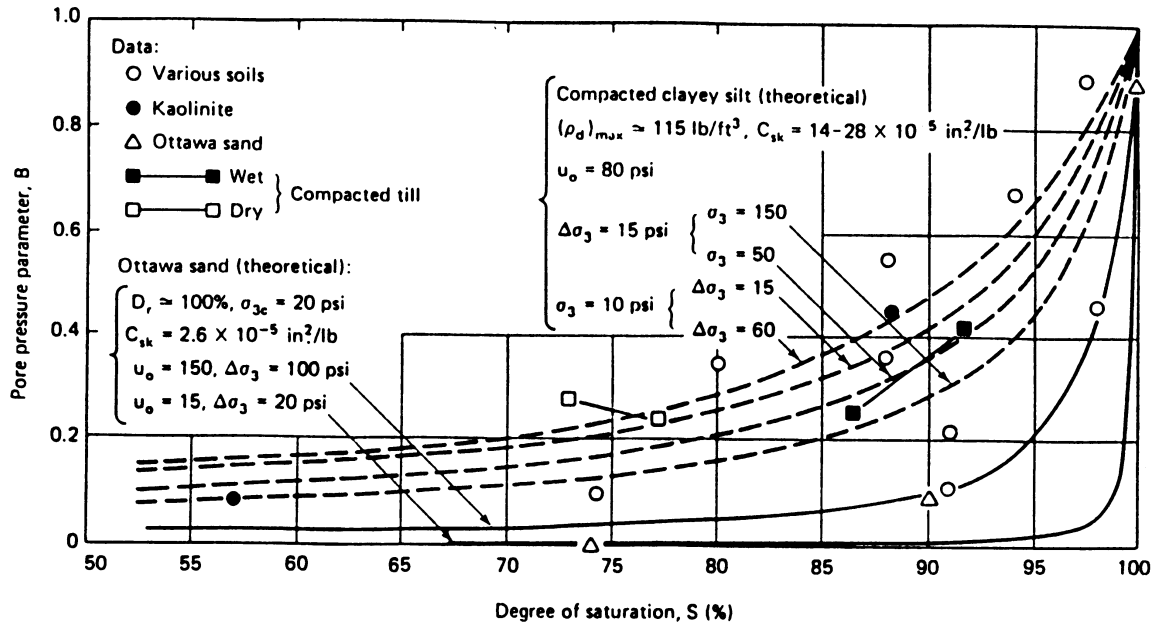


Fig. 1: Skempton's B -parameter versus degree of saturation

In the following the above mentioned relationships are reviewed in different modes.

11.3 Classical mode

In the classical mode of PLAXIS, it is assumed that the degree of saturation is 1 when soil is undrained and is 0 when soil is drained in all types of calculation excepting in the consolidation type of calculation, therefore K_e is either K_w/n or 0. Thus when the material is undrained, K_e is K_w/n for plastic undrained and K_e is 0 for plastic drained. In consolidation type of calculation, all materials are assumed to be fully saturated and the bulk modulus of water is calculated according to Eq. (5) for drained and undrained types of materials. In this case, the mechanical behaviour of soil is mainly governed by the permeability of layers. Therefore, if the user needs to reduce the bulk modulus of water in a layer, which is the case for considering partially saturated soils (degree of saturation less than 1), the user needs to lower Skempton's B -parameter (Eq 15) in the respective layer. This is one of the main differences between the new kernel and the previous one (version 9.0). Because in the old kernel, the bulk modulus of water for drained materials is assumed to be 10% of the bulk modulus of water of the undrained material.

For the newly activated cluster, due to the fact that the soil is not fully saturated, the bulk modulus of water is neglected to avoid generation of excess water pore pressure.

Tables 1 shows the summary of the bulk moduli of water used in the classical mode of PLAXIS. As seen, in this mode, the same K_w is utilised for below and above the phreatic level. This means that, in this mode, it is possible to generate high excess pore water pressure in the area where lower amount of water exists.

11.4 Advanced mode

In the advanced mode, K_w is reduced in partially saturated zones according to Eq. (16). This reduction is done for undrained materials in the undrained calculations. However, it is possible to reduce the bulk modulus of water by reducing Skempton B -parameter in the material database according to Eq. (15). Therefore K_w^{sat} is not always based on $v_u=0.495$.

Since the degree of saturation depends on the amount of active pore pressures, all undrained calculations are suction dependent and therefore the global stiffness matrix has to be updated in the beginning of each load step.

Eq. (17) shows the finite element formulation of the consolidation used in the advanced mode.

$$\begin{bmatrix} \underline{\underline{K}} & \underline{\underline{Q}} \\ \underline{\underline{C}} & -\underline{\underline{S}}^* \end{bmatrix}^{i+\alpha} \begin{bmatrix} \Delta \underline{\underline{v}} \\ \Delta \underline{\underline{p}}_w \end{bmatrix} = \begin{bmatrix} 0 & 0 \\ 0 & \Delta t \underline{\underline{H}} \end{bmatrix}^{i+\alpha} \begin{bmatrix} \underline{\underline{v}}^i \\ \underline{\underline{p}}_w^i \end{bmatrix} + \begin{bmatrix} \Delta t \underline{\underline{G}} + \Delta t (\underline{\underline{q}}_p^i + \alpha \Delta \underline{\underline{q}}_p) \end{bmatrix} \quad (17)$$

with

$$\underline{\underline{S}}^* = (\underline{\underline{S}} + \alpha \Delta t \underline{\underline{H}}) \quad (17.1)$$

$$\underline{\underline{H}} = \int_V (\nabla \underline{\underline{N}})^T \frac{k_{rel}}{\gamma_w} k^{sat} (\nabla \underline{\underline{N}}) dV \quad (17.2)$$

$$\underline{\underline{S}} = \int_V \underline{\underline{N}}^T \left(\frac{nS}{K_w} - n \frac{dS}{dp_w} \right) \underline{\underline{N}} dV \quad (17.3)$$

$$\underline{\underline{G}} = - \int_V (\nabla \underline{\underline{N}})^T \frac{k_{rel}}{\gamma_w} k^{sat} \rho_w \underline{\underline{g}} dV \quad (17.4)$$

$$\underline{\underline{q}}_p = \int_{\Gamma} \underline{\underline{N}}^T \hat{q}_w dS \quad (17.5)$$

$$\underline{\underline{K}} = \int_V \underline{\underline{B}}^T \underline{\underline{M}} \underline{\underline{B}} dV \quad (17.6)$$

$$\underline{\underline{Q}} = \int_V \underline{\underline{S}} \underline{\underline{B}}^T \underline{\underline{m}} \underline{\underline{N}} dV \quad (17.7)$$

$$\underline{\underline{C}} = \int_V \underline{\underline{N}} \underline{\underline{S}} \underline{\underline{L}} \underline{\underline{N}} dV \quad (17.8)$$

$$\Delta \underline{f}_u = \int_v \underline{N}^T \Delta \underline{b} dV + \int_r \underline{N}^T \Delta \underline{t} dS \quad (17.9)$$

The bulk modulus of water appears in Eq (17.3). Here, the bulk modulus of water is not reduced because the saturation is involved in the matrix \underline{S} . Therefore, for partially saturated zones, the storage is reduced according to the degree of saturation.

Similar to the classical mode, the bulk modulus of water is decreased in all types of calculations for materials which are just switched on to decrease the generation of excess water pore pressure.

Tables 2 shows the summary of the bulk moduli of water used in the advanced mode of PLAXIS.

11.5 Flow mode

In the flow mode, K_w is only reduced in the transient type of calculation for the materials just switched on to prevent flow in the material which is almost dry. Similar to the other modes the bulk modulus of water can be modified by changing Skempton B -parameter in the material database according to Eq. (15). Therefore K_w^{sat} is not always based on $v_u=0.495$.

Tables 3 shows the summary of the bulk moduli of water used in the flow mode of PLAXIS.

Tab. 1: Bulk modulus of water in the classical mode

Type of material	Classical mode				
	Plastic (drained)	Plastic (undrained)	Consolidation	Safety or dynamics (drained)	Safety or dynamics (undrained)
Undrained (below and above phreatic level)	$K_w = 0$	$K_w = \frac{2 \cdot G}{3} \left(\frac{1 + \nu_u}{1 - 2\nu_u} - \frac{1 + \nu'}{1 - 2\nu'} \right)$	$K_w = \frac{2 \cdot G}{3} \left(\frac{1 + \nu_u}{1 - 2\nu_u} - \frac{1 + \nu'}{1 - 2\nu'} \right)$	$K_w = 0$	$K_w = \frac{2 \cdot G}{3} \left(\frac{1 + \nu_u}{1 - 2\nu_u} - \frac{1 + \nu'}{1 - 2\nu'} \right)$
Drained (below and above phreatic level)	$K_w = 0$	$K_w = 0$	$K_w = \frac{2 \cdot G}{3} \left(\frac{1 + \nu_u}{1 - 2\nu_u} - \frac{1 + \nu'}{1 - 2\nu'} \right)$	$K_w = 0$	$K_w = 0$
Material just switched on (below and above phreatic level)	$K_w = 0$	$K_w = 0$	$K_w = \frac{2 \cdot G}{3} \left(\frac{1 + \nu_u}{1 - 2\nu_u} - \frac{1 + \nu'}{1 - 2\nu'} \right) \cdot 1 \times 10^{-8}$	Not relevant.	Not relevant.
Non-porous or dry cluster	$K_w = 0$	$K_w = 0$	$K_w = 0$	$K_w = 0$	$K_w = 0$

Tab. 2: Bulk modulus of water in the advanced mode

Type of material	Advanced mode				
	Plastic (drained)	Plastic (undrained)	Consolidation	Safety or dynamics (drained)	Safety or dynamics (undrained)
Undrained ($p_w \leq 0$)	$K_w = 0$	$K_w^{sat} = \frac{2 \cdot G}{3} \left(\frac{1 + \nu_u}{1 - 2\nu_u} - \frac{1 + \nu'}{1 - 2\nu'} \right)$	$K_w^{sat} = \frac{2 \cdot G}{3} \left(\frac{1 + \nu_u}{1 - 2\nu_u} - \frac{1 + \nu'}{1 - 2\nu'} \right)$	$K_w = 0$	$K_w^{sat} = \frac{2 \cdot G}{3} \left(\frac{1 + \nu_u}{1 - 2\nu_u} - \frac{1 + \nu'}{1 - 2\nu'} \right)$
Undrained ($p_w > 0$)	$K_w = 0$	$K_w^{unsat} = \frac{K_w^{sat} K_{air}}{SK_{air} + (1 - S)K_w^{sat}}$	$K_w^{sat} = \frac{2 \cdot G}{3} \left(\frac{1 + \nu_u}{1 - 2\nu_u} - \frac{1 + \nu'}{1 - 2\nu'} \right)$	$K_w = 0$	$K_w^{unsat} = \frac{K_w^{sat} K_{air}}{SK_{air} + (1 - S)K_w^{sat}}$
Drained ($p_w \leq 0$)	$K_w = 0$	$K_w = 0$	$K_w^{sat} = \frac{2 \cdot G}{3} \left(\frac{1 + \nu_u}{1 - 2\nu_u} - \frac{1 + \nu'}{1 - 2\nu'} \right)$	$K_w = 0$	$K_w = 0$
Drained ($p_w > 0$)	$K_w = 0$	$K_w = 0$	$K_w^{sat} = \frac{2 \cdot G}{3} \left(\frac{1 + \nu_u}{1 - 2\nu_u} - \frac{1 + \nu'}{1 - 2\nu'} \right)$	$K_w = 0$	$K_w = 0$

Material just switched on (below and above phreatic level)	$K_w = 0$	$K_w = 0$	$K_w = (K_w^{sat}) \cdot 1 \times 10^{-8}$	Not relevant.	Not relevant.
Non-porous or dry cluster	$K_w = 0$	$K_w = 0$	$K_w = 0$	$K_w = 0$	$K_w = 0$

Tab. 3: Bulk modulus of water in flow mode

Type of material	Flow mode	
	Steady state	Transient
Undrained ($p_w \leq 0$)	$K_w = \frac{2 \cdot G}{3} \left(\frac{1 + \nu_u}{1 - 2\nu_u} - \frac{1 + \nu'}{1 - 2\nu'} \right)$	$K_w^{sat} = \frac{2 \cdot G}{3} \left(\frac{1 + \nu_u}{1 - 2\nu_u} - \frac{1 + \nu'}{1 - 2\nu'} \right)$
Undrained ($p_w > 0$)	$K_w = \frac{2 \cdot G}{3} \left(\frac{1 + \nu_u}{1 - 2\nu_u} - \frac{1 + \nu'}{1 - 2\nu'} \right)$	$K_w^{sat} = \frac{2 \cdot G}{3} \left(\frac{1 + \nu_u}{1 - 2\nu_u} - \frac{1 + \nu'}{1 - 2\nu'} \right)$
Drained ($p_w \leq 0$)	$K_w = \frac{2 \cdot G}{3} \left(\frac{1 + \nu_u}{1 - 2\nu_u} - \frac{1 + \nu'}{1 - 2\nu'} \right)$	$K_w^{sat} = \frac{2 \cdot G}{3} \left(\frac{1 + \nu_u}{1 - 2\nu_u} - \frac{1 + \nu'}{1 - 2\nu'} \right)$
Drained ($p_w > 0$)	$K_w = \frac{2 \cdot G}{3} \left(\frac{1 + \nu_u}{1 - 2\nu_u} - \frac{1 + \nu'}{1 - 2\nu'} \right)$	$K_w^{sat} = \frac{2 \cdot G}{3} \left(\frac{1 + \nu_u}{1 - 2\nu_u} - \frac{1 + \nu'}{1 - 2\nu'} \right)$
Material just switched on (below and above phreatic level)	$K_w = \frac{2 \cdot G}{3} \left(\frac{1 + \nu_u}{1 - 2\nu_u} - \frac{1 + \nu'}{1 - 2\nu'} \right)$	$K_w = (K_w^{sat}) \cdot 1 \times 10^{-8}$
Non-porous or dry cluster	$K_w = 0$	$K_w = 0$

11.6 Examples

In this section one example has been chosen to show effects of the new formulation in generating excess water pore pressures in the advanced mode. It is attempted to show how the Soil Water Characteristic Curve affects the undrained behaviour of soil.

Figure 2 shows the geometry of the problem which is 1 m wide and 2 m high. The initial phreatic level is at 1 m high. This example is performed in two phases as follows:

1. *Phase 0*: Gravity loading
2. *Phase 1*: Activating a distributed load of 10 kPa on top of the model and doing plastic analysis

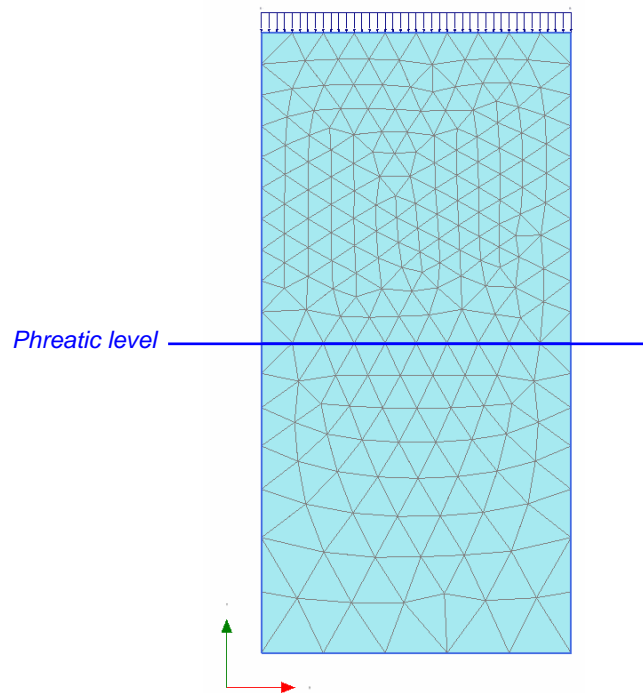


Fig. 2: Geometry and finite element model of the problem

Three cases are studied here, namely fully saturated behaviour, partially saturated behaviour by using *coarse* material and partially saturated behaviour by using *fine* material. The terms *coarse* and *fine* are defined according to the similar names used in the upper soils of *Hypres* series, Table 3.1, PlaxFlow manual.

The mechanical and hydraulic properties of the materials are given in Tables 4 to 6. As the Van Genuchten parameter g_l is not used in these calculations, because this parameter is related to the relative permeability k_r , which is not the case in this example, it is not reported in the tables.

Tab. 4: Input data (fully saturated behaviour)

Description	Symbol	Unit	Value
Elastic modulus	E^{ref}	[kN/m ²]	1000
Poisson's ratio	ν	[-]	0
initial void ratio	e_{init}	[-]	0.50
Water weight	γ_w	[kN/m ³]	10.0
Soil weight (sat)	γ_{sat}	[kN/m ³]	20.0
Soil weight (dry)	γ_{unsat}	[kN/m ³]	20.0

Tab. 5: Input data (partially saturated behaviour-coarse material)

Description	Symbol	Unit	Value
Elastic modulus	E^{ref}	[kN/m ²]	1000
Poisson's ratio	ν	[-]	0
initial void ratio	e_{init}	[-]	0.50
Van Genuchten	g_n	[-]	1.3774
Van Genuchten	g_a	[m ⁻¹]	3.830
Water weight	γ_w	[kN/m ³]	10.0
Soil weight (sat)	γ_{sat}	[kN/m ³]	20.0
Soil weight (dry)	γ_{unsat}	[kN/m ³]	20.0

Tab. 6: Input data (partially saturated behaviour-fine material)

Description	Symbol	Unit	Value
Elastic modulus	E^{ref}	[kN/m ²]	1000
Poisson's ratio	ν	[-]	0
initial void ratio	e_{init}	[-]	0.50
Van Genuchten	g_n	[-]	1.1012
Van Genuchten	g_a	[m ⁻¹]	3.670
Water weight	γ_w	[kN/m ³]	10.0
Soil weight (sat)	γ_{sat}	[kN/m ³]	20.0
Soil weight (dry)	γ_{unsat}	[kN/m ³]	20.0

11.7 Case 1: Fully saturated behaviour

Figure 3 shows the results of the initial phase. As this example is done in the advanced mode, Bishop's stress is used (Eq. 2). It can be seen, the results are in

agreement with Eq. (2). It should be noted that in this example, everywhere is fully saturated ($S=1.0$).

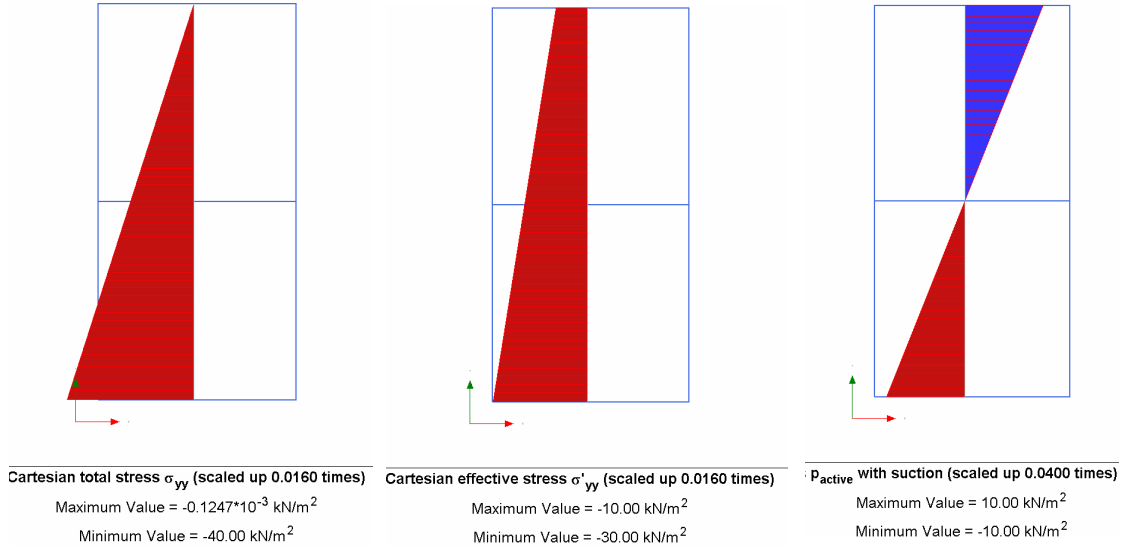


Fig. 3: Results after the initial phase for fully saturated soil: left) vertical total stress; middle) vertical effective stress; right) active pore pressure

The external load is applied in phase 1 which is a distributed load of 10 kPa on top of the model. As the material is defined as undrained, this causes to generate excess pore pressure. Eq. 16 is used for calculating the bulk modulus of water. It follows from this equation when $S=1$ the $K_w^{usat} = K_w^{sat}$. Therefore, there is no distinction between below and above the phreatic level. The bulk modulus of water in this example is $K_e^{sat} = K_w^{sat}/n = 49.5 \text{e3 kPa}$ (Eq. 5).

Figure 4 shows the results of phase 1. By applying 10 kPa on top of the model, the vertical total stress increases by 10 kPa as expected. From the undrained elastic moduli (Eqs. 6), it can be found that the $E_{oed,u} = 50499.99 \text{ kPa}$ and therefore $\Delta \varepsilon_y = \Delta \varepsilon_v = 0.198 \times 10^{-3}$ and $P_{excess} = 9.802 \text{ kPa}$ (Figure 5). The difference between the total stress and the excess pore pressure is added to the effective stress ($10 - 9.802 = 0.2 \text{ kPa}$). As seen, the results are the same as analytical solution.

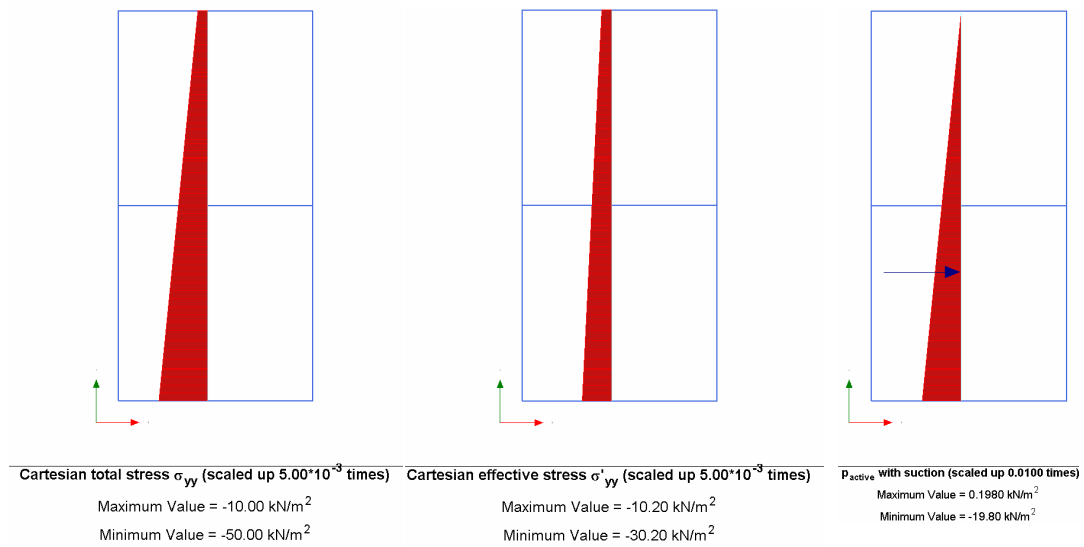


Fig. 4: Results after the phase 1 for fully saturated soil: left) vertical total stress; middle) vertical effective stress; right) active pore pressure

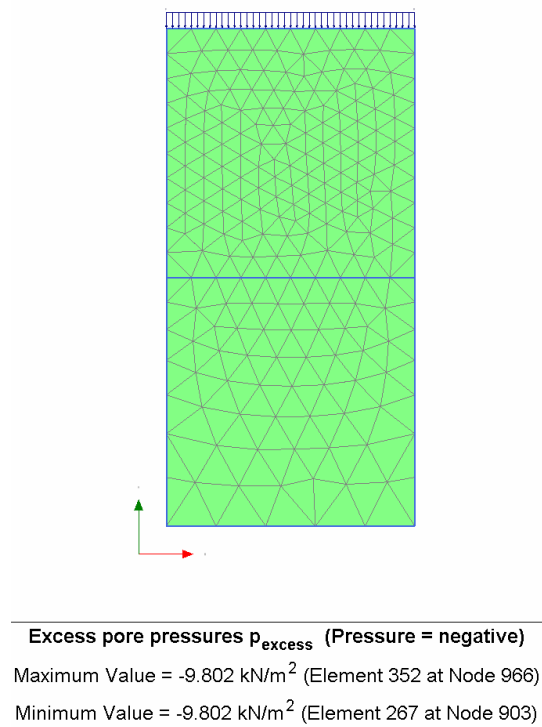


Fig. 5: Excess water pore pressure after the phase 1 for fully saturated soil

11.8 Case 2 and 3: Unsaturated behaviour - coarse and fine materials

In case of unsaturated behaviour, as the behaviour is governed by the SWCC parameters, here two different types of material are analysed, namely coarse and fine materials. The mechanical and hydraulic properties can be found in Tables 5 and 6. Usually, the degree of saturation is degraded faster with increasing suction in coarse material and therefore less excess pore pressure is expected in unsaturated area.

First of all, results of each case are provided and then the results are compared with each other. Figure 6 shows the stresses and active water pore pressures at the end of the initial phase (gravity loading). As Bishop stress is used, to explain how the effective stresses are calculated, degree of saturation is needed (Eq. 2) which is plotted in Figure 7.

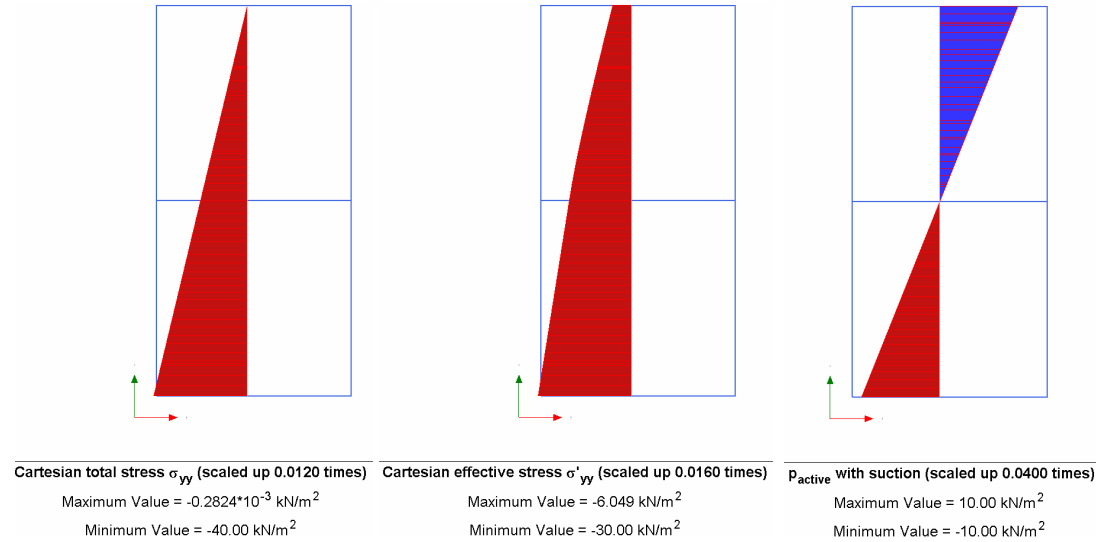


Fig. 6: Results after the initial phase for coarse material: left) vertical total stress; middle) vertical effective stress; right) active pore pressure

Verification:

Bishop stress reads:

$$\sigma = \sigma' + m(S p_w) \quad (2)$$

As the same weight for dry and saturated soil is used, the vertical total stress at the bottom can be simply calculated by:

$$\sigma = h \cdot \gamma = -2 \times 20 = -40 \text{ kPa}$$

The degree of saturation is 1 at the bottom and 0.6049 at the top. Therefore Bishop's effective stresses at the top and bottom are:

$$\sigma'_{top} = \sigma_{top} - S \cdot p_w = 0 - 0.6049 \times 10 = -6.049 \text{ kPa}$$

$$\sigma'_{bottom} = \sigma_{bottom} - S \cdot p_w = -40 - 1 \times 10 = -30.0 \text{ kPa}$$

It can be seen that the calculated results from PLAXIS are the same as the analytical solution.

It should be noted that the degree of saturation is not linear in the unsaturated area and consequently the resulting effective stress is not linear in this area (Figure 6).

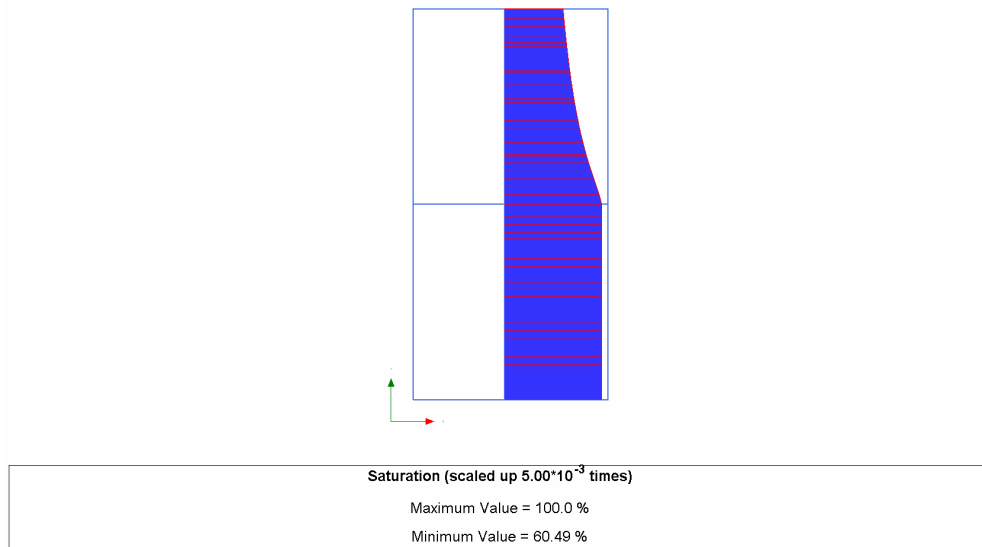


Fig. 7: Results after the initial phase for coarse material: Degree of saturation

Figure 8 and 9 show the results of the fine material after the initial phase. In the same manner done for the coarse material, the results can be verified. As seen in this case, higher degree of saturation and higher effective stresses are generated in the unsaturated area.

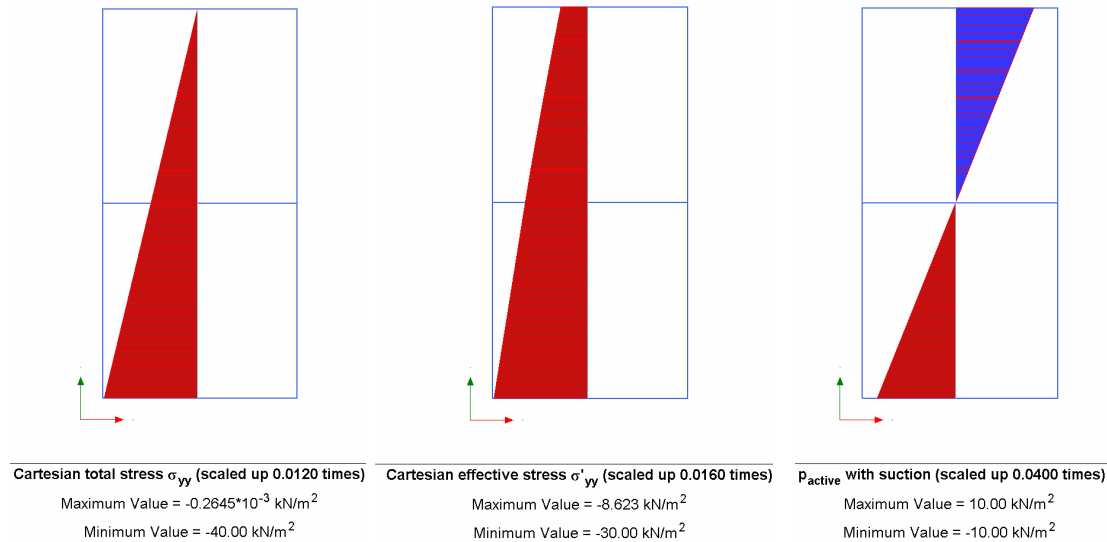


Fig. 8: Results after the initial phase for fine material: left) vertical total stress; middle) vertical effective stress; right) active pore pressure

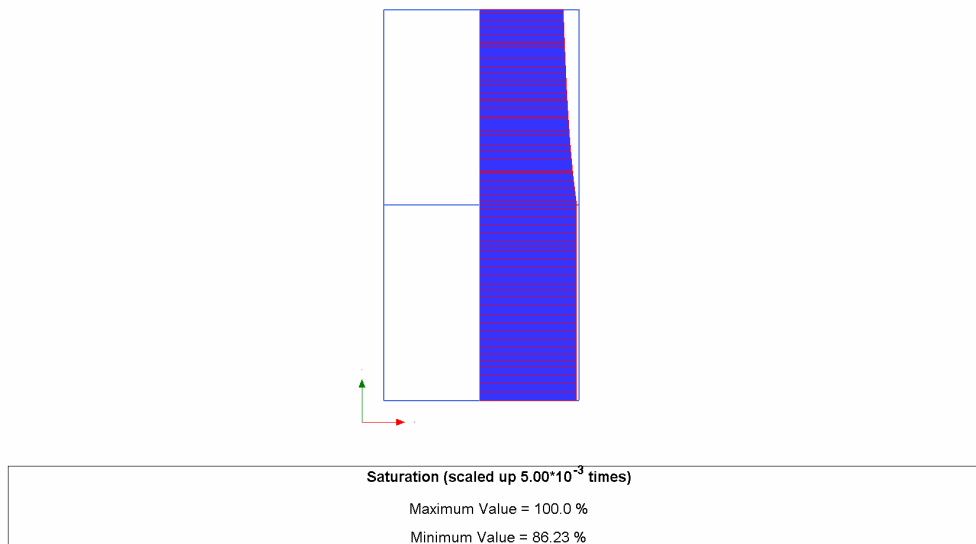


Fig. 9: Results after the initial phase for fine material: Degree of saturation

In phase 1, undrained behaviour is assumed and consequently excess water pore pressure is generated. As the bulk modulus of water, weight of soil, degree of saturation and the effective stress are suction dependent, the undrained calculations are always non-linear in the advanced mode even for linear elastic materials as used in this example.

The total and effective stresses as well as the active pore pressures of phase 1 in coarse material are plotted in Figure 10.

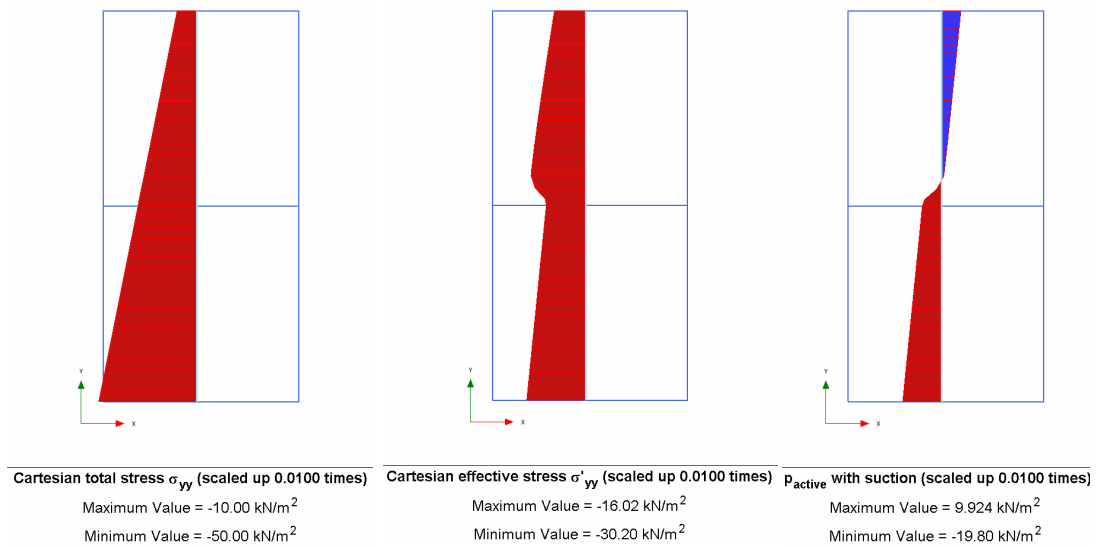


Fig. 10: Results after the phase 1 for coarse material: left) vertical total stress; middle) vertical effective stress; right) active pore pressure

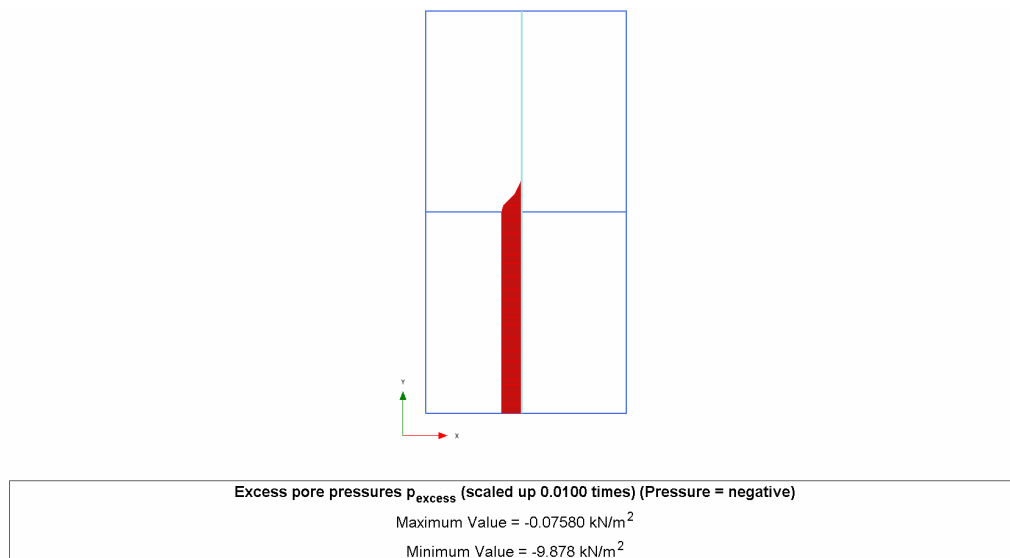


Fig. 11: Excess water pore pressure in coarse material at the end of phase 1.

In the same way done in for phase 0, the stresses can be verified in this phase. Due to the highly non-linearity behaviour, it is difficult to verify water excess pore pressure analytically as done for the saturated case.

In Figure 10, it can be observed that the vertical total stress on top of the model is 9.968 kPa which slightly less than the analytical solution, 10 kPa (error = 0.32%). This difference is due to the non-linearity mentioned above.

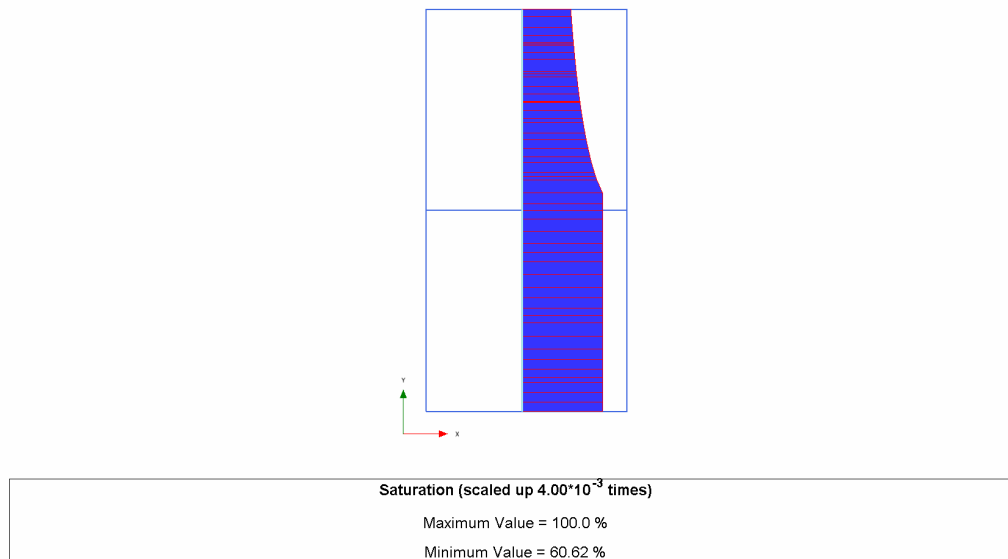


Fig. 12: Results after phase 1 for coarse material: Degree of saturation

Results of the fine material at the end of phase 1 are plotted in Figures 13-15. By comparing the results from the coarse and fine materials, it can be seen that more excess pore pressure (and consequently less effective stress) is developed in the fine material which is in agreement with reality.

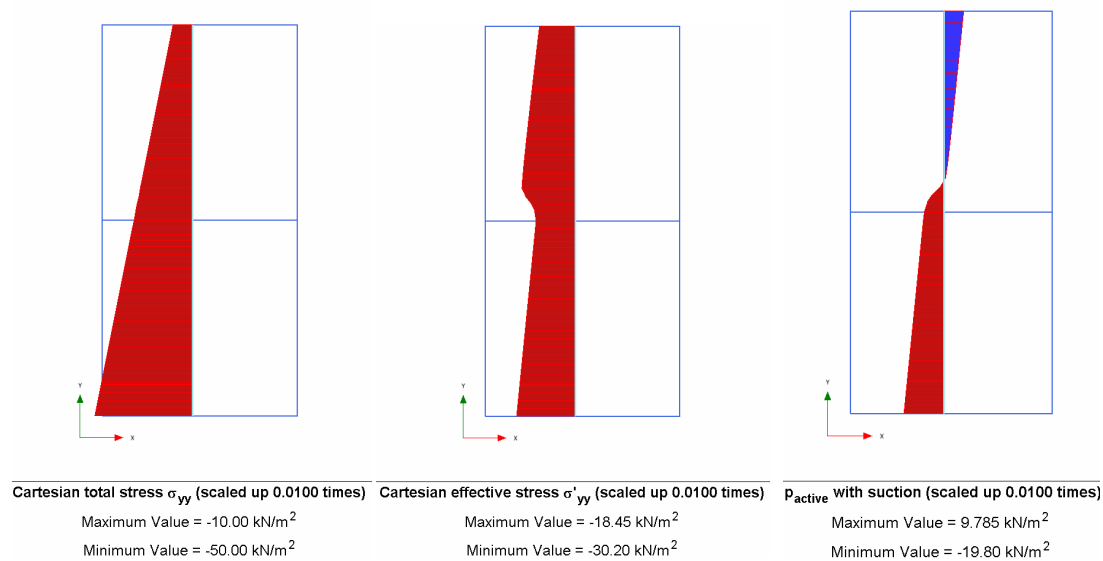


Fig. 13: Results after the phase 1 for fine material: left) vertical total stress; middle) vertical effective stress; right) active pore pressure

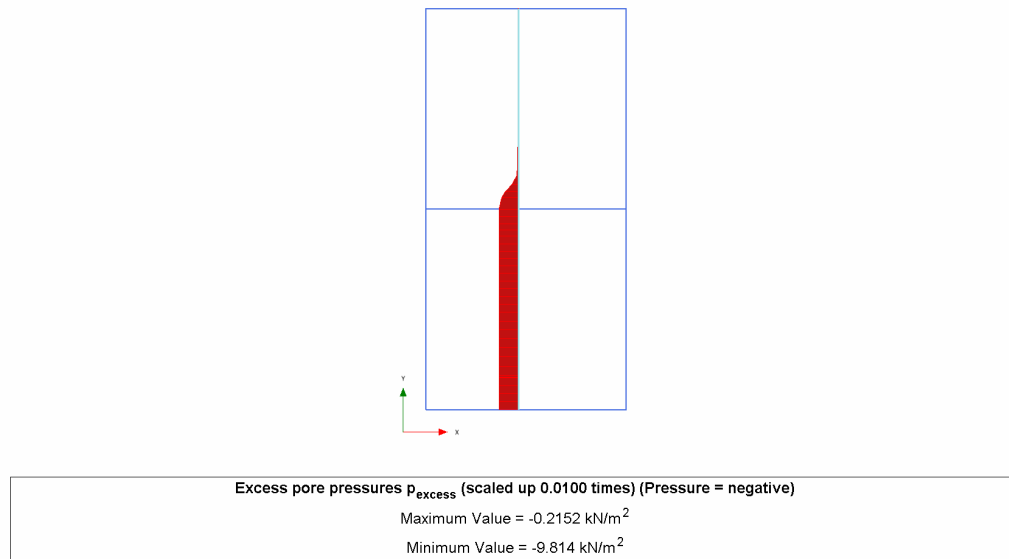


Fig. 14: Excess water pore pressure in fine material at the end of phase 1.

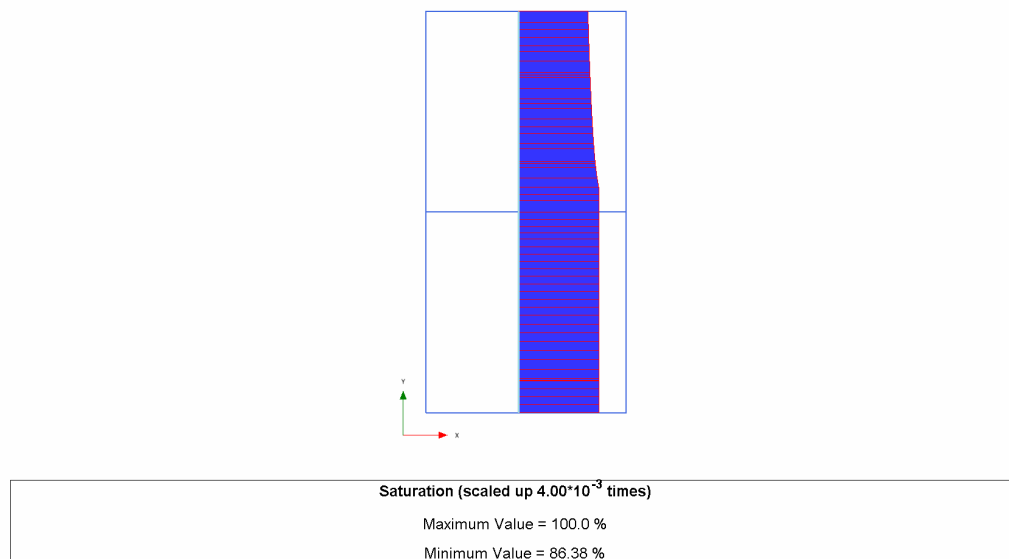


Fig. 15: Results after phase 1 for fine material: Degree of saturation

The results of the coarse material (effective stress, total stress, degree of saturation, active and excess pore pressures versus depth) are plotted in Figures 16-20 and the results of the fine material in Figures 21-25. It can be seen that, according to the SWCC used in the calculation, different effective stresses are developed in the model. As the degradation of the degree of saturation increases with increasing suction, effective stress in the unsaturated zone are increases and the problem becomes more non-linear (because the properties of the soil changes more by changing the suction).

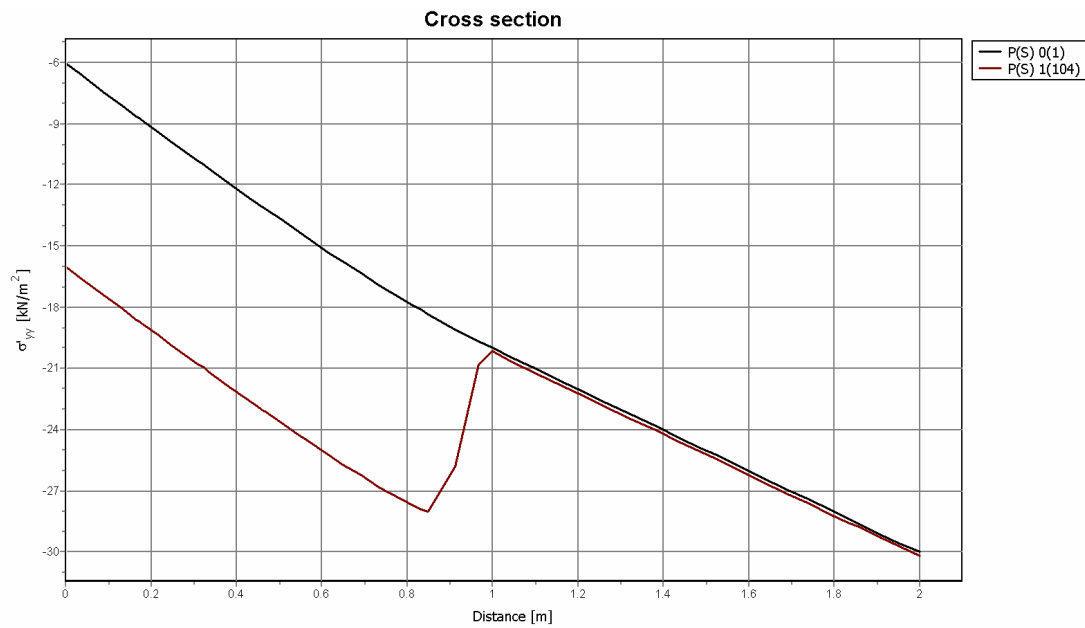


Fig. 16: Effective stresses at the end of phase 0 (step 1) and phase 1 (step 104) in coarse material

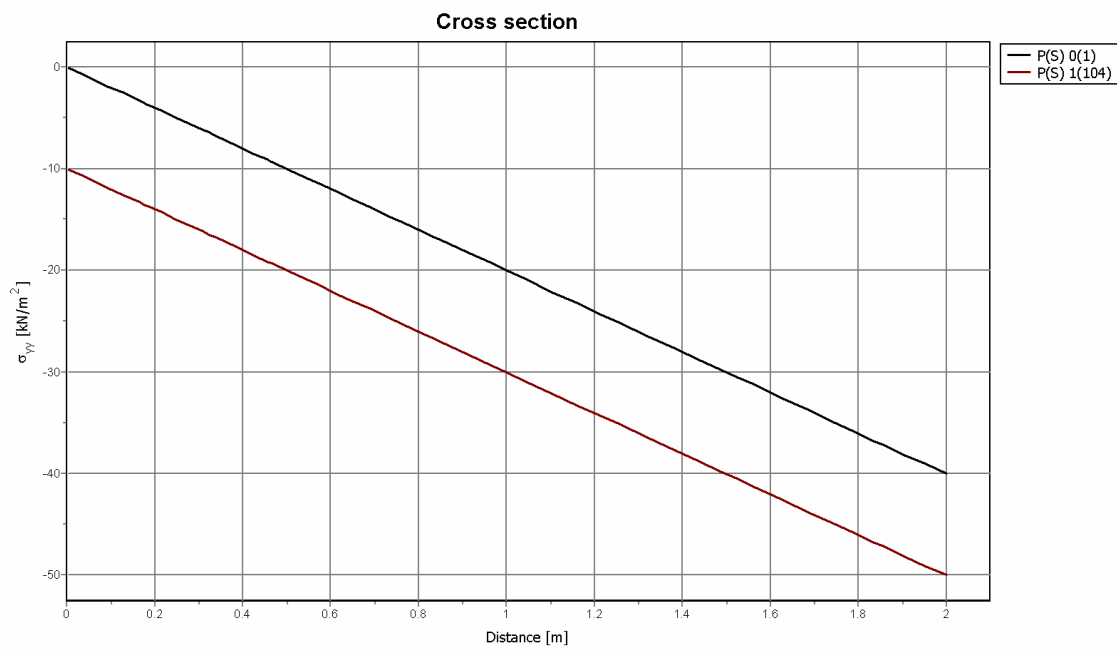


Fig. 17: Vertical total stress at the end of phase 0 (step 1) and phase 1 (step 104) in coarse material

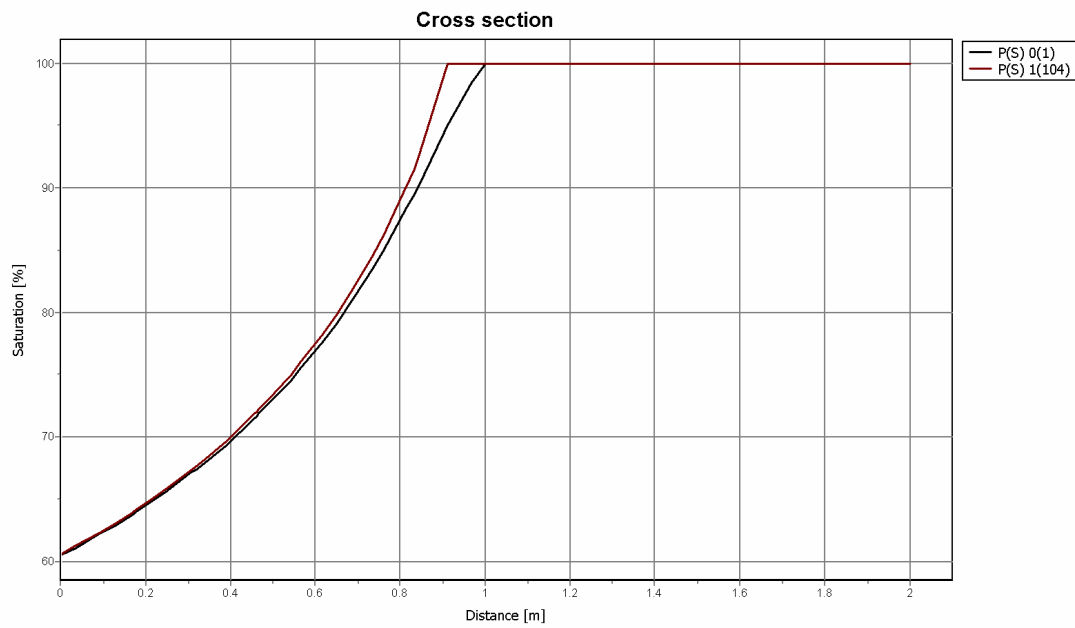


Fig. 18: Degree of saturation at the end of phase 0 (step 1) and phase 1 (step 104) in coarse material

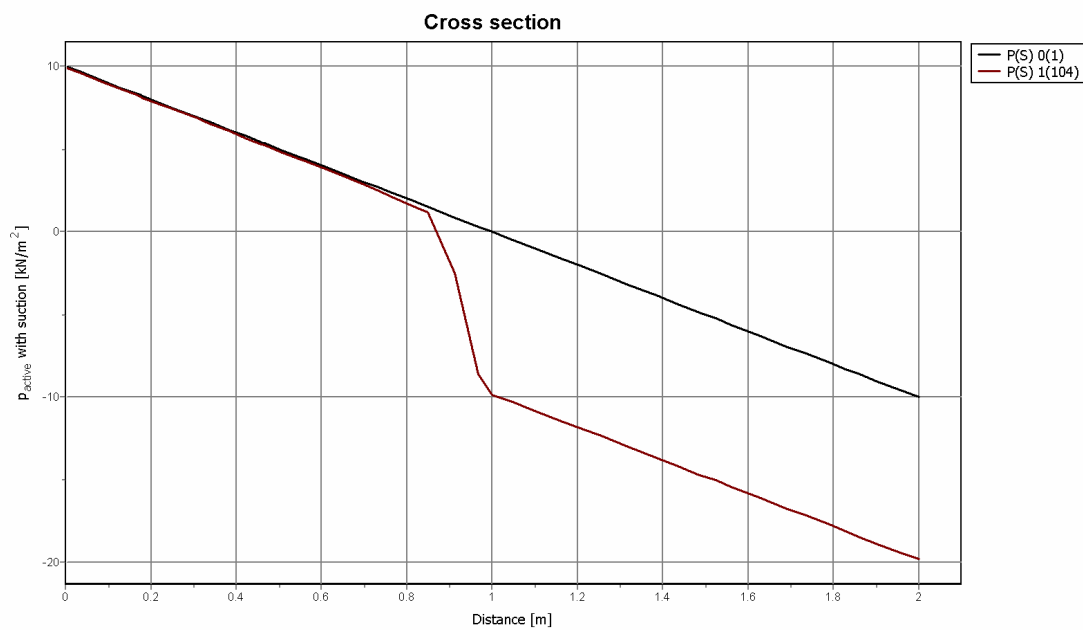


Fig. 19: Active pore pressure at the end of phase 0 (step 1) and phase 1 (step 104) in coarse material

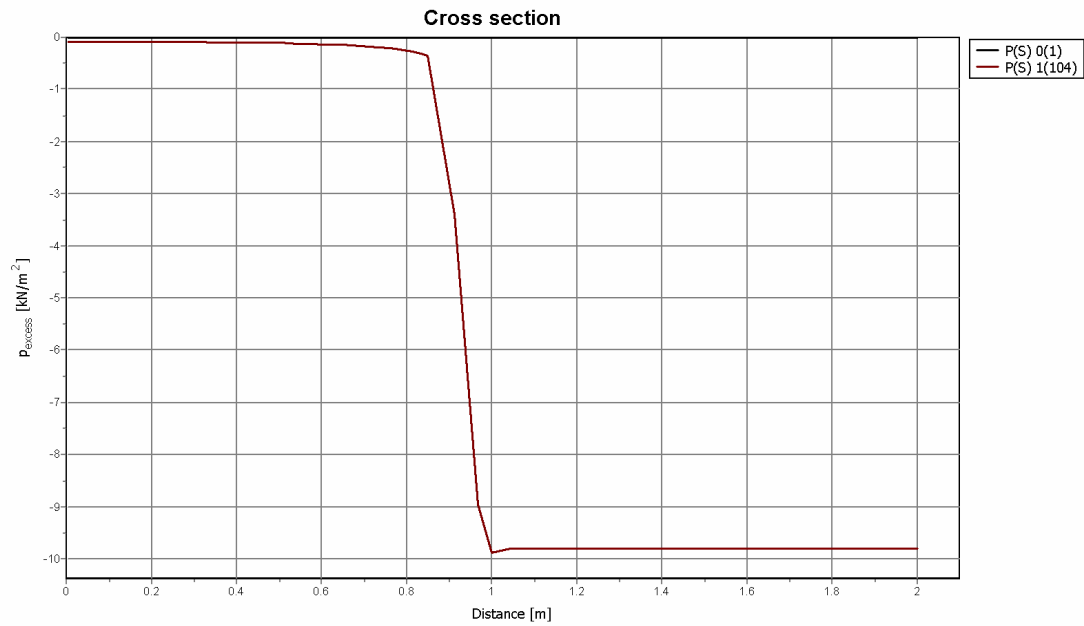


Fig. 20: Excess pore pressure at the end of phase 0 (step 1) and phase 1 (step 104) in coarse material

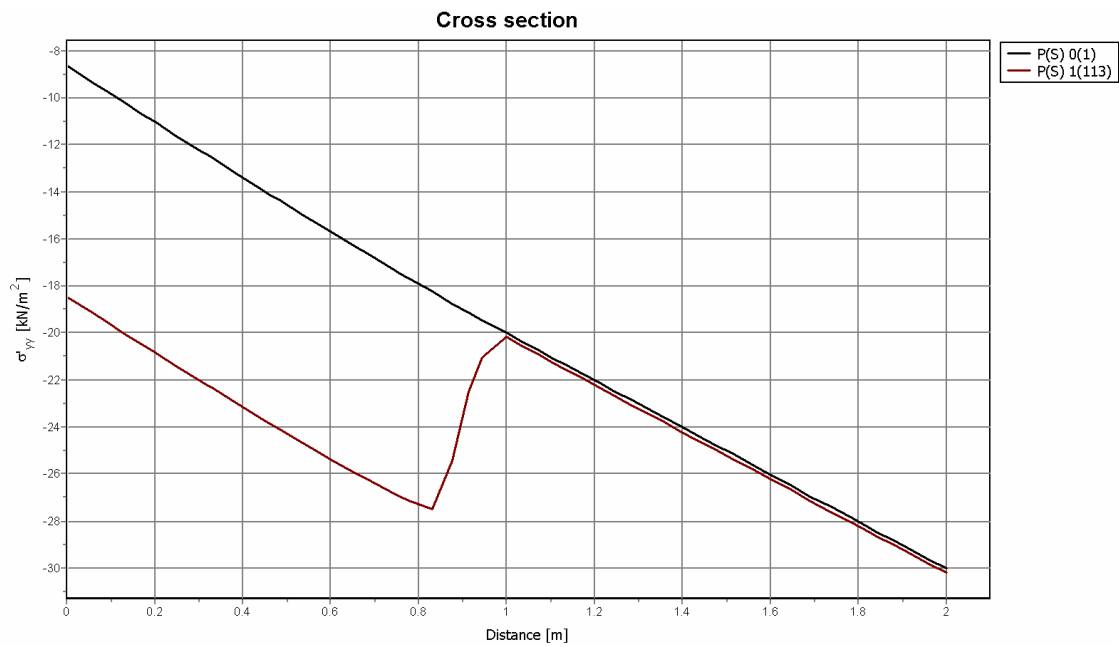


Fig. 21: Effective stresses at the end of phase 0 (step 1) and phase 1 (step 113) in fine material

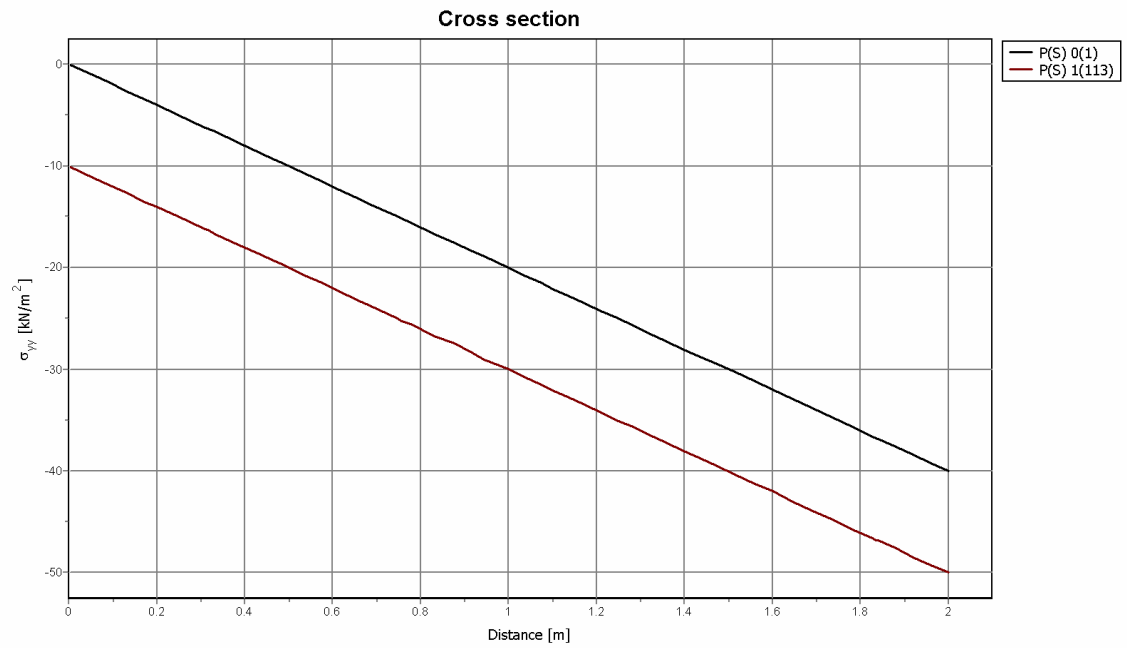


Fig. 22: Vertical total stress at the end of phase 0 (step 1) and phase 1 (step 113) in fine material

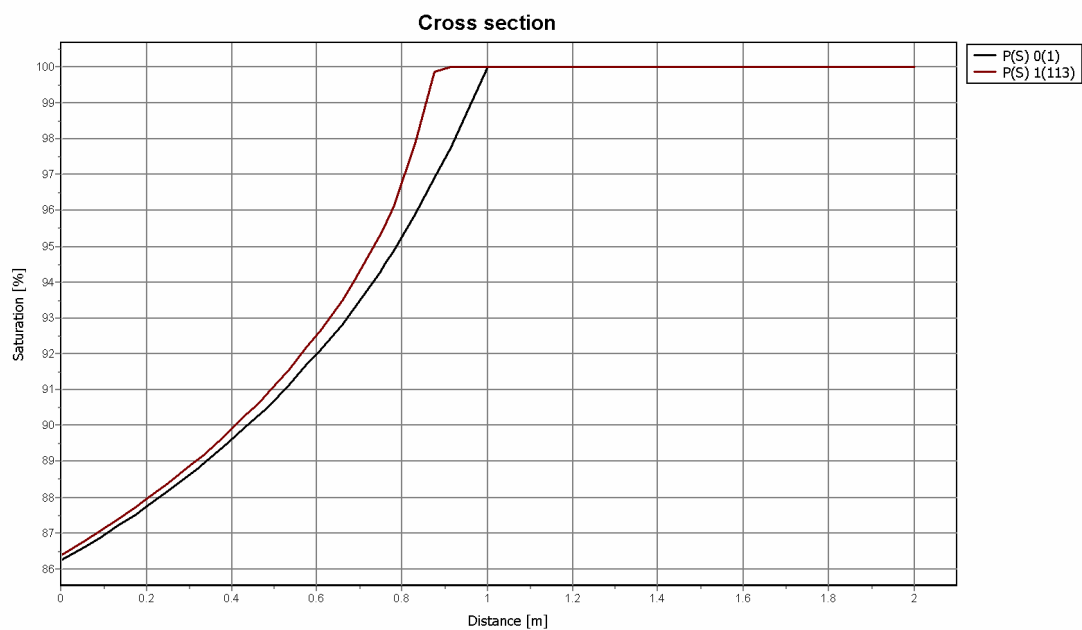


Fig. 23: Degree of saturation at the end of phase 0 (step 1) and phase 1 (step 113) in fine material

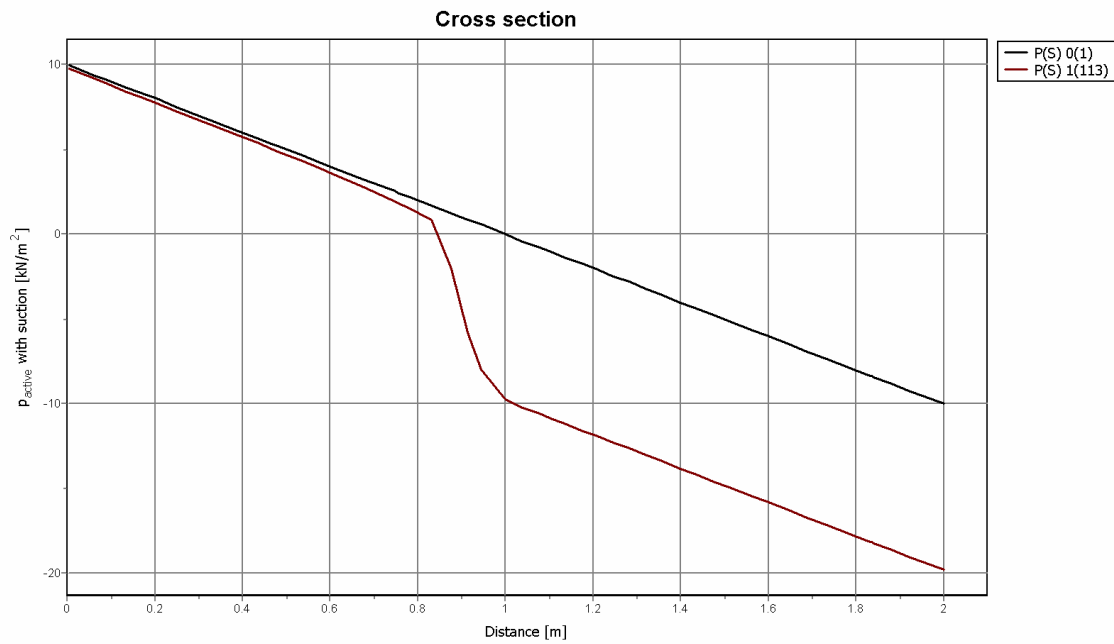


Fig. 24: Active pore pressure at the end of phase 0 (step 1) and phase 1 (step 113) in fine material

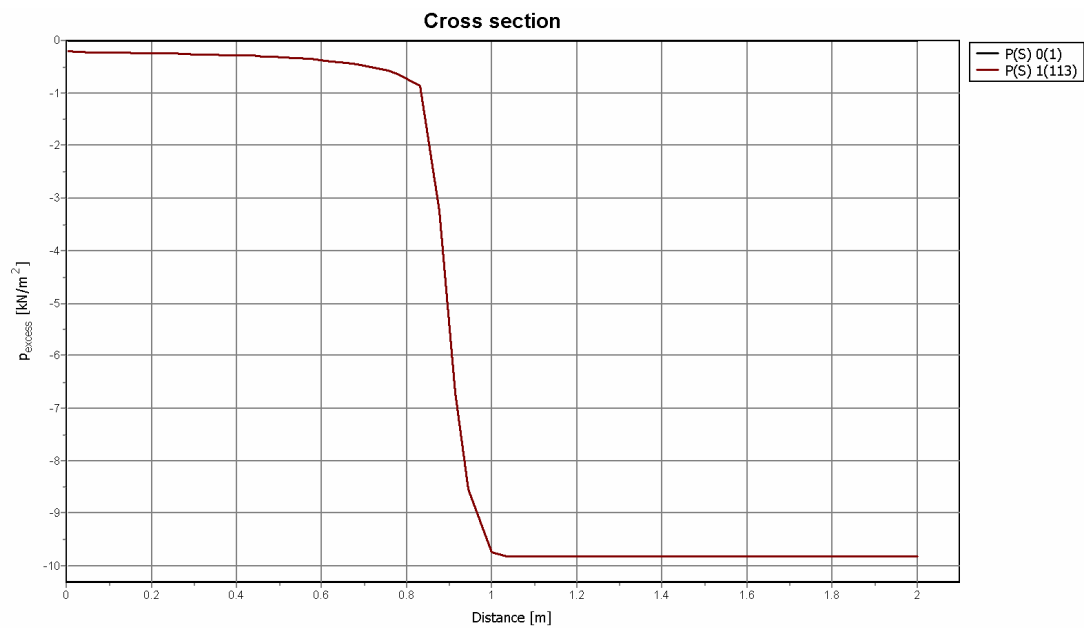


Fig. 25: Excess pore pressure at the end of phase 0 (step 1) and phase 1 (step 113) in fine material

12 Bibliography

- Alonso, E.E., Gens, A. & Josa, A. (1990), "A constitutive model for partially saturated soils". *Géotechnique*, 40: 405-430.
- Barrera, M., Romero, E., Sánchez, M. & Lloret, A. (2002). "Laboratory tests to validate and determine parameters of an elastoplastic model for unsaturated soils". International Symposium on identification and determination of soil and rock parameters for geotechnical design. Jean-Pierre MAGNAN. LCPC.
- Bardet, J-P & Tobita, T. (2002). "A practical method for solving free-surface seepage problems". *Computer and Geotechnics*, 29: 451-475.
- Biot, M.A. (1941). "General theory of three dimensional consolidation". *Journal of Applied Physics*, 12, 155-164.
- Bishop, A.W. & Blight, A.K.G. (1963). "Some aspects of effective stress in saturated and partially saturated soils". *Géotechnique*, 13: 177-197.
- Bishop, A. W. & Eldin, A. K. G. (1950). "Undrained triaxial tests on saturated sands and their significance in the general theory of shear strength". *Géotechnique*, 2: 13-32.
- Bolzon, G., Screfler, B.A. & Zienkiewicz, O.C. (1996). "Elastoplastic soil constitutive laws generalised to partially saturated states". *Géotechnique*, 46(2), 279-289.
- Booker, J.R. & Small, J.C. (1975). "An investigation of the stability of numerical solutions of Biot's equations of consolidation". *Int. J. Solids Struct.*, 11, 907-917.
- Borja, R.I., Kishnani, S.S. (1991). "On the solution of elliptic free-boundary problems via Newton's method". *Computer Methods in Applied Mechanics and Engineering*, 88: 341-361.
- Brinkgreve, R.B.J, Broere, W. & Waterman, D. (2006), *Plaxis, Finite element code for soil and rock analyses, users manual*. The Netherlands.
- Darcy, H. (1856). *Histoire Des Fontaines Publique de Dijon*. Paris, Dalmont, pp. 590-594.
- Dogan, A. & Motz, L. H. (2005). "Saturated-unsaturated 3D groundwater model. I: Development". *Journal of Hydrological Engineering, ASCE*, Vol. 10, No. 6, 492-504.

- Fredlund, D.G. (1996). *The Emergence of Unsaturated Soil Mechanics*. The Fourth Spencer J. Buchanan Lecture, College Station, Texas, A & M University Press, p. 39.
- Fredlund, D.G. & Rahardjo, H. (1993). *Soil mechanics for unsaturated soils*. New York: Wiley.
- Gallipoli, D., Gens, A., Sharma, R. & Vaunat, J. (2003). “An elasto-plastic model unsaturated soil incorporating the effects of suction and degree of saturation on mechanical behaviour”. *Géotechnique*, 53: 123-135.
- Geiser, F., Laloui L & Vulliet L (2000). Modelling the behaviour of unsaturated silt. Experimental evidence and theoretical approaches in unsaturated soils. Balkema, Rotterdam, pp 155–175.
- Gonzalez, N.A. & Gens, A. (2008). Report: Implementation of unsaturated soil model in Plaxis.
- Harr, M.E. (1962). *Groundwater and Seepage*. McGraw-Hill, New York.
- Jeremic, B. & Sture, S. (1997). “Implicit integration in elastoplastic geotechnics”. *Mech. Cohes.-Frict. Mater.*, 2: 165-183.
- Kang-Kun Lee & Darrell I. Leap (1997). “Simulation of a free-surface and seepage face using boundary-fitted coordinate system method”. *Journal of Hydrology*, 196: 297-309.
- Lacy, S.J. & Prevost, J.H. (1987). “Flow through porous media: a procedure for locating the free surface”. *International Journal for numerical and Analytical Methods in Geomechanics*. 11: 585-601.
- Mualem, Y. (1976). “A new model for predicting the hydraulic conductivity of unsaturated porous media”. *Water Resour. Res.*, 12: 513–522.
- Muskat, M. (1937). *Flow of Homogeneous Fluids through Porous Media*. McGraw-Hill.
- Oden, J.T. & Kikuchi, N. (1980). “Recent advances: theory of variational inequalities with applications to problems of flow through porous media”. *International Journal of Engineering Science*. 18, 1173-1284.
- Pérez A., Rodríguez A. & Huerta, A. (2001). “Consistent tangent matrices for substepping schemes”. *Comput. Methods Appl. Mech. Engrg.* 190: 4627–4647.

- Roscoe, K.H. & Burland, J.B. (1968). "On the generalised stress-strain behaviour of "wet" clay". Engineering Plasticity. Cambridge University Press: Cambridge, MA, 535-609.
- Schwab, R. (2008). Report: Implementation of total pore pressure approach in Plaxis.
- Sheng, D., Sloan, S.W., Gens, A., & Smith, D.W. (2003). "Finite element formulation and algorithms for unsaturated soils". Part II: Verification and application. Int. J. for Numerical and Analytical Meth. in Geomech., 27: 767- 790.
- Song, E.X. (1990). Elasto-plastic consolidation under steady state and cyclic loads". Dissertation, Delft University of Technology, Delft, Netherlands.
- Strack, O.D. & Asgian, M.I. (1978). "A new function for use in the hodograph method". Water Resource Research, No. 14(6), 1045-1058.
- Van Genuchten, M.T. (1980). "A closed-form equation for predicting the hydraulic conductivity of unsaturated soil". Soil Science Society of America Journal, 44: 892-898.
- Verruijt, A. (2001). *Soil mechanics*, Delft University of Technology.
- Zhang, C.-L., Kröhn, K.-P., & Rothfuchs, T. (2003). Applications of CODE-BRIGHT to thermal-hydromechanical experiments on clays. Proceedings of the International Conference from Experimental Evidence towards Numerical Modelling. Numerical and Theoretical Approaches Unsaturated. Volume II. T. Schanz (Ed.). pp: 341-358.

Appendix A

In the following definitions of invariants and first and second derivatives of yield function and plastic potential used in Barcelona Basic Model are given.

Definitions of invariants

Stress tensor:

$$\sigma_{ij} = p\delta_{ij} + s_{ij}$$

Volumetric stress tensor:

$$p = \sigma_{ij} \frac{\delta_{ij}}{3} = \frac{\sigma_{kk}}{3}$$

Deviatoric stress tensor:

$$s_{ij} = \sigma_{ij} - p\delta_{ij}$$

Second invariant of deviatoric stress tensor:

$$J_2 = \frac{1}{2} s_{ij} s_{ij} = \frac{1}{6} \left[(\sigma_{11} - \sigma_{22})^2 + (\sigma_{11} - \sigma_{33})^2 + (\sigma_{22} - \sigma_{33})^2 \right] + \sigma_{12}^2 + \sigma_{13}^2 + \sigma_{23}^2$$

$$J_2 = \frac{1}{6} \left[(\sigma_1 - \sigma_2)^2 + (\sigma_1 - \sigma_3)^2 + (\sigma_2 - \sigma_3)^2 \right]$$

Square root of second invariant of deviatoric stress tensor: $J = \sqrt{J_2}$

Third invariant of deviatoric stress tensor:

$$J_3 = \frac{1}{3} s_{ij} s_{jk} s_{ki} = \begin{vmatrix} s_{11} & s_{12} & s_{13} \\ s_{21} & s_{22} & s_{23} \\ s_{31} & s_{32} & s_{33} \end{vmatrix}$$

$$J_3 = \frac{1}{3} (s_1^3 + s_2^3 + s_3^3) = s_1 s_2 s_3$$

Lode angle:

$$\theta = \frac{1}{3} \sin^{-1} \left(\frac{-3\sqrt{3}}{2} \frac{J_3}{J^3} \right)$$

Derivatives of invariants

First derivatives of invariants:

$$\frac{\partial p}{\partial \bar{\sigma}_j} = \begin{pmatrix} \frac{1}{3} & \frac{1}{3} & \frac{1}{3} & 0 & 0 & 0 \end{pmatrix}$$

$$\frac{\partial J}{\partial \bar{\sigma}_j} = \begin{pmatrix} \frac{s_1}{2J} & \frac{s_2}{2J} & \frac{s_3}{2J} & \frac{s_4}{J} & \frac{s_5}{J} & \frac{s_6}{J} \end{pmatrix}$$

$$\frac{\partial \theta}{\partial \bar{\sigma}_j} = \tan(3\theta) \left(\frac{1}{3J_3} \frac{\partial J_3}{\partial \bar{\sigma}_j} - \frac{1}{J} \frac{\partial J}{\partial \bar{\sigma}_j} \right) = \frac{-\sqrt{3} \left(\frac{\partial J_3}{\partial \bar{\sigma}_j} - \frac{3J_3}{J} \frac{\partial J}{\partial \bar{\sigma}_j} \right)}{\sqrt{4J^6 - 27J_3^3}}$$

$$\frac{\partial J_3}{\partial \bar{\sigma}_j} = \begin{bmatrix} \frac{2}{3}(s_{11}^2 - s_{23}^2) - \frac{1}{3}(s_{22}^2 - s_{13}^2) - \frac{1}{3}(s_{33}^2 - s_{12}^2) \\ \frac{2}{3}(s_{22}^2 - s_{13}^2) - \frac{1}{3}(s_{11}^2 - s_{23}^2) - \frac{1}{3}(s_{33}^2 - s_{12}^2) \\ \frac{2}{3}(s_{33}^2 - s_{12}^2) - \frac{1}{3}(s_{11}^2 - s_{23}^2) - \frac{1}{3}(s_{22}^2 - s_{13}^2) \\ 2[s_{12}(s_{11} + s_{22}) + s_{13}s_{23}] \\ 2[s_{13}(s_{11} + s_{33}) + s_{12}s_{23}] \\ 2[s_{23}(s_{22} + s_{33}) + s_{12}s_{13}] \end{bmatrix}$$

Derivatives of gradients to the plastic potential: $\partial m_{ij} / \partial \sigma_{kl}$

- a) Derivatives of gradients to the plastic potential ∇Q_i with respect to stress vector σ_j

$$\frac{\partial \nabla Q_i^\sigma}{\partial \bar{\sigma}_j} = \frac{\partial^2 Q}{\partial \bar{\sigma}_i \partial \bar{\sigma}_j} = \begin{bmatrix} \frac{\partial^2 Q}{\partial \bar{\sigma}_1 \partial \bar{\sigma}_1} & \frac{\partial^2 Q}{\partial \bar{\sigma}_1 \partial \bar{\sigma}_2} & \frac{\partial^2 Q}{\partial \bar{\sigma}_1 \partial \bar{\sigma}_3} & \frac{\partial^2 Q}{\partial \bar{\sigma}_1 \partial \bar{\sigma}_4} & \frac{\partial^2 Q}{\partial \bar{\sigma}_1 \partial \bar{\sigma}_5} & \frac{\partial^2 Q}{\partial \bar{\sigma}_1 \partial \bar{\sigma}_6} \\ \frac{\partial^2 Q}{\partial \bar{\sigma}_2 \partial \bar{\sigma}_1} & \frac{\partial^2 Q}{\partial \bar{\sigma}_2 \partial \bar{\sigma}_2} & \frac{\partial^2 Q}{\partial \bar{\sigma}_2 \partial \bar{\sigma}_3} & \frac{\partial^2 Q}{\partial \bar{\sigma}_2 \partial \bar{\sigma}_4} & \frac{\partial^2 Q}{\partial \bar{\sigma}_2 \partial \bar{\sigma}_5} & \frac{\partial^2 Q}{\partial \bar{\sigma}_2 \partial \bar{\sigma}_6} \\ \frac{\partial^2 Q}{\partial \bar{\sigma}_3 \partial \bar{\sigma}_1} & \frac{\partial^2 Q}{\partial \bar{\sigma}_3 \partial \bar{\sigma}_2} & \frac{\partial^2 Q}{\partial \bar{\sigma}_3 \partial \bar{\sigma}_3} & \frac{\partial^2 Q}{\partial \bar{\sigma}_3 \partial \bar{\sigma}_4} & \frac{\partial^2 Q}{\partial \bar{\sigma}_3 \partial \bar{\sigma}_5} & \frac{\partial^2 Q}{\partial \bar{\sigma}_3 \partial \bar{\sigma}_6} \\ \frac{\partial^2 Q}{\partial \bar{\sigma}_4 \partial \bar{\sigma}_1} & \frac{\partial^2 Q}{\partial \bar{\sigma}_4 \partial \bar{\sigma}_2} & \frac{\partial^2 Q}{\partial \bar{\sigma}_4 \partial \bar{\sigma}_3} & \frac{\partial^2 Q}{\partial \bar{\sigma}_4 \partial \bar{\sigma}_4} & \frac{\partial^2 Q}{\partial \bar{\sigma}_4 \partial \bar{\sigma}_5} & \frac{\partial^2 Q}{\partial \bar{\sigma}_4 \partial \bar{\sigma}_6} \\ \frac{\partial^2 Q}{\partial \bar{\sigma}_5 \partial \bar{\sigma}_1} & \frac{\partial^2 Q}{\partial \bar{\sigma}_5 \partial \bar{\sigma}_2} & \frac{\partial^2 Q}{\partial \bar{\sigma}_5 \partial \bar{\sigma}_3} & \frac{\partial^2 Q}{\partial \bar{\sigma}_5 \partial \bar{\sigma}_4} & \frac{\partial^2 Q}{\partial \bar{\sigma}_5 \partial \bar{\sigma}_5} & \frac{\partial^2 Q}{\partial \bar{\sigma}_5 \partial \bar{\sigma}_6} \\ \frac{\partial^2 Q}{\partial \bar{\sigma}_6 \partial \bar{\sigma}_1} & \frac{\partial^2 Q}{\partial \bar{\sigma}_6 \partial \bar{\sigma}_2} & \frac{\partial^2 Q}{\partial \bar{\sigma}_6 \partial \bar{\sigma}_3} & \frac{\partial^2 Q}{\partial \bar{\sigma}_6 \partial \bar{\sigma}_4} & \frac{\partial^2 Q}{\partial \bar{\sigma}_6 \partial \bar{\sigma}_5} & \frac{\partial^2 Q}{\partial \bar{\sigma}_6 \partial \bar{\sigma}_6} \end{bmatrix}$$

where:

$$\frac{\partial \nabla Q_i^\sigma}{\partial \bar{\sigma}_j} = \frac{\partial^2 Q}{\partial \bar{\sigma}_i \partial \bar{\sigma}_j} = \underbrace{\frac{\partial Q}{\partial p} \frac{\partial^2 p}{\partial \bar{\sigma}_j^2}}_{=0} + \frac{\partial p}{\partial \bar{\sigma}_i} \otimes \frac{\partial^2 Q}{\partial p \partial \bar{\sigma}_j} + \frac{\partial Q}{\partial J} \frac{\partial^2 J}{\partial \bar{\sigma}_j^2} + \frac{\partial J}{\partial \bar{\sigma}_i} \otimes \frac{\partial^2 Q}{\partial J \partial \bar{\sigma}_j} + \frac{\partial Q}{\partial \theta} \frac{\partial^2 \theta}{\partial \bar{\sigma}_j^2} + \frac{\partial \theta}{\partial \bar{\sigma}_i} \otimes \frac{\partial^2 Q}{\partial \theta \partial \bar{\sigma}_j}$$

$$\frac{\partial^2 J}{\partial \bar{\sigma}_i \partial \bar{\sigma}_j} = \begin{bmatrix} \frac{1}{3J} - \frac{s_1^2}{4J^3} & -\frac{1}{6J} - \frac{s_1 s_2}{4J^3} & -\frac{1}{6J} - \frac{s_1 s_3}{4J^3} & -\frac{s_1 s_{12}}{2J^3} & -\frac{s_1 s_{13}}{2J^3} & -\frac{s_1 s_{23}}{2J^3} \\ & \frac{1}{3J} - \frac{s_2^2}{4J^3} & -\frac{1}{6J} - \frac{s_2 s_3}{4J^3} & -\frac{s_2 s_{12}}{2J^3} & -\frac{s_2 s_{13}}{2J^3} & -\frac{s_2 s_{23}}{2J^3} \\ & & \frac{1}{3J} - \frac{s_3^2}{4J^3} & -\frac{s_3 s_{12}}{2J^3} & -\frac{s_3 s_{13}}{2J^3} & -\frac{s_3 s_{23}}{2J^3} \\ & & & \frac{1}{J} - \frac{s_{12}^2}{J^3} & -\frac{s_{12} s_{13}}{2J^3} & -\frac{s_{12} s_{23}}{2J^3} \\ & & & & \frac{1}{J} - \frac{s_{13}^2}{J^3} & -\frac{s_{13} s_{23}}{2J^3} \\ & & & & & \frac{1}{J} - \frac{s_{23}^2}{J^3} \end{bmatrix}$$

SYM

$$\begin{aligned} \frac{\partial^2 \theta}{\partial \bar{\sigma}_j^2} &= \frac{\partial^2 \theta}{\partial \sigma_{ij} \partial \sigma_{kl}} = \tan \theta \left[\frac{\sin^2 \theta}{J_3^2 \cos^2 \theta} \frac{\partial J_3}{\partial \sigma_{ij}} \frac{\partial J_3}{\partial \sigma_{kl}} + \frac{1 + \cos^2 \theta}{\cos^2 \theta} \frac{\partial J}{\partial \sigma_{ij}} \frac{\partial J}{\partial \sigma_{kl}} - \right. \\ &\quad \left. - \frac{1}{\cos^2 \theta J J_3} \left(\frac{\partial J}{\partial \sigma_{ij}} \frac{\partial J_3}{\partial \sigma_{kl}} + \frac{\partial J_3}{\partial \sigma_{ij}} \frac{\partial J}{\partial \sigma_{kl}} \right) + \frac{1}{J_3} \frac{\partial^2 J_3}{\partial \sigma_{ij} \partial \sigma_{kl}} - \frac{1}{J} \frac{\partial^2 J}{\partial \sigma_{ij} \partial \sigma_{kl}} \right] \\ \frac{\partial^2 \theta}{\partial \bar{\sigma}_j^2} &= \tan 3\theta \underbrace{\frac{\partial \left[\frac{1}{3J_3} \frac{\partial J_3}{\partial \bar{\sigma}_j} - \frac{1}{J} \frac{\partial J}{\partial \bar{\sigma}_j} \right]}{\partial \bar{\sigma}_j}}_{A_{6 \times 6}} + \underbrace{\left[\frac{1}{3J_3} \frac{\partial J_3}{\partial \bar{\sigma}_j} - \frac{1}{J} \frac{\partial J}{\partial \bar{\sigma}_j} \right]}_{B_{6 \times 1}} \otimes \underbrace{\frac{\partial \tan 3\theta}{\partial \bar{\sigma}_j}}_{C_{6 \times 1}} \end{aligned}$$

where:

$$A_{6 \times 6} = \frac{1}{3J_3} \frac{\partial^2 J_3}{\partial \bar{\sigma}_j^2} + \frac{\partial J_3}{\partial \bar{\sigma}_j} \otimes \frac{\partial \frac{1}{3J_3}}{\partial \bar{\sigma}_j} - \frac{1}{J} \frac{\partial^2 J}{\partial \bar{\sigma}_j^2} - \frac{\partial J}{\partial \bar{\sigma}_j} \otimes \frac{\partial \frac{1}{J}}{\partial \bar{\sigma}_j}$$

$$\frac{\partial^2 J_3}{\partial \bar{\sigma}_j^2} = \begin{pmatrix} \frac{2}{3}s_1 & \frac{2}{3}s_3 & \frac{2}{3}s_2 & \frac{2}{3}s_{12} & \frac{2}{3}s_{13} & -\frac{4}{3}s_{23} \\ \frac{2}{3}s_3 & \frac{2}{3}s_2 & \frac{2}{3}s_1 & \frac{2}{3}s_{12} & -\frac{4}{3}s_{13} & \frac{2}{3}s_{23} \\ \frac{2}{3}s_2 & \frac{2}{3}s_1 & \frac{2}{3}s_3 & -\frac{4}{3}s_{12} & \frac{2}{3}s_{13} & \frac{2}{3}s_{23} \\ \frac{2}{3}s_{12} & \frac{2}{3}s_{12} & -\frac{4}{3}s_{12} & -2s_3 & 2s_{23} & 2s_{13} \\ \frac{2}{3}s_{13} & -\frac{4}{3}s_{13} & \frac{2}{3}s_{13} & 2s_{23} & -2s_2 & 2s_{12} \\ -\frac{4}{3}s_{23} & \frac{2}{3}s_{23} & \frac{2}{3}s_{23} & 2s_{13} & 2s_{12} & -2s_1 \end{pmatrix}^T$$

$$\frac{\partial}{\partial \bar{\sigma}_j} \frac{1}{3J_3} = \frac{\partial (3J_3)^{-1}}{\partial \bar{\sigma}_j} = -3 \frac{\frac{\partial J_3}{\partial \bar{\sigma}_j}}{(3J_3)^2} = -\frac{\frac{\partial J_3}{\partial \bar{\sigma}_j}}{3J_3^2}$$

$$\frac{\partial \tan 3\theta}{\partial \bar{\sigma}_j} = 3(1 + \tan^2 3\theta) \frac{\partial \theta}{\partial \bar{\sigma}_j}$$

b) Derivatives of gradients to the plastic potential ∇Q_i with respect to hardening parameters χ_j

$$\frac{\partial \nabla Q_i^\sigma}{\partial \chi_j} = \frac{\partial^2 Q}{\partial \bar{\sigma}_i \partial \chi_j} = \begin{bmatrix} \frac{\partial^2 Q}{\partial \bar{\sigma}_1 \partial \chi_1} \\ \frac{\partial^2 Q}{\partial \bar{\sigma}_2 \partial \chi_1} \\ \frac{\partial^2 Q}{\partial \bar{\sigma}_3 \partial \chi_1} \\ \frac{\partial^2 Q}{\partial \bar{\sigma}_4 \partial \chi_1} \\ \frac{\partial^2 Q}{\partial \bar{\sigma}_5 \partial \chi_1} \\ \frac{\partial^2 Q}{\partial \bar{\sigma}_6 \partial \chi_1} \end{bmatrix}$$

where,

$$\frac{\partial^2 Q}{\partial \bar{\sigma}_i \partial \chi_j} = \frac{\partial Q}{\partial p} \underbrace{\frac{\partial^2 p}{\partial \bar{\sigma}_i \partial \chi_j}}_{=0} + \frac{\partial p}{\partial \bar{\sigma}_i} \otimes \frac{\partial^2 Q}{\partial p \partial \chi_j} + \frac{\partial Q}{\partial J} \underbrace{\frac{\partial^2 J}{\partial \bar{\sigma}_i \partial \chi_j}}_{=0} + \frac{\partial J}{\partial \bar{\sigma}_i} \otimes \frac{\partial^2 Q}{\partial J \partial \chi_j} + \frac{\partial Q}{\partial \theta} \underbrace{\frac{\partial^2 \theta}{\partial \bar{\sigma}_i \partial \chi_j}}_{=0} + \frac{\partial \theta}{\partial \bar{\sigma}_i} \otimes \frac{\partial^2 Q}{\partial \theta \partial \chi_j}$$

First and second derivatives of yield function and plastic potential

First derivatives:

$$\frac{\partial F}{\partial p} = \frac{\partial G}{\partial p} = \left(\frac{g(\theta)}{g(-30^\circ)} \right)^2 M^2 (2p + p_s - P_c)$$

$$\frac{\partial F}{\partial J} = 6J; \quad \frac{\partial G}{\partial J} = 6\alpha J$$

$$\frac{\partial F}{\partial g(\theta)} = \frac{\partial G}{\partial g(\theta)} = -\frac{2g(\theta)M^2(p + p_s)(P_c - p)}{g(-30^\circ)^2}$$

$$\frac{\partial g(\theta)}{\partial \theta} = -\frac{\sin \phi \left\{ -\sin \theta + \frac{\cos \theta \sin \phi}{\sqrt{3}} \right\}}{\left(\cos \theta + \frac{\sin \theta \sin \phi}{\sqrt{3}} \right)^2}$$

$$\frac{\partial F}{\partial P_c} = \frac{\partial G}{\partial P_c} = -\left(\frac{g(\theta)}{g(-30^\circ)^2} \right)^2 M^2 (p + p_s)$$

$$\frac{\partial P_c}{\partial P_o} = \frac{P_r \left(\frac{P_o}{P_r} \right)^{\frac{\lambda_o^* - \kappa^*}{\lambda_s^* - \kappa^*}} (\lambda_o^* - \kappa^*)}{(\lambda_s^* - \kappa^*) P_o}$$

$$\frac{\partial P_c}{\partial s} = \frac{P_c (\lambda_o^* - \kappa^*) \lambda_o^* (1-r) \beta \exp(-\beta s) \ln \left(\frac{P_o}{P_r} \right)}{(\lambda_s^* - \kappa^*)^2}$$

$$\frac{\partial F}{\partial p_s} = \frac{\partial G}{\partial p_s} = -\left(\frac{g(\theta)}{g(-30^\circ)} \right)^2 M^2 (P_c - p)$$

$$\frac{\partial p_s}{\partial s} = \kappa_s$$

Second derivatives:

a) p:
$$\frac{\partial^2 F}{\partial p^2} = 2 \left(\frac{g(\theta)}{g(-30^\circ)} \right)^2 M^2$$

$$\frac{\partial^2 F}{\partial p \partial J} = 0$$

$$\frac{\partial^2 F}{\partial p \partial \theta} = 2 \left(\frac{g(\theta)}{g(-30^\circ)} \right)^2 \frac{M^2 (P_c - 2p - p_s) \left(-\sin \theta + \frac{\cos \theta \sin \phi}{\sqrt{3}} \right)}{\left(\cos \theta + \frac{\sin \theta \sin \phi}{\sqrt{3}} \right)}$$

$$\frac{\partial^2 F}{\partial p \partial P_o} = - \left(\frac{g(\theta)}{g(-30^\circ)} \right)^2 M^2 \frac{\partial P_c}{\partial P_o}$$

b) J $\frac{\partial^2 F}{\partial J \partial p} = 0$

$$\frac{\partial^2 F}{\partial J^2} = 6; \quad \frac{\partial^2 G}{\partial J^2} = 6\alpha$$

$$\frac{\partial^2 F}{\partial J \partial \theta} = 0$$

$$\frac{\partial^2 F}{\partial J \partial P_c} = 0$$

c) θ $\frac{\partial^2 F}{\partial \theta \partial p} = \frac{\partial^2 F}{\partial p \partial \theta}$

$$\frac{\partial^2 F}{\partial \theta \partial J} = 0$$

$$\begin{aligned} \frac{\partial^2 F}{\partial \theta^2} = & -6 \left(\frac{g(\theta)}{g(-30^\circ)} \right)^2 \frac{M^2 (p + p_s) (P_c - p) \left(-\sin \theta + \frac{\cos \theta \sin \phi}{\sqrt{3}} \right)}{\left(\cos \theta + \frac{\sin \theta \sin \phi}{\sqrt{3}} \right)^2} + \\ & 2 \left(\frac{g(\theta)}{g(-30^\circ)} \right)^2 \frac{M^2 (p + p_s) (P_c - p) \left(-\cos \theta - \frac{\sin \theta \sin \phi}{\sqrt{3}} \right)}{\left(\cos \theta + \frac{\sin \theta \sin \phi}{\sqrt{3}} \right)} \end{aligned}$$

$$\frac{\partial^2 F}{\partial \theta \partial P_c} = 2 \left(\frac{g(\theta)}{g(-30^\circ)} \right)^2 \frac{M^2 (p + p_s) \left(-\sin \theta + \frac{\cos \theta \sin \phi}{\sqrt{3}} \right)}{\left(\cos \theta + \frac{\sin \theta \sin \phi}{\sqrt{3}} \right)} \frac{\partial P_c}{\partial P_o}$$

Appendix B

Here it is shown how Skempton B-parameter, the undrained Poisson's ratio ν_u and the equivalent bulk modulus of pore fluid K_w/n can be derived if one of them is known.

Note: In all cases, the effective Poisson's ratio ν' and shear stiffness G are known.

- **Case 1:**

	Known	Unknown
Parameters	B	$\nu_u, K_w/n$
Conditions	$0 \leq B \leq 0.995$	$\nu' \leq \nu_u \leq 0.4988$

Step 1: Calculate the undrained Poisson's ratio ν_u

$$\nu_u = \frac{3\nu' + B(1 - 2\nu')}{3 - B(1 - 2\nu')} \quad (15)$$

Step 2: the equivalent bulk modulus of pore fluid K_w/n

$$\frac{K_w}{n} = \frac{2 \cdot G}{3} \left(\frac{1 + \nu_u}{1 - 2\nu_u} - \frac{1 + \nu'}{1 - 2\nu'} \right) \quad (5)$$

- **Case 2:**

	Known	Unknown
Parameters	ν_u	$B, K_w/n$
Conditions	$\nu' \leq \nu_u \leq 0.4988$	$0 \leq B \leq 0.995$

Step 1: Calculate Skempton B-parameter

$$B = 1 - \frac{(1 + \nu')(1 - 2\nu_u)}{(1 + \nu_u)(1 - 2\nu')} \quad (14)$$

Step 2: the equivalent bulk modulus of pore fluid K_w/n

$$\frac{K_w}{n} = \frac{2 \cdot G}{3} \left(\frac{1 + \nu_u}{1 - 2\nu_u} - \frac{1 + \nu'}{1 - 2\nu'} \right) \quad (5)$$

- **Case 3:**

	Known	Unknown
Parameters	K_w/n	B, ν_u
Conditions	$0 \leq \frac{K_w}{n} \leq \frac{2 \cdot G}{3} \left(624.5 - \frac{1 + \nu'}{1 - 2\nu'} \right)$	$0 \leq B \leq 0.995$ $\nu' \leq \nu_u \leq 0.4988$

Step 1: Calculate the undrained Poisson's ratio ν_u

$$\nu_u = \frac{\alpha - 1}{2\alpha + 1}$$

where

$$\alpha = \frac{2 \cdot G}{3} \cdot \frac{K_w}{n} + \frac{1 + \nu'}{1 - 2\nu'}$$

Step 2: Calculate Skempton B-parameter

$$B = 1 - \frac{(1 + \nu')(1 - 2\nu_u)}{(1 + \nu_u)(1 - 2\nu')} \quad (14)$$

Here it is shown how to convert old PlaxFlow material data set to the new one. In the new material data set, C_{sat} is removed because it can simply be derived from the equivalent bulk modulus of water K_w/n and water weight γ_w :

$$C_{sat} = \frac{n\gamma_w}{K_w} \quad (1)$$

and

$$\frac{K_w}{n} = \frac{2 \cdot G}{3} \left(\frac{1 + \nu_u}{1 - 2\nu_u} - \frac{1 + \nu'}{1 - 2\nu'} \right) \quad (2)$$

or

$$\frac{K_w}{n} = \frac{E'}{3(1 + \nu')} \left(\frac{1 + \nu_u}{1 - 2\nu_u} - \frac{1 + \nu'}{1 - 2\nu'} \right) \quad (3)$$

Therefore:

$$E' = \frac{\gamma_w}{C_{sat}} \cdot \frac{1}{\alpha} \quad (4)$$

in which

$$\alpha = \frac{1}{3(1 + \nu')} \left(\frac{1 + \nu_u}{1 - 2\nu_u} - \frac{1 + \nu'}{1 - 2\nu'} \right) \quad (5)$$

How to convert:

Step 1: Choose “linear elastic” material.

Step 2: Choose “Undrained (A)” as type of drainage.

Step 3: Set $\nu' = 0.3$ and $\nu_u = 0.495$ (standard setting of undrained behaviour).

Step 4: Calculate α :

$$\alpha = \frac{1}{3(1 + \nu')} \left(\frac{1 + \nu_u}{1 - 2\nu_u} - \frac{1 + \nu'}{1 - 2\nu'} \right)$$

Step 5: Calculate E' :

$$E' = \frac{\gamma_w}{C_{sat}} \cdot \frac{1}{\alpha}$$